# PREDICTIVE, PROGNOSTIC BIOMARKERS AND THERAPEUTIC TARGETS IN TRIPLE NEGATIVE BREAST CANCER

EDITED BY: Shengtao Zhou, Zhi-Ming Shao, Zhijie Jason Liu and Yi-Zhou Jiang

PUBLISHED IN: Frontiers in Oncology

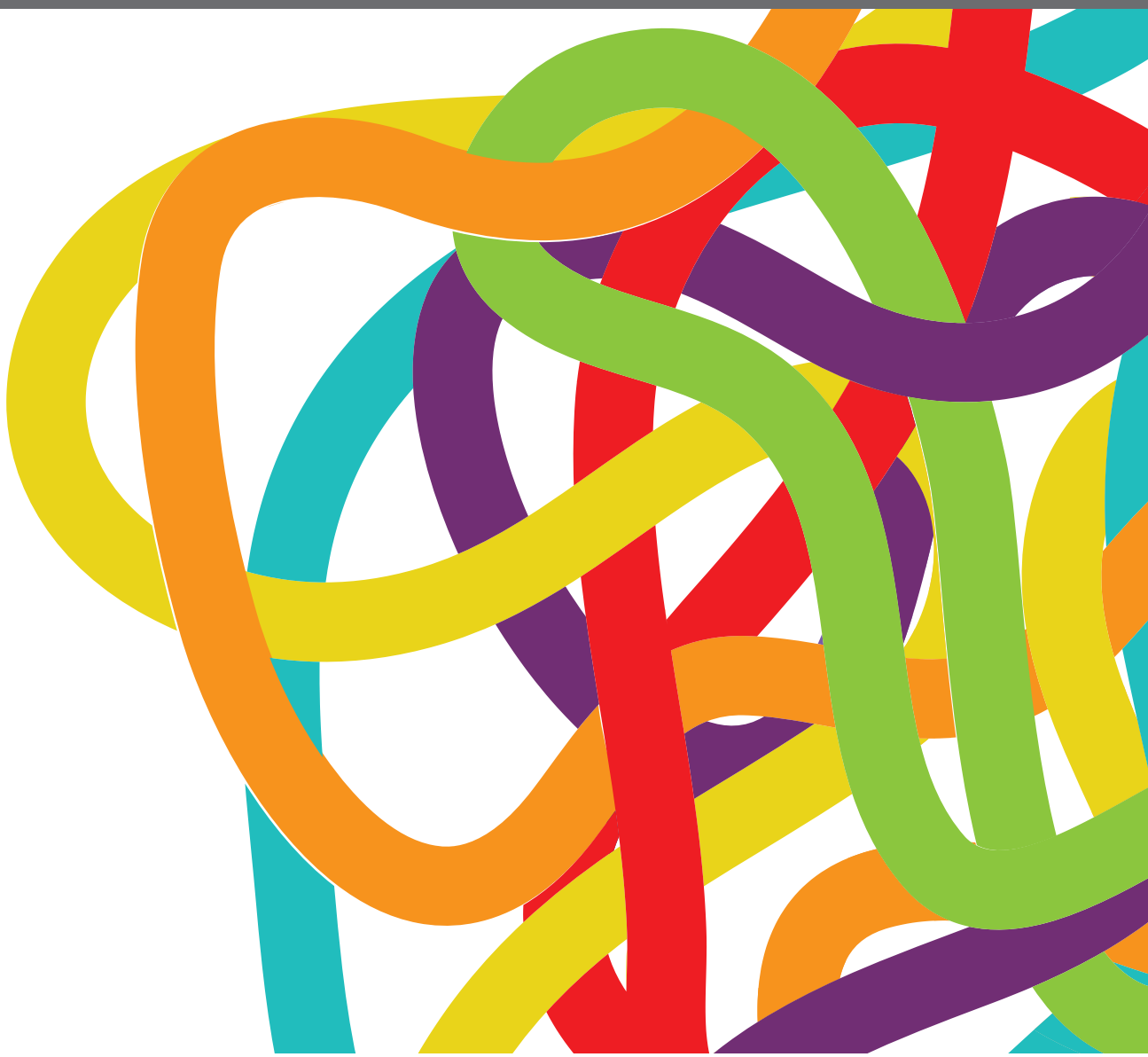

frontiers Research Topics

frontiers



ISSN 1664-8714
ISBN 978-2-88971-746-0
DOI 10.3389/978-2-88971-746-0

## About Frontiers

Frontiers is more than just an open-access publisher of scholarly articles: it is a pioneering approach to the world of academia, radically improving the way scholarly research is managed. The grand vision of Frontiers is a world where all people have an equal opportunity to seek, share and generate knowledge. Frontiers provides immediate and permanent online open access to all its publications, but this alone is not enough to realize our grand goals.

## Frontiers Journal Series

The Frontiers Journal Series is a multi-tier and interdisciplinary set of open-access, online journals, promising a paradigm shift from the current review, selection and dissemination processes in academic publishing. All Frontiers journals are driven by researchers for researchers; therefore, they constitute a service to the scholarly community. At the same time, the Frontiers Journal Series operates on a revolutionary invention, the tiered publishing system, initially addressing specific communities of scholars, and gradually climbing up to broader public understanding, thus serving the interests of the lay society, too.

## Dedication to Quality

Each Frontiers article is a landmark of the highest quality, thanks to genuinely collaborative interactions between authors and review editors, who include some of the world's best academicians. Research must be certified by peers before entering a stream of knowledge that may eventually reach the public - and shape society; therefore, Frontiers only applies the most rigorous and unbiased reviews.
Frontiers revolutionizes research publishing by freely delivering the most outstanding research, evaluated with no bias from both the academic and social point of view. By applying the most advanced information technologies, Frontiers is catapulting scholarly publishing into a new generation.

## What are Frontiers Research Topics?

Frontiers Research Topics are very popular trademarks of the Frontiers Journals Series: they are collections of at least ten articles, all centered on a particular subject. With their unique mix of varied contributions from Original Research to Review Articles, Frontiers Research Topics unify the most influential researchers, the latest key findings and historical advances in a hot research area! Find out more on how to host your own Frontiers Research Topic or contribute to one as an author by contacting the Frontiers Editorial Office: frontiersin.org/about/contact

# PREDICTIVE, PROGNOSTIC BIOMARKERS AND THERAPEUTIC TARGETS IN TRIPLE NEGATIVE BREAST CANCER

Topic Editors:
**Shengtao Zhou,** Sichuan University, China
**Zhi-Ming Shao,** Fudan University, China
**Zhijie Jason Liu,** The University of Texas Health Science Center at San Antonio, United States
**Yi-Zhou Jiang,** Fudan University, China

**Citation:** Zhou, S., Shao, Z.-M., Liu, Z. J., Jiang, Y.-Z., eds. (2021). Predictive, Prognostic Biomarkers and Therapeutic Targets in Triple Negative Breast Cancer. Lausanne: Frontiers Media SA. doi: 10.3389/978-2-88971-746-0

# Table of Contents

frontiers in Oncology

ORIGINAL RESEARCH
published: 04 December 2020
doi: 10.3389/fonc.2020.608334

# Nomogram for Predicting Lymph Node Involvement in Triple-Negative Breast Cancer

*Xiang Cui**, *Hao Zhu* and *Jisheng Huang**

*Department of Thyroid and Breast Surgery, The First People's Hospital of Shangqiu, Shangqiu, China*

**Background:** Lymph node metastasis of triple-negative breast cancer (TNBC) is essential in treatment strategy formulation. This study aimed to build a nomogram that predicts lymph node metastasis in patients with TNBC.

**Materials and Methods:** A total of 28,966 TNBC patients diagnosed from 2010 to 2017 in the Surveillance, Epidemiology and End Results (SEER) database were enrolled, and randomized 1:1 into the training and validation sets, respectively. Univariate and multivariate logistic regression analysis were applied to identify the predictive factors, which composed the nomogram. The receiver operating characteristic curves showed the efficacy of the nomogram.

**Result:** Multivariate logistic regression analyses revealed that age, race, tumor size, tumor primary site, and pathological grade were independent predictive factors of lymph node status. Integrating these independent predictive factors, a nomogram was successfully developed for predicting lymph node status, and further validated in the validation set. The areas under the receiver operating characteristic curves of the nomogram in the training and validation sets were 0.684 and 0.689 respectively, showing a satisfactory performance.

**Conclusion:** We constructed a nomogram to predict the lymph node status in TNBC patients. After further validation in additional large cohorts, the nomogram developed here would do better in predicting, providing more information for staging and treatment, and enabling tailored treatment in TNBC patients.

**Keywords: lymph node involvement, triple-negative breast cancer, nomogram, prediction, Surveillance, Epidemiology and End Results**

OPEN ACCESS

***Edited by:***
*Yi-Zhou Jiang,*
*Fudan University, China*

***Reviewed by:***
*Li-Ping Ge,*
*Fudan University, China*
*Gen-Hong Di,*
*Fudan University, China*

****Correspondence:***
*Xiang Cui*
*xiangcui223@163.com*
*Jisheng Huang*
*jishenghuang01@163.com*

***Specialty section:***
*This article was submitted to Women's Cancer, a section of the journal Frontiers in Oncology*

***Received:*** *20 September 2020*
***Accepted:*** *02 November 2020*
***Published:*** *04 December 2020*

***Citation:***
*Cui X, Zhu H and Huang J (2020) Nomogram for Predicting Lymph Node Involvement in Triple-Negative Breast Cancer. Front. Oncol. 10:608334. doi: 10.3389/fonc.2020.608334*

## INTRODUCTION

Breast cancer, the most common malignant tumor in women, is a heterogeneous disease. Triple-negative breast cancer (TNBC) represents one of the subtypes described in recent years, which does not express estrogen receptor (ER), progesterone receptor (PR) or human epidermal growth factor receptor 2 (HER2). It shows a variety of biological, clinicopathological and molecular characteristics, responses significantly differently to treatment and achieves divergent prognosis (1, 2). Despite the low incidence, accounting for about 10 to 20% of all breast cancer cases, TNBC

shows strong invasiveness, high malignancy and short relapse-free survival, reflecting the vital role of early diagnosis and accurate staging (3). Compared with other subtypes, patients with TNBC are more likely to show lymph node metastasis at the initial diagnosis (4).

Studies have shown that lymph node status is crucial for prognosis prediction and treatment decision in TNBC (5–7). At present, sentinel lymph node biopsy (SLNB), axillary lymph node dissection (ALND) and subsequent pathological diagnosis are commonly used methods to evaluate lymph node status in TNBC. The false negative rate of SLNB is 5–10%, which may result in improper patient management. Sufficient ALND can effectively reduce the risk of TNBC metastasis, but may cause chronic side effects such as numbness, stiffness in the upper body, and lymphedema. Moreover, extra-axillary lymph node metastasis also occurs (8), implying that SLNB or ALND might not be sufficient for the diagnosis of lymph node metastasis in TNBC. Therefore, it is helpful to classify TNBC cases preoperatively based on clinicopathologic factors, which contributes to the development of individualized surgical treatments and reducing overall mortality and morbidity in TNBC.

Clinical researchers and clinicians always make unremitting effort in predicting lymph node (LN) status. Several studies have developed multiple models for LN status prediction, but mostly are based on limited cases (9). Tan et al. constructed an immune-related genes (IRGS)-based nomogram to accurately estimate the preoperative ALN status of 214 operable TNBC cases (10). Despite its strong performance, the gene-based model may be difficult to promote. Therefore, this study aimed to develop a risk nomogram based on clinical data to determine lymph node metastasis, which could help to identify TNBC patients with positive lymph nodes more quickly.

# MATERIALS AND METHODS

## Patients

We extracted the data of 28,966 triple-negative breast cancer patients registered between January 1, 2010 and December 31, 2017 from the SEER program. HER2 status was absent in SEER's breast cancer cohort before 2010, and an enormous number of patients diagnosed before this time point were not included. Analysis cohorts were identified according to the following criteria: unilateral, invasive carcinoma of the breast (ICD-O-3 8500); diagnosis confirmed by positive histology and not by autopsy or a death certificate, as the first and only primary tumor; adjusted AJCC stage I–III; known tumor size; histological grade I–III; known regional lymph node status; ER, PR, HER2 negative. Patients with Paget's disease or younger than 18 years old were excluded. The patients were randomized 1:1 to the training and validation sets, respectively, for the construction and verification the nomogram. The following information was collected and transformed into categorical variables: age, race, gender, laterality, grade, location, histological type, and T stage.

## Construction and Validation of the Nomogram

Lymph node status was determined according to the Regional Nodes Positive term. We first screened the lymph node status-related clinicopathological characteristics, and found that statistically significant variables included age, race, grade, location, histological type, and T stage ($P<0.05$). All these variables were analyzed by univariate logistic regression analysis, and the correlated ones ($P<0.05$) are estimated through multivariate logistic regression analysis. As a result, significantly independent predictors were identified to construct a well-calibrated nomogram. Odds ratios (ORs) and 95% confidence intervals (CIs) were also calculated. Nomogram performance was quantified with respect to calibration and discrimination. Calibration was assessed graphically by plotting the relationship between actual (observed) and predicted probabilities by the Hosmer goodness-of-fit test (11). Internal validation of performance was estimated by the bootstrapping method (1,000 replications). According to the nomogram, total points for all patients were determined with the "nomogramFormula" package in the R software. Discrimination (ability of a nomogram to separate patients with different lymph node statuses) was quantified by the area under the receiver operating characteristic (ROC) curve (AUC). A larger AUC (range 0.5–1.0) reflected a more accurate prediction.

Finally, the best cut-off value is determined by the Youden's index, according to which, the training and validation cohorts were divided into two subgroups. The correlation between the nomogram and the risk of lymph node metastasis was estimated by univariate logistic regression analysis.

## Statistical Analyses

The chi-square test was performed to evaluate the associations of lymph node status with appropriate variables. Fisher's exact test was carried out if necessary. Statistically significant was defined as two-sided $P<0.05$ was considered, unless otherwise stated. All statistical analyses were performed using STATA (version 14.1) and R (version 3.6.1). The R packages caret, rms, pROC, ggplot2, parallel, and nomogramFormula were applied.

# RESULTS

## Patient Characteristics

There were 28,966 patients enrolled in this study, with 8,710 (30.07%) lymph node positive (**Table 1**). The demographics and clinicopathologic characteristics related to lymph node status included age, race, grade, location, histological type and T stage. Younger patients (age<60) have a higher rate of lymph node involvement (32.43%) compared with older ones (age≥60, 26.98%) ($P < 0.001$). As for race, 33.79% black patients had positive lymph nodes versus 29.00% for white patients and 30.00% for others ($P < 0.001$). The positive rate of lymph nodes was higher in patients with grade III cancer than grade II and grade I (31.33% vs. 25.88% and 12.20%, respectively; $P < 0.001$). Patients with primary tumor located in the axillary tail of the breast were more likely to have positive lymph nodes (46.26%), while cases primarily located in the central portion of the breast ranked second

**TABLE 1 |** Patients' demographics and clinicopathologic characteristics by lymph node status.

| | Whole cohort | | | | Training cohort | | | | Validation cohort | | | |
|---|---|---|---|---|---|---|---|---|---|---|---|---|
| | **LN- (%)** | **LN+ (%)** | **Total** | **P** | **LN- (%)** | **LN+ (%)** | **Total** | **P** | **LN- (%)** | **LN+ (%)** | **Total** | **P** |
| **All** | 20,256 (69.93) | 8,710 (30.07) | 28,966 | | 10,142 (70.03) | 4,341 (29.97) | 14,483 | | 10,114 (69.83) | 4369 (30.17) | 14,483 | |
| **Age** | | | | **<0.001** | | | | **<0.001** | | | | **<0.001** |
| <60 | 11,094 (67.57) | 5,325 (32.43) | 16,419 | | 5,493 (67.37) | 2,661 (32.63) | 8,154 | | 5,601 (67.77) | 2,664 (32.23) | 8,265 | |
| ≥60 | 9,162 (73.02) | 3,385 (26.98) | 12,547 | | 4,649 (73.46) | 1,680 (26.54) | 6,329 | | 4,513 (72.58) | 1,705 (27.42) | 6218 | |
| **Race** | | | | **<0.001** | | | | **<0.001** | | | | **<0.001** |
| White | 14,666 (71.00) | 5,990 (29.00) | 20,656 | | 7,341 (71.20) | 2,970 (28.8) | 10,311 | | 7,325 (70.81) | 3,020 (29.19) | 10,345 | |
| Black | 3,968 (66.21) | 2,025 (33.79) | 5,993 | | 1,987 (65.59) | 1,038 (34.31) | 3,025 | | 1,981 (66.75) | 987 (30.94) | 2,968 | |
| Others[#] | 1,622 (70.00) | 695 (30.00) | 2,317 | | 814 (70.97) | 333 (29.03) | 1,147 | | 808 (69.05) | 362 (30.94) | 1,170 | |
| **Gender** | | | | 0.351 | | | | 1.000 | | | | 0.181 |
| Female | 20,240 (69.94) | 8,700 (30.06) | 28,940 | | 10,131 (70.03) | 4,336 (29.97) | 14,467 | | 10,109 (69.85) | 4,364 (30.15) | 14,473 | |
| Male | 16 (61.54) | 10 (39.46) | 26 | | 11 (68.75) | 5 (31.25) | 16 | | 5 (50.00) | 5 (50.00) | 10 | |
| **Grade** | | | | **<0.001** | | | | **<0.001** | | | | **<0.001** |
| I | 475 (87.80) | 66 (12.20) | 541 | | 249 (89.89) | 28 (10.11) | 277 | | 226 (85.61) | 38 (14.39) | 264 | |
| II | 3,546 (74.12) | 1,238 (25.88) | 4,784 | | 1,796 (73.94) | 633 (26.06) | 2,429 | | 1,750 (74.31) | 605 (25.69) | 2,355 | |
| III | 16,235 (68.67) | 7,406 (31.33) | 23,641 | | 8,097 (68.75) | 3,680 (31.25) | 11,777 | | 8,138 (68.59) | 3,726 (31.41) | 11,864 | |
| **Laterality** | | | | 0.369 | | | | 0.194 | | | | 0.98 |
| Left | 10,316 (69.69) | 4,486 (30.31) | 14,802 | | 5,163 (69.54) | 2,261 (30.46) | 7,424 | | 5,153 (69.84) | 2,225 (30.16) | 7,378 | |
| Right | 9,940 (70.18) | 4,224 (30.07) | 14,164 | | 4,979 (70.53) | 2,080 (29.47) | 7,059 | | 4,961 (69.82) | 2,144 (30.18) | 7,105 | |
| **Location*** | | | | **<0.001** | | | | **<0.001** | | | | **<0.001** |
| Central | 624 (60.94) | 400 (39.06) | 1,024 | | 336 (63.16) | 196 (36.84) | 532 | | 288 (58.54) | 204 (41.46) | 492 | |
| Inner | 4,943 (79.82) | 1,250 (20.18) | 6,193 | | 2,458 (79.86) | 620 (20.14) | 3,078 | | 2,485 (79.78) | 630 (20.22) | 3,115 | |
| Outer | 9,738 (66.46) | 4,915 (33.54) | 14,653 | | 4,874 (66.52) | 2,453 (33.48) | 7,327 | | 4,864 (66.39) | 2,462 (33.61) | 7,326 | |
| Overlap | 4,836 (70.27) | 2,046 (29.73) | 6,882 | | 2,414 (70.22) | 1,024 (29.78) | 3,438 | | 2,422 (70.33) | 1,022 (29.67) | 3,444 | |
| Tail | 115 (53.74) | 99 (46.26) | 214 | | 60 (55.56) | 48 (44.44) | 108 | | 55 (51.89) | 51 (48.11) | 106 | |
| **Histological type** | | | | **<0.001** | | | | **<0.001** | | | | **<0.001** |
| IDC | 17,512 (69.57) | 7,661 (30.43) | 25,173 | | 8,710 (69.50) | 3,823 (30.50) | 12,533 | | 8,802 (69.64) | 3,838 (30.36) | 12,640 | |
| ILC | 141 (55.95) | 111 (44.05) | 252 | | 82 (62.12) | 50 (37.88) | 132 | | 59 (49.17) | 61 (50.83) | 120 | |
| IDC/ILC | 184 (56.62) | 141 (43.38) | 325 | | 97 (58.08) | 70 (41.92) | 167 | | 87 (55.06) | 71 (44.94) | 158 | |
| Others | 2,419 (75.22) | 797 (24.78) | 3,216 | | 1,253 (75.89) | 398 (24.11) | 1,651 | | 1,166 (74.50) | 399 (25.50) | 1,565 | |
| **T stage** | | | | **<0.001** | | | | **<0.001** | | | | **<0.001** |
| T1 | 10,553 (81.77) | 2,353 (18.23) | 12,906 | | 5,261 (81.91) | 1,162 (18.09) | 6,423 | | 5,292 (81.63) | 1,191 (18.37) | 6,483 | |
| T2 | 8,330 (65.03) | 4,479 (34.97) | 12,809 | | 4,145 (64.44) | 2,287 (35.56) | 6,432 | | 4,185 (65.63) | 2,192 (34.37) | 6,377 | |
| T3 | 1,066 (46.82) | 1,211 (53.18) | 2,277 | | 573 (49.87) | 576 (50.13) | 1,149 | | 493 (43.71) | 635 (56.29) | 1,128 | |
| T4 | 307 (31.52) | 667 (68.48) | 974 | | 163 (34.03) | 316 (65.97) | 479 | | 144 (29.09) | 351 (70.91) | 495 | |

[#]*American Indian/AK Native, Asian/Pacific Islander.*

**Central, code C50.0 and C50.1; Inner, code C50.2 and C50.3; Outer, code C50.4 and C50.5; Tail, code C50.6; Overlap, code C50.8. From SEER Coding Guidelines Breast 2018 manual, coding guideline breast C500-C509.*

*IDC, invasive ductal carcinoma; IDC/ILC, Infiltrating duct and lobular carcinoma; ILC, invasive lobular carcinoma; LN, lymph nodes.*

*Bold value indicates statistical significance.*

(39.06%) ($P < 0.001$). Patients with invasive lobular carcinoma (ILC) (44.05%) had higher positive rate of lymph nodes than invasive ductal carcinoma (IDC), IDC/ILC, and other histological types (30.43%, 43.38% and 24.78%, respectively) ($P < 0.001$). It was found that lymph nodes are positive correlated with T stage. Stage T4 cases had the highest rate of positive lymph nodes (68.48%), versus T1, T2, and T3 patients (18.23%, 34.97% and 53.18%, respectively) ($P < 0.001$) (**Table 1**).

## Independent Predictors in Training Set

According to univariate Cox analysis, age, race, location, grade, histologic type, and T stage were significantly associated with the positive rate of lymph nodes (**Table S1**). These factors were included in multivariate logistic regression analysis (**Table 2**). The result confirmed that grade was not an independent predictor (P=0.421) and the others were statistically significant and independent predictors for lymph node status (P<0.05).

## Construction and Validation of the Nomogram

We established a nomogram based on significant and independent predictors determined by multivariate analysis (**Figure 1**), including age, race, location, histological type, and T stage. By adding up the scores of all the variables, the probability of a specific patient to have positive lymph nodes could be predicted. As we can see, younger black patients with T4 and IDC/ILC tumor at the axillary tail had highest scores, while elderly white cases with non-ILC or non-IDC, and T1 tumors had a lower risk of lymph node metastasis. The novel nomogram predicted the risk of positive lymph nodes between 0.05 and 0.8.

In order to test the performance of the new nomogram, 1,000 bootstrap resampling was carried out for internal verification through the calibration chart in the training set (**Figure 2**). The calibration curve indicated a good calibration effect of the nomogram. The effectiveness of the nomogram for predicting lymph node status was further evaluated using ROC curves for the training (**Figure 3A**) and validation (**Figure 3B**) sets. In the training set, AUC was 0.684 (95%CI: 0.675–0.693), which is similar to the AUC observed in the validation set (0.689, 95%CI: 0.679–0.698). These results indicated that the nomogram is a useful predictor for lymph node status in TNBC.

**TABLE 2** | Multivariate logistic regression analysis of possible factors independently predicting positive lymph nodes in the training cohort.

| | Training cohort | | |
|---|---|---|---|
| | **OR** | **95%CI** | **P** |
| **Age** | | | **<0.001** |
| <60 | Ref. | Ref. | |
| ≥60 | 0.85 | 0.79–0.92 | |
| **Race** | | | **0.010** |
| White | Ref. | Ref. | |
| Black | 1.22 | 1.11–1.33 | |
| Others[#] | 0.98 | 0.85–1.13 | |
| **Grade** | | | 0.421 |
| I | 0.38 | 0.25–0.57 | |
| II | 0.93 | 0.84–1.04 | |
| III | Ref. | Ref. | |
| **Location*** | | | **<0.001** |
| Central | 1.07 | 0.88–1.30 | |
| Inner | 0.51 | 0.46–0.56 | |
| Outer | Ref. | Ref. | |
| Overlap | 0.82 | 0.75–0.90 | |
| Tail | 1.60 | 1.07–2.38 | |
| **Histological type** | | | **<0.001** |
| IDC | Ref. | Ref. | |
| ILC | 1.66 | 1.20–2.31 | |
| IDC/ILC | 1.45 | 0.99–2.12 | |
| Others | 0.66 | 0.58–0.75 | |
| **T stage** | | | **<0.001** |
| T1 | Ref. | Ref. | |
| T2 | 2.40 | 2.21–2.61 | |
| T3 | 4.28 | 3.74–4.90 | |
| T4 | 8.60 | 7.02–10.53 | |

[#]*American Indian/AK Native, Asian/Pacific Islander.*

**Central, code C50.0 and C50.1; Inner, code C50.2 and C50.3; Outer, code C50.4 and C50.5; Tail, code C50.6; Overlap, code C50.8. From SEER Coding Guidelines Breast 2018 manual, coding guideline breast C500-C509.*

*CI, confidence interval; IDC, invasive ductal carcinoma; IDC/ILC, Infiltrating duct and lobular carcinoma; ILC, invasive lobular carcinoma; LN, lymph nodes; OR, odds ratio; Ref., Reference.*

*Bold value indicates statistical significance.*

## Risk Stratification by the Nomogram

The cut-off value of total scores for predicting lymph node status was determined by Youden's index in the training set. Both the training and validation sets were subdivided into the low score groups (total points ≤ 82) and high score groups (total points>82), respectively. After applying the cut-off value to the training set, univariate analysis found a significant difference in the probability of lymph node metastasis between the high and low score groups (OR=3.24, 95%CI:3.03–3.49; P<0.001), consistent with the results obtained in the validation set (OR=3.30, 95%CI 3.07–3.56; P<0.001; **Table 3**).

# DISCUSSION

In this study, the risk factors associated with lymph node metastasis in triple-negative breast cancer were determined, and a predictive model was developed by logistic regression, with a nomogram attached. We found that age, race, T stage, primary site, grade, and histological subtype were related to lymph node status by univariate logistic regression analysis. These variables were independent predictors of lymph node status confirmed by multivariate logistic regression except for grade. These factors were shown to be predictors of axillary lymph node metastasis. As shown above, the risk of lymph node metastasis was positively correlated with T stage. The increase in T stage was significantly associated with the risk of lymph node metastasis, which was previously reported (12). Young patients had higher odds of developing lymph node metastasis compared with older ones. Patients with the axillary tail as the primary site were more likely to have metastatic lymph nodes. These results indicate that the primary site of the tumor is important in predicting lymph node metastasis. It was also confirmed that the pathological type of ILC is more prone to lymph nodes metastasis. To validate the

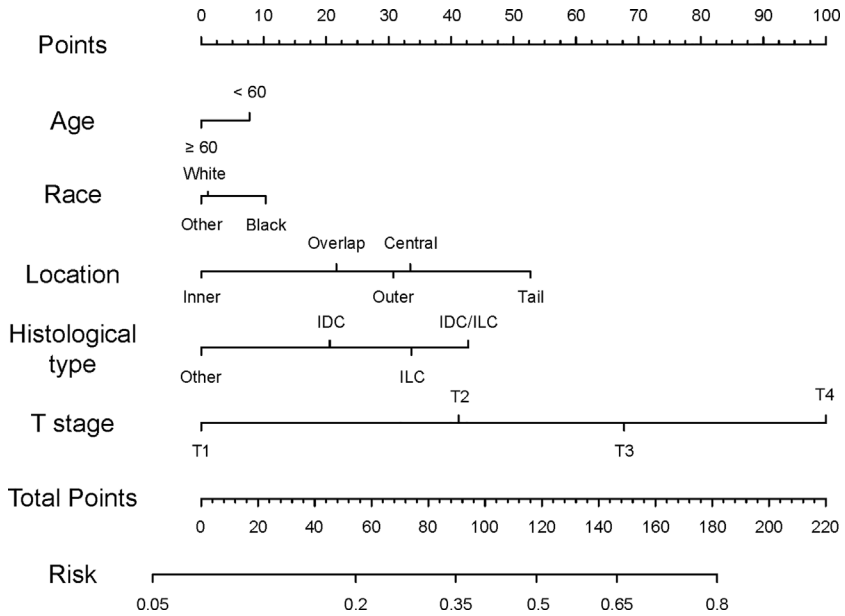


**FIGURE 1** | Nomogram predicting lymph node status of TNBC patients. Instructions for the nomogram: First, quantify each characteristic of the patient by drawing a vertical line from corresponding scale to the points scale. Then, sum all the points and draw a vertical line from the total points scale to the risk scale to obtain the probability of lymph node metastasis.

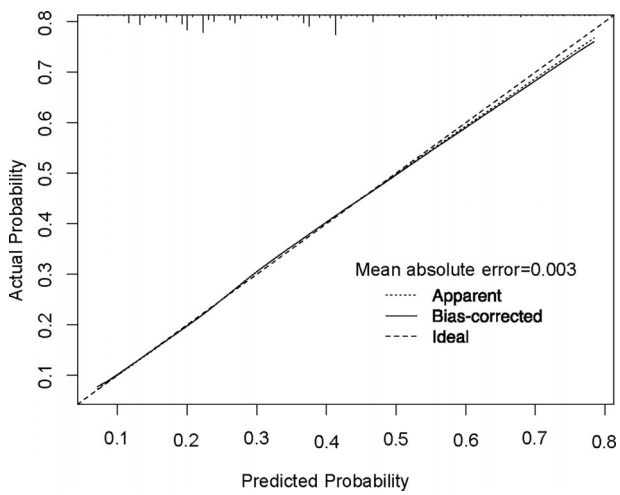


**FIGURE 2** | Calibration plot of the nomogram for predicting lymph node status. The performance is estimated by bootstrap 1,000 repetitions. The X-axis plots the nomogram-predicted survival; the Y-axis plots the actual survival.

developed model, the bootstrapping method (1,000 times) was used. Moreover, the relatively high AUC of 0.684, also referred as concordance index in our study, confirmed the validation of this nomogram. Thus, this nomogram can be utilized by surgeons to more effectively counsel individual patients, thereby helping to personalize the surgical treatment of TNBC.

Previous studies have constructed nomograms to predict both sentinel and non-sentinel lymph node metastases in breast cancer, performing well in cohorts at different institutions (13–15). Several well-designed nomograms have been accepted worldwide, with some adopted by clinicians (16–20). For example, Hwang et al. incorporated sentinel lymph node metastasis size into a nomogram that accurately predicts the likelihood of having additional axillary metastasis (16). Nevertheless, these models only show limited performance in triple-negative breast cancer. For predicting non-sentinel lymph node metastasis in TNBC, some of these widely used nomograms are not much better than coin tossing, with AUCs around 0.55. It is noteworthy that such nomograms still work well in ER positive patients in the same institute (21). This phenomenon can be partly attributed to that rather than being a single subtype, triple-negative breast cancer is a general concept covering a group of diseases, with a variety in biological behavior, as well as great differences compared with other subtypes (22). To settle this, the cohort used to build a model should be large enough to cover each "subtype" of TNBC with an adequate number. SEER, a nationwide program covering nearly a quarter of the US population, is an optimal cohort for building such a model.

Apart from the excellent cohort as the data source for the nomogram, this model has other advantages. First, our research used the clinical information of TNBC patients to predict lymph node metastasis. Meanwhile, existing researches (10, 13) assessed TNBC at the genetic level, using IRGS to predict lymph node metastasis, and the obtained results were also good.

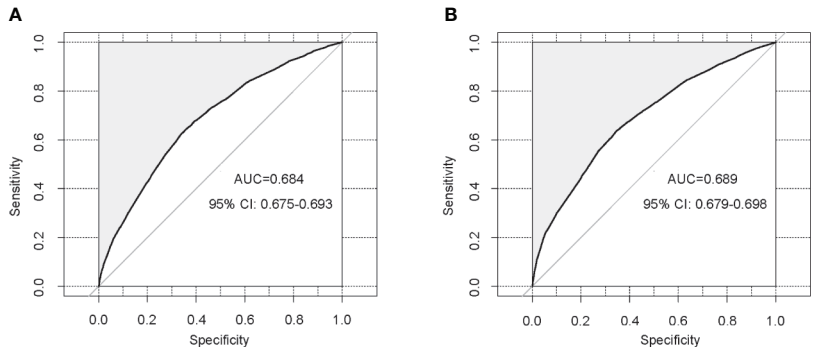


**FIGURE 3** | Validation of the nomogram using receiver operating characteristic curves. **(A)** Internal validation in the training cohort; **(B)** External validation in the validation cohort. AUC: area under curve; CI: confidence intervals.

**TABLE 3** | Univariate logistic regression analysis of total points in predicting positive lymph nodes in the training and validation cohorts.

| Group[#] | Training cohort | | P | Validation cohort | | P |
|---|---|---|---|---|---|---|
| | OR | 95%CI | | OR | 95%CI | |
| Low score | Ref. | Ref. | – | Ref. | Ref. | – |
| High score | 3.24 | 3.03-3.49 | **<0.001** | 3.30 | 3.07–3.56 | **<0.001** |

[#]*Low score, ≤82; high score,>82.*
*CI, confidence interval; OR, odds ratio; Ref., Reference.*
*Bold value indicates statistical significance.*

However, clinical information is more intuitive to make decisions easily in clinic. Secondly, compared with the long and complicated formulas of Cox and logistic predictive models, nomograms, composed of several simple scaled parallel lines, provide a reliable prognostic information that is unique to a given patient.

Limited by the data and the characteristics of analysis, this study had some limitations. We were unable to obtain more information from the SEER database, including invasion of lymphatic or blood vessels, multifocality and even molecular biomarkers, which, if included, could improve the sensitivity and specificity of the present nomogram. In addition, as a retrospective study, selection or information bias was hardly avoidable. The main cohort in this study was the American population, and it is worth considering whether the results are applicable to other populations.

## CONCLUSION

In summary, a predictive nomogram for lymph node metastasis detection in TNBC patients was developed. Evaluating lymph node metastasis remains a major concern in the treatment and staging of breast cancer. The present findings reveal the features of lymph node metastasis in TNBC, providing a reference for future treatment which would take neoadjuvant chemotherapy and sentinel lymph node biopsy into consideration, eventually optimizing clinical diagnosis and treatment.

## DATA AVAILABILITY STATEMENT

Publicly available datasets were analyzed in this study. This data can be found here: Surveillance, Epidemiology, and End Results (SEER) database (https://seer.cancer.gov/).

## AUTHOR CONTRIBUTIONS

XC: conception of the work, data collection, data analysis and interpretation, drafting the article, critical revision of the article, and final approval of the version to be published. HZ and JH: conception of the work, critical revision of the article, and final approval of the version to be published. All authors contributed to the article and approved the submitted version.

## FUNDING

This work was supported by grants from the Training Plan of Excellent Talents of The First People's Hospital of Shangqiu (SQFPH2019). The funder had no role in the study design, data collection and analysis, decision to publish, or preparation of the manuscript.

## SUPPLEMENTARY MATERIAL

The Supplementary Material for this article can be found online at: https://www.frontiersin.org/articles/10.3389/fonc.2020.608334/full#supplementary-material

**SUPPLEMENTARY TABLE 1** | Univariate logistic regression analysis of different variables in predicting positive lymph nodes in the training cohort. [#] American Indian/AK Native, Asian/Pacific Islander. * Central, code C50.0 and C50.1; Inner, code C50.2 and C50.3; Outer, code C50.4 and C50.5; Tail, code C50.6; Overlap, code C50.8. From SEER Coding Guidelines Breast 2018 manual, coding guideline breast C500-C509. CI, confidence interval; IDC, invasive ductal carcinoma; IDC/ILC, Infiltrating duct and lobular carcinoma; ILC, invasive lobular carcinoma; LN, lymph nodes; OR, odds ratio; Ref., Reference.

## REFERENCES


1. Siegel R, Miller K, Jemal A. Cancer statistics, 2018. *CA: Cancer J Clin* (2018) 68:7–30. doi: 10.3322/caac.21442
2. DeSantis C, Ma J, Gaudet M, Newman L, Miller K, Goding Sauer A, et al. Breast cancer statistics, 2019. *CA: Cancer J Clin* (2019) 69:438–51. doi: 10.3322/caac.21583
3. Pan K, Zhang L, Gerhard M, Ma J, Liu W, Ulm K, et al. A large randomised controlled intervention trial to prevent gastric cancer by eradication of Helicobacter pylori in Linqu County, China: baseline results and factors affecting the eradication. *Gut* (2016) 65:9–18. doi: 10.1136/gutjnl-2015-309197
4. Barry P, Vatsiou A, Spiteri I, Nichol D, Cresswell G, Acar A, et al. The Spatiotemporal Evolution of Lymph Node Spread in Early Breast Cancer. *Clin Cancer Res an Off J Am Assoc Cancer Res* (2018) 24:4763–70. doi: 10.1158/1078-0432.Ccr-17-3374
5. Taylor K, O'Keeffe S, Britton P, Wallis M, Treece G, Housden J, et al. Ultrasound elastography as an adjuvant to conventional ultrasound in the preoperative assessment of axillary lymph nodes in suspected breast cancer: a pilot study. *Clin Radiol* (2011) 66:1064–71. doi: 10.1016/j.crad.2011.05.015
6. Nathanson S, Krag D, Kuerer H, Newman L, Brown M, Kerjaschki D, et al. Breast cancer metastasis through the lympho-vascular system. *Clin Exp Metastasis* (2018) 35:443–54. doi: 10.1007/s10585-018-9902-1
7. Morrow M, Jagsi R, McLeod M, Shumway D, Katz S. Surgeon Attitudes Toward the Omission of Axillary Dissection in Early Breast Cancer. *JAMA Oncol* (2018) 4:1511–6. doi: 10.1001/jamaoncol.2018.1908
8. Hindié E, Groheux D, Brenot-Rossi I, Rubello D, Moretti J, Espié M. The sentinel node procedure in breast cancer: nuclear medicine as the starting point. *J Nuclear Med Off Publication Soc Nuclear Med* (2011) 52:405–14. doi: 10.2967/jnumed.110.081711
9. Koca B, Kuru B, Ozen N, Yoruker S, Bek Y. A breast cancer nomogram for prediction of non-sentinel node metastasis - validation of fourteen existing models. *Asian Pacific J Cancer Prev APJCP* (2014) 15:1481–8. doi: 10.7314/apjcp.2014.15.3.1481
10. Tan W, Xie X, Huang Z, Chen L, Tang W, Zhu R, et al. Construction of an immune-related genes nomogram for the preoperative prediction of axillary lymph node metastasis in triple-negative breast cancer. *Artif Cells Nanomed Biotechnol* (2020) 48:288–97. doi: 10.1080/21691401.2019.1703731
11. Hosmer DW, Hosmer T, Le Cessie S. Lemeshow S. A comparison of goodness-of-fit tests for the logistic regression model. *Stat med* (1997) 16:965–80. doi: 10.1002/(sici)1097-0258(19970515)16:9<965::aid-sim509>3.0.co;2-o
12. Rivadeneira DE, Simmons RM, Christos PJ, Hanna K, Daly JM, Osborne MP. Predictive factors associated with axillary lymph node metastases in T1a and T1b breast carcinomas: analysis in more than 900 patients. *J Am Coll Surgeons* (2000) 191:1–6. doi: 10.1016/s1072-7515(00)00310-0 discussion -8.
13. Wang N, Yang Z, Wang X, Chen L, Zhao H, Cao W, et al. A mathematical prediction model incorporating molecular subtype for risk of non-sentinel lymph node metastasis in sentinel lymph node-positive breast cancer patients: a retrospective analysis and nomogram development. *Breast Cancer (Tokyo Japan)* (2018) 25:629–38. doi: 10.1007/s12282-018-0863-7
14. Tapia G, Ying V, Di Re A, Stellin A, Cai T, Warrier S. Predicting non-sentinel lymph node metastasis in Australian breast cancer patients: are the nomograms still useful in the post-Z0011 era? *ANZ J Surg* (2019) 89:712–7. doi: 10.1111/ans.15173
15. Han L, Zhu Y, Liu Z, Yu T, He C, Jiang W, et al. Radiomic nomogram for prediction of axillary lymph node metastasis in breast cancer. *Eur Radiol* (2019) 29:3820–9. doi: 10.1007/s00330-018-5981-2
16. Mittendorf EA, Hunt KK, Boughey JC, Bassett R, Degnim AC, Harrell R, et al. Incorporation of sentinel lymph node metastasis size into a nomogram predicting nonsentinel lymph node involvement in breast cancer patients with a positive sentinel lymph node. *Ann Surg* (2012) 255:109–15. doi: 10.1097/SLA.0b013e318238f461
17. Vaysse C, Sroussi J, Mallon P, Feron JG, Rivain AL, Ngo C, et al. Prediction of axillary lymph node status in male breast carcinoma. *Ann Oncol Off J Eur Soc Med Oncol* (2013) 24:370–6. doi: 10.1093/annonc/mds283
18. Park J, Fey JV, Naik AM, Borgen PI, Van Zee KJ, Cody HS. 3rd. A declining rate of completion axillary dissection in sentinel lymph node-positive breast cancer patients is associated with the use of a multivariate nomogram. *Ann Surg* (2007) 245:462–8. doi: 10.1097/01.sla.0000250439.86020.85
19. Werkoff G, Lambaudie E, Fondrinier E, Levêque J, Marchal F, Uzan M, et al. Prospective multicenter comparison of models to predict four or more involved axillary lymph nodes in patients with breast cancer with one to three metastatic sentinel lymph nodes. *J Clin Oncol Off J Am Soc Clin Oncol* (2009) 27:5707–12. doi: 10.1200/jco.2009.21.9139
20. Katz A, Smith BL, Golshan M, Niemierko A, Kobayashi W, Raad RA, et al. Nomogram for the prediction of having four or more involved nodes for sentinel lymph node-positive breast cancer. *J Clin Oncol Off J Am Soc Clin Oncol* (2008) 26:2093–8. doi: 10.1200/jco.2007.11.9479
21. Ozbas S, Ozmen V, Igci A, Muslumanoglu M, Ozcinar B, Balkan M, et al. Predicting the likelihood of nonsentinel lymph node metastases in triple negative breast cancer patients with a positive sentinel lymph node: Turkish Federation of Breast Disease Associations protocol MF09-01. *Clin Breast Cancer* (2012) 12:63–7. doi: 10.1016/j.clbc.2011.07.004
22. Bryan B, Schnitt S, Collins L. Ductal carcinoma in situ with basal-like phenotype: a possible precursor to invasive basal-like breast cancer. *Modern Pathol an Off J U States Can Acad Pathol Inc* (2006) 19:617–21. doi: 10.1038/modpathol.3800570


**Conflict of Interest:** The authors declare that the research was conducted in the absence of any commercial or financial relationships that could be construed as a potential conflict of interest.

frontiers in Oncology

ORIGINAL RESEARCH
published: 19 January 2021
doi: 10.3389/fonc.2020.587422

# Sonographic Features of Triple-Negative Breast Carcinomas Are Correlated With mRNA–lncRNA Signatures and Risk of Tumor Recurrence

*Jia-wei Li*[1,2†], *Jin Zhou*[1,2†], *Zhao-ting Shi*[1,2], *Na Li*[1,2], *Shi-chong Zhou*[1,2] *and Cai Chang*[1,2*]

[1] Department of Medical Ultrasound, Fudan University Shanghai Cancer Center, Shanghai, China, [2] Department of Oncology, Shanghai Medical College, Fudan University, Shanghai, China

OPEN ACCESS

**Edited by:**
*Zhijie Jason Liu,*
*The University of Texas Health Science Center at San Antonio, United States*

**Reviewed by:**
*Hui-Xiong Xu,*
*Tongji University, China*
*Li Cuiying,*
*Nanjing Medical University, China*

***Correspondence:**
*Cai Chang*
*changc61@163.com*

[†]*These authors have contributed equally to this work*

**Specialty section:**
*This article was submitted to Women's Cancer, a section of the journal Frontiers in Oncology*

**Received:** *26 July 2020*
**Accepted:** *30 November 2020*
**Published:** *19 January 2021*

**Citation:**
*Li J-w, Zhou J, Shi Z-t, Li N, Zhou S-c and Chang C (2021) Sonographic Features of Triple-Negative Breast Carcinomas Are Correlated With mRNA–lncRNA Signatures and Risk of Tumor Recurrence. Front. Oncol. 10:587422. doi: 10.3389/fonc.2020.587422*

**Background:** To determine a correlation between mRNA and lncRNA signatures, sonographic features, and risk of recurrence in triple-negative breast cancers (TNBC).

**Methods:** We retrospectively reviewed the data from 114 TNBC patients having undergone transcriptome analysis. The risk of tumor recurrence was determined based on the correlation between transcriptome profiles and recurrence-free survival. Ultrasound (US) features were described according to the Breast Imaging Reporting and Data System. Multivariate logistic regression analysis determined the correlation between US features and risk of recurrence. The predictive value of sonographic features in determining tumor recurrence was analyzed using receiver operating characteristic curves.

**Results:** Three mRNAs (CHRDL1, FCGR1A, and RSAD2) and two lncRNAs (HIF1A-AS2 and AK124454) were correlated with recurrence-free survival in patients with TNBC. Among the three mRNAs, two were upregulated (FCGR1A and RSAD2) and one was downregulated (CHRDL1) in TNBCs. LncRNAs HIF1A-AS2 and AK124454 were upregulated in TNBCs. Based on these signatures, an integrated mRNA–lncRNA model was established using Cox regression analysis to determine the risk of tumor recurrence. Benign-like sonographic features, such as regular shape, circumscribed margin, posterior acoustic enhancement, and no calcifications, were associated with HIF1A-AS2 expression and high risk of tumor recurrence ($P<0.05$). Malignant-like features, such as irregular shape, uncircumscribed margin, no posterior acoustic enhancement, and calcifications, were correlated with CHRDL1 expression and low risk of tumor recurrence ($P<0.05$).

**Conclusions:** Sonographic features and mRNA–lncRNA signatures in TNBCs represent the risk of tumor recurrence. Taken together, US may be a promising technique in determining the prognosis of patients with TNBC.

**Keywords: long non-coding RNA, messenger RNA, triple-negative breast cancer, tumor recurrence, ultrasound**

## HIGHLIGHTS

1. Sonographic features of TNBCs correlated with the expression of mRNAs and lncRNAs.
2. Benign-like sonographic features correlated with the expression of lncRNA HIF1A-AS2; malignant-like sonographic features correlated with CHRDL1 mRNA levels.
3. Sonographic features of TNBCs correlated with the risk of tumor recurrence predicted using the mRNA and lncRNA signatures.
4. TNBCs with benign-like sonographic features exhibited higher rate of recurrence than those with malignant sonographic features.

## BACKGROUND

Triple-negative breast cancer (TNBC) is the most aggressive breast cancer subtype. Patients with TNBC lack the expression of estrogen receptor (ER), progesterone receptor (PR), and human epidermal growth factor receptor 2 (HER2). The aggressive nature of the cancer and limited availability of effective targeted therapy against molecular biomarkers result in poor prognosis of patients with TNBC (1).

Numerous studies have analyzed the genome and transcriptome signatures to identify the therapeutic target for TNBCs (2–6). TNBC heterogeneity has gained considerable attention in understanding therapeutic strategies and clinical outcomes (2–4, 7). Using the largest TNBC database at Fudan University Shanghai Cancer Center, a recent study confirmed the importance of personalized therapy based on the gene expression profile in patients with TNBC (3). They found that PIK3CA mutations and LAR subtype are more common in Chinese TNBC patients. Substantial evidence was established for the biological heterogeneity of TNBCs based on the genomic and transcriptomic profiles (3).

In accordance with TNBC heterogeneity, we have previously demonstrated that these tumors present with a wide variety of sonographic features (8) that correlate with cancer grade and score based on immunohistochemical (IHC) biomarkers, such as Ki-67 and HER2. However, these protein biomarkers have limited significance in the sonographic variations. In this study, we analyzed the sonographic variations based on messenger RNA (mRNA) and long non-coding RNA (lncRNA) signatures. Moreover, we have determined a correlation between sonographic features and risk of tumor recurrence.

## METHODS

### Patients

Based on a prospective study between 1st January 2010 and 31st December 2013, 165 consecutive breast cancer patients having undergone transcriptome analysis were retrospectively reviewed for their clinical data and ultrasound (US) images. All patients were primarily treated by surgery after excluding surgical contraindications based on standard preoperative examination. None of the patients expressed ER, PR, and HER2 (characteristic of TNBC).

### Transcriptome Microarray, Identifying Candidate RNAs, and Integrated mRNA–lncRNA Model

A study in 2016 described the correlation between mRNAs and lncRNAs with recurrence-free survival (RFS) and established an integrated mRNA–lncRNA model to predict the risk of recurrence (2).

Differentially expressed RNAs were first identified from 33 paired TNBC tissues and adjacent normal breast tissues using HTA 2.0 microarray analysis. The inclusion criteria for these mRNAs included: fold change >2 or <0.33 and false discovery rate (FDR) <0.001. For lncRNAs, the inclusion criteria were: fold change >1.5 and FDR <0.001. Based on this, there were 183 and 195 differentially expressed mRNAs and lncRNAs, respectively, between TNBC and normal breast tissues. Combining the RNA expression data from a microarray with the clinical follow-up data from 165 TNBC patients, 16 mRNAs ($P<0.1$) and 11 lncRNAs ($P<0.2$) correlated with RFS using the log-rank test. Duplicated mRNAs were excluded and only intergenic lncRNAs were included and 13 mRNAs and 6 lncRNAs were identified using real-time quantitative polymerase chain reaction from 33 paired TNBC and normal tissues. Nineteen RNAs were consistently amplified in 137 training samples undergoing real-time quantitative polymerase chain reaction using the correlation with survival analysis as the filtration standard. The expression of RNA candidates that did not correlate with RFS were excluded. After this round of filtration, the remaining seven mRNAs and four lncRNAs were tested for their prognostic signature until the area under curve (AUC) in the time-dependent receiver operating characteristic model arrived at the best performance. Finally, there were three mRNAs (CHRDL1, FCGR1A, and RSAD2) and two lncRNAs (HIF1A-AS2 and AK124454) in the model (derived and rephrased from the **Supplementary File** of Jiang et al., 2016) (2). Of the three mRNAs, two were upregulated (FCGR1A and RSAD2) and one was downregulated (CHRDL1) during the progression of TNBC. LncRNAs HIF1A-AS2 and AK124454 were upregulated during TNBC progression.

The signature model for predicting the risk of recurrence was established with Cox proportional hazards regression modeling as: $-1.225\times$CHRDL1$+0.74\times$FCGR1A$+0.219\times$RSAD2$+0.482\times$HIF1A-AS2$+0.571\times$AK124454. The cut-off score was set to 0.793 to classify patients into high-risk and low-risk groups (2).

### Pathological and Immunohistochemical Data

After measuring the gross tumor size, postoperative breast cancer samples were subjected to hematoxylin-eosin staining and IHC analysis. Pathological type, histological grade (I, II, and III), and lymph node status were determined based on the stained samples. Based on IHC analysis and *in situ* hybridization, the expression of ER, PR, and HER2 was confirmed by two pathologists with more than 10 years of working experiences. ER and PR negative

expression was defined as less than 1% staining in nuclei. HER2 negative expression was defined by score 0 or 1 by IHC staining and <4 gene copies/nucleus and ratio of <1.8 using fluorescence *in situ* hybridization (9). Thus, TNBCs are defined as ER, PR, and HER2 negative (10). Ki-67 expression was also acquired from the IHC samples.

## Sonographic Feature Assessment

US images were retrospectively collected from the data archives. Fifty-one patients without US images were excluded. Images from 114 patients were blind reviewed by two US physicians with more than five years' experience on breast US. TNBC masses were assessed for sonographic features based on orientation (parallel/non-parallel), shape (regular/irregular), margin (circumscribed/uncircumscribed), angular or spiculated margin (yes/no), echo pattern (hypoechoic, mixed solid echo, complex cystic and solid echo), posterior acoustic pattern (shadow, enhancement, no change, or mixed pattern), and calcification (yes/no). These sonographic features were based on the Breast Imaging Reporting and Data System published in 2013 (8, 11, 12). A final assessment report was established after incorporating the reviews by two US physicians.

According to our previous study (8), typical malignant sonographic features for TNBCs included irregular shape, angular or spiculated margin, posterior acoustic shadow, and presence of calcification. TNBCs were divided into three groups based on the number of sonographic features in the US images of the malignancies: Group 1, no malignant sonographic features; Group 2, one or two malignant sonographic features; and Group 3, three or four malignant sonographic features (13).

All data included in our study were ethically approved by the institutional review board at Fudan University Shanghai Cancer Center. The approval number for the data from the breast cancer microarray and clusters was 050432-4-1212B; all the patients provided written informed consent. The approval number for the review of data from the US images was 1802181-22-NSFC; due to the retrospective design of the study, patient written consent was waived.

## Statistical Analysis

Statistical analysis was performed using SPSS version 22.0 for Windows (SPSS Inc., Chicago, IL, USA) and MedCalc Statistical Software version 19.0.7 (MedCalc Software bvba, Ostend, Belgium). Continuous numerical variables were compared using the independent samples t-test, while categorical data were compared by Pearson's chi-square test using a two-tailed P value <0.05 as statistically significant. Univariate and multivariate logistic regression analyses were used to determine the sonographic features associated with the risk of recurrence. Odds ratio (OR) with 95% confidence interval (CI) was calculated to identify the correlation between sonographic features and risk of recurrence. The prediction model for the risk of recurrence was established based on sonographic features and clinicopathological characteristics of patients. Receiver operating characteristic curves were used to determine the performance of the prediction model. Sensitivity, specificity, and AUC with 95% CI were calculated.

# RESULTS

**Table 1** summarizes the clinicopathological and IHC data from the 114 patients. **Table 2** summarizes the expression profiles of five RNAs categorized by sonographic features. Malignant-like sonographic features, such as irregular shape, uncircumscribed margin, presence of angular/spiculated margin, and absence of posterior acoustic enhancement, were associated with high expression of CHRDL1 (P<0.05, **Figure 1**). Benign-like sonographic features, such as regular shape, no angular/spiculated margin, posterior acoustic enhancement, and no calcification, positively associated with HIF1A-AS2 (P ≤ 0.05, **Figure 2**). **Figure 3** illustrates TNBC masses with malignant-like sonographic appearances with low rates of cellular proliferation. **Figure 4** illustrates TNBC masses with benign-like sonographic appearances with high cellular proliferation.

As shown in **Table 3**, benign-like sonographic features correlated with high risk of recurrence (P<0.05). In contrast, malignant-like sonographic features correlated with low risk of tumor recurrence (P<0.05). **Table 4** shows that the fewer number of malignant sonographic features, the higher is the risk of recurrence. The tumor margin in the TNBC mass tended to be associated with the risk of recurrence (P=0.058). However, multivariate logistic regression analysis showed that there was no correlation between sonographic features and risk of tumor recurrence (P>0.05, **Table 5**). Regular shape, posterior acoustic enhancement, and the absence of calcification were "not" significantly associated with high risk of tumor recurrence (P=0.091, OR=2.04 for regular shape; P=0.166, OR=1.79 for posterior acoustic enhancement; and P=0.097, OR=2.21 for absence of calcification). To predict the risk of recurrence, the model based on sonographic features of regular shape, posterior acoustic enhancement, and absence of calcification were comparable (AUC=0.674, 95% CI 0.573–0.774) in the model based on the clinicopathological characteristics, such as tumor size, histological grade, Ki-67 expression, and axillary lymph node metastasis (LNM, AUC=0.678, 95% CI 0.580–0.775). The US-based and

**TABLE 1** | Clinicopathological and IHC characteristics of all TNBC patients.

| | | | |
|---|---|---|---|
| **Age (yrs)** | 53.4 ± 9.7 | **Tumor size (cm)** | 2.44 ± 0.84 |
| **Surgical type** | | **Pathological type** | |
| MRM | 82 (71.9%) | IDC | 104 (91.2%) |
| M+SLNB | 32 (28.1%) | DCIS | 2 (1.8%) |
| **Chemotherapy** | | ILC | 2 (1.8%) |
| Taxane-based | 87 (76.3%) | Others | 6 (5.3%) |
| Non-taxane-based | 18 (15.8%) | **Histological grade** | |
| Unknown | 9 (7.9%) | I and II | 38 (33.3%) |
| **Radiotherapy** | | III | 76 (66.7%) |
| Yes | 31 (27.2%) | **LNM** | |
| No | 73 (64.0%) | Yes | 35 (30.7%) |
| Unknown | 10 (8.8%) | No | 79 (69.3%) |
| **Follow up (month)** | 63 (57–70) | **Ki-67 (%)** | 60 (30–70) |

*Categorical data are presented as number (%). Numerical data are presented as mean ± SD or median (IQR).*

*DCIS, Ductal carcinoma in situ; IDC, Infiltrative ductal carcinoma; ILC, Infiltrative lobular carcinoma; IQR, Interquartile range; LNM, Lymph node metastasis; M, Mastectomy; MRM, Modified radical mastectomy; SLNB, Sentinel lymph node biopsy.*

**TABLE 2 |** Expression level of mRNAs and lncRNAs in associated with sonographic features of TNBC patients.

| | CHRDL1 | FCGR1A | RSAD2 | HIF1A-AS2 | AK124454 |
|---|---|---|---|---|---|
| **Shape** | | | | | |
| Regular | 5.44 ± 1.66 | 4.94±0.77 | 5.84±1.00 | 1.16 ± 0.36 | 3.58±0.97 |
| Irregular | 6.11 ± 1.55 | 4.74±0.75 | 5.65±1.17 | 1.00±0.18 | 3.53±0.84 |
| **P value** | **0.031*** | 0.176 | 0.382 | **0.011*** | 0.778 |
| **Margin** | | | | | |
| Circumscribed | 4.73 ± 1.60 | 5.30 ± 0.76 | 5.77 ± 0.82 | 1.07±0.24 | 3.44±0.75 |
| Uncircumscribed | 5.99 ± 1.58 | 4.76 ± 0.74 | 5.71±1.14 | 1.06±0.28 | 3.56±0.90 |
| **P value** | **0.01*** | **0.019*** | 0.873 | 0.893 | 0.66 |
| **Angular margin** | | | | | |
| Yes | 6.25 ± 1.44 | 4.76±0.77 | 5.63±1.06 | 1.00 ± 0.18 | 3.58±0.90 |
| No | 5.66 ± 1.68 | 4.84±0.76 | 5.77±1.13 | 1.09 ± 0.31 | 3.54±0.88 |
| **P value** | **0.049*** | 0.601 | 0.531 | **0.05*** | 0.786 |
| **Echo pattern** | | | | | |
| Hypoechoic | 5.81 ± 1.54 | 5.01 ± 0.74 | 5.99 ± 1.06 | 1.10±0.33 | 3.55±0.79 |
| Mixed | 6.00 ± 1.64 | 4.60 ± 0.73 | 5.48 ± 1.10 | 1.03±0.21 | 3.56±0.98 |
| Solid and cystic | 3.05 ± 0.12 | 5.70 ± 0.20 | 4.92 ± 0.62 | 1.15±0.32 | 3.43±1.04 |
| **P value** | **0.038*** | **0.003*** | **0.029*** | 0.377 | 0.980 |
| **Posterior acoustic pattern** | | | | | |
| Shadow | 6.57 ± 1.18 | 4.88±0.99 | 5.75±1.38 | 0.96 ± 0.13 | 3.51±1.07 |
| Enhancement | 5.32 ± 1.70 | 4.97±0.76 | 5.88±1.09 | 1.19 ± 0.36 | 3.56±0.88 |
| No change | 6.08 ± 1.51 | 4.71±0.72 | 5.59±1.06 | 0.98 ± 0.16 | 3.55±0.90 |
| Mixed | 6.44 ± 1.65 | 4.70±0.79 | 5.67±1.26 | 1.05 ± 0.22 | 3.54±0.83 |
| **P value** | **0.033*** | 0.366 | 0.642 | **0.001*** | 0.999 |
| **Posterior acoustic enhancement** | | | | | |
| Yes | 5.32 ± 1.70 | 4.97±0.76 | 5.88±1.09 | 1.19 ± 0.36 | 3.56±0.88 |
| No | 6.18 ± 1.49 | 4.72±0.75 | 5.62±1.11 | 0.99 ± 0.17 | 3.55±0.90 |
| **P value** | **0.005*** | 0.094 | 0.216 | **0.001*** | 0.940 |
| **Calcification** | | | | | |
| Yes | 6.13±1.60 | 4.68±0.68 | 5.71±1.10 | 0.98 ± 0.13 | 3.56±0.83 |
| No | 5.75±1.62 | 4.87±0.79 | 5.72±1.12 | 1.09 ± 0.31 | 3.52±1.03 |
| **P value** | 0.267 | 0.243 | 0.958 | **0.01*** | 0.82 |

*Data are presented as mean ± SD for RNAs. * Indicates significant difference.*
*Bold values indicate P values less than 0.05.*

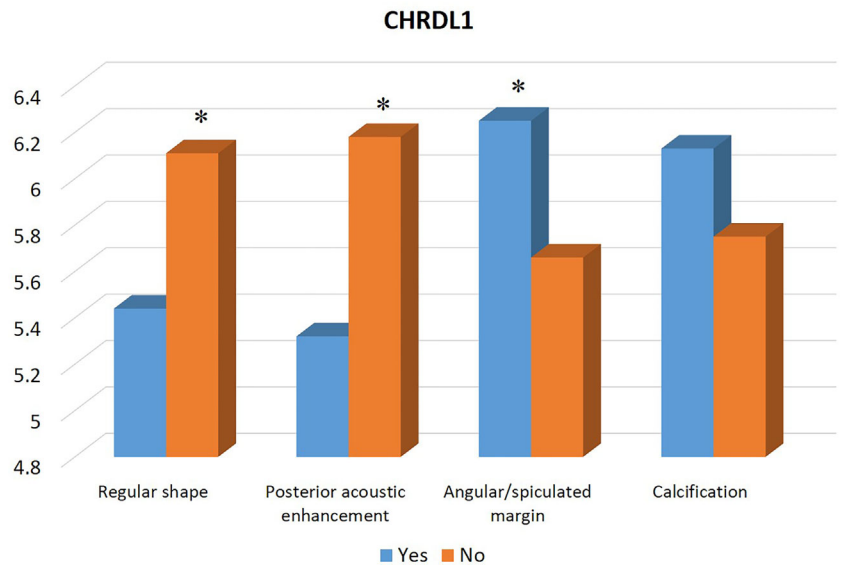


**FIGURE 1 |** Association between the expression profile of mRNA CHRDL1 and sonographic features of TNBCs. The high expression of CHRDL1 is significantly associated with malignant sonographic features of irregular shape, absence of posterior acoustic enhancement, and presence of angular/spiculated margin.
* indicates significant difference between the two groups with and without the specific sonographic feature.

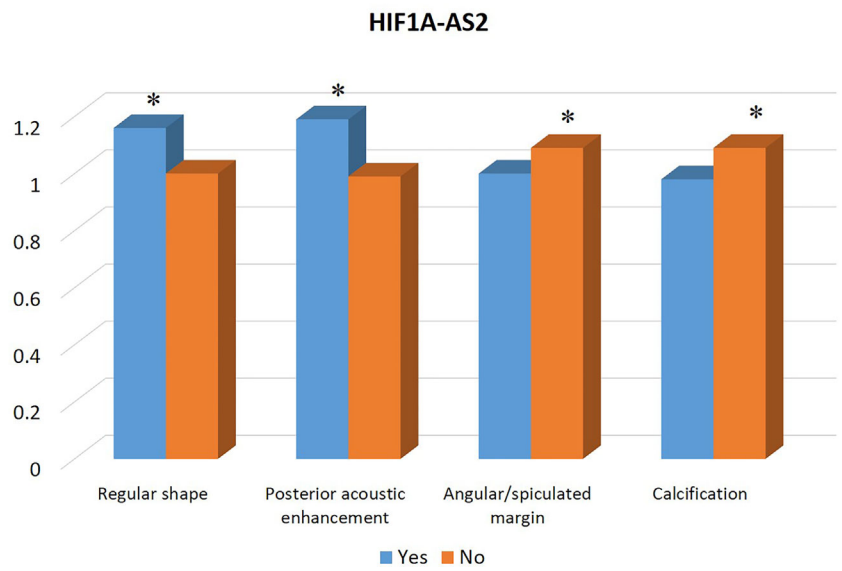


**FIGURE 2** | Association between the expression profile of lncRNA HIF1A-AS2 and sonographic features of TNBCs. The high expression of HIF1A-AS2 is significantly associated with benign sonographic features of regular shape, presence of posterior acoustic enhancement, absence of angular/spiculated margin, and no calcification. * indicates significant difference between the two groups with and without the specific sonographic feature.

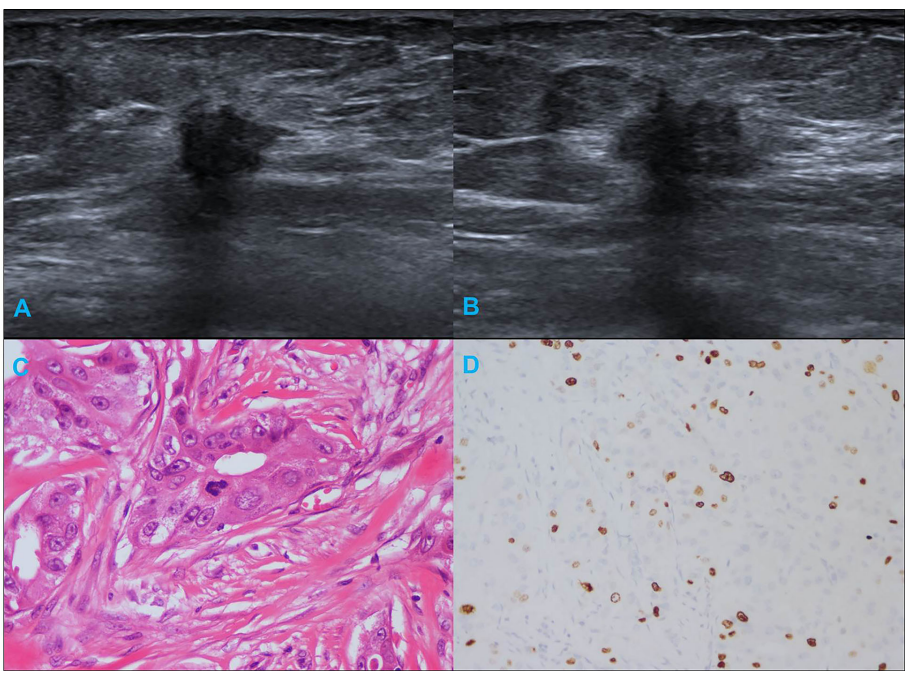


**FIGURE 3** | Illustration of TNBC in a 66-year-old female patient. **(A, B)** Irregular shape, angular margin and posterior acoustic shadow in sonogram (BI-RADS:4C); **(C)** Histological grade II in HE staining (original magnification × 400); **(D)** Twenty percent Ki-67 expression in IHC staining (original magnification × 200).

clinicopathology-based models showed equivalent results as seen by the AUC (P=0.956). As illustrated in **Table 6** and **Figure 5**, the combination of sonographic features and clinicopathological characteristics improved the prediction model (AUC=0.737, 95% CI 0.644–0.829). AUC was similar between the two types of models (combined model vs US-based model: P=0.083; combined model vs clinicopathology-based model: P=0.112).

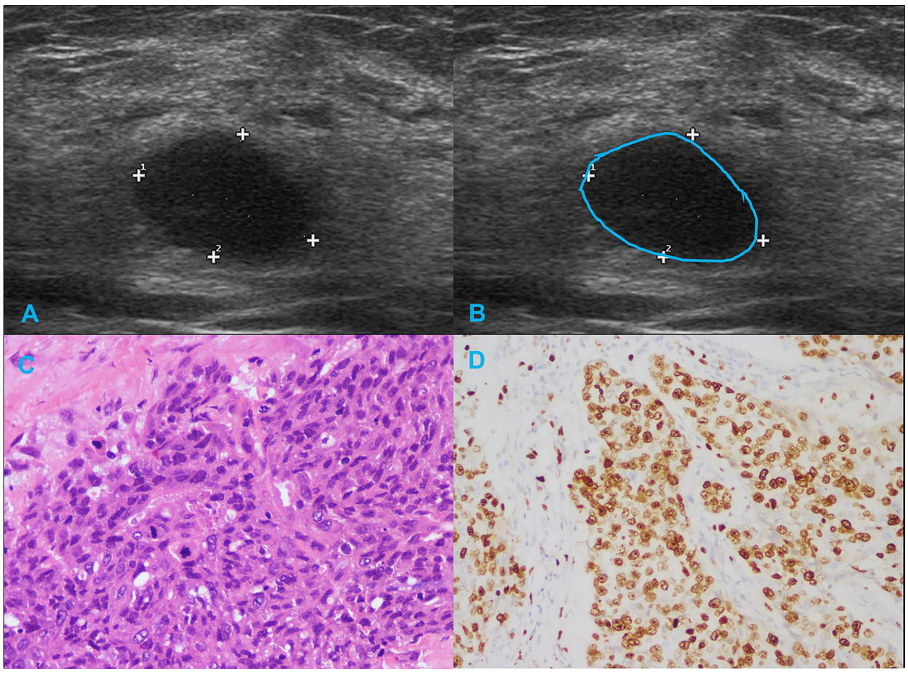


**FIGURE 4** | Illustration of TNBC in a 29-year-old female patient. **(A, B)** Regular shape, circumscribed margin and posterior acoustic enhancement in sonogram (BI-RADS:4A); **(C)** Histological grade III in HE staining (original magnification × 400); **(D)** Eighty percent Ki-67 expression in IHC staining (original magnification × 200).

**TABLE 3** | Association between sonographic features of TNBCs and risk of recurrence (Univariate Logistic regression analysis).

| | High risk of recurrence | Low risk of recurrence | P value |
|---|---|---|---|
| **Shape** | | | 0.014* |
| Regular | 24 (51.1%) | 19 (28.4%) | |
| Irregular | 23 (48.9%) | 48 (71.6%) | |
| **Margin** | | | 0.058 |
| Circumscribed | 8 (17.0%) | 4 (6.0%) | |
| Uncircumscribed | 39 (83.0%) | 63 (94.0%) | |
| **Posterior acoustic enhancement** | | | 0.038* |
| Yes | 23 (48.9%) | 20 (29.9%) | |
| No | 24 (51.1%) | 47 (70.1%) | |
| **Calcification** | | | 0.028* |
| Yes | 8 (17.0%) | 24 (35.8%) | |
| No | 39 (83.0%) | 43 (64.2%) | |

**Indicates statistical significance.*

**TABLE 4** | Association between the number of sonographic features with the risk of recurrence of TNBCs.

| US feature group | Risk of recurrence group | |
|---|---|---|
| | Low risk | High risk |
| No malignant features | 11 (35.5%) | 20 (64.5%) |
| 1–2 malignant features | 42 (63.6%) | 24 (36.4%) |
| 3–4 malignant features | 14 (82.4%) | 3 (17.6%) |
| **P value** | **0.003** | |

**TABLE 5** | Multivariate Logistic regression analysis for sonographic features associated with high risk of recurrence.

| Sonographic features | Multivariate Analysis | | | |
|---|---|---|---|---|
| | B | SE | P value | OR (95%CI) |
| Regular shape | 0.71 | 0.42 | 0.091 | 2.04 (0.89–4.66) |
| Posterior acoustic enhancement | 0.58 | 0.42 | 0.166 | 1.79 (0.79–4.06) |
| Without calcification | 0.79 | 0.48 | 0.097 | 2.21 (0.87–5.66) |

*B, regression coefficient; SE, standard error; OR, odds ratio; CI, confidence interval.*

## DISCUSSION

TNBCs bear genomic, clinical, and imaging heterogeneity (2–4, 6, 8, 14–16). This study demonstrated the correlation between gene expression and sonographic features. Benign-like sonographic features correlated with the upregulated signature of HIF1A-AS2; while malignant-like sonographic features correlated with the downregulated signature of CHRDL1 in TNBCs. Sonographic features of TNBCs represent the risk of tumor recurrence that is based on the mRNA and lncRNA signatures. TNBCs with benign-like sonographic appearances have a higher risk of recurrence than those with malignant sonographic appearances.

CHRDL1 mRNA has been reported to have tumor suppressing effects on melanoma (17) and TNBC (2). lncRNAs cannot encode proteins, but they can regulate the expression of

**TABLE 6 |** Performance using sonographic features, clinicopathological characteristics and combined sonographic–clinical–pathological parameters to predict the high risk of recurrence of TNBCs.

| Method | Sensitivity (%) | Specificity (%) | AUC (95%CI) | P value |
|---|---|---|---|---|
| US features | 59.6 | 70.2 | 0.674 (0.573–0.774) | 0.0006 |
| Clinicopathology | 76.6 | 53.7 | 0.678 (0.580–0.775) | 0.0003 |
| Combined | 85.1 | 59.7 | 0.737 (0.644–0.829) | <0.0001 |

*US, ultrasound; AUC, area under curve; CI, confidence interval.*
*Sonographic features include regular shape, posterior acoustic enhancement and without calcification; Clinicopathological characteristics include tumor size >2cm, histological grade III, Ki-67 ≥40% and presence of LNM.*

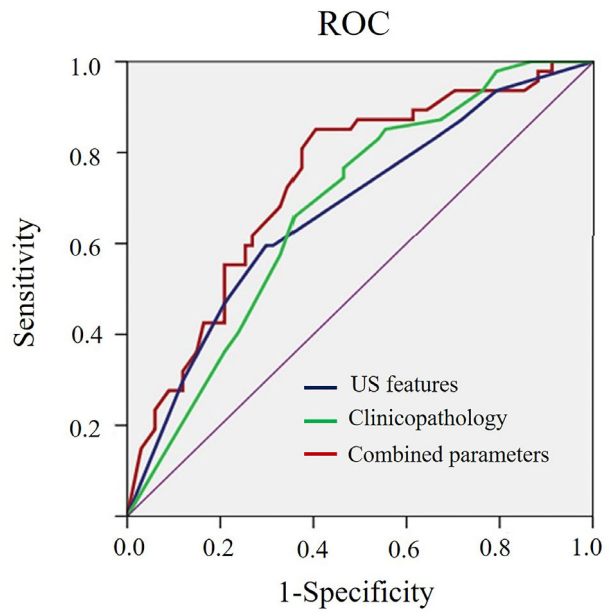


**FIGURE 5 |** ROC curve for the prediction model of risk of recurrence based on sonographic features, clinicopathological characteristics, and the combined sonographic-clinical-pathological parameters of TNBCs.

protein encoding genes involved in epigenetics, transcription, post-transcriptional modification, and translation. They also affect the occurrence, development, invasion, and metastasis of various tumors, such as breast cancer (18), bladder cancer (19), gastric cancer (20), colorectal cancer (21), and glioblastoma (22). The expression of HIF1A-AS2 is higher in TNBC than that in non-TNBC cancers and surrounding normal breast tissue (2, 18). HIF1A-AS2 improves the tolerance of tumor cells to hypoxic conditions, induces angiogenesis, and promotes growth and invasion of tumors by regulating the HIF-1α pathway (23). Jiang et al. suggested that HIF1A-AS2 affect the coding process by interrupting metabolism; AK124454 is involved in cell division and cell cycle (2). We have also previously reported the correlation between high expression of HIF1A-AS2 and AK124454 and increased risk of TNBC recurrence (2).

The integrated mRNA–lncRNA model predicted the risk of tumor recurrence reliably since it was based on 33 paired TNBC and normal tissues and a training set of 137 TNBCs with follow-up data on RFS. The reliability of the integrated model was further verified using 138 TNBC patients and 82 TNBC patients undergoing taxane-based neoadjuvant chemotherapy (2). However, to the best of our knowledge, this is the first report demonstrating that high risk of recurrence represents increased invasiveness that correlated with benign-like sonographic features.

In this study, sonographic features of TNBCs correlated with specific mRNAs and lncRNAs that are key regulators of TNBC cell proliferation. The sonographic features that were obtained using US rely on the acoustic characteristics of the tumor region that results from the interaction between tumor and normal tissues. The rate of TNBC tumor proliferation determines the possibility of interactions with the normal breast tissues. Enhanced cell proliferation allows specific cellular components to dominate in the tumor, thereby resulting in reduced fibrosis, infiltration, and reflection interferences (24, 25). Posterior acoustic enhancement results from the enhanced propagation of US energy owing to the lack of reflective interfaces. Upregulated RNAs that are involved in cell proliferation result in the occurrence of benign-like sonographic features, whereas downregulated RNAs reduce the rate of cell proliferation and result in the occurrence of malignant-like sonographic features. Our results are in accordance with this regulatory pattern. The extent of cell proliferation and differentiation is an important index for predicting tumor malignancy. Therefore, sonographic features of TNBCs may be an indirect indicator for tumor invasiveness. We have previously reported that sonogram features of breast cancers are reflective of tumor proliferation and invasiveness (26, 27). However, in this study, the effect of HIF1A-AS2 and CHRDL1 in determining the growth pattern of the tumor based on US was not studied in animals. Thus, exploring this in the future will enhance the utility of US as an important auxiliary technique to determine tumor characteristics and clinical outcomes in patients.

The sonographic difference between TNBCs and non-TNBCs was reported (28–30). However, the diversity in the sonographic features have not been studied. We have previously reported the variety of sonographic features of TNBCs and their correlation with clinicopathological and IHC characteristics (8). Understanding the biological basis for the variety in sonographic features is crucial in improving the reliability of diagnosing benign breast tumors by US specialists (8). We have demonstrated in this study that benign-like TNBCs correlate with higher risk of recurrence. US appearance of TNBCs can be used as an auxiliary parameter in addition to clinicopathological characteristics to stratify patients based on risk of relapse and develop personalized treatment in lieu of surgery.

However, this study has some limitations. First, the sample size of only 114 cases and the subpar quality of US imaging that were collected 6–8 years ago may affect the data interpretation. Second, we were not able to determine the correlation between sonographic features and RFS outcomes in this study; however, this is one of our

ongoing projects. The last but not the least, there were only data on US images with no MRI data which may warrant further study.

## CONCLUSION

Sonographic features of TNBCs correlated with the risk of tumor recurrence that was predicted using the mRNA–lncRNA signatures. However, this correlation should be further verified using a larger patient cohort.

## DATA AVAILABILITY STATEMENT

The raw data supporting the conclusions of this article will be made available by the authors, without undue reservation.

## ETHICS STATEMENT

The studies involving human participants were reviewed and approved by Institutional review board at Fudan University Shanghai Cancer Center. The patients/participants provided their written informed consent to participate in this study.

## AUTHOR CONTRIBUTIONS

Conception and design: J-WL. Administrative support: S-CZ, CC. Provision of study materials or patients: CC. Collection and assembly of data: JZ, NL. Data analysis and interpretation: J-WL, Z-TS. Manuscript writing: all authors. Final approval of manuscript: all authors. All authors contributed to the article and approved the submitted version.

## FUNDING

This study was funded by National Natural Science Foundation of China (No. 81627804, 81830058), Shanghai Science and Technology Development Foundation of China (No. 18411967400), and Shanghai Anticancer Association SOAR Project (No. SACA-AX201905).

## ACKNOWLEDGMENTS

We thank Prof Shao (M.D) and Dr Jiang (M.S) for sharing the transcriptome data. We would like to thank Editage (www.editage.cn) for English language editing.

## REFERENCES

1. Jiang YZ, Liu Y, Xiao Y, Hu X, Jiang L, Zuo WJ, et al. Molecular subtyping and genomic profiling expand precision medicine in refractory metastatic triple-negative breast cancer: the FUTURE trial. *Cell Res* (2020) 27(10):020–0375. doi: 10.1038/s41422-020-0375-9
2. Jiang YZ, Liu YR, Xu XE, Jin X, Hu X, Yu KD, et al. Transcriptome analysis of triple-negative breast cancer reveals an integrated mRNA-lncRNA signature with predictive and prognostic value. *Cancer Res* (2016) 76(8):2105–14. doi: 10.1158/0008-5472.CAN-15-3284
3. Jiang YZ, Ma D, Suo C, Shi J, Xue M, Hu X, et al. Genomic and transcriptomic landscape of triple-negative breast cancers: subtypes and treatment strategies. *Cancer Cell* (2019) 35(3):428–40.e5. doi: 10.1016/j.ccell.2019.02.001
4. Liu YR, Jiang YZ, Xu XE, Yu KD, Jin X, Hu X, et al. Comprehensive transcriptome analysis identifies novel molecular subtypes and subtype-specific RNAs of triple-negative breast cancer. *Breast Cancer Res* (2016) 18 (1):33. doi: 10.1186/s13058-016-0690-8
5. Lehmann BD, Bauer JA, Chen X, Sanders ME, Chakravarthy AB, Shyr Y, et al. Identification of human triple-negative breast cancer subtypes and preclinical models for selection of targeted therapies. *J Clin Invest* (2011) 121(7):2750–67. doi: 10.1172/JCI45014
6. Burstein MD, Tsimelzon A, Poage GM, Covington KR, Contreras A, Fuqua SA, et al. Comprehensive genomic analysis identifies novel subtypes and targets of triple-negative breast cancer. *Clin Cancer Res* (2015) 21(7):1688–98. doi: 10.1158/1078-0432.CCR-14-0432
7. Zhao S, Zuo WJ, Shao ZM, Jiang YZ. Molecular subtypes and precision treatment of triple-negative breast cancer. *Ann Transl Med* (2020) 8(7):499. doi: 10.21037/atm.2020.03.194
8. Li JW, Zhang K, Shi ZT, Zhang X, Xie J, Liu JY, et al. Triple-negative invasive breast carcinoma: the association between the sonographic appearances with clinicopathological feature. *Sci Rep* (2018) 8(1):9040. doi: 10.1038/s41598-018-27222-6
9. Wolff AC, Hammond ME, Schwartz JN, Hagerty KL, Allred DC, Cote RJ, et al. American Society of Clinical Oncology/College of American Pathologists guideline recommendations for human epidermal growth factor receptor 2 testing in breast cancer. *J Clin Oncol* (2007) 25(1):118–45. doi: 10.1200/jco.2006.09.2775
10. Goldhirsch A, Winer EP, Coates AS, Gelber RD, Piccart-Gebhart M, Thurlimann B, et al. Personalizing the treatment of women with early breast cancer: highlights of the St Gallen International Expert Consensus on the Primary Therapy of Early Breast Cancer 2013. *Ann Oncol* (2013) 24 (9):2206–23. doi: 10.1093/annonc/mdt303
11. Mendelson EB, Böhm-Vélez M, Berg WA. *ACR BI-RADS® Ultrasound*. ACR BI-RADS® Atlas, Breast Imaging Reporting and Data System. Reston: American College of Radiology (2013).
12. Li JW, Tong YY, Jiang YZ, Shui XJ, Shi ZT, Chang C. Clinicopathologic and ultrasound variables associated with a heavy axillary nodal tumor burden in invasive breast carcinoma. *J Ultras Med* (2019) 38:1747–55. doi: 10.1002/jum.14863
13. Li JW, Li N, Jiang YZ, Liu YR, Shi ZT, Chang C, et al. Ultrasonographic appearance of triple-negative invasive breast carcinoma is associated with novel molecular subtypes based on transcriptomic analysis. *Ann Trans Med* (2020) 8(7):435. doi: 10.21037/atm.2020.03.204
14. Elsawaf Z, Sinn HP, Rom J, Bermejo JL, Schneeweiss A, Aulmann S. Biological subtypes of triple-negative breast cancer are associated with distinct morphological changes and clinical behaviour. *Breast* (2013) 22(5):986–92. doi: 10.1016/j.breast.2013.05.012
15. Li CY, Zhang S, Zhang XB, Wang P, Hou GF, Zhang J. Clinicopathological and prognostic characteristics of triple- negative breast cancer (TNBC) in Chinese patients: a retrospective study. *Asian Pac J Cancer Prev* (2013) 14 (6):3779–84. doi: 10.7314/APJCP.2013.14.6.3779
16. Golshan M, Wong SM, Loibl S, Huober JB, O'Shaughnessy J, Rugo HS, et al. Early assessment with magnetic resonance imaging for prediction of pathologic response to neoadjuvant chemotherapy in triple-negative breast cancer: Results from the phase III BrighTNess trial. *Eur J Surg Oncol* (2020) 46 (2):223–8. doi: 10.1016/j.ejso.2019.10.002
17. Mithani SK, Smith IM, Califano JA. Use of integrative epigenetic and cytogenetic analyses to identify novel tumor-suppressor genes in malignant melanoma. *Melanoma Res* (2011) 21(4):298–307. doi: 10.1097/CMR.0b013e328344a003
18. Wang Y, Zhang G, Han J. HIF1A-AS2 predicts poor prognosis and regulates cell migration and invasion in triple-negative breast cancer. *J Cell Biochem* (2019) 120(6):10513–8. doi: 10.1002/jcb.28337

19. Chen M, Zhuang C, Liu Y, Li J, Dai F, Xia M, et al. Tetracycline-inducible shRNA targeting antisense long non-coding RNA HIF1A-AS2 represses the malignant phenotypes of bladder cancer. *Cancer Lett* (2016) 376(1):155–64. doi: 10.1016/j.canlet.2016.03.037
20. Mei D, Song H, Wang K, Lou Y, Sun W, Liu Z, et al. Up-regulation of SUMO1 pseudogene 3 (SUMO1P3) in gastric cancer and its clinical association. *Med Oncol* (2013) 30(4):709. doi: 10.1007/s12032-013-0709-2
21. Lin J, Shi Z, Yu Z, He Z. LncRNA HIF1A-AS2 positively affects the progression and EMT formation of colorectal cancer through regulating miR-129-5p and DNMT3A. *BioMed Pharmacother* (2018) 98:433–9. doi: 10.1016/j.biopha.2017.12.058
22. Mineo M, Ricklefs F, Rooj AK, Lyons SM, Ivanov P, Ansari KI, et al. The long non-coding RNA HIF1A-AS2 facilitates the maintenance of mesenchymal glioblastoma stem-like cells in hypoxic niches. *Cell Rep* (2016) 15(11):2500–9. doi: 10.1016/j.celrep.2016.05.018
23. Bertozzi D, Iurlaro R, Sordet O, Marinello J, Zaffaroni N, Capranico G. Characterization of novel antisense HIF-1alpha transcripts in human cancers. *Cell Cycle* (2011) 10(18):3189–97. doi: 10.4161/cc.10.18.17183
24. Costantini M, Belli P, Bufi E, Asunis AM, Ferra E, Bitti GT. Association between sonographic appearances of breast cancers and their histopathologic features and biomarkers. *J Clin Ultrasound* (2016) 44(1):26–33. doi: 10.1002/jcu.22312
25. Sannomiya N, Hattori Y, Ueda N, Kamida A, Koyanagi Y, Nagira H, et al. Correlation between ultrasound findings of tumor margin and clinicopathological findings in patients with invasive ductal carcinoma of the breast. *Yonago Acta Med* (2016) 59(2):163–8.
26. Tong YY, Sun PX, Zhou J, Shi ZT, Chang C, Li JW. The association between sonographic features and biological property of invasive breast carcinoma is modified by age, tumor size and preoperative axilla status. *J Ultras Med* (2020) 39(6):1125–34. doi: 10.1002/jum.15196
27. Li JW, Tong YY, Zhou J, Shi ZT, Sun PX, Chang C. Tumor proliferation and invasiveness derived from sonographic appearances of invasive breast cancers: Moving beyond the routine differential diagnosis. *J Ultrasound Med* (2020) 39:1589–99. doi: 10.1002/jum.15250
28. Celebi F, Pilanci KN, Ordu C, Agacayak F, Alco G, Ilgun S, et al. The role of ultrasonographic findings to predict molecular subtype, histologic grade, and hormone receptor status of breast cancer. *Diagn Interv Radiol* (2015) 21 (6):448–53. doi: 10.5152/dir.2015.14515
29. Yang Q, Liu HY, Liu D, Song YQ. Ultrasonographic features of triple-negative breast cancer: a comparison with other breast cancer subtypes. *Asian Pac J Cancer Prev* (2015) 16(8):3229–32. doi: 10.7314/APJCP.2015.16.8.3229
30. Zheng FY, Lu Q, Huang BJ, Xia HS, Yan LX, Wang X, et al. Imaging features of automated breast volume scanner: Correlation with molecular subtypes of breast cancer. *Eur J Radiol* (2017) 86:267–75. doi: 10.1016/j.ejrad.2016.11.032

**Conflict of Interest:** The authors declare that the research was conducted in the absence of any commercial or financial relationships that could be construed as a potential conflict of interest.

frontiers in Oncology

ORIGINAL RESEARCH
published: 20 January 2021
doi: 10.3389/fonc.2020.575317

# Analysis of CK5/6 and EGFR and Its Effect on Prognosis of Triple Negative Breast Cancer

*Zhen Wang*[1,2,3,4], *Lei Liu*[1,2,3,4], *Ying Li*[1,2,3,4], *Zi'an Song*[1,2,3,4], *Yi Jing*[1,2,3,4], *Ziyu Fan*[1,2,3,4] *and Sheng Zhang*[1,2,3,4]*

[1] The Third Department of Breast Cancer, Tianjin Medical University Cancer Institute and Hospital, National Clinical Research Center for Cancer, Tianjin, China, [2] Key Laboratory of Breast Cancer Prevention and Therapy, Tianjin Medical University, Ministry of Education, Tianjin, China, [3] Key Laboratory of Cancer Prevention and Therapy, Tianjin, China, [4] Tianjin's Clinical Research Center for Cancer, Tianjin, China

OPEN ACCESS

**Edited by:**
*Zhi-Ming Shao,*
*Fudan University, China*

**Reviewed by:**
*Camila O. Dos Santos,*
*Cold Spring Harbor Laboratory, United States*
*Julio de la Torre-Montero,*
*Comillas Pontifical University, Spain*

***Correspondence:**
*Sheng Zhang*
*szhang138@163.com*

**Specialty section:**
*This article was submitted to Women's Cancer, a section of the journal Frontiers in Oncology*

**Received:** *23 June 2020*
**Accepted:** *30 November 2020*
**Published:** *20 January 2021*

**Citation:**
*Wang Z, Liu L, Li Y, Song Z, Jing Y, Fan Z and Zhang S (2021) Analysis of CK5/6 and EGFR and Its Effect on Prognosis of Triple Negative Breast Cancer. Front. Oncol. 10:575317. doi: 10.3389/fonc.2020.575317*

**Background:** Triple-negative breast cancer (TNBC) is considered to be higher grade, more aggressive and have a poorer prognosis than other types of breast cancer. Discover biomarkers in TNBC for risk stratification and treatments that improve prognosis are in dire need.

**Methods:** Clinical data of 195 patients with triple negative breast cancer confirmed by pathological examination and received neoadjuvant chemotherapy (NAC) were collected. The expression levels of EGFR and CK5/6 were measured before and after NAC, and the relationship between EGFR and CK5/6 expression and its effect on prognosis of chemotherapy was analyzed.

**Results:** The overall response rate (ORR) was 86.2% and the pathological complete remission rate (pCR) was 29.2%. Univariate and multivariate logistic regression analysis showed that cT (clinical Tumor stages) stage was an independent factor affecting chemotherapy outcome. Multivariate Cox regression analysis showed pCR, chemotherapy effect, ypT, ypN, histological grades, and post- NAC expression of CK5/6 significantly affected prognosis. The prognosis of CK5/6-positive patients after NAC was worse than that of CK5/6-negative patients (p=0.036). Changes in CK5/6 and EGFR expression did not significantly affect the effect of chemotherapy, but changes from positive to negative expression of these two markers are associated with a tendency to improve prognosis.

**Conclusion:** For late-stage triple negative breast cancer patients receiving NAC, patients who achieved pCR had a better prognosis than those with non- pCR. Patients with the change in expression of EGFR and CK5/6 from positive to negative after neoadjuvant chemotherapy predicted a better prognosis than the change from negative to positive group.

**Keywords: triple-negative breast cancer, CK5/6, EGFR, clinical pathological response, prognosis**

## INTRODUCTION

Triple negative breast cancer (TNBC) which is defined by the lack of estrogen receptor (ER), progesterone receptor (PR), and human epidermal growth factor receptor-2 (Her-2) accounts for 10–20% of all breast cancer. Due to a lack of available therapeutic targets that often lead to poor prognosis, those patients with triple-negative disease were left as the only group without an option for targeted therapy (1). Many clinical trials focused on identifying specific therapeutic targets for TNBC. In particular, Masuda et al. reported that 7 subtypes of TNBC were identified by cluster analysis of mRNA expression profiles: basal-like 1, basal-like 2, mesenchymal stem-like, mesenchymal, immunization immunomodulatory, androgen receptor type (AR+), and unsatable. Additionally, this study indicated that different subtypes have different drug susceptibility, and that patients with different gene subtypes have significantly different prognosis (2).

Basal-like breast cancer (BLBC) is a distinct pathological subtype that is characterized by expression of cytokeratin (including CK5/6, CK14, CK17, and etc.) and/or human epidermal growth factor receptor (EGFR). In particular, CK5/6 is an important molecular marker for the recognition of TNBC, and may be an independent factor that influences TNBC prognosis (3, 4). EGFR is a member of the erbB family of casein kinase receptor protein and it has been shown to play an important role during tumor cell proliferation process, including cell movement, tissue invasion, and angiogenesis. As a result, EGFR appears to be a highly attractive target for tumor-specific therapies. Over expression of EGFR in most basal-like breast cancer suggests that basal-like tumors may be caused by excessive activation of the growth factor receptor pathway in a manner similar to Her-2+ breast cancer. Since anti-Her-2 therapy has shown to be effective in treating Her-2+ breast cancer, a similar strategy using anti-Her-1 antibodies or blockers of Her-1 tyrosine kinase may also be beneficial. This is especially important as it may offer new prospects for the treatment of triple negative BCBL (5, 6).

The current treatment strategy does not differ between distinct TNBC subtypes. While genetic analysis classification will be a direct solution to this need, classifying a cancer using gene expression subtype is impractical in clinics. The most widely accepted clinical practice is to identify substitute biomarkers by immunohistochemistry (IHC) for BLBC, such as EGFR and CK5/6. Therefore, screening for CK5/6 and EGFR is necessary for predicting prognosis and treatment strategy for TNBC. In this study, we adopted the widely accepted definition in which CK5/6- and/or EGFR-positive breast cancers are classified as BLBC while CK5/6- and EGFR-negative breast cancers are defined as non-basal-like breast cancer (NBLBC). Previous studies have observed in BLBC a significantly lower response to chemotherapy than in NBLBC, in addition to a higher risk of recurrence and a worse prognosis. Yet there has been no study to date that looked at the effect of treatment on these two distinct subtypes (4, 7). Therefore, evaluation of the use of the two biomarkers in TNBC for risk stratification and treatments that improve prognosis is in dire need.

Neoadjuvant chemotherapy (NAC) has been widely used as a standard treatment for locally advanced breast cancer. It has been increasingly applied by researchers to observe the efficacy of preoperative chemotherapy and to determine the sensitivity of individuals to chemotherapy drugs which together guide the clinical comprehensive treatment program. Increasing number of studies have shown that patients with good clinical outcomes after NAC, especially patients with pathologic complete response (pCR), have significantly improved disease-free survival (DFS) and overall survival (OS) rates (8–10). For patients receiving NAC, pCR rate of TNBC patients is about two times that of non-TNBC patients and TNBC exhibits a better response to NAC than non-TNBC (11). Thus, the need of biomarkers that respond to the better prognoses of TNBC receiving NAC is crucial for future treatment manipulation in this setting.

In sum, the aim of this study was to evaluate the prognostic value of biomarkers CK5/6 and EGFR in patients with TNBC receiving NAC. In this retrospective study, IHC methods were used to (1) detect the expression of CK5/6 and EGFR for classification of TNBC subtypes (including BLBC and NBLBC), and to (2) compare the expression change of CK5/6 and EGFR before and after NAC, and lastly to (3) assess the ability of both markers in predicting NAC chemotherapy outcome and survival rate as well as their impact on TNBC treatment strategies.

## MATERIALS AND METHODS

### Patient Selection

We retrospectively collected all clinical, imaging, and pathological data from TNBC patients from clinical stages II to III who underwent NAC at Tianjin Medical University Cancer Institute and Hospital between June 2014 to June 2018. The study protocol conformed to the ethical guidelines of the 1975 Declaration of Helsinki and was approved by the Medical Ethics Committee of Tianjin Medical University Cancer Institute and Hospital. Patient inclusion criteria were: 1) TNBCs both before and after chemotherapy were determined by IHC. This criterion includes some patients who could not undergo immunohistochemistry after pathological complete remission (pCR) but were diagnosed with triple-negative breast cancer before chemotherapy. Patients that exhibited changes in ER, PR, Her-2 status due to chemotherapy as well as advanced (stage IV) patients for whom surgery is not possible are excluded from the study.; 2) Cases of invasive ductal carcinoma confirmed by histology were selected; 3) All patients had radical mastectomy, modified radical mastectomy or breast tumor resection (mammography) which is the main surgical treatment option; and 4) All patients with a chemotherapy regimen in which they were treated with anthracyclines combined with sequential taxane were also selected. Informed consent was obtained from the studied patients.

### Material and Indicator Evaluation Criteria

Before NAC, needle biopsy was used to obtain histopathological specimens of breast cancer. After NAC, the postoperative breast

specimens were analyzed by IHC staining on paraffin-embedded tissue sections made from post treatment needle biopsy. Tumor tissues analyzed was confirmed with a component of over >95% tumor cells. Triple-negative breast cancer (TNBC), characterized by absence of expression of ER, PR, and Her-2; For ER and PR expression, moderate to strong nuclear staining in ≥1% of tumor cells was considered positive. Her-2 positivity was defined as either Her-2 gene amplification by fluorescent *in situ* hybridization or scored as 3+ by IHC. In case of Her-2 2(+), fluorescent *in situ* hybridization was performed to determine Her-2 positivity.

In our clinical evaluation, Ki-67 values were expressed as the percentage of positive cell counts among at least 100 tumor cells in each case. Patients with positive staining of Ki-67 at 20% or more were defined as high Ki-67 patients (12). Similarly, the expression levels of CK5/6, EGFR, and P53 are considered to be negative if the nuclear staining is less than 1%, and positive if it is 1% or more. BLBC is defined as positive expression of EGFR and/or CK5/6. All IHC readings were independently verified by two blinded pathologists.

## Evaluation of Chemotherapy Response

According to RECIST (Response Evaluation Criteria In Solid Tumors, version 1.1), the patients were classified into two groups: the overall response group (ORR), into which all patients classified as complete response (CR) or partial response (PR) were placed, and the no response group (NR), containing all patients classified as stable disease (SD) or progressive disease (PD).

Tumor size was determined as tumor length × width ($cm^2$). A clinical complete response (CR) was defined as the disappearance of the palpable tumor deposits. Clinical partial response (PR) is when > 50% reduction in tumor volume occurred. Tumor reduction < 50% or an increase in volume up to 25% was considered as stable disease (SD). An increase of > 25% of tumor volume was scored as progressive disease (PD). Pathological complete response (pCR): after NAC, the tumor of the breast cancer and the axillary lymph node surgical specimens showed no invasive tumor cell residual, or the intraductal carcinoma were found in the tissue section, but no infiltrating components were observed.

## Follow-Up

Follow-ups are mainly conducted as phone interviews or outpatient questionnaires in order to obtain prognostic information such as recurrence of the local region or distant metastasis and survival state after the treatment. Disease-free survival (DFS) and overall survival (OS) are used as end points of survival analysis. DFS was defined as the date from the initial treatment date (first accepted to NAC) to the first local recurrence or distant metastasis. The OS was defined as the date from the initial treatment (first accepted to NAC) to the date of death or loss of follow-up.

## Statistical Analysis

Statistical and prognostic analysis was performed using SPSS 22.0 (IBM SPSS Statistics for Windows, Version 22.0. Armonk, NY: IBM Corp.) and multiple comparisons test was performed using Graph pad Prism 7.0.0 (San Diego, California USA). Correlation factors were compared between the groups using the Pearson$\chi^2$ test. For those whose theoretical frequency does not meet the application conditions of Person chi-square test, continuous correction is adopted. The significant index of univariate analysis is included in the analysis of multivariate logistic regression model. Correlation between clinical and pathological variables, and survival was done by using univariate and multivariable Cox proportional risk regression analysis. In addition, log-rank test and Kaplan-Meier (K-M) curve were used to evaluate the influencing factors and the difference in survival between groups. A *P*-value of 0.05 was considered significant.

# RESULTS

## Characteristics of BLBC and NBLBC Before NAC

The age of the patients (n=195) at the time of initial diagnosis ranged from 26 to 78 years with a mean of 49 ± 11.09 years. The median follow-up time was 30 months (range, 13–64) and the median DFS and OS were 29 ± 13.1 months and 30 ± 12.46 months respectively. During the follow-up period, recurrence and/or metastasis occurred in 24.1% (47/195) of patients and 5.1% (10/195) of patients died during follow-up.

Out of the 195 TNBC cases, 70.7% (138/195) were CK5/6-positive and 87.1% (170/195) were EGFR-positive. According to the definition used in our study, out of the 195 TNBC case, 89.7% were BLBC and 10.3% were NBLBC. After chemotherapy, 29.2% patients achieved pCR. Only 138 of 195 cases were feasible for IHC testing in which BLBC accounted for 92.7% (123/138) while NBLBC accounted for only 7.3% (15/138). The clinical pathological variables of the two groups before NAC were assessed and presented in **Table 1**. The results showed that there was no significant difference in age, menopausal status, cT stage, Ki-67 and p53 expression between the two groups.

## The Response of TNBC to NAC

The clinical overall response rate (ORR=CR+PR) to NAC in 195 TNBC cases was 86.2% (168/195) and the non-response rate (NR=SD+PD) was 13.8% (27/195). The pCR rate was 29.2% (n=57), the CR rate was 31.7% (n=62), the PR rate was 54.3% (n=106), the SD rate was 12.3% (n=24), and the PD rate was 1.5% (n=3). Within the BLBC group, 52 cases reached pCR, accounting for 29.7% of all BLBC cases. 5 cases of NBLBC reached pCR, accounting for 25% of all NBLBC. The data showed no statistical difference in the pCR between the two groups (p=0.661, **Table 1**). Univariate and multivariate logistic analyses showed that cT staging was an independent factor influencing the effects of chemotherapy (p<0.001) (**Tables 2** and **3**).

## Biomarkers Change Before and After NAC (Including 138 Patients That Did Not Reach pCR)

Considering the effect of chemotherapy on the expression of molecular biomarkers, we analyzed changes in CK5/6, EGFR, Ki-

**TABLE 1 |** Clinical pathological variables of the BLBC and NBLBC before NAC treatment.

| Variables | No. of cases (% of total 195) | NBLBC (n = 20, 10.3%) | BLBC (n = 175, 89.7%) | p-value |
|---|---|---|---|---|
| Age(year) | | | | 0.113 |
| ≤50years | 101 (51.8) | 7 | 94 | |
| >50years | 94 (48.2) | 13 | 81 | |
| Menopausal state | | | | 0.316 |
| Not menopause | 127 (65.1) | 11 | 116 | |
| Menopause | 68 (34.9) | 9 | 59 | |
| Tumor stage (cT) | | | | 0.714 |
| cT1 | 12 (6.2) | 1 | 11 | |
| cT2 | 137 (70.3) | 16 | 121 | |
| cT3 | 40 (20.5) | 3 | 37 | |
| cT4 | 6 (3.1) | 0 | 6 | |
| Ki-67 staining | | | | 1.0 |
| <20% | 7 (3.6) | 0 | 7 | |
| ≥20% | 188 (96.4) | 20 | 168 | |
| P53 expression | | | | 0.437 |
| – | 63 (32.3) | 8 | 55 | |
| + | 132 (67.6) | 12 | 120 | |
| Pathological response | | | | 0.857 |
| Non-pCR | 138 (70.8) | 15 | 123 | |
| pCR | 57 (29.2) | 4 | 23 | |
| Chemotherapy response | | | | 0.617 |
| ORR | 168 (86.2) | 16 | 152 | |
| NR | 27 (13.8) | 4 | 27 | |

*NAC, neoadjuvant chemotherapy; NBLBC, non-basal-like breast cancer; BLBC, basal-like breast cancer; ORR, overall response group; NR, no response group.*

**TABLE 2 |** The association of clinical pathological variables with the pCR and NAC efficiency using univariate logistic analysis.

| Variables | Non-pCR (n = 138) | pCR (n = 57) | P-value (Non-Pcr vs. pCR) | ORR (n = 168) | NR (n = 27) | P-value (ORR vs. NR) |
|---|---|---|---|---|---|---|
| Age(year) | | | 0.881 | | | 0.403 |
| ≤50years | 71 | 30 | | 85 | 16 | |
| >50years | 67 | 27 | | 83 | 11 | |
| Menopausal state | | | 0.535 | | | 0.857 |
| Not menopause | 88 | 39 | | 109 | 18 | |
| Menopause | 50 | 18 | | 59 | 9 | |
| Tumor stage (cT) | | | 0.002 | | | <0.001 |
| cT1 | 6 | 6 | | 6 | 6 | |
| cT2 | 90 | 47 | | 127 | 10 | |
| cT3 | 36 | 4 | | 31 | 9 | |
| cT4 | 6 | 0 | | 4 | 2 | |
| Ki-67 staining | | | 0.108 | | | 1.0 |
| <20% | 7 | 0 | | 6 | 1 | |
| ≥20% | 131 | 57 | | 162 | 26 | |
| P53 expression | | | 0.384 | | | 0.445 |
| – | 42 | 21 | | 56 | 7 | |
| + | 96 | 36 | | 112 | 20 | |
| CK5/6 expression | | | 0.133 | | | 0.961 |
| – | 36 | 21 | | 49 | 8 | |
| + | 102 | 36 | | 119 | 19 | |
| EGFR expression | | | 0.885 | | | 0.115 |
| – | 18 | 7 | | 19 | 6 | |
| + | 120 | 50 | | 149 | 21 | |
| Classification | | | 0.661 | | | 0.617 |
| NBLBC | 15 | 5 | | 16 | 4 | |
| BLBC | 123 | 52 | | 152 | 23 | |

*NAC, neoadjuvant chemotherapy; NBLBC, non-basal-like breast cancer; BLBC, basal-like breast cancer; ORR, overall response group; NR, no response group.*

67, and p53 expression before and after NAC. We observed significant difference in these molecular indexes, including changes between BLBC and NBLBC and before and after NAC (**Table 4**). As a result, we further divided the results into subgroups using changes in expression of CK5/6 and EGFR which includes positive→negative group, negative→positive group, positive before and after NAC group, and negative before and after NAC group. Basal/non-basal group changes

**TABLE 3 |** The association of clinicopathological variables with the NAC efficiency using multivariate logistic analysis.

| Variables | B | S.E. | Wald | p-value | 95% CI | |
|---|---|---|---|---|---|---|
| | | | | | Lower limit | Upper limit |
| cT | −1.214 | 0.356 | 11.608 | 0.001 | 0.148 | 0.597 |
| CK5/6 expression | −0.688 | 0.406 | 2.875 | 0.090 | 0.227 | 1.113 |
| EGFR expression | −1.080 | 1.014 | 1.134 | 0.287 | 0.047 | 2.480 |

*cT, Tumor stage; NAC, neoadjuvant chemotherapy; EGFR, human epidermal growth factor receptor.*

**TABLE 4 |** Biomakers changes before and after NAC treatment.

| Variables | | | | Chi-square value | p value |
|---|---|---|---|---|---|
| *CK5/6* | | After NAC | | | |
| | Before NAC | − | + | 28.02 | <0.001 |
| | − | 23 | 13 | | |
| | + | 18 | 86 | | |
| *EGFR* | | After NAC | | | |
| | Before NAC | − | + | 21.457 | <0.001 |
| | − | 10 | 8 | | |
| | + | 14 | 108 | | |
| *Ki-67* | | After NAC | | | |
| | Before NAC | <20% | ≥20% | 11.924 | 0.001 |
| | <20% | 5 | 2 | | |
| | ≥20% | 23 | 108 | | |
| *P53* | | After NAC | | | |
| | Before NAC | − | + | 66.076 | <0.001 |
| | − | 33 | 9 | | |
| | + | 9 | 87 | | |
| *BLBC/NBLBC* | | After NAC | | | |
| | Before NAC | NBLBC | BLBC | 38.909 | <0.001 |
| | NBLBC | 7 | 8 | | |
| | BLBC | 3 | 120 | | |

*NAC, neoadjuvant chemotherapy; NBLBC, non-basal-like breast cancer; BLBC, basal-like breast cancer; EGFR, epidermal growth factor receptor; CK5/6, cytokeratin5/6.*

were divided into BLBC→NBLBC (after NAC) group, NBLBC→BLBC (after NAC) group, BLBC before and after NAC group, and NBLBC before and after NAC group (**Table 5**).

We first analyzed the relationship between changes in CK5/6 and EGFR and the effect of chemotherapy: the statistical results showed that the number of cases in which chemotherapeutic effects reached ORR in the positive→negative group was higher than that in the negative→positive group. However, due to the small number of enrolled cases, we were unable to observe a statistically significant correlation between the two biomarkers and the chemotherapy effect (p>0.05, **Table 6**).

## Survival Analysis of TNBC Patients Receiving NAC

We analyzed the effects of clinical and pathological variables on long-term prognosis in patients using the Cox univariate and multivariate models. The results showed that the histological grades, chemotherapy effect, pCR, ypT, ypN, and expression of CK5/6 after NAC all significantly affected the prognosis (**Table 7**). The mean DFS of CK5/6-positive after NAC was 41 months and the mean DFS of CK5/6-negative after NAC was 47 months (**Figure 1A**).

The K-M survival analysis of pCR and non-pCR was compared in the **Figure 1B**. The survival prognosis of patients who achieved pCR (mean DFS was 54 months) was significantly better than those in non-pCR (mean DFS was 44 months) (p=0.0109).

Next, we analyzed whether the changes in expression of CK5/6 and EGFR before and after NAC affected prognosis. The DFS analysis of CK5/6 expression change was shown in **Figures 2A–C**, the mean DFS of positive→negative CK5/6 group was 53 months and 40 months for the negative→positive group. The mean DFS of the positive→positive group was 41 months and 46 months for the negative→negative group. Though the prognostic comparison did not show statistical difference, the DFS of the positive→negative CK5/6 group saw an improvement compared to the negative→positive group and positive→positive group (p=0.814, 0.0707, respectively), and the DFS of the negative→positive group was slightly worse than that of the negative→negative group.

A similar trend can also be seen in changes of EGFR expression and its effect on K-M prognosis analysis (**Figures 2D–F**). The mean DFS of the positive→negative EGFR group was 48 months while the DFS for the negative→positive group was 38 months. The mean DFS of the positive→positive group was 43 months and 49 months for the negative→negative group. It can also be observed that the EGFR change from positive to negative after NAC has a tendency to improve prognosis. Due to the cases of the changes of BLBC and NBLBC with recurrence and metastasis was less and no prognostic analysis was performed.

**TABLE 5 |** Number of recurrence and metastasis (R&M) cases of biomarkers changes.

| Variables | No. of cases |
|---|---|
| *CK5/6 expression* | |
| Pos→Neg. | 18 |
| BLBC →NBLBC | 3 |
| Neg.→Pos. | 13 |
| NBLBC→BLBC | 6 |
| Neg→Neg. | 23 |
| NBLBC→NBLBC | 4 |
| Pos.→Pos. | 84 |
| BLBC→BLBC | 31 |
| *EGFR expression* | |
| Pos→Neg. | 14 |
| BLBC →NBLBC | 3 |
| Neg.→Pos. | 8 |
| NBLBC→BLBC | 3 |
| Neg→Neg. | 4 |
| NBLBC→NBLBC | 10 |
| Pos.→Pos. | 31 |
| BLBC→BLBC | 106 |
| *BLBC/NBLBC groups* | |
| Pos→Neg. | 3 |
| BLBC →NBLBC | 0 |
| Neg.→Pos. | 8 |
| NBLBC→BLBC | 1 |
| Neg→Neg. | 7 |
| NBLBC→NBLBC | 1 |
| Pos.→Pos. | 118 |
| BLBC→BLBC | 41 |

*NBLBC, non-basal-like breast cancer; BLBC, basal-like breast cancer; EGFR, epidermal growth factor receptor; CK5/6, cytokeratin5/6; Neg., Negative; Pos., Positive.*

**TABLE 6 |** The relationship between changes of biomarkers and the efficacy of chemotherapy.

| Variables | Grouping | Chemotherapy effect | | p-value |
|---|---|---|---|---|
| | | ORR | NR | |
| CK5/6 | Pos→Neg. | 15 | 3 | 0.676 |
| | Neg.→Pos. | 10 | 3 | |
| EGFR | Pos→Neg. | 12 | 2 | 0.602 |
| | Neg.→Pos. | 6 | 2 | |

*EGFR, epidermal growth factor receptor; CK5/6, cytokeratin5/6; ORR, overall response group; NR, no response group; Neg., Negative; Pos., Positive.*

## DISCUSSION

TNBC presents are with a poor prognosis and is comprised of 7 subtypes including basal-like 1, basal-like 2, mesenchymal, mesenchymal stem-like, immunomodulatory, androgen receptor, and unsatable. While BLBC is usually defined based on gene expression analysis, its actual clinical application is greatly limited due to the complexity and cost of genetic analysis. Many research groups have recommended IHC detection be used in place of the gene chip to diagnose the genetically-defined BLBC, which is a more common type of TNBC accounting for approximately 70–80% of all cases (13). In this study, the BLBC before NAC accounts for 89.7%.

In BLBC, expressions of CK5/6, CK14, and/or CK17 among basal cytokeratins (CKs) are often positive. Thike et al. reported that basal cytokeratin demonstrated significant prognostic value (14). CK5/6 is one of the most commonly expressed cytokeratins in basal-like breast cancer, and it is oftentimes one of the markers detected by immunohistochemistry. Previous studies have shown that 60–70% of all TNBCs is CK5/6-positive, and many studies have also shown that patients with high expression of CK5/6 have a poor prognosis (15–18). EGFR pathway is a complex signal transduction network. In breast cancer, there is usually a disorder of EGFR family kinase activity. Viale and Zhang et al. reported poor prognosis for EGFR-positive breast cancer among all breast cancers (19, 20).

Currently, CK5/6 and EGFR have been widely accepted as biomarkers for the identification of BLBC. Most studies classified BLBC as TNBC with positive expression of CK5/6 and/or EGFR. Additionally, detection of BLBC with these two biomarkers is inexpensive and clinically convenient (7, 21). It has been reported that a combination of high expression in CK5/6 and EGFR in addition to expression of Ki-67, cT (tumor stage), and cN for stratification has great clinical significance (18). Further, there is a statistically significant association between the CK5/6 and/or EGFR expression and the presence of tumor necrosis, which provide the clue of exploratory study on the molecular mechanisms of how CK5/6 and EGFR impact on prognosis of TNBC (22).

For locally advanced breast cancer patients that either have large tumor size, in late stage, or cannot receive surgery, the tumor is usually taken out by coarse needle puncture. Neoadjuvant chemotherapy scheme is then selected based on the results of IHC in order to reduce the size of primary tumor and the stage such that the patients can keep the breast or eventually receive surgery (21, 23). Patients with locally advanced TNBC have a worse prognosis and a lower survival rate. There are currently no randomized controlled clinical studies demonstrating whether the use of NAC in TNBC subtypes can improve patient outcomes. Therefore, the expression of EGFR and CK5/6 were classified and their ability to predict the chemotherapy response and survival rate of NAC was evaluated.

We used CK5/6 and EGFR expression to divide TNBC cases into NBLBC and BLBC groups, of which CK5/6 and EGFR positive expressions accounted for 70.7 and 87.1%, respectively, and double expression was found in 68.2% (133/195) of all cases. We analyzed patients' response to NAC, in which 29.2% of TNBC patients who received anthracyclines combined with or sequential taxane achieved pCR. Liedtke et al. (24) found that 22% of patients with triple-negative breast cancer achieved pCR while Fisher et al. (25) reported a similar rate of 17% in which 26 patients achieved pCR among 151 TNBC patients receiving neoadjuvant chemotherapy (17%). The slight variance between these results can be easily explained by the differences in the NAC schemes used in these studies. While Hiroko Masuda and Rouzier et al. reported that the pCR rate of the non-base-like phenotype is higher than that of the basal-like phenotype (2, 26), our results showed that there is no significant difference in the achievement of pCR between the NBLBC and BLBC. This inconsistency could be explained by the small sample size

**TABLE 7** | Prognostic value of clinicopathological variables in predicting disease free survival of 138 patients using Cox univariate and multivariate models.

| Variables | Cox Univariate analysis (DFS) | | Cox multivariate analysis (DFS) | |
|---|---|---|---|---|
| | p-value | HR (95%CI) | p-value | HR (95%CI) |
| ***Pre NAV*** | | | | |
| Tumor stage (cT) | 0.010 | 1.139–2.555 | 0.057 | – |
| Ki-67 (<20/≥20) | 0.542 | 0.255–13.453 | | |
| p53 (+/–) | 0.973 | 0.52–1.883 | | |
| CK5/6 (+/–) | 0.950 | 0.538–1.937 | | |
| EGFR (+/–) | 0.875 | 0.453–2.533 | | |
| BLBC/NBLBC | 0.275 | 0.595–6.196 | | |
| Histological grades | 0.001 | 1.174–1.782 | 0.016 | 1.056–1.696 |
| ***Post NAC*** | | | | |
| Ki-67 (<20/≥20) | 0.779 | 0.532–2.324 | | |
| p53 (+/–) | 0.813 | 0.456–1.851 | | |
| CK5/6 (+/–) | 0.036 | 1.06–5.337 | 0.041 | 1.035–5.381 |
| EGFR (+/–) | 0.177 | 0.748–4.853 | | |
| BLBC/NBLBC | 0.190 | 0.519–27.459 | | |
| ORR/NR | 0.0151 | 1.581–5.534 | 0.023 | 1.11–3.98 |
| ypT | <0.001 | 1.381–2.393 | 0.009 | 1.112–2.083 |
| ypN | <0.001 | 1.436–2.289 | 0.001 | 1.237–2.065 |

*EGFR, epidermal growth factor receptor; CK5/6, cytokeratin5/6; ORR, overall response group; NR, no response group; NBLBC, non-basal-like breast cancer; BLBC, basal-like breast cancer; ypT, post neoadjuvant chemotherapy Tumor; ypN, post neoadjuvant chemotherapy Lymph note.*

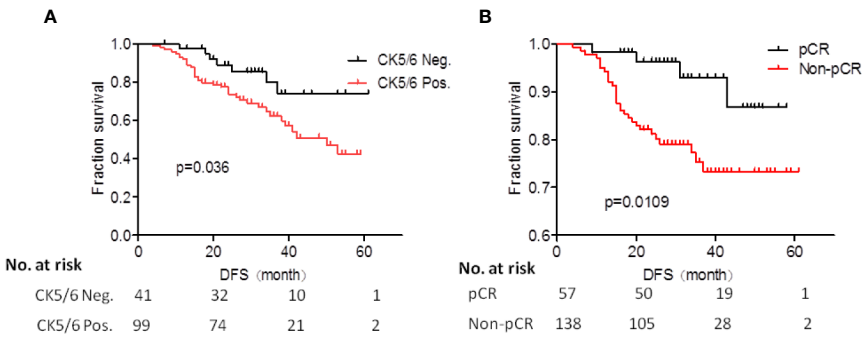


**FIGURE 1** | **(A)** Prognostic analysis of CK5/6 expression after neoadjuvant chemotherapy (NAC) treatment of studied patients. **(B)** K-M survival analysis of pCR and non-pCR patients.

(only 20 of the NBLBC). At the same time, univariate and multivariate logistic analysis in our study showed that cT is an independent factor that affects the efficacy of chemotherapy.

Our data also confirmed that approximately 86.2% of all patients with TNBC had clinical response to NAC. DFS rate in patients with chemotherapy response to ORR was significantly higher than that in patients with poor response (NR) ($p$=0.0151). At the same time, we demonstrated that DFS in patients that achieved pCR was significantly higher than that in non-pCR group, which is consistent with most studies: pCR achievement is a prognostic factor in patients receiving NAC (25, 27, 28).

We used univariate and multivariate COX model to analyze the impact of clinical pathology variables on long-term prognosis. CK5/6 expression after NAC showed a significant correlation with prognosis (p=0.036). In other words, although we verified that chemotherapeutic drugs did cause significant changes in CK5/6, EGFR, and Ki-67, p53 expression (**Table 4**), patients with positive expression of CK5/6 after NAC still showed worse prognosis than patients with negative expression. The results also showed that pCR achievement, chemotherapy response, histological grades, ypT, and ypN are all also factors affecting prognosis.

We further analyzed whether change in biomarkers affects prognosis before and after chemotherapy. We used the changes to group, and the final results showed that changes in CK5/6 and EGFR after NAC did not show a significant effect on the prognosis (p<0.05). We reasoned this is due to too few cases in the group with change in biomarkers (**Table 5**). It is also worth to note that there is a limitation of the study that other genetic backgrounds including BRCA1/2 mutations, ATM mutation and family history should be revealed to exclude genetic basis with CK5/6 and EGFR as prognostic markers. However, we would still like to point out that based on the K-M analysis, prognosis of the CK5/6 or EGFR positive-to-negative group was improved compared with the (positive-to-positive) and (negative-to-

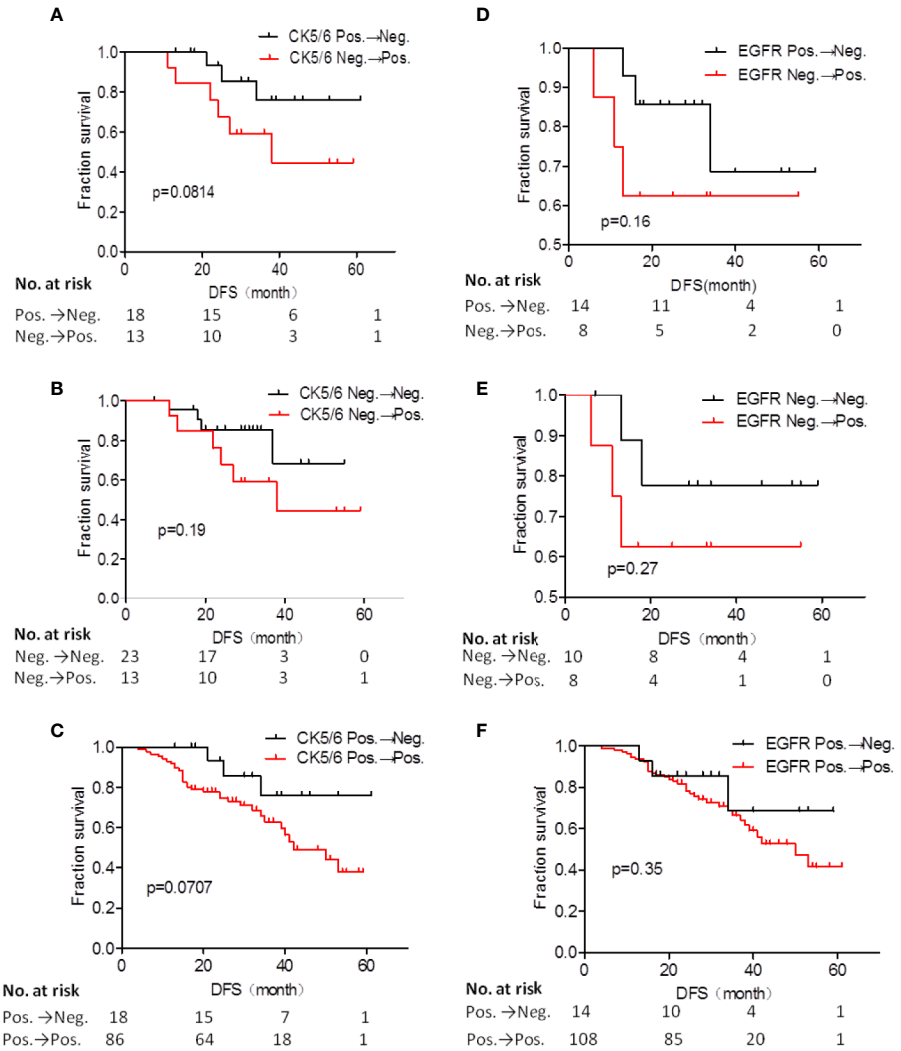


**FIGURE 2** | Disease free survival (DFS) analysis of CK5/6 **(A–C)** and EGFR **(D–F)** expression before and after NAC affected prognosis.

positive) groups. Together, these observations suggest that changes of CK5/6 or EGFR expression from positive to negative after NAC is correlated with improved prognosis and larger sample size is needed for further validation.

## CONCLUSIONS

In sum, we have demonstrated that late- stage TNBC patients receiving NAC that achieved pCR had a better prognosis than those in non-pCR in the population of patients we studied. Although the final results did not confirm whether changes in the expressions of EGFR and CK5/6 can be used to predict the survival rate of TNBC patients, changes of the two biomarkers from positive to negative are strongly indicative of an improved prognosis. While a larger number of TNBC cases are needed to further confirm our results, it will be interesting for future studies to research drugs targeting CK5/6 and EGFR as they may aid efforts towards developing the best individualized treatment options for patients.

## DATA AVAILABILITY STATEMENT

The raw data supporting the conclusions of this article will be made available by the authors, without undue reservation.

## ETHICS STATEMENT

The studies involving human participants were reviewed and approved by Medical Ethics Committee of Tianjin Medical University Cancer Institute and Hospital. The patients/

participants provided their written informed consent to participate in this study. Written informed consent was obtained from the individual(s) for the publication of any potentially identifiable images or data included in this article.

## AUTHOR CONTRIBUTIONS

ZW performed the data analyses and was involved in the writing and editing of this article. LL contributed to analysis and wrote the manuscript. YL, ZS, YJ, and ZF helped perform the analysis with constructive discussions. SZ contributed to the conception and design. All authors agree to be accountable for the content of the work. All authors contributed to the article and approved the submitted version.

## FUNDING

This work was supported by the National Natural Science Foundation of China [81672623] and Tianjin Science and Technology Committee [19YFZCSY00030].

## REFERENCES

1. Lund MJ, Trivers KF, Porter PL, Coates RJ, Leyland-Jones B, Brawley OW, et al. Race and triple negative threats to breast cancer survival: a population-based study in Atlanta, GA. *Breast Cancer Res Treat* (2009) 113:357–70. doi: 10.1007/s10549-008-9926-3
2. Masuda H, Baggerly KA, Wang Y, Zhang Y, Gonzalez-Angulo AM, Meric-Bernstam F, et al. Differential response to neoadjuvant chemotherapy among 7 triple-negative breast cancer molecular subtypes. *Clin Cancer Res* (2013) 19:5533–40. doi: 10.1158/1078-0432.CCR-13-0799
3. Alluri P, Newman LA. Basal-like and triple-negative breast cancers: searching for positives among many negatives. *Surg Oncol Clin N Am* (2014) 23:567–77. doi: 10.1016/j.soc.2014.03.003
4. Kutomi G, Ohmura T, Suzuki Y, Kameshima H, Shima H, Takamaru T, et al. Clinicopathological characteristics of basal type breast cancer in triple-negative breast cancer. *J Cancer Ther* (2012) 3:836–40. doi: 10.4236/jct.2012.325106
5. Yarden Y, Sliwkowski MX. Untangling the ErbB signaling network. *Nat Rev Mol Cell Biol* (2001) 2:127–37. doi: 10.1038/35052073
6. Da Silva L, Clarke C, Lakhani SR. Demystifying basal-like breast carcinomas. *J Clin Pathol* (2007) 60:1328–32. doi: 10.1136/jcp.2006.041731
7. Cheang MC, Voduc D, Bajdik C, Leung S, McKinney S, Chia SK, et al. Basal-Like Breast Cancer Defined by Five Biomarkers Has Superior prognostic Value than Triple-Negative Phenotype. *Clin Cancer Res* (2008) 14:1368–76. doi: 10.1158/1078-0432.CCR-07-1658
8. Carey LA, Dees EC, Sawyer L, Gatti L, Moore DT, Collichio F, et al. The triple negative paradox: primary tumor chemosensitivity of breast cancer subtypes. *Clin Cancer Res* (2007) 13:2329–34. doi: 10.1158/1078-0432.CCR-06-1109
9. Cortazar P, Zhang L, Untch M, Mehta K, Costantino JP, Wolmark N, et al. Pathological complete response and long-term clinical benefit in breast cancer: the CTNeoBC pooled analysis. *Lancet* (2014) 384:164–72. doi: 10.1016/S0140-6736(13)62422-8
10. Von Minckwitz G, Untch M, Blohmer JU, Costa SD, Eidtmann H, Fasching PA, et al. Definition and impact of pathologic complete response on prognosis after neoadjuvant chemotherapy in various intrinsic breast cancer subtypes. *J Clin Oncol* (2012) 30:1796–804. doi: 10.1016/S0140-6736(13)62422-8
11. Wu K, Yang Q, Liu Y, Wu A, Yang Z. Meta-analysis on the association between pathologic complete response and triple-negative breast cancer after neoadjuvant chemotherapy. *World J Surg Oncol* (2014) 12:95. doi: 10.1186/1477-7819-12-95
12. Dowsett M, Nielsen TO, A'Hern R, Bartlett J, Coombes RC, Cuzick J, et al. Assessment of Ki67 in breast cancer: recommendations from the International Ki67 in Breast Cancer working group. *J Natl Cancer Inst* (2011) 103:1656–64. doi: 10.1093/jnci/djr393
13. Prat A, Adamo B, Cheang MC, Anders CK, Carey LA and Perou CM. Molecular Characterization of Basal-Like and Non-Basal-Like Triple-Negative Breast Cancer. *Oncologist* (2013) 18:123–33. doi: 10.1634/theoncologist.2012-0397
14. Thike AA, Iqbal J, Cheok PY, Chong AP, Tse GM, Tan B, et al. Triple Negative Breast Cancer: Outcome Correlation With Immunohistochemical Detection of Basal Markers. *Am J Surg Pathol* (2010) 34:956–64. doi: 10.1097/PAS.0b013e3181e02f45
15. Nielsen TO, Hsu FD, Jensen K, Cheang M, Karaca G, Hu Z, et al. Immunohistochemical and clinical characterization of the basal-like subtype of invasive breast carcinoma. *Clin Cancer Res* (2004) 10:5367–74. doi: 10.1158/1078-0432.CCR-04-0220
16. Livasy CA, Karaca G, Nanda R, Tretiakova MS, Olopade OI, Moore DT, et al. Phenotypic evaluation of the basal-like subtype of invasive breast carcinoma. *Mod Pathol* (2006) 19:264–71. doi: 10.1038/modpathol.3800528
17. Thike AA, Cheok PY, Jara-Lazaro AR, Tan B, Tan P and Tan PH. Triple-negative breast cancer: clinicopathological characteristics and relationship with basal-like breast cancer. *Mod Pathol* (2010) 23:123–33. doi: 10.1038/modpathol
18. Abdelrahman AE, Rashed HE. Abdelgawad M and Abdelhamid MI. prognostic impact of EGFR and cytokeratin 5/6 immunohistochemical expression in triple-negative breast cancer. *Ann Diagn Pathol* (2017) 28:43–53. doi: 10.1016/j.anndiagpath
19. Viale G, Rotmensz N, Maisonneuve P, Bottiglieri L, Montagna E, Luini A, et al. Invasive ductal carcinoma of the breast with the "triple-negative" phenotype: prognostic implications of EGFR immunoreactivity. *Breast Cancer Res Treat* (2009) 116:317–28. doi: 10.1007/s10549-008-0206-z
20. Zhang M, Zhang X, Zhao S, Wang Y, Di W, Zhao G, et al. prognostic value of survivin and EGFR protein expression in triple-negative breast cancer (TNBC) patients. *Target Oncol* (2014) 9:349–57. doi: 10.1007/s11523-013-0300-y
21. Fisher B, Bryant J, Wolmark N, Mamounas E, Brown A, Fisher ER, et al. Effect of preoperative chemotherapy on the outcome of women with operable breast cancer. *J Clin Oncol* (1998) 16:2672–85. doi: 10.1200/JCO.1998.16.8.2672
22. Rao C, Shetty J, Prasad KHL. Immunohistochemical Profile and Morphology in Triple – Negative Breast Cancers. *J Clin Diagn Res* (2013) 7:7. doi: 10.7860/JCDR/2013/5823.3129
23. Wolmark N, Wang J, Mamounas E, Bryant J and Fisher B. Preoperative chemotherapy in patients with operable breast cancer: nine-year results from National Surgical Adjuvant Breast and Bowel Project B-18. *J Natl Cancer Inst Monogr* (2001) 30:96–102. doi: 10.1093/oxfordjournals.jncimonographs.a003469
24. Liedtke C, Mazouni C, Hess KR, André F, Tordai A, Mejia JA, et al. Response to neoadjuvant therapy and long-term survival in patients with triple-negative breast cancer. *J Clin Oncol* (2008) 26:1275–81. doi: 10.1200/JCO.2007.14.4147
25. Fisher CS, Ma CX, Gillanders WE, Aft RL, Eberlein TJ, Gao F, et al. Neoadjuvant chemotherapy is associated with improved survival compared with adjuvant chemotherapy in patients with triple-negative breast cancer only after complete pathologic response. *Ann Surg Oncol* (2012) 19:253–8. doi: 10.1245/s10434-011-1877-y
26. Rouzier R, Perou CM, Symmans WF, Ibrahim N, Cristofanilli M, Anderson K, et al. Breast Cancer Molecular Subtypes Respond Differently to Preoperative Chemotherapy. *Clin Cancer Res* (2005) 11:5678–85. doi: 10.1158/1078-0432.CCR-04-2421
27. Brown JR, Di Giovanna MP, killelea B, Lannin DR3, Rimm DL. Quantitative assessment Ki-67 score for prediction of response to neoadjuvant chemotherapy in breast cancer. *Lab Invest* (2014) 94:98–106. doi: 10.1038/labinvest.2013.128

28. Shao Z, Chaudhri S, Guo M, Zhang L and Rea D. Neoadjuvant Chemotherapy in Triple Negative Breast Cancer: An Observational Study. *Oncol Res* (2016) 23:291–302. doi: 10.3727/096504016x14562725373879

**Conflict of Interest:** The authors declare that the research was conducted in the absence of any commercial or financial relationships that could be construed as a potential conflict of interest.

frontiers in Oncology

ORIGINAL RESEARCH
published: 08 February 2021
doi: 10.3389/fonc.2020.636549

# Construction and Validation of Nomograms Predicting Survival in Triple-Negative Breast Cancer Patients of Childbearing Age

*Xiang Cui*, Deba Song and Xiaoxu Li*

*Department of Thyroid and Breast Surgery, The First People's Hospital of Shangqiu, Shangqiu, China*

**Background:** Triple-negative breast cancer (TNBC) is one of the most aggressive subtypes of breast cancer with poorest clinical outcomes. Patients of childbearing age have a higher probability of TNBC diagnosis, with more demands on maintenance and restoration of physical and psychosocial function. This study aimed to design effective and comprehensive nomograms to predict survival in these patients.

**Methods:** We used the SEER database to identify patients with TNBC aged between 18 and 45 and randomly classified these patients into a training (n=2,296) and a validation (n=2,297) cohort. Nomograms for estimating overall survival (OS) and breast cancer-specific survival (BCSS) were generated based on multivariate Cox proportional hazards models and competing-risk models in the training cohort. The performances of the nomograms were quantified in the validation cohort using calibration curves, time-dependent receiver operating characteristic (ROC) curves and Harrell's concordance index (C-index).

**Results:** A total of 4,593 TNBC patients of childbearing age were enrolled. Four prognostic factors for OS and six for BCSS were identified and incorporated to construct nomograms. In the validation cohort, calibration curves showed excellent agreement between nomogram-predicted and actual survival data. The nomograms also achieved relatively high Harrell's C-indexes and areas under the time-dependent ROC curves for estimating OS and BCSS in both training and validation cohorts.

**Conclusions:** Independent prognostic factors were identified, and used to develop nomograms to predict OS and BCSS in childbearing-age patients with TNBC. These models could enable individualized risk estimation and risk-adapted treatment for these patients.

**Keywords: nomogram, triple-negative breast cancer, overall survival, breast cancer-specific survival, SEER, prognosis, prediction, childbearing age**

OPEN ACCESS

***Edited by:***
*Yi-Zhou Jiang,*
*Fudan University, China*

***Reviewed by:***
*Zhi-Ming Shao,*
*Fudan University, China*
*Gen-Hong Di,*
*Fudan University, China*

****Correspondence:***
*Xiang Cui*
*xiangcui223@163.com*

***Specialty section:***
*This article was submitted to Women's Cancer, a section of the journal Frontiers in Oncology*

***Received:*** *01 December 2020*
***Accepted:*** *21 December 2020*
***Published:*** *08 February 2021*

***Citation:***
*Cui X, Song D and Li X (2021) Construction and Validation of Nomograms Predicting Survival in Triple-Negative Breast Cancer Patients of Childbearing Age. Front. Oncol. 10:636549. doi: 10.3389/fonc.2020.636549*

## INTRODUCTION

Breast cancer is the most prevalent malignancy among females, which ranks first in new cases and second in deaths according to estimation from the American Cancer Society in 2019 (1). And as of 2019, there were more than 3.8 million women with a history of invasive breast cancer in the United States (2). Triple-negative breast cancer (TNBC) is a subset of breast cancer that lacks expression of estrogen receptor (ER), progesterone receptor (PR), and human epidermal growth factor receptor 2 (HER2). TNBC represents one of the most aggressive subtypes of breast cancer and remains the most challenging subtype to treat (3). The proportion of patients of childbearing age was higher in TNBC than in other breast cancer subtypes (4), and childbearing females were also more likely to be diagnosed with TNBC than with the other subtypes (5). In addition, childbearing-age patients have relatively different demographics and clinicopathologic characteristics and treatment strategies compared with patients in other physiological stages (6–8). Childbearing age refers to nearly 30 years after a woman reaches the age of 18. In this period, the reproductive and endocrine functions of the ovaries attained full growth or maturity, and the mammary glands undergo periodic changes under the regulation of ovarian hormones. The ovarian dysfunction, delayed childbearing, inability to breastfeed, and job changes, which may result from cancer treatment, have a tremendous impact on the physical, psychosocial well-being of these patients, resulting a reduction of disability adjusted life years (DALYs) (9–12). Therefore, it is of great significance to differentiate these patients with different risk of death, especially breast cancer specific death, and implement different treatment strategies.

With the increased use of neoadjuvant chemotherapy in TNBC patients, pathologic response has been recognized as an important prognostic factor (13). However, neoadjuvant has adverse therapeutic effects and takes time, which have an impact on the childbearing patients' willingness to treatment (14). Even worse, some non-pathologic responding patients do not benefit from it and may delay prompt treatment. So, if the level of risk can be identified based on other characteristics, it will facilitate the identification and implementation of a tailored treatment. Our previous study described the molecular characteristics of TNBC patients of childbearing age, which provide a rationale for clinical management (15). However, in clinical practice, clinicopathologic characteristics are more accessible for clinicians than molecular profiling. Thus, the urgent clinical need for risk estimation prompted us to construct a clinicopathological information-based model for predicting survival in childbearing-age TNBC patients.

Nomograms are reliable and effective tools to quantify individual risk by incorporating and illustrating multiple important prognostic factors. They performed well in predicting survival in a variety of cancer types (16). In addition to nomogram for all four subtypes of breast cancer (17), researchers established specific nomograms for different histological subtypes (18–23), clinical subtypes (24–26), metastatic status (27–30), and age group (31–35) of breast cancer. However, to the best of our knowledge, nomograms for predicting the survival of childbearing-age patients with TNBC have not been reported. In this study, we aimed to formulate comprehensive nomograms based on complete clinical data selected from the Surveillance, Epidemiology, and End Results (SEER) database to estimate survival in TNBC patients of childbearing age.

## MATERIALS AND METHODS

### Data Source and Patient Screening

Data were extracted from the SEER*Stat version 8.3.6.1, SEER 18 Cancer Registry [1976-2016] (with additional treatment fields) of the National Cancer Institute. The following criteria were used to identify eligible patients: female gender; age of 18–45 years at diagnosis; diagnosed between 2010 and 2015; pathologically confirmed invasive ductal carcinoma of the breast (ICD-O-3 8500/3); diagnosis confirmed by positive histology and not by autopsy or a death certificate; breast cancer as the first and only primary tumor; unilateral breast cancer; adjusted AJCC stage I-III; histological grade I-III; known tumor size; known regional lymph nodes status; and ER, PR, and HER2 negativity. Since the HER2 status was not recorded in the database until 2010, patients diagnosed before 2010 were not included. Patients diagnosed after 2015 were also excluded to ensure adequate follow-up time. Exclusion criteria were as follows: no record of regional lymph node status or tumor size; Paget's disease and inflammatory breast cancer; incomplete survival data and unspecified tumor laterality or location information; survival month less than 1. Eventually, 4,593 patients were included after the screening. The following data were collected and transformed into categorical variables: age, race, marital status, laterality, grade, location, tumor size, positive lymph nodes, breast surgery, radiation, and chemotherapy.

### Identification of Prognostic Factors in the Training Cohort

Patients were randomly classified into a training and a validation cohort at a 1:1 ratio (36). The primary endpoint were overall survival (OS) and breast cancer-specific survival (BCSS). OS was defined as the interval from breast cancer diagnosis to the last follow-up or death from any cause. BCSS was define as the interval from the time of diagnosis to last follow-up or death from breast cancer. Independent prognostic factors for OS were identified by multivariate Cox proportional hazards models, and the results were reported using hazard ratios (HRs) and 95% confidence intervals (CIs). The cumulative incidence rates of breast cancer specific death (CIBCSD) were calculated based on competing-risk models, and differences among groups were assessed by the Gray's test (37, 38). In the competing-risk regression model, deaths from non-breast cancer specific causes were considered as competing risks.

## Model Construction in the Training Cohort

Two nomograms were constructed to predict survival in the training cohort (39). Independent prognostic factors in multivariate Cox proportional hazards models were used to construct the nomogram for 3- and 5-year OS. Factors associated with CIBCSD in the competing-risk models were used to build the BCSS nomogram. The BCSS nomogram was also constructed based on the Cox regression model, in which patients succumbing to non-breast cancer specific causes were considered to be censored.

## Model Validation in Both Cohorts

The nomograms were validated in both training and validation cohorts. First, the predictive accuracies of the nomograms were validated by bootstrapping with 1000 repetitions, and the discriminative ability was quantified by the concordance index (C-index). The C-index ranges from 0.5 (occurring by random chance) to 1.0 (perfectly correct discrimination). Second, calibration curves were generated to obtain nomogram-predicted survival, which is then compared with the corresponding Kaplan-Meier estimates. Third, according to the nomogram, we calculated the total points for all patients (40). The predictive precision of the risk score as a continuous variable was evaluated by time-dependent receiver operating characteristic (ROC) curves, and areas under the curves (AUCs) were used as the criterion (41). The ROC curves plotted the predictive sensitivity and specificity; a larger AUC (range 0.5~1.0) reflected a more accurate prediction. Finally, to demonstrate the clinical values of the nomograms that included all meaningful variables, two normal TNBC patients were assessed as examples.

## Statistical Analysis

All statistical analyses were performed with STATA (version 14.1) and R (version 3.6.1). The R packages including caret, rms, cmprsk, survivalROC, and nomogramFormula were used. Statistical significance was defined as $P < 0.05$.

# RESULTS

## Patient Characteristics

A total of 4,593 patients from the SEER program were enrolled in our study. The demographics and clinicopathologic characteristics of these patients are listed in **Table 1**. Among these patients, median follow-up months were 37 months (25%–75%, 22–58 months). Nearly half of them were aged between 40 and 45 (45.8%), while those between 35 and 40 (29.0%), and less than 35 (25.2%) composed the remaining half. Most of the patients were white (69.4%) and more than half of the patients were unmarried (58.8%). All assessed factors showed similar distribution between the training and validation cohorts.

**TABLE 1** | Patients' demographics and clinicopathologic characteristics.

| | All patients N=4,593 (%) | Training cohort N=2,296 (%) | Validation cohort N=2,297 (%) |
|---|---|---|---|
| **Median follow-up months (IQR)** | | 37 (22–58) | |
| **Age (years)** | | | |
| ≤ 35 | 1158 (25.2) | 571 (24.9) | 587 (25.6) |
| 35–40 | 1331 (29.0) | 670 (29.2) | 661 (28.8) |
| 40–45 | 2104 (45.8) | 1055 (45.9) | 1049 (45.7) |
| **Race** | | | |
| White | 3188 (69.4) | 1571 (68.4) | 1617 (70.4) |
| Black | 915 (19.9) | 471 (20.5) | 444 (19.3) |
| Others[#] | 490 (10.7) | 254 (11.1) | 236 (10.3) |
| **Marital status[$]** | | | |
| Married | 1892 (41.2) | 952 (41.5) | 940 (40.9) |
| Unmarried | 2701 (58.8) | 1344 (58.5) | 1357 (59.1) |
| **Laterality** | | | |
| Left | 2355 (51.3) | 1179 (51.4) | 1176 (51.2) |
| Right | 2238 (48.7) | 1117 (48.6) | 1121 (48.8) |
| **Grade** | | | |
| I | 24 (0.5) | 14 (0.6) | 10 (0.4) |
| II | 426 (9.3) | 211 (9.2) | 215 (9.4) |
| III | 4143 (90.2) | 2071 (90.2) | 2072 (90.2) |
| **Location*** | | | |
| Central | 95 (2.1) | 50 (2.2) | 45 (2.0) |
| Inner | 910 (19.8) | 439 (19.1) | 471 (20.5) |
| Outer | 2167 (47.2) | 1111 (48.4) | 1056 (46.0) |
| Tail | 41 (0.9) | 21 (0.9) | 20 (0.9) |
| Overlap | 1380 (30.0) | 675 (29.4) | 705 (30.7) |
| **Tumor Size (cm)** | | | |
| ≤ 2 | 1510 (32.9) | 746 (32.5) | 764 (33.3) |
| 2–5 | 2455 (53.5) | 1222 (53.2) | 1233 (53.7) |
| > 5 | 628 (13.7) | 328 (14.3) | 300 (13.1) |
| **Positive lymph nodes** | | | |
| 0 | 2752 (59.9) | 1370 (59.7) | 1382 (60.2) |
| 1–3 | 1017 (22.1) | 526 (22.9) | 491 (21.4) |
| > 3 | 824 (17.9) | 400 (17.4) | 424 (18.5) |
| **Breast Surgery** | | | |
| BCS | 1924 (41.9) | 934 (40.7) | 990 (43.1) |
| Mastectomy | 2669 (58.1) | 1362 (59.3) | 1307 (56.9) |
| **Radiation** | | | |
| Yes | 2144 (46.7) | 1062 (46.3) | 1082 (47.1) |
| No | 2449 (53.3) | 1234 (53.7) | 1215 (52.9) |
| **Chemotherapy** | | | |
| Yes | 4183 (91.1) | 2091 (91.1) | 2092 (91.1) |
| No/Unknown | 410 (8.9) | 205 (8.9) | 205 (8.9) |

[#]*American Indian/AK Native, Asian/Pacific Islander.*

[$]*Unmarried included single (never married), widowed, separated, divorced, and unmarried or domestic partner.*

**Central, codes C50.0 and C50.1; Inner, codes C50.2 and C50.3; Outer, codes C50.4 and C50.5; Tail, code C50.6; Overlap, codes C50.8 and C50.9. From SEER Coding Guidelines Breast 2018 manual, coding guideline breast C500–C509.*

*BCS, breast conservation surgery; IQR, interquartile range.*

## Factors Associated With Overall Survival in the Training Cohort

In univariate Cox analysis, race, marital status, tumor location, tumor size, number of positive lymph nodes and breast surgery type were significantly correlated with OS (all $P < 0.001$ except for race and breast surgery, with $P = 0.009$ and $P = 0.003$, respectively). These prognostic factors were included in multivariate Cox analysis. The results confirmed that unmarried status, overlapped tumor location, large tumor, and more positive lymph nodes were independent adverse prognostic factors (**Table 2**). These variables were included in a weighted scoring system to estimate 3- and 5-year OS.

**TABLE 2 |** Univariate and multivariate analyses of overall survival in the training cohort.

| | Training cohort | | |
|---|---|---|---|
| | **Univariate P value** | **Multivariate HR (95% CI)** | **P value** |
| **Age (years)** | 0.762 | | |
| ≤ 35 | | | |
| 35–40 | | | |
| 40–45 | | | |
| **Race** | **0.009** | | |
| White | | Ref. | - |
| Black | | 1.06 (0.83–1.37) | 0.621 |
| Others[#] | | 0.73 (0.50–1.08) | 0.114 |
| **Marital status[$]** | **<0.001** | | |
| Married | | Ref. | - |
| Unmarried | | 1.49 (1.19–1.85) | **<0.001** |
| **Laterality** | 0.637 | | |
| Left | | | |
| Right | | | |
| **Grade** | 0.134 | | |
| I | | | |
| II | | | |
| III | | | |
| **Location*** | **<0.001** | | |
| Central | | 1.51 (0.90–2.55) | 0.190 |
| Inner | | 0.92 (0.67–1.26) | 0.594 |
| Outer | | Ref. | - |
| Tail | | 0.62 (0.15–2.55) | 0.503 |
| Overlap | | 1.22 (1.03–1.81) | **0.045** |
| **Tumor Size (cm)** | **<0.001** | | |
| ≤ 2 | | 0.62 (0.46–0.82) | **0.001** |
| 2–5 | | Ref. | – |
| >5 | | 2.02 (1.59–2.57) | **<0.001** |
| **Positive lymph nodes** | **<0.001** | | |
| 0 | | Ref. | – |
| 1–3 | | 2.54 (1.94–3.32) | **<0.001** |
| > 3 | | 4.47 (3.44–5.82) | **<0.001** |
| **Breast Surgery** | **0.003** | | |
| BCS | | Ref. | – |
| Mastectomy | | 1.20 (0.96–1.51) | 0.111 |
| **Radiation** | 0.169 | | |
| Yes | | | |
| No | | | |
| **Chemotherapy** | 0.782 | | |
| Yes | | | |
| No/Unknown | | | |

[#]*American Indian/AK Native, Asian/Pacific Islander.*

[$]*Unmarried included single (never married), widowed, separated, divorced, and unmarried or domestic partner.*

**Central, codes C50.0 and C50.1; Inner, codes C50.2 and C50.3; Outer, codes C50.4 and C50.5; Tail, code C50.6; Overlap, code C50.8. From SEER Coding Guidelines Breast 2018 manual, coding guideline breast C500–C509.*

*BCS, breast conservation surgery; CI, confidence interval; HR, hazard ratio; Ref., Reference.*

**TABLE 3 |** Three- and 5-year cumulative incidence rates of death among patients in the training cohort.

| | Cumulative incidence of breast cancer-specific death | | | Cumulative incidence of non-breast cancer-specific death | | |
|---|---|---|---|---|---|---|
| | **3-year** | **5-year** | **P value** | **3-year** | **5-year** | **P value** |
| **Age (years)** | | | 0.586 | | | 0.627 |
| ≤ 35 | 0.147 | 0.173 | | 0.013 | 0.016 | |
| 35–40 | 0.162 | 0.216 | | 0.009 | 0.016 | |
| 40–45 | 0.131 | 0.192 | | 0.010 | 0.024 | |
| **Race** | | | **0.006** | | | 0.383 |
| White | 0.133 | 0.187 | | 0.001 | 0.023 | |
| Black | 0.192 | 0.246 | | 0.011 | 0.015 | |
| Others[#] | 0.122 | 0.142 | | 0.004 | 0.004 | |
| **Marital status[$]** | | | **<0.001** | | | 0.210 |
| Married | 0.113 | 0.153 | | 0.009 | 0.017 | |
| Unmarried | 0.188 | 0.253 | | 0.014 | 0.023 | |
| **Laterality** | | | 0.688 | | | 0.813 |
| Left | 0.137 | 0.200 | | 0.014 | 0.019 | |
| Right | 0.152 | 0.190 | | 0.007 | 0.021 | |
| **Grade** | | | 0.368 | | | 0.643 |
| I | 0.000 | 0.000 | | 0.000 | 0.000 | |
| II | 0.123 | 0.190 | | 0.014 | 0.034 | |
| III | 0.147 | 0.197 | | 0.010 | 0.018 | |
| **Location*** | | | **<0.001** | | | 0.958 |
| Central | 0.293 | 0.378 | | 0.021 | 0.021 | |
| Inner | 0.099 | 0.148 | | 0.005 | 0.019 | |
| Outer | 0.134 | 0.187 | | 0.011 | 0.022 | |
| Tail | 0.056 | 0.134 | | 0.000 | 0.000 | |
| Overlap | 0.182 | 0.227 | | 0.012 | 0.015 | |
| **Tumor Size (cm)** | | | **<0.001** | | | 0.665 |
| ≤ 2 | 0.065 | 0.093 | | 0.009 | 0.017 | |
| 2–5 | 0.133 | 0.191 | | 0.011 | 0.020 | |
| >5 | 0.356 | 0.432 | | 0.015 | 0.024 | |
| **Positive lymph nodes** | | | **<0.001** | | | 0.356 |
| 0 | 0.059 | 0.099 | | 0.006 | 0.019 | |
| 1–3 | 0.203 | 0.265 | | 0.013 | 0.016 | |
| > 3 | 0.359 | 0.428 | | 0.022 | 0.026 | |
| **Breast Surgery** | | | **<0.001** | | | 0.474 |
| BCS | 0.111 | 0.146 | | 0.010 | 0.015 | |
| Mastectomy | 0.166 | 0.227 | | 0.011 | 0.022 | |
| **Radiation** | | | 0.088 | | 0.395 | 0.395 |
| Yes | 0.166 | 0.216 | | 0.009 | 0.016 | |
| No | 0.125 | 0.176 | | 0.012 | 0.023 | |
| **Chemotherapy** | | | 0.444 | | | **0.001** |
| Yes | 0.146 | 0.199 | | 0.009 | 0.015 | |
| No/Unknown | 0.125 | 0.162 | | 0.024 | 0.058 | |
| All Patients | 0.144 | 0.195 | | 0.011 | 0.020 | |

[#]*American Indian/AK Native, Asian/Pacific Islander.*

[$]*Unmarried included single (never married), widowed, separated, divorced, and unmarried or domestic partner.*

**Central, codes C50.0 and C50.1; Inner, codes C50.2 and C50.3; Outer, codes C50.4 and C50.5; Tail, code C50.6; Overlap, code C50.8. From SEER Coding Guidelines Breast 2018 manual, coding guideline breast C500–C509.*

*BCS, breast conservation surgery.*

## Factors Associated With Breast Cancer-Specific Survival in the Training Cohort

To identify prognostic factors associated with BCSS, we determined CIBCSD and cumulative incidence of non-breast cancer specific death (CINBCSD) based on the developed competing-risk models. At 3 and 5 years after diagnosis, CIBCSD rates in the training cohort were 0.144 and 0.195, respectively, while CINBCSD rates were 0.011 and 0.020, respectively. Estimates of CIBCSD and other causes according to the clinicopathological variables are shown in **Table 3**. Black patients had the highest CIBCSD (0.192 and 0.246 for 3 and 5 years, respectively), while white and patients of other race had lower CIBCSD (white, 0.133 and 0.187 for 3 and 5 years, respectively; other race, 0.122 and 0.142 for 3 and 5 years, respectively; P = 0.006). Other factors significantly associated with CIBCSD are marital status, tumor size, tumor location, lymph node status, and surgery type (all P < 0.001). All these

factors were used to construct a nomogram to predict 3- and 5-year BCSS.

## Nomograms

Based on the prognostic factors identified in the training cohort, nomograms were formulated to predict 3- and 5-year OS and BCSS (**Figure 1**). To clarify the applications of these nomograms, two representative TNBC patients were assessed. Both patients were married, underwent surgery, and diagnosed with grade III, invasive ductal carcinoma with outer location. The first patient was a 36-year-old white patient diagnosed with a tumor of 1.5 cm in diameter and without positive lymph node, while the second was a 37-year-old patient of other race (American Indian/AK Native, Asian/Pacific Islander) diagnosed with a tumor of 5.5 cm in diameter and with 5 positive lymph nodes. According to the nomograms, the first patient scored 59.1 and 47.9 in the OS and BCSS nomograms, respectively, which indicated that her odds of 3- and 5-year OS were greater than 0.85, and those of 3- and 5-year BCSS were greater than 0.95. Scores of the second patient in OS and BCSS nomograms were 214.3 and 205.1, respectively, which indicated that the odds of both 3- and 5-year OS and BCSS were less than 0.7. These results can help to guide individualized treatment for these two patients.

## Model Validation

Nomogram validation was processed in both the training and validation cohorts. In the training cohort, the Harrell's C-indexes for the nomograms for predicting OS and BCSS were 0.766 and 0.776, respectively. In the validation cohort, the C-indexes were slightly lower, i.e., 0.763 and 0.765, respectively (**Table S1**). The external and internal calibration curves were shown in **Figure 2** and **Figure S1**, which demonstrated an excellent agreement between the actual and nomogram-predicted survival rates. The time-dependent ROC curves for predicting 3- and 5-year OS and BCSS in the training and validation cohorts were presented in **Figure 3**. With the risk score as a continuous variable, the AUCs for 3- and 5-year OS and BCSS predictions were all above 0.74. These results demonstrated that the nomograms were useful tools for the prediction of survival in TNBC patients of childbearing age.

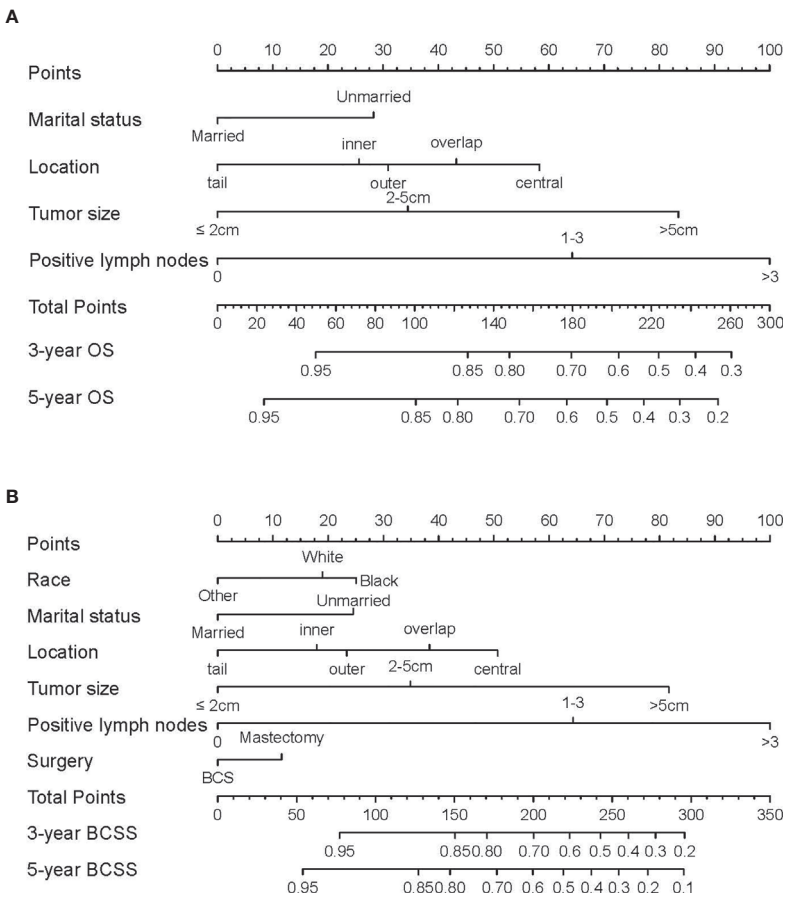


**FIGURE 1** | Nomograms predicting 3- and 5-year **(A)** overall survival (OS) and **(B)** breast cancer-specific survival (BCSS) in TNBC patients of childbearing age. Instructions for nomogram use were as follows. First, assign points to each characteristic for a given patient by drawing a vertical line from that variable to the points scale. Then, sum all the points and draw a vertical line from the total points scale to the 3- and 5-year OS or BCSS to obtain the likelihood of 3- or 5-year survival.

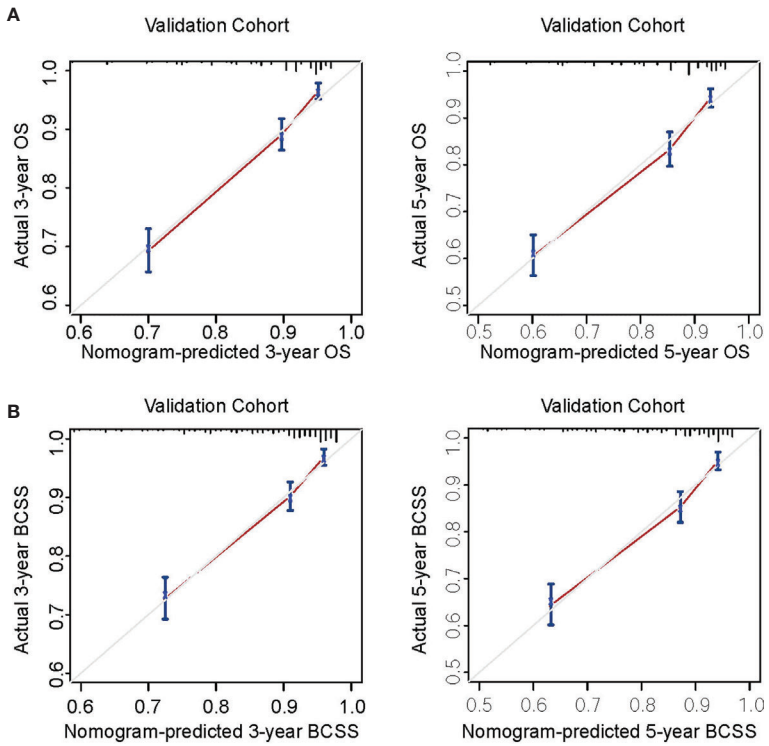


**FIGURE 2** | Calibration curves for external validation. **(A)** Nomogram calibration curves for 3- and 5-year overall survival (OS). **(B)** Nomogram calibration curves for 3- and 5-year breast cancer-specific survival (BCSS). X-axis, nomogram-predicted survival; Y-axis, actual survival.

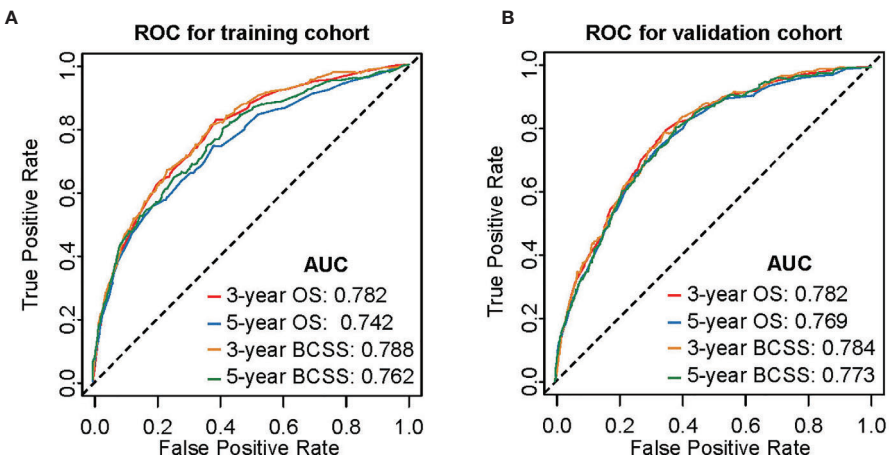


**FIGURE 3** | Time-dependent receiver operating characteristic (ROC) curves for predicting 3- and 5-year OS and BCSS. **(A)** Internal validation in the training cohort. **(B)** External validation in the validation cohort. AUC, area under curve; OS, overall survival; BCSS, breast cancer-specific survival.

## DISCUSSION

In the light of the relatively high mobility and invasiveness of tumor, strong desire to preserve and restore physiological and social functions, high requirements for quality of life, and unique clinicopathological features of TNBC patients of childbearing age, a brief nomogram based on follow-up data of a large cohort for predicting OS and BCSS should be quite practical in clinic. Although nomograms predicting survival of patients with TNBC or of a specific age group have been reported (20, 22, 31–33, 35), there is no nomogram for TNBC patients of childbearing age, a period of highly active physiological and social function.

Using data from the SEER program, we established reliable nomograms to predict the 3- and 5-year OS and BCSS of these patients based on Cox regression and competing-risk models. The calibration curves, time-dependent ROC analysis and Harrell's C-indexes demonstrated satisfactory performances of our nomograms. Therefore, our nomograms can be used for personalized risk prediction and to guide treatment for TNBC patients of childbearing age.

In the current study, several demographics and clinicopathologic characteristics were shown to be prognosis factors of 3- and 5-year OS and BCSS, including marital status, tumor location, tumor size, number of positive lymph nodes, race and surgery, corroborating previous studies of TNBC patients (42–46). The primary tumor site is considered as an important independent prognostic factor of breast cancer, and several studies have shown that tumor location in lower inner zone suggests a poor prognosis (47, 48). In the univariate analysis of OS in the training cohort, OS was significantly different among the five groups of tumor location. In multivariate analysis, though only the "overlap" site was significantly associated with poor prognosis, the hazard ratios of various groups confirmed the impact of tumor location on OS. Therefore, this factor was incorporated in the nomogram for predicting OS. As for BCSS, different groups of location were significantly different in CIBCSD and showed no differences in CINBCSD, indicating that tumor location is a significant prognosis factor of breast cancer-specific death. According to the CIBCSD of each group, we developed a scoring system to qualify the risk caused by tumor location. Previous studies have shown higher incidence of TNBC among black women compared with other races, which is determined by biological differences and socioeconomic factors (45, 49). In addition, African ethnicity is a significant and independent predictor of poor outcome (50). In this study, race was a significant but not independent prognosis factor of OS. However, regarding BCSS, black women had higher CIBCSD compared with white and "other" patients. Therefore, race was included in our scoring system for BCSS prediction but not for OS prediction.

Despite the above strengths, there were some limitations in this study. First, the undetailed data of adjuvant chemotherapy and radiotherapy in the SEER database cannot distinguish "no treatment" and "unknown if patients received treatment", which were combined into a group in our study. Moreover, the lack of information on neoadjuvant therapy in SEER database made it impossible to evaluate the relationship between neoadjuvant therapy and survival in this paper. Some other proven prognostic factors of breast cancer in childbearing age, including breastfeeding, adiposity, and oral contraceptive use (51), were also not available in the SEER database. Although more detailed treatment information is available in other databases, i.e., the National Cancer Database (NCDB) database, we chose SEER as our data source because NCDB is a hospital-based rather than population-based database without available BCSS data (52–54). Second, breast cancer that occurs in patients before the age of 45 has a higher potential to result from hereditary causes. Patients with hereditary breast cancer have a higher risk of recurrence and death. However, because of the lack of genetic data in SEER datasets, we cannot incorporate this important factor into our nomograms, which may lead to predictive bias. Third, patients with incomplete clinical information or survival data were excluded from this study, which could result in selection bias. Further, limited by its single data source and retrospective nature, the nomograms should be further validated in other cohorts, and a prospective research should be performed before its clinical application.

## CONCLUSION

We developed nomograms to predict OS and BCSS in TNBC patients of childbearing age based on a relatively large cohort with detailed follow-up. The nomograms had excellent performances in both training and validation cohorts. It may serve as an efficient tool for clinicians to predict the prognosis of these patients and to guide individualized treatment.

## DATA AVAILABILITY STATEMENT

The original contributions presented in the study are included in the article/**Supplementary Materials**; further inquiries can be directed to the corresponding author.

## ETHICS STATEMENT

Since the data were from the SEER database, informed patient consent and ethical approval were not required.

## AUTHOR CONTRIBUTIONS

XC conceptualized the work, collected, analyzed, and interpreted the date, drafted the article, critically revised the article, and gave the final approval of the version to be published. DS and XL conceptualized the work, critically revised the article, and gave the final approval of the version to be published. All authors contributed to the article and approved the submitted version.

## FUNDING

This work was supported by grants from the Training Plan of Excellent Talents of The First People's Hospital of Shangqiu (SQFPH2019). The funder had no role in the study design, data collection and analysis, decision to publish, or preparation of the manuscript.

## SUPPLEMENTARY MATERIAL

The Supplementary Material for this article can be found online at: https://www.frontiersin.org/articles/10.3389/fonc.2020.636549/full#supplementary-material

## REFERENCES


1. Siegel RL, Miller KD, Jemal A. Cancer statistics, 2019. *CA: A Cancer J Clin* (2019) 69(1):7–34. doi: 10.3322/caac.21551
2. DeSantis CE, Ma J, Gaudet MM, Newman LA, Miller KD, Goding Sauer A, et al. Breast cancer statistics, 2019. *CA: Cancer J Clin* (2019) 69(6):438–51. doi: 10.3322/caac.21583
3. Garrido-Castro AC, Lin NU, Polyak K. Insights into Molecular Classifications of Triple-Negative Breast Cancer: Improving Patient Selection for Treatment. *Cancer Discov* (2019) 9(2):176–98. doi: 10.1158/2159-8290.Cd-18-1177
4. Sajid MT, Ahmed M, Azhar M, Mustafa QU, Shukr I, Ahmed M, et al. Age-related frequency of triple negative breast cancer in women. *J Coll Physicians Surgeons–Pakistan JCPSP* (2014) 24(6):400–3.
5. Scott LC, Mobley LR, Kuo T-M, Il'yasova D. Update on triple-negative breast cancer disparities for the United States: A population-based study from the United States Cancer Statistics database, 2010 through 2014. *Cancer* (2019) 125(19):3412–7. doi: 10.1002/cncr.32207
6. Aapro M, Wildiers H. Triple-negative breast cancer in the older population. *Ann Oncol* (2012) Suppl 6:vi52–5. doi: 10.1093/annonc/mds189
7. Liedtke C, Hess KR, Karn T, Rody A, Kiesel L, Hortobagyi GN, et al. The prognostic impact of age in patients with triple-negative breast cancer. *Breast Cancer Res Treat* (2013) 138(2):591–9. doi: 10.1007/s10549-013-2461-x
8. Plichta JK, Thomas SM, Vernon R, Fayanju OM, Rosenberger LH, Hyslop T, et al. Breast cancer tumor histopathology, stage at presentation, and treatment in the extremes of age. *Breast Cancer Res Treat* (2020) 180(1):227–35. doi: 10.1007/s10549-020-05542-4
9. Lambertini M, Goldrat O, Clatot F, Demeestere I, Awada A. Controversies about fertility and pregnancy issues in young breast cancer patients: current state of the art. *Curr Opin Oncol* (2017) 29(4):243–52. doi: 10.1097/cco.0000000000000380
10. Paluch-Shimon S, Pagani O, Partridge AH, Abulkhair O, Cardoso MJ, Dent RA, et al. ESO-ESMO 3rd international consensus guidelines for breast cancer in young women (BCY3). *Breast* (2017) 35:203–17. doi: 10.1016/j.breast.2017.07.017
11. Oktay K, Harvey BE, Partridge AH, Quinn GP, Reinecke J, Taylor HS, et al. Fertility Preservation in Patients With Cancer: ASCO Clinical Practice Guideline Update. *J Clin Oncol* (2018) 36(19):1994–2001. doi: 10.1200/jco.2018.78.1914
12. Christinat A, Pagani O. Fertility after breast cancer. *Maturitas* (2012) 73(3):191–6. doi: 10.1016/j.maturitas.2012.07.013
13. Murphy BL, Day CN, Hoskin TL, Habermann EB, Boughey JC. Neoadjuvant Chemotherapy Use in Breast Cancer is Greatest in Excellent Responders: Triple-Negative and HER2+ Subtypes. *Ann Surg Oncol* (2018) 25(8):2241–8. doi: 10.1245/s10434-018-6531-5
14. Rosenberg SM, Newman LA, Partridge AH. Breast Cancer in Young Women: Rare Disease or Public Health Problem? *JAMA Oncol* (2015) 1(7):877–8. doi: 10.1001/jamaoncol.2015.2112
15. Ma D, Jiang YZ, Xiao Y, Xie MD, Zhao S, Jin X, et al. Integrated molecular profiling of young and elderly patients with triple-negative breast cancer indicates different biological bases and clinical management strategies. *Cancer* (2020) 126(14):3209–18. doi: 10.1002/cncr.32922
16. Balachandran VP, Gonen M, Smith JJ, DeMatteo RP. Nomograms in oncology: more than meets the eye. *Lancet Oncol* (2015) 16(4):e173–80. doi: 10.1016/s1470-2045(14)71116-7
17. Chu JL, Yang DH, Wang L, Xia JL. Nomograms predicting survival for all four subtypes of breast cancer: a SEER-based population study. *Ann Trans Med* (2020) 8(8):544. doi: 10.21037/atm-20-2808
18. Luo CX, Zhong XR, Wang Z, Wang Y, Wang YP, He P, et al. Prognostic nomogram for patients with non-metastatic HER2 positive breast cancer in a prospective cohort. *Int J Biol Markers* (2019) 34(1):41–6. doi: 10.1177/1724600818824786
19. Li D, Zhong CH, Cheng Y, Zhu N, Tan YN, Zhu LZ, et al. A Competing Nomogram to Predict Survival Outcomes in Invasive Micropapillary Breast Cancer. *J Cancer* (2019) 10(27):6801–12. doi: 10.7150/jca.27955
20. Guo LW, Jiang LM, Gong Y, Zhang HH, Li XG, He M, et al. Development and validation of nomograms for predicting overall and breast cancer-specific survival among patients with triple-negative breast cancer. *Cancer Manage Res* (2018) 10:5881–94. doi: 10.2147/cmar.S178859
21. Ye FG, Xia C, Ma D, Lin PY, Hu X, Shao ZM. Nomogram for predicting preoperative lymph node involvement in patients with invasive micropapillary carcinoma of breast: a SEER population-based study. *BMC Cancer* (2018) 18(1):1085. doi: 10.1186/s12885-018-4982-5
22. Dai DJ, Jin HC, Wang X. Nomogram for predicting survival in triple-negative breast cancer patients with histology of infiltrating duct carcinoma: a population-based study. *Am J Cancer Res* (2018) 8(8):1576–85.
23. Sun W, Jiang YZ, Liu YR, Ma D, Shao ZM. Nomograms to estimate long-term overall survival and breast cancer-specific survival of patients with luminal breast cancer. *Oncotarget* (2016) 7(15):20496–506. doi: 10.18632/oncotarget.7975
24. Diao JD, Ma LX, Sun MY, Wu CJ, Wang LJ, Liu YL, et al. Construction and validation of a nomogram to predict overall survival in patients with inflammatory breast cancer. *Cancer Med* (2019) 8(12):5600–8. doi: 10.1002/cam4.2470
25. Zhang HG, Ma GF, Du SS, Sun J, Zhang Q, Yuan BY, et al. Nomogram for predicting cancer specific survival in inflammatory breast carcinoma: a SEER population-based study. *Peerj* (2019) 7:e7659. doi: 10.7717/peerj.7659
26. Pan XX, Yang W, Chen YF, Tong LH, Li CR, Li H. Nomogram for predicting the overall survival of patients with inflammatory breast cancer: A SEER-based study. *Breast* (2019) 47:56–61. doi: 10.1016/j.breast.2019.05.015
27. Zhao W, Wu L, Zhao AD, Zhang M, Tian Q, Shen YW, et al. A nomogram for predicting survival in patients with de novo metastatic breast cancer: a population-based study. *BMC Cancer* (2020) 20(1):982. doi: 10.1186/s12885-020-07449-1
28. Xiong Y, Cao H, Zhang YQ, Pan Z, Dong SY, Wang GSY, et al. Nomogram-Predicted Survival of Breast Cancer Brain Metastasis: a SEER-Based Population Study. *World Neurosurg* (2019) 128:E823–E34. doi: 10.1016/j.wneu.2019.04.262
29. Wang Z, Cheng YG, Chen S, Shao HY, Chen XW, Wang ZN, et al. Novel prognostic nomograms for female patients with breast cancer and bone metastasis at presentation. *Ann Trans Med* (2020) 8(5):197. doi: 10.21037/atm.2020.01.37
30. Lin ZH, Yan SC, Zhang JY, Pan Q. A Nomogram for Distinction and Potential Prediction of Liver Metastasis in Breast Cancer Patients. *J Cancer* (2018) 9(12):2098–106. doi: 10.7150/jca.24445
31. Gong Y, Ji P, Sun W, Jiang YZ, Hu X, Shao ZM. Development and Validation of Nomograms for Predicting Overall and Breast Cancer-Specific Survival in Young Women with Breast Cancer: A Population-Based Study. *Transl Oncol* (2018) 11(6):1334–42. doi: 10.1016/j.tranon.2018.08.008
32. Lu X, Li X, Ling H, Gong Y, Guo L, He M, et al. Nomogram for Predicting Breast Cancer-Specific Mortality of Elderly Women with Breast Cancer. *Med Sci Monit* (2020) 26:e925210. doi: 10.12659/MSM.925210
33. Sun Y, Li Y, Wu J, Tian H, Liu H, Fang Y, et al. Nomograms for prediction of overall and cancer-specific survival in young breast cancer. *Breast Cancer Res Treat* (2020) 184(2):597–613. doi: 10.1007/s10549-020-05870-5
34. Li X, Dai D, Chen B, He S, Zhang J, Wen C, et al. Prognostic Values Of Preoperative Serum CEA And CA125 Levels And Nomograms For Young Breast Cancer Patients. *Onco Targets Ther* (2019) 12:8789–800. doi: 10.2147/OTT.S221335
35. Lin H, Zhang F, Wang L, Zeng. Use of clinical nomograms for predicting survival outcomes in young women with breast cancer. *Oncol Lett* (2019) 17(2):1505–16. doi: 10.3892/ol.2018.9772
36. Kuhn M. caret: Classification and Regression Training. (2020). Available at: https://cran.r-project.org/web/packages/caret/index.html.
37. Gray R. A Class of $K$-Sample Tests for Comparing the Cumulative Incidence of a Competing Risk. *Ann Stat* (1988) 16:1141–54. doi: 10.1214/aos/1176350951
38. Gary B. cmprsk: Subdistribution Analysis of Competing Risk. (2014). Available at: https://cran.r-project.org/web/packages/cmprsk/index.html.
39. Harrell Jr FE. rms: Regression Modeling Strategies. (2017). Available at: https://cran.r-project.org/web/packages/rms/index.html.
40. Zhang J, Jin Z. nomogramFormula: Calculate Total Points and Probabilities for Nomogram. (2020). Available at: https://cran.r-project.org/web/packages/nomogramFormula/index.html.
41. Patrick J. Heagerty and packaging by Paramita Saha-Chaudhuri. survivalROC: Time-dependent ROC curve estimation from censored survival data. (2013). Available at: https://cran.r-project.org/web/packages/survivalROC/index.html.

42. Yu KD, Jiang YZ, Chen S, Cao ZG, Wu J, Shen ZZ, et al. Effect of large tumor size on cancer-specific mortality in node-negative breast cancer. *Mayo Clinic Proc* (2012) 87(12):1171–80. doi: 10.1016/j.mayocp.2012.07.023
43. Falagas ME, Zarkadoulia EA, Ioannidou EN, Peppas G, Christodoulou C, Rafailidis PI. The effect of psychosocial factors on breast cancer outcome: a systematic review. *Breast Cancer Res BCR* (2007) 9(4):R44. doi: 10.1186/bcr1744
44. Carter CL, Allen C, Henson DE. Relation of tumor size, lymph node status, and survival in 24,740 breast cancer cases. *Cancer* (1989) 63(1):181–7. doi: 10.1002/1097-0142(19890101)63:1<181::aid-cncr2820630129>3.0.co;2-h
45. Jemal A, Robbins AS, Lin CC, Flanders WD, DeSantis CE, Ward EM, et al. Factors That Contributed to Black-White Disparities in Survival Among Nonelderly Women With Breast Cancer Between 2004 and 2013. *J Clin Oncol* (2018) 36(1):14–24. doi: 10.1200/jco.2017.73.7932
46. Orecchia R. Breast cancer: post-mastectomy radiotherapy reduces recurrence and mortality. *Nat Rev Clin Oncol* (2014) 11(7):382–4. doi: 10.1038/nrclinonc.2014.95
47. Yang J, Tang S, Zhou Y, Qiu J, Zhang J, Zhu S, et al. Prognostic implication of the primary tumor location in early-stage breast cancer: focus on lower inner zone. *Breast Cancer (Tokyo Japan)* (2018) 25(1):100–7. doi: 10.1007/s12282-017-0797-5
48. Wu S, Zhou J, Ren Y, Sun J, Li F, Lin Q, et al. Tumor location is a prognostic factor for survival of Chinese women with T1-2N0M0 breast cancer. *Int J Surg (London England)* (2014) 12(5):394–8. doi: 10.1016/j.ijsu.2014.03.011
49. Jatoi I, Anderson WF, Rao SR, Devesa SS. Breast cancer trends among black and white women in the United States. *J Clin Oncol* (2005) 23(31):7836–41. doi: 10.1200/jco.2004.01.0421
50. Newman LA, Griffith KA, Jatoi I, Simon MS, Crowe JP, Colditz GA. Meta-analysis of survival in African American and white American patients with breast cancer: ethnicity compared with socioeconomic status. *J Clin Oncol* (2006) 24(9):1342–9. doi: 10.1200/jco.2005.03.3472
51. Chollet-Hinton L, Olshan AF, Nichols HB, Anders CK, Lund JL, Allott EH, et al. Biology and Etiology of Young-Onset Breast Cancers among Premenopausal African American Women: Results from the AMBER Consortium. *Cancer Epidemiol Biomarkers Prev Publ Am Assoc Cancer Research Cosponsored by Am Soc Prevent Oncol* (2017) 26(12):1722–9. doi: 10.1158/1055-9965.Epi-17-0450
52. Mettlin CJ, Menck HR, Winchester DP, Murphy GP. A comparison of breast, colorectal, lung, and prostate cancers reported to the National Cancer Data Base and the Surveillance, Epidemiology, and End Results Program. *Cancer* (1997) 79(10):2052–61. doi: 10.1002/(sici)1097-0142(19970515)79:10<2052::aid-cncr29>3.0.co;2-s
53. Lin CC, Virgo KS, Robbins AS, Jemal A, Ward EM. Comparison of Comorbid Medical Conditions in the National Cancer Database and the SEER-Medicare Database. *Ann Surg Oncol* (2016) 23(13):4139–48. doi: 10.1245/s10434-016-5508-5
54. Janz TA, Graboyes EM, Nguyen SA, Ellis MA, Neskey DM, Harruff EE, et al. A Comparison of the NCDB and SEER Database for Research Involving Head and Neck Cancer. *Otolaryngol Head Neck Surg* (2019) 160(2):284–94. doi: 10.1177/0194599818792205


**Conflict of Interest:** The authors declare that the research was conducted in the absence of any commercial or financial relationships that could be construed as a potential conflict of interest.

frontiers in Oncology

ORIGINAL RESEARCH
published: 16 February 2021
doi: 10.3389/fonc.2020.624493

# GPRC5A Is a Negative Regulator of the Pro-Survival PI3K/Akt Signaling Pathway in Triple-Negative Breast Cancer

*Lu Yang*[1,2,3,4], *Shaorong Zhao*[1,2,3,4], *Tong Zhu*[1,2,3,4] *and Jin Zhang*[1,2,3,4*]

[1] *The Third Department of Breast Cancer, Tianjin Medical University Cancer Institute and Hospital, National Clinical Research Center for Cancer, Tianjin, China,* [2] *Key Laboratory of Cancer Prevention and Therapy, Tianjin Medical University Cancer Institute and Hospital, Tianjin, China,* [3] *Tianjin's Clinical Research Center for Cancer, Tianjin Medical University Cancer Institute and Hospital, Tianjin, China,* [4] *Key Laboratory of Breast Cancer Prevention and Therapy, Tianjin Medical University, Ministry of Education, Tianjin, China*

Breast cancer is one of the most common types of malignancy worldwide; however, its underlying mechanisms remain unclear. In the present study, we investigated the roles of G-protein-coupled receptor family C, member 5, group A (GPRC5A) in cell apoptosis in triple-negative breast cancer (TNBC). The expression of GPRC5A in breast cancer cell lines was detected by real time PCR and western blot. And the results suggested that GPRC5A was downregulated in breast cancer cell lines compared to normal breast epithelial cell lines. Additionally, the expression of GPRC5A in TCGA database was analyzed *in silico*. GPRC5A exhibited the lowest expression levels in TNBC compared to $ER^+$ and $HER2^+$ breast cancer. Overexpression of GPRC5A in MDA-MB-231 and MDA-MB-468 cells promoted apoptosis, whereas depletion of GPRC5A in T47D and MCF7 cells inhibited cell apoptosis *via* the intrinsic apoptotic pathway. We performed RNA-sequencing in GPRC5A overexpressed MDA-MB-231 and the control cells. The results facilitated the identification of a number of signaling pathways involved in this process, and the PI3K/Akt signaling pathway was found to be one the most important. A specific activator of the PI3K/Akt signaling pathway inhibited apoptosis of breast cancer cells, whereas cotreatment of this activator with a GPRC5A-expressing plasmid reduced this effect. Similarly, a specific inhibitor of the PI3K/Akt signaling pathway increased cell apoptosis by activating caspase-3 and caspase-9, whereas co-incubation of the inhibitor with a short hairpin RNA targeting GPRC5A significantly reduced the cell apoptotic rate. Additionally, the overexpression of GPRC5A suppressed tumor growth by inducing cell apoptosis *in vivo*. Taken together, the present study identified GPRC5A as a protective factor against the progression of human triple-negative breast cancer by increasing cell apoptosis *via* the regulation of the PI3K/Akt signaling pathway.

**Keywords: G-protein-coupled receptor family C, member 5, group A (Gprc5a), cell apoptosis, PI3K/Akt, breast cancer, triple-negative breast cancer (TNBC)**

OPEN ACCESS

***Edited by:***
*Yi-Zhou Jiang,*
*Fudan University, China*

***Reviewed by:***
*Yizi Cong,*
*Yantai Yuhuangding Hospital, China*
*Elena Gershtein,*
*Russian Cancer Research Center NN Blokhin, Russia*

****Correspondence:***
*Jin Zhang*
*zhangjintjmuch1@163.com*

***Specialty section:***
*This article was submitted to Women's Cancer, a section of the journal Frontiers in Oncology*

***Received:*** *31 October 2020*
***Accepted:*** *30 December 2020*
***Published:*** *16 February 2021*

***Citation:***
*Yang L, Zhao S, Zhu T and Zhang J (2021) GPRC5A Is a Negative Regulator of the Pro-Survival PI3K/Akt Signaling Pathway in Triple-Negative Breast Cancer. Front. Oncol. 10:624493. doi: 10.3389/fonc.2020.624493*

## INTRODUCTION

Breast cancer is one of the most common diseases among females, with ~200,000 new cases diagnosed every year worldwide, and is a major cause of mortality in females despite age or ethnicity. Triple-negative breast cancer (TNBC) is the most challenging subtype of breast cancer to treat. TNBC refers to breast cancer where the genes encoding estrogen receptor (ER), progesterone receptor and human epidermal growth factor receptor 2 are not upregulated (1). TNBC is poorly differentiated and can migrate and proliferate in distant locations faster compared with other types of breast cancer, which leads to a worse prognosis and a short 5-year survival rate (2, 3). The lack of targetable receptors in TNBC makes targeted therapy an important topic of research and a number of studies are trying to identify novel markers for the treatment and diagnosis of breast cancer.

G-protein-coupled receptor family C, member 5, group A (GPRC5A), also termed retinoic acid-inducible 3, belongs to the largest protein superfamily containing >700 genes within the human genome (4, 5). GPRC5A was first identified in 1998 in numerous types of human cancer, including colon cancer (6), colorectal cancer (7), and pancreatic cancer (8). A high prevalence of GPRC5A germline mutations have been identified in BRCA1-mutant breast cancer (9). Furthermore, GPRC5A has been demonstrated to be a potential therapeutic target (10), and can inhibit epidermal growth factor receptor and its downstream pathway (11). However, the detailed mechanisms underlying the regulatory roles of GPRC5A remain unclear.

Cell apoptosis is a form of programmed cell death that occurs in multicellular organisms (12) and serves significant roles in various types of cancer (13). Our previous researches implicate GPRC5A as a tumor suppressor in breast cancer cells, and GPRC5A exerts its tumor-suppressive function by inhibiting EGFR related cell proliferation. Meanwhile, we found GPRC5A as a tumor suppressor has effect on breast cancer cell apoptosis (11). Thus, the present study aimed to examine whether the role of GPRC5A is associated with cell apoptosis. Cultured breast cancer cells were used in the present study to detect the expression of GPRC5A. RNA-sequencing (RNA-seq) analysis was performed to investigate the detailed mechanism underlying the protective role of GPRC5A. A specific activator and an inhibitor of the PI3K/Akt signaling pathway were also used in the presence or absence of a GPRC5A expressing plasmid or short hairpin RNA (shRNA) targeting GPRC5A (shGPRC5A). The present results suggested a protective role of GPRC5A in human breast cancer and investigated its underlying mechanism, facilitating the development of novel clinical treatments for patients with TNBC.

## MATERIALS AND METHODS

*Cell Culture and Transfection*. The human breast cancer cell lines T47D, MDA-MB-231, MDA-MB-468, MCF7, and SK-BR-3 were purchased from the Cell Bank of Shanghai Biological Institute, Chinese Academy of Science. The breast epithelial cell line MCF10A was obtained from the American Type Culture Collection and was used as control cell line to assess the expression level of GPRC5A. All cell lines were cultured in DMEM (Gibco; Thermo Fisher Scientific, Inc.) supplemented with 10% FBS (Gibco; Thermo Fisher Scientific, Inc.) and maintained at 37˚C with 5% $CO_2$.

Specific shRNAs against GPRC5A were designed and synthesized by Shanghai GenePharm Co., Ltd. and dissolved in 20 μM. The GPRC5A-expressing plasmid was cloned by PCR with *Xho*I and *Hind*III restriction enzymes into pcDNA3.1 and validated by DNA sequencing. Cell transfection was performed with Lipofectamine® 3000 (Invitrogen; Thermo Fisher Scientific, Inc.), according to the manufacturer's protocol. Cells transfected with empty vector or a non-targeting shRNA were used as controls.

SF1670, a specific PTEN inhibitor, and deguelin were used as the activator and inhibitor of the PI3K/Akt signaling pathway, respectively, and both were obtained from Selleck Chemicals and used at a final concentration of 10 μM.

*Reverse Transcription-Quantitative PCR*. Total RNA from cultured breast cancer cells was extracted using TRIzol® reagent (Invitrogen; Thermo Fisher Scientific, Inc.) and quantified with Nanodrop 2000 by measuring the absorbance at 260 and 280 nm. A total of 1 μg RNA was reverse transcribed into cDNA by Prime Script Master mix (Takara Biotechnology Co., Ltd.) according to the manufacturer's protocol. qPCR was performed with SYBR Premix EX Taq TM II (Takara Biotechnology Co., Ltd.) on an ABI 7900 qPCR detection system (Thermo Fisher Scientific, Inc.) with the following conditions: Initial denaturation at 95˚C for 5 min, followed by 45 cycles of 10 s at 95˚C (denaturation), 10 s at 60˚C (primer annealing), and 10 s at 72˚C (elongation), and a final extension step for 10 min at 72˚C. GAPDH was used as the internal reference. Relative mRNA expression levels were calculated using the $2^{-\Delta\Delta Cq}$ method. The following primer sequences were used for the qPCR analysis: GPRC5A forward, 5'-ATGGCTACA ACAGTCCCTGAT-3' and reverse, 5'-CCACCGTTTCTAG GACGATGC-3'; PI3K forward, 5'-GTCCTATTGTCGTG CATGTGG-3' and reverse, 5'-TGGGTTCTCCCAAT TCAACC-3'; Akt forward, 5'-TTCTATGGCGCTGA GATTGTGT-3' and reverse, 5'-GCCGTAGTCATTGTC CTCCAG-3'; mTOR forward, 5'-ATGCTTGGAACCGG ACCTG-3' and reverse, 5'-TCTTGACTCATCTCTCGGAGTT-3'; and GAPDH forward, 5'-GTGGACATCCGCAAAGAC-3' and reverse, 5'-AAAGGGTGTAACGCAACTA-3'.

*Vector Construction, Virus Production, and the Construction of Stable Cell Lines*. The GPRC5A plasmid was purchased in HANHENG Co. (China). Then GPRC5A were amplified by reverse transcription PCR and then inserted into pLV-cDNA-MCS-bsd cloning vector (Biosettia). Lentivirus stocks were produced by transfecting a 4-plasmid system from 293T in accordance with the manufacturer's instruction (Biosettia). The lentivirus stocks were added to MDA-MB-231 cell line for 16h. After 48h, 10 μg/ml blasticidin S was added for 3 days to obtained MDA-MB-231-GPRC5A cell lines.

*Cell Apoptosis Assays*. The annexin V/propidium iodide (PI) assay was performed according to the manufacturer's protocol (Invitrogen; Thermo Fisher Scientific, Inc.). Briefly, MDA-MB-231 and MDA-MB-468 cells were transfected with GPRC5A-expressing plasmid and treated with or without SF1670. In addition, T47D and MCF7 cells were transfected with shGPRC5A in the presence or absence of deguelin. Subsequently, cells were washed twice with pre-cold PBS, trypsinized and re-suspended in 100 µl binding buffer with 2.5 µl FITC-conjugated annexin-V and 1 µl PI (100 µg/ml). Cells were then incubated at room temperature for 15 min in the dark. A total of ~10,000 cells were collected and analyzed with a flow cytometer.

*Relative Caspase Activities*. The relative activities of caspase-3, caspase-8, and caspase-9 were determined using caspase activity kits (cat. nos. C1115, C1151, and C1157, respectively; Beyotime Institute of Biotechnology), according to the manufacturer's protocols. Briefly, MDA-MB-231 and MDA-MB-468 cells were transfected with GPRC5A expressing plasmid with or without SF1670, and T47D and MCF7 cells were treated with shGPRC5A in the presence or absence of deguelin. Subsequently, cell lysates were collected by low speed centrifugation at 1,000 x g for 5 min at 4°C. An equal amount of protein (10 µl) was added into 96-well plates in triplicate and mixed with 80 µl reaction buffer supplemented with caspase substrates (2 mM). Following incubation at 37°C for 4 h, caspase activities were determined at an absorbance of 450 nm.

*Western Blot Assays*. Cells were transfected with shGPRC5A or GPRC5A-expressing plasmid for 48 h and then lysed with RIPA lysis buffer (Beyotime Institute of Biotechnology) and fresh protease inhibitor cocktail (Thermo Fisher Scientific, Inc.). The protein concentration was assessed using a bicinchoninic assay kit (Thermo Fisher Scientific, Inc.), according to the manufacturer's protocol. A total of 40 µg protein extract was loaded into each well of a 12% SDS-PAGE gel and transferred to a nitrocellulose membrane (EMD Millipore). Following blocking with 5% milk, the membranes were incubated with primary antibodies against GPRC5A (cat. no. CSB-PA818781DSR1HU; Cusabio Biotech Co., Ltd.), caspase-3 (cat. no. ab13585; Abcam), caspase-9 (cat. no. ab2324; Abcam), cytochrome C (cat. no. ab13575; Abcam) and GAPDH (cat. no. sc-32233; Santa Cruz Biotechnology, Inc.) overnight. The secondary antibodies were purchased from Santa Cruz Biotechnology, Inc. All antibodies were diluted at a ratio of 1:1,000. Subsequently, proteins were detected using an enhanced chemiluminescence kit (EMD Millipore). The immunoreactive bands were quantified by densitometry with ImageJ software (National Institutes of Health).

*RNA-Seq Analysis*. MDA-MB-231 cells were transfected with or without GPRC5A expressing plasmid for 48 h and total RNA was then extracted for RNA-seq in triplicate. RNA-seq was performed and analyzed by AnNuoNeng Co. Different signaling pathways were investigated and the significant differentially expressed genes ($P<0.05$) were classified into corresponding signaling pathways.

*Tumor Xenograft*. The female NOD/SCID mice at 6–8 weeks were chosen and randomly separated into two groups ($n=5$ each). 2 × 106 cells (MDA-MB-231-MCS and -GPRC5A) were injected subcutaneously into each mouse at the fourth mammary fat pad.

Tumor volume was measured once every 3 days and calculated by the formula: length × width$^2$/2. All animal experiments were conducted according to the standard operating procedures approved by the Institute Research Ethics Committee of Tianjin Medical University Cancer Hospital.

*Immunohistochemistry and TUNEL Assay*. Immunohistochemistry and TUNEL staining were performed using standard protocols with paraffin-embedded mouse xenograft tumors. These tissues were stained using GPRC5A antibody (YT3995, immunoway, 1:1000). TUNEL staining was performed according to the manufacturer's protocol (12156792910, invitrogen).

*Statistical Analysis*. GraphPad Prism 5.0 software (GraphPad Software, Inc.) was used for statistical analysis. Data are presented as the mean ± SD. Two-tailed Student's t-test was used for comparisons between groups, while differences between tumor and adjacent normal control samples were analyzed using a paired Student's t-test. For comparisons among multiple groups (≥3 groups), one-way ANOVA was used followed by Fisher's least significant difference post-hoc test. $P<0.05$ was considered to indicate a statistically significant difference. All experiments were performed in triplicate.

## RESULTS

*GPRC5A Expression Is Downregulated in Human Breast Cancer Cells*. First, the expression of GPRC5A in breast cancer cells was examined. The mRNA expression levels of GPRC5A were significantly lower in breast cancer cells compared with MCF10A control cells (**Figure 1**). Similarly, the protein expression levels of GPRC5A were significantly lower in breast cancer cells compared with the MCF10A (**Figure 1B**). Notably, MDA-MB-231 and MDA-MB-468 cells exhibited the lowest expression levels of GPRC5A, while T47D and MCF7 cells exhibited the highest mRNA expression levels of GPRC5A among the breast cancer cell lines investigated. Therefore, MDA-MB-231 and MDA-MB-468 cells were selected for subsequent overexpression experiments, and T47D and MCF7 cells were selected for knockdown experiments. Additionally, GPRC5A is significantly downregulated in TNBC breast cancer compared to $ER^+$ and $HER2^+$ breast cancer from TCGA database. (**Figure 1**). And Immunohistochemistry staining assay showed the similar results (**Figure S1**). In summary, the present data suggested that GPRC5A was downregulated in human breast cancer, especially in triple negative breast cancer.

*Overexpression of GPRC5A Promotes Cell Apoptosis by Increasing the Activity of the Intrinsic Apoptotic Pathway*. The detailed role of GPRC5A in human breast cancer was then investigated. GPRC5A-expressing plasmid was transfected into MDA-MB-231 and MDA-MB-468 cells. The relative mRNA level of GPRC5A was significantly increased in transfected cells compared with the control cells for both cell lines (**Figure 2**). In

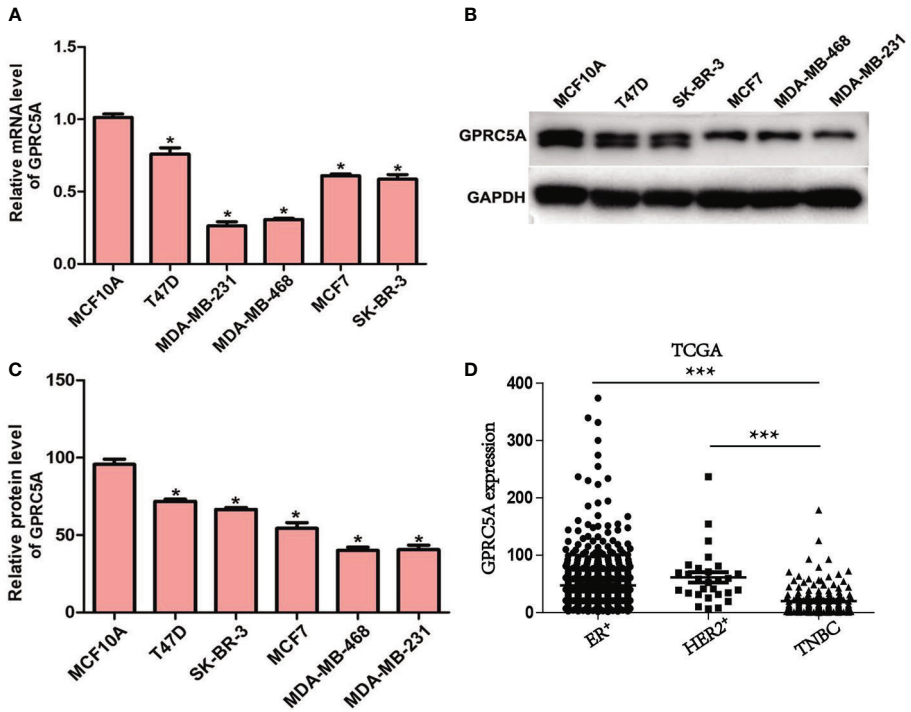


**FIGURE 1** | Expression of GPRC5A is downregulated in human breast cancer. **(A)** Relative mRNA expression levels of GPRC5A were examined in breast cancer cell lines and a control normal breast epithelial cell line using reverse transcription-quantitative PCR. **(B)** Protein expression levels of GPRC5A were examined in cultured human breast cancer cell lines and the control normal breast epithelial cell line MCF10A by western blot analysis. **(C)** Quantification of the western blot analysis results. *$P < 0.05$ vs. MCF10A. GPRC5A, G-protein-coupled receptor family C, member 5, group A. **(D)** The expression of GPRC5A in TNBC was compared to $ER^+$ and $HER2^+$ breast cancer from TCGA database. ***$P < 0.05$.

addition, the cell apoptotic rates were increased by 3.5- and 3-fold following transfection in MDA-MB-231 and MDA-MB-468 cells, respectively (**Figure 2**, **Figure S1**). Cell apoptosis includes two distinct pathways; the intrinsic pathway, where caspase-3 and 9 are the major factors involved in the process, and the extrinsic pathway, where caspase-8 serves a crucial role (14). Following overexpression of GPRC5A in MDA-MB-231 and MDA-MB-468 cells, the relative activities of caspase-3 (**Figure 2**) and caspase-9 (**Figure 2**) were significantly increased compared with the control cells; however, no significant difference was identified in the relative activity of caspase-8 (**Figure 2**). Furthermore, protein expression levels were detected using western blot analysis. The protein expression levels of cleaved-caspase-3, cleaved-caspase-9 and cytochrome C, key molecules involved in the intrinsic pathway of cell apoptosis, were higher in MDA-MB-231 and MDA-MB-468 cells transfected with GPRC5A-expressing plasmid compared with the control cells (**Figure 2**). The present results suggested that overexpression of GPRC5A increased cell apoptosis in MDA-MB-231 and MDA-MB-468 cells.

*Knockdown of GPRC5A Inhibits Cell Apoptosis by Suppressing the Activity of the Intrinsic Apoptotic Pathway*. In addition, the present study performed knockdown of GPRC5A using a specific shRNA and investigated its effects on cell apoptosis. The relative mRNA levels of GPRC5A were significantly decreased in transfected cells compared with control cells (**Figure 3**). In addition, cell apoptosis was significantly suppressed by GPRC5A shRNA in both cell lines (**Figure 3**, **Figure S1**). The relative activities of different caspases were also detected, and the activity of caspase-3 (**Figure 3**) and caspase-9 (**Figure 3**) significantly decreased in the transfected cells compared with the control cells; however, no significant difference in the activity of capase-8 was detected in T47D and MCF7 cells (**Figure 3**). Similarly, the protein expression levels of cleaved-caspase-3, cleaved-caspase-9 and cytochrome C were markedly decreased when T47D and MCF7 cells were transfected with shGPRC5A for 48 h (**Figure 3**). The present data suggested that GPRC5A promoted cell apoptosis *via* the intrinsic apoptotic pathway in human breast cancer cells *in vitro*.

*Overexpression of GPRC5A Inhibits the PI3K/Akt Signaling Pathway in MDA-MB-231 Cells*. The detailed mechanisms underlying the regulatory role of GPRC5A in cell apoptosis were then investigated using RNA-seq techniques. Among all genes that were identified to be differentially expressed in MDA-MB-231 cells transfected with GPRC5A expressing plasmid, those with significant differential expression ($P<0.05$) were selected and their associated signaling pathways were determined. Notably, 18 genes differentially expressed in MDA-MB-231 cells following GPRC5A overexpression were identified to be associated with the PI3K/Akt signaling

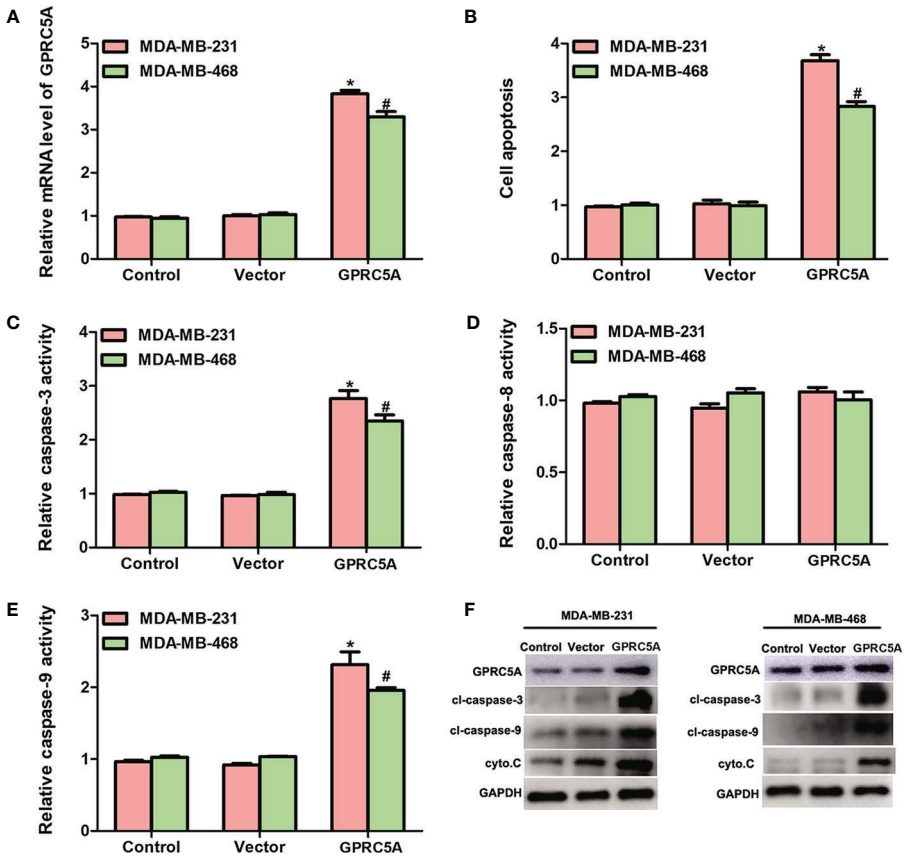


**FIGURE 2** | Overexpression of GPRC5A promotes cell apoptosis by increasing the activity of the intrinsic pathway. **(A)** Relative mRNA expression levels of GPRC5A in MDA-MB-231 and MDA-MB-468 cells transfected with a GPRC5A-overexpressing plasmid. **(B)** Cell apoptotic rates were assessed in MDA-MB-231 and MDA-MB-468 cells transfected with GPRC5A expressing plasmid. **(C)** Relative caspase-3 activity levels were examined in MDA-MB-231 and MDA-MB-468 cells transfected with GPRC5A-expressing plasmid. **(D)** Relative caspase-8 activity levels were evaluated in MDA-MB-231 and MDA-MB-468 cells transfected with GPRC5A expressing plasmid. **(E)** Relative caspase-9 activity levels were examined in MDA-MB-231 and MDA-MB-468 cells transfected with GPRC5A expressing plasmid. **(F)** Western blot analysis was performed to examine the levels of factors associated with the intrinsic pathway of cell apoptosis. *$P$<0.05 vs. control in MDA-MB-231 cells. #$P$<0.05 vs. control in MDA-MB-468 cells. GPRC5A, G-protein-coupled receptor family C, member 5, group A; cyto.C, cytochrome C; cl, cleaved.

pathway (**Figure 4**). These 18 genes were presented in a heat map and it was identified that the expression levels of a number of genes, including B-cell adaptor for phosphoinositide 3-kinase, PI3K and Akt, were downregulated, while numerous genes associated with the PI3K/Akt signaling pathway, including Bad and Bax, were upregulated following overexpression of GPRC5A (**Figure 4**).

*Pharmacologic Interference of the PI3K/Akt Signaling Pathway Reduces the Effects of GPRC5A on Cell Apoptosis in Breast Cancer Cells*. To elucidate the importance of the PI3K/Akt signaling pathway in the regulatory role of GPRC5A, the PTEN inhibitor SF1670 and deguelin were used to activate and inhibit, respectively, the PI3K/Akt signaling pathway. The present results suggested that MDA-MB-231 cells treated with SF1670 exhibited significantly increased mRNA expression levels of PI3K, Akt and mTOR, while cotreatment with SF1670 and GPRC5A-overexpressing plasmid significantly reduced this effect (**Figure 5**). Furthermore, when MCF7 cells were treated with deguelin, the mRNA expression levels of PI3K, Akt and mTOR were significantly decreased, while cotreatment with deguelin and shGPRC5A significantly restored the expression levels of these factors (**Figure 5**). Subsequently, cell apoptosis was examined, and MDA-MB-231 and MDA-MB-468 cells treated with SF1670 presented significantly reduced cell apoptosis (**Figure 5**, **Figure S2**), and decreased activities of caspase-3 (**Figure 5**) and caspase-9 (**Figure 5**). Notably, overexpression of GPRC5A significantly reversed these effects. Similarly, treatment of T47D and MCF7 cells with deguelin significantly increased cell apoptosis (**Figure 5**, **Figure S2**), as well as the activities of caspase-3 (**Figure 5**) and caspase-9 (**Figure 5**), while knockdown of GPRC5A significantly reversed these effects. In summary, the present results suggested that GPRC5A promoted cell apoptosis by regulating the PI3K/Akt signaling pathway in breast cancer cells.

*GPRC5A Inhibited TNBC Tumor Progression In Vivo*. To investigate the role of GPRC5A on TNBC tumor progression, the MDA-MB-231 mouse xenograft was established. Stable MDA-MB-231-MCS and MDA-MB-231-GPRC5A cells were injected subcutaneously. As shown in **Figure 6A**, GPRC5A

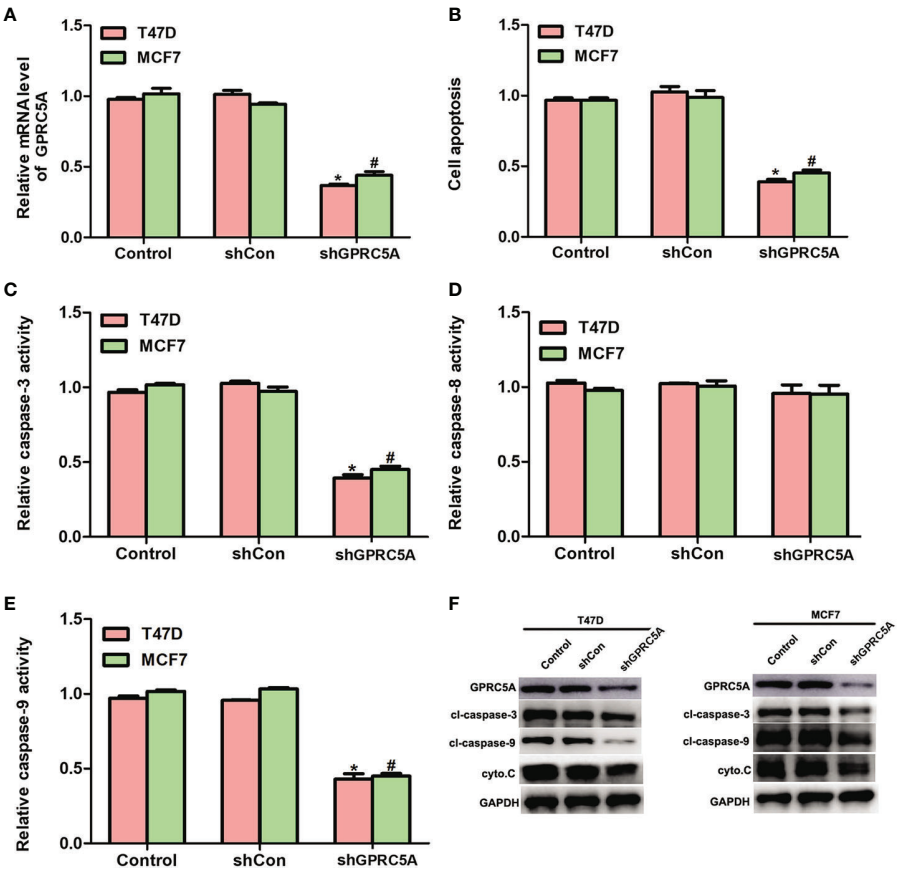


**FIGURE 3** | Knockdown of GPRC5A inhibits cell apoptosis by suppressing the activity of the intrinsic pathway. **(A)** Relative mRNA expression levels of GPRC5A in MDA-MB-231 and MDA-MB-468 cells transfected with shGPRC5A. **(B)** Cell apoptotic rates were assessed in MDA-MB-231 and MDA-MB-468 cells transfected with shRNA against GPRC5A. **(C)** Relative caspase-3 activity levels were examined in MDA-MB-231 and MDA-MB-468 cells transfected with shRNA against GPRC5A. **(D)** Relative caspase-8 activity levels were investigated in MDA-MB-231 and MDA-MB-468 cells transfected with shRNA against GPRC5A. **(E)** Relative caspase-9 activity levels were evaluated in MDA-MB-231 and MDA-MB-468 cells transfected with shRNA against GPRC5A. **(F)** Western blot analysis was performed to examine the levels of proteins associated with the intrinsic pathway of cell apoptosis. $^{*}P < 0.05$ vs. control in MDA-MB-231 cells. $^{\#}P < 0.05$ vs. control in MDA-MB-468 cells. GPRC5A, G-protein-coupled receptor family C, member 5, group A; cyto.C, cytochrome C; cl, cleaved; shCon, small hairpin RNA control; shGPRC5A, GPRC5A small hairpin RNA.

significantly inhibited MDA-MB-231 xenograft tumor growth. The western blot assay showed that upregulated GPRC5A promotes the expression of cleavage-caspase 3, cleavage-caspase 9 and cytochrome C, the markers of apoptosis, *via* suppressing the activity of PI3K/Akt signaling pathway (**Figure 6**). Immunohistochemistry staining and TUNEL assay showed that the upregulation of GPRC5A promoted the apoptosis in mouse xenograft model (**Figure 6**). These results collectively demonstrated that GPRC5A leads to TNBC tumor progression *via* PI3K/Akt pathway *in vivo*.

## DISCUSSION

Breast cancer is one of the most common types of malignancy in females worldwide and affects ~12% of females (15). Breast cancer cases contribute to 22.9% of invasive cancer cases and 16% of all cases of cancer in females (16). According to a European study, 523,000 new cases were diagnosed in 2018 and 138,000 breast cancer-associated mortalities occurred, making the incidence rate of breast cancer one of the highest of all cancer types, with a morbidity rate that ranked third among all cancer types (17). TNBC accounts for 15–25% of all breast cancer cases and the incidence rate is very similar among all age groups (18). Despite significant efforts in the past decades, the 5-year survival rate remains low. Therefore, there is an urgent requirement to identify novel therapeutic methods for the diagnosis and treatment of breast cancer. In the present study, GPRC5A was identified to be downregulated in breast cancer cells. Using an *in silico* assay, a previous study has suggested that GPRC5A is highly expressed in breast cancer, particularly in ER-positive breast cancer compared with the normal breast cancer cell line MCF-10A (19). However, the present results suggested that the expression of GPRC5A was decreased in cultured breast cancer cells, in line with a previous study (11). Other studies have reported that GPRC5A is an orphan G-protein coupled receptor

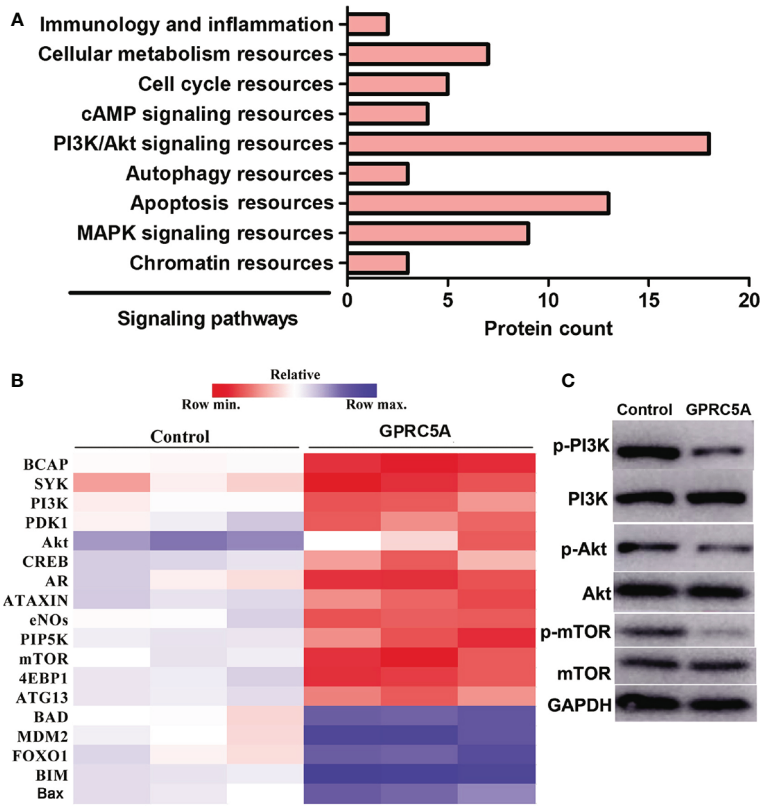


**FIGURE 4** | Overexpression of GPRC5A inhibits the PI3K/Akt signaling pathway in MDA-MB-231 cells. **(A)** RNA-sequencing analysis revealed the top nine signaling pathways associated with the GPRC5A regulatory network in MDA-MB-231 cells transfected with GPRC5A expressing plasmid. **(B)** Heatmap of the 18 differentially expressed proteins that are associated with the PI3K/Akt signaling pathway. Red indicates downregulated and blue indicates upregulated genes. GPRC5A, G-protein-coupled receptor family C, member 5, group A; p-, phosphorylated; MAPK, mitogen-activated protein kinase; BCAP, B-cell adaptor for phosphoinositide 3-kinase; PDK1, phosphoinositide-dependent kinase-1; CREB, CAMP responsive element binding protein; AR, androgen receptor; eNOs, endothelial nitric oxide synthase; PIP5K, phosphatidylinositol-4-phosphate 5-kinase; 4EBP1, eukaryotic translation initiation factor 4E-binding protein 1; ATG13, autophagy-related protein 13; MDM2, mouse double minute 2 homolog; FOXO1, forkhead box protein O1; BIM, Bcl-2-like protein 11. **(C)** Western blot analysis was performed to examine the levels of proteins associated with PI3K/Akt signaling pathway.

with an intriguing dual behavior, acting as an oncogene in certain cancer types and as a tumor suppressor in other cancer types (20). GPRC5A-KO mice was highly associated with lung metastasis and poor prognosis (21, 22). In breast cancer, GPRC5A has been reported to be downregulated and was identified to act as a tumor suppressor by RhoA/C (23) and EGFR related signaling pathway (11). GPRC5A could be a malignant biomarker in breast cancer progression. Thus, the role and mechanism of GPRC5A in breast cancer, especially in different breast cancer subtypes, still need elucidated for further application of GPRC5A as a prospective clinical target.

Since cell apoptosis is an irreversible process, it is highly regulated (24). Apoptosis can be divided into two pathways; in the intrinsic pathway, apoptosis occurs following intracellular stresses, while in the extrinsic pathway, apoptosis occurs following extrinsic signals (25). In the intrinsic pathway, cytochrome C is released from the mitochondria and binds to apoptotic protease activating factor-1 and ATP, forming a complex that binds to pro-caspase-9 and forms an apoptosome, which cleaves pro-caspase-9 to its active form caspase-9, which activates the effector caspase-3 (26). In total, two theories of the extrinsic pathway have been suggested; the tumor necrosis factor-induced model and the Fas-Fas ligand-mediated model, the former of which involves the activation of caspase-8 (27). The present study identified that overexpression of GPRC5A promoted apoptosis and the activities of caspase-3 and caspase-9, while knockdown of GPRC5A inhibited these processes. These results suggested that GPRC5A affected cell apoptosis *via* the intrinsic pathway.

The PI3K/Akt signaling pathway is an intracellular signaling pathway that is directly associated with cell proliferation, tumorigenesis, cellular quiescence, longevity and apoptosis (28). Briefly, PI3K activation phosphorylates and activates Akt, leading to its translocation to the plasma membrane and the subsequent activation of its downstream genes, including CAMP responsive element binding protein, forkhead box O and mTOR (29). Using RNA-seq analysis, the expression levels of 18 genes associated with the PI3K/Akt signaling pathway were identified to be significantly altered following GPRC5A overexpression in MDA-MB-231 cells. Therefore, the PI3K/Akt signaling pathway was selected for

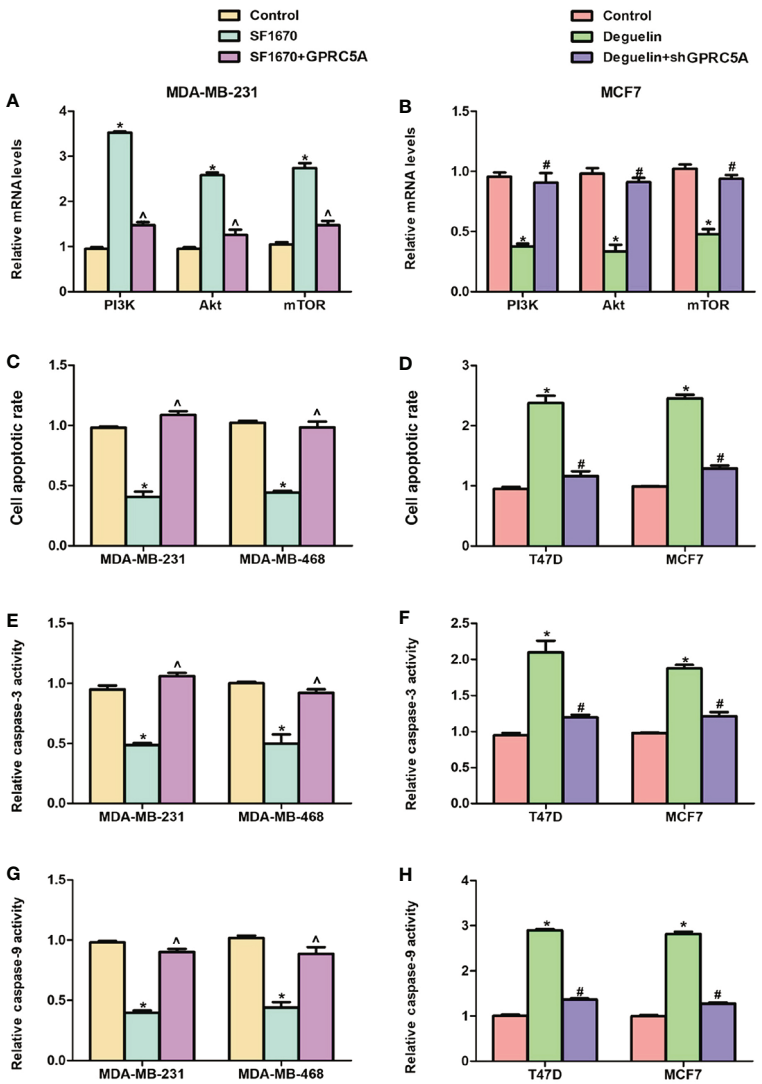


**FIGURE 5** | Interference of the PI3K/Akt signaling pathway reverses the effects of GPRC5A on cell apoptosis in breast cancer cells. **(A)** Relative mRNA expression levels of PI3K, Akt and mTOR in MDA-MB-231 cells treated with SF1670 in presence or absence of GPRC5A. **(B)** Relative mRNA expression levels of PI3K, Akt and mTOR in MCF7 cells treated with deguelin in the presence or absence of shGPRC5A. **(C)** Cell apoptosis was assessed in MDA-MB-231 and MDA-MB-468 cells following treatment with SF1670 with or without GPRC5A overexpression. **(D)** Cell apoptosis was assessed in T47D and MCF7 cells following treatment with deguelin with or without shGPRC5A. **(E)** Relative activity levels of caspase-3 were examined following treatment with SF1670 and GPRC5A-overexpressing plasmid in MDA-MB-231 and MDA-MB-468 cells. **(F)** Relative activity levels of caspase-3 were examined following treatment with deguelin and shGPRC5A in T47D and MCF7 cells. **(G)** Relative activity levels of caspase-9 were examined following treatment with SF1670 and GPRC5A-overexpressing plasmid in MDA-MB-231 and MDA-MB-468 cells. **(H)** Relative activity levels of caspase-9 were examined following treatment with deguelin and shGPRC5A in T47D and MCF7 cells. $^{*}P<0.05$ vs. corresponding control; $^{\#}P<0.05$ vs. deguelin; $^{\wedge}P<0.5$ vs. SF1670. GPRC5A, G-protein-coupled receptor family C, member 5, group A; sh, small hairpin.

further investigation. A number of factors can enhance PI3K/Akt signaling, including epidermal growth factor, insulin-like growth factor 1 and insulin (30). In addition, numerous factors can inhibit the PI3K/Akt signaling pathway, PTEN, glycogen synthase kinase 3 β and homeobox protein 9 (31). Therefore, the PTEN inhibitor SF1670 was selected as an activator of the PI3K/Akt signaling pathway and deguelin was selected as an inhibitor of PI3K/Akt signaling in the present study. The activation of PI3K/Akt pathway has been a focus of interest in breast cancer due to its role in cell growth, cell migration and deregulated apoptosis (32). The inactivation of PI3K/Akt pathway is an important approach in triple negative breast cancer (33). The present results suggested that the effects of SF1670 and deguelin were reversed by GPRC5A overexpression and knockdown, respectively. The present results supported the aforementioned hypothesis that GPRC5A can act as an upstream regulator of the PI3K/Akt signaling pathway.

In conclusion, the present study suggested that GPRC5A was downregulated in human breast cancer cell lines. Overexpression of GPRC5A promoted cell apoptosis by increasing the activity of the intrinsic pathway and inhibition of GPRC5A exhibited the

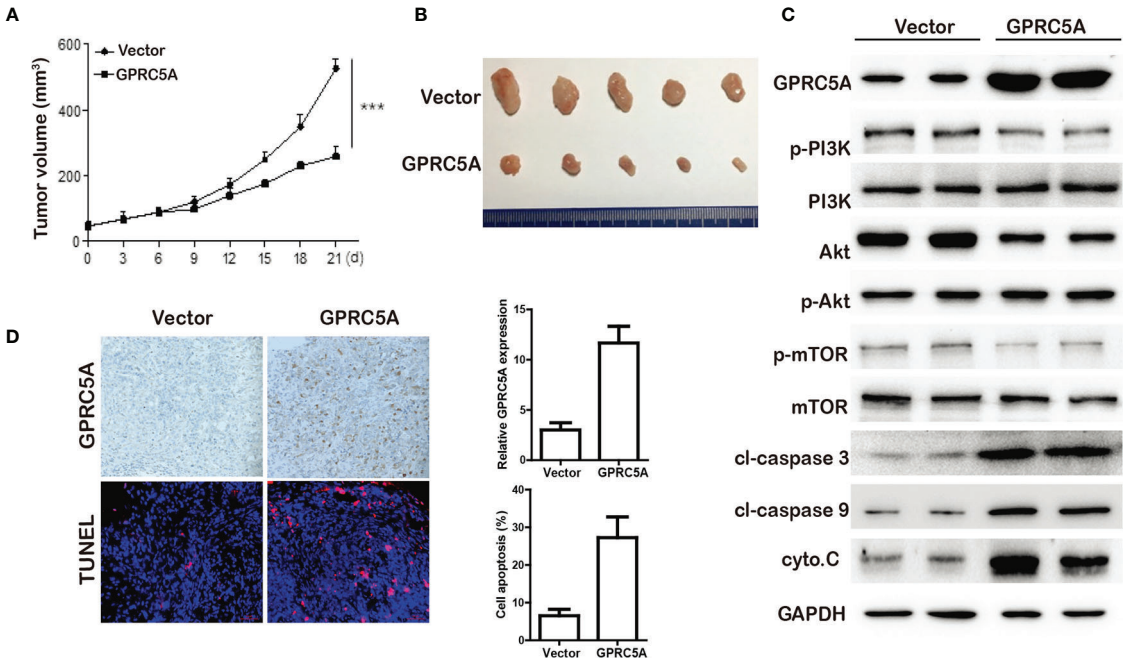


**FIGURE 6** | GPRC5A inhibited TNBC tumor growth *in vivo*. **(A)** The tumor volume were measured. ***$P$<0.05 vs. control. **(B)** Tumors from MDA-MB-231-MCS and MDA-MB-231-GPRC5A xenograft mouse model. **(C)** Western blot analysis was performed to examine the levels of proteins associated with cell apoptosis. **(D)** The expression of GPRC5A was examined by immunohistochemistry. The cell apoptosis was measured by TUNEL staining. *$P$<0.5, ***$P$<0.05 vs. control. GPRC5A, G-protein-coupled receptor family C, member 5, group A; cyto.C, cytochrome C; cl, cleaved.

opposite effect. GPRC5A was identified to regulate cell apoptosis *via* the PI3K/Akt signaling pathway. In summary, the present study identified GPRC5A as a potential protective factor against breast cancer progression and provided novel insights on the mechanism of GPRC5A on TNBC cell apoptosis.

## DATA AVAILABILITY STATEMENT

The original contributions presented in the study are included in the article/**Supplementary Material**. Further inquiries can be directed to the corresponding author.

## ETHICS STATEMENT

The animal study was reviewed and approved by Institute Research Ethics Committee of Tianjin Medical University Cancer Hospital.

## AUTHOR CONTRIBUTIONS

LY designed the study, performed the analysis, and wrote the paper. JZ supervised the work. TZ edited the paper. SZ made contribution to the revised manuscript. All authors contributed to the article and approved the submitted version.

## FUNDING

This study was supported by the National Natural Science Fund (No. 81672623) and Key Projects in Tianjin Science & Technology Pillar Program (No. 19YFZCSY00030).

## SUPPLEMENTARY MATERIAL

The Supplementary Material for this article can be found online at: https://www.frontiersin.org/articles/10.3389/fonc.2020.624493/full#supplementary-material

## REFERENCES

1. Siegel RL, Miller KD, Jemal A. 2018, Cancer statistics. *CA Cancer J Clin* (2018) 68(1):7–30. doi: 10.3322/caac.21442
2. Katayama A, Handa T, Komatsu K, Togo M, Horiguchi J, Nishiyama M, et al. Expression patterns of claudins in patients with triple-negative breast cancer are associated with nodal metastasis and worse outcome. *Pathol Int* (2017) 67 (8):404–13. doi: 10.1111/pin.12560
3. Dent R, Trudeau M, Pritchard KI, Hanna WM, Kahn HK, Sawka CA, et al. Triple-negative breast cancer: clinical features and patterns of recurrence. *Clin Cancer Res* (2007) 13(15 Pt 1):4429–34. doi: 10.1158/1078-0432.CCR-06-3045
4. Langer I, Robberecht P. Molecular mechanisms involved in vasoactive intestinal peptide receptor activation and regulation: current knowledge, similarities to and differences from the A family of G-protein-coupled receptors. *Biochem Soc Trans* (2007) 35(Pt 4):724–8. doi: 10.1042/BST0350724

5. Venkatakrishnan AJ, Deupi X, Lebon G, Tate CG, Schertler GF, Babu MM. Molecular signatures of G-protein-coupled receptors. *Nature* (2013) 494 (7436):185–94. doi: 10.1038/nature11896
6. Cheng Y, Lotan R. Molecular cloning and characterization of a novel retinoic acid-inducible gene that encodes a putative G protein-coupled receptor. *J Biol Chem* (1998) 273(52):35008–15. doi: 10.1074/jbc.273.52.35008
7. Zhang L, Li L, Gao G, Wei G, Zheng Y, Wang C, et al. Elevation of GPRC5A expression in colorectal cancer promotes tumor progression through VNN-1 induced oxidative stress. *Int J Cancer* (2017) 140(12):2734–47. doi: 10.1002/ijc.30698
8. Liu B, Yang H, Pilarsky C, Weber GF. The Effect of GPRC5a on the Proliferation, Migration Ability, Chemotherapy Resistance, and Phosphorylation of GSK-3beta in Pancreatic Cancer. *Int J Mol Sci* (2018) 19(7):1–14. doi: 10.3390/ijms19071870
9. Sokolenko AP, Bulanova DR, Iyevleva AG, Aleksakhina SN, Preobrazhenskaya EV, Ivantsov AO, et al. High prevalence of GPRC5A germline mutations in BRCA1-mutant breast cancer patients. *Int J Cancer* (2014) 134(10):2352–8. doi: 10.1002/ijc.28569
10. Nagahata T, Sato T, Tomura A, Onda M, Nishikawa K, Emi M. Identification of RAI3 as a therapeutic target for breast cancer. *Endocr Relat Cancer* (2005) 12(1):65–73. doi: 10.1677/erc.1.00890
11. Yang L, Ma L, Zhang J. GPRC5A exerts its tumor-suppressive effects in breast cancer cells by inhibiting EGFR and its downstream pathway. *Oncol Rep* (2016) 36(5):2983–90. doi: 10.3892/or.2016.5062
12. Bohm I, Schild H. Apoptosis: the complex scenario for a silent cell death. *Mol Imaging Biol* (2003) 5(1):2–14. doi: 10.1016/S1536-1632(03)00024-6
13. El-Metwally SA, Khalil AK, El-Naggar AM, El-Sayed WM. Novel Tetrahydrobenzo Thiophene Compounds Exhibit Anticancer Activity through Enhancing Apoptosis and Inhibiting Tyrosine Kinase. *Anticancer Agents Med Chem* (2018) 18(12):1761–9. doi: 10.2174/1871520618666180813120558
14. Zhang TG, Wang YM, Zhao J, Xia MY, Peng SQ, Ikejima T. Induction of protective autophagy against apoptosis in HepG2 cells by isoniazid independent of the p38 signaling pathway. *Toxicol Res (Camb)* (2016) 5 (3):963–72. doi: 10.1039/C5TX00470E
15. McGuire A, Brown JA, Malone C, McLaughlin R, Kerin MJ. Effects of age on the detection and management of breast cancer. *Cancers (Basel)* (2015) 7 (2):908–29. doi: 10.3390/cancers7020815
16. Bray F, Soerjomataram I. The Changing Global Burden of Cancer: Transitions in Human Development and Implications for Cancer Prevention and Control. *Cancer Disease Control Priorities* (2015) 3. doi: 10.1596/978-1-4648-0349-9_ch2
17. Ferlay J, Colombet M, Soerjomataram I, Dyba T, Randi G, Bettio M, et al. Cancer incidence and mortality patterns in Europe: Estimates for 40 countries and 25 major cancers in 2018. *Eur J Cancer* (2018) 103:356–87. doi: 10.1016/j.ejca.2018.07.005
18. Hudis CA, Gianni L. Triple-negative breast cancer: an unmet medical need. *Oncologist* (2011) 16(Suppl 1):1–11. doi: 10.1634/theoncologist.2011-S1-01
19. Wu Q, Ding W, Mirza A, Van Arsdale T, Wei I, Bishop WR, et al. Integrative genomics revealed RAI3 is a cell growth-promoting gene and a novel P53 transcriptional target. *J Biol Chem* (2005) 280(13):12935–43. doi: 10.1074/jbc.M409901200
20. Zhou H, Telonis AG, Jing Y, Xia NL, Biederman L, Jimbo M, et al. GPRC5A is a potential oncogene in pancreatic ductal adenocarcinoma cells that is upregulated by gemcitabine with help from HuR. *Cell Death Dis* (2016) 7: e2294. doi: 10.1038/cddis.2016.169
21. Wang T, Jing B, Xu D, Liao Y, Song H, Sun B, et al. PTGES/PGE2 signaling links immunosuppression and lung metastasis in Gprc5a-knockout mouse model. *Oncogene* (2020) 39:3179–94. doi: 10.1038/s41388-020-1207-6
22. Guo W, Hu M, Wu J, Zhou A, Liao Y, Song H, et al. Gprc5a depletion enhances the risk of smoking-induced lung tumorigenesis and mortality. *Biomed Pharmacother Biomed Pharmacother* (2019) 114:108791. doi: 10.1016/j.biopha.2019.108791
23. Richter L, Oberlander V, Schmidt G. RhoA/C inhibits proliferation by inducing the synthesis of GPRC5A. *Sci Rep* (2020) 10:12532. doi: 10.1038/s41598-020-69481-2
24. Kerr JF. A histochemical study of hypertrophy and ischaemic injury of rat liver with special reference to changes in lysosomes. *J Pathol Bacteriol* (1965) 90(2):419–35. doi: 10.1002/path.1700900210
25. Raychaudhuri S. A minimal model of signaling network elucidates cell-to-cell stochastic variability in apoptosis. *PloS One* (2010) 5(8):e11930. doi: 10.1371/journal.pone.0011930
26. Hardy S, El-Assaad W, Przybytkowski E, Joly E, Prentki M, Langelier Y. Saturated fatty acid-induced apoptosis in MDA-MB-231 breast cancer cells. A role for cardiolipin. *J Biol Chem* (2003) 278(34):31861–70. doi: 10.1074/jbc.M300190200
27. Thomas MP, Liu X, Whangbo J, McCrossan G, Sanborn KB, Basar E, et al. Apoptosis Triggers Specific, Rapid, and Global mRNA Decay with 3' Uridylated Intermediates Degraded by DIS3L2. *Cell Rep* (2015) 11(7):1079–89. doi: 10.1016/j.celrep.2015.04.026
28. King D, Yeomanson D, Bryant HE, Yeomanson, Bryant HE. PI3King the lock: targeting the PI3K/Akt/mTOR pathway as a novel therapeutic strategy in neuroblastoma. *J Pediatr Hematol Oncol* (2015) 37(4):245–51. doi: 10.1097/MPH.0000000000000329
29. Rafalski VA, Brunet A. Energy metabolism in adult neural stem cell fate. *Prog Neurobiol* (2011) 93(2):182–203. doi: 10.1016/j.pneurobio.2010.10.007
30. Ojeda L, Gao J, Hooten KG, Wang E, Thonhoff JR, Dunn TJ, et al. Critical role of PI3K/Akt/GSK3beta in motoneuron specification from human neural stem cells in response to FGF2 and EGF. *PloS One* (2011) 6(8):e23414. doi: 10.1371/journal.pone.0023414
31. Wyatt LA, Filbin MT, Keirstead HS. PTEN inhibition enhances neurite outgrowth in human embryonic stem cell-derived neuronal progenitor cells. *J Comp Neurol* (2014) 522(12):2741–55. doi: 10.1002/cne.23580
32. Verret B, Cortes J, Bachelot T, Andre F, Arnedos M. Efficacy of PI3K inhibitors in advanced breast cancer. *Ann Oncol* (2019) 30(Suppl 10):x12–20. doi: 10.1093/annonc/mdz381
33. Delaloge S, DeForceville L. Targeting PI3K/AKT pathway in triple-negative breast cancer. *Lancet Oncol* (2017) 18:1293–4. doi: 10.1016/S1470-2045(17)30514-4


**Conflict of Interest:** The authors declare that the research was conducted in the absence of any commercial or financial relationships that could be construed as a potential conflict of interest.

frontiers in Oncology

ORIGINAL RESEARCH
published: 25 February 2021
doi: 10.3389/fonc.2021.569295

# Resveratrol Mediates the Apoptosis of Triple Negative Breast Cancer Cells by Reducing POLD1 Expression

*Zhi-Jie Liang[1,2†], Yan Wan[1†], Dan-Dan Zhu[2], Meng-Xin Wang[1], Hong-Mian Jiang[3], Dong-Lin Huang[4], Li-Feng Luo[3], Mao-Jian Chen[1], Wei-Ping Yang[5], Hong-Mian Li[4*] and Chang-Yuan Wei[1*]*

[1] Department of Breast Surgery, Guangxi Medical University Cancer Hospital, Nanning, China, [2] Department of Wound Repair Surgery, The Fifth Affiliated Hospital of Guangxi Medical University & The First People's Hospital of Nanning, Nanning, China, [3] Department of Pathology, The Fifth Affiliated Hospital of Guangxi Medical University & The First People's Hospital of Nanning, Nanning, China, [4] Department of Plastic and Aesthetic Surgery, The Fifth Affiliated Hospital of Guangxi Medical University & The First People's Hospital of Nanning, Nanning, China, [5] Department of Ultrasonography, Guangxi Medical University Cancer Hospital, Nanning, China

OPEN ACCESS

**Edited by:**
Shengtao Zhou,
Sichuan University, China

**Reviewed by:**
Giuseppina Roscigno,
University of Naples Federico II, Italy
Yuba Raj Pokharel,
South Asian University, India
Kui Wang,
Sichuan University, China

***Correspondence:**
Chang-Yuan Wei
weichangyuan@gxmu.edu.cn
Hong-Mian Li
lihongmian@gxmu.edu.cn

†These authors have contributed equal to this work

**Specialty section:**
This article was submitted to Women's Cancer, a section of the journal Frontiers in Oncology

**Received:** 03 June 2020
**Accepted:** 12 January 2021
**Published:** 25 February 2021

**Citation:**
Liang Z-J, Wan Y, Zhu D-D, Wang M-X, Jiang H-M, Huang D-L, Luo L-F, Chen M-J, Yang W-P, Li H-M and Wei C-Y (2021) Resveratrol Mediates the Apoptosis of Triple Negative Breast Cancer Cells by Reducing POLD1 Expression. Front. Oncol. 11:569295. doi: 10.3389/fonc.2021.569295

Resveratrol (RSV) is known to possess anticancer properties in many types of cancers like breast cancer, in which POLD1 may serve as a potential target. However, the anticancer mechanism of RSV on triple negative breast cancer (TNBC) remains unclear. In the present study, the antitumor effects and mechanism of RSV on TNBC cells were analyzed by RNA sequencing (RNA-seq), which was then verified *via* cell counting kit-8 (CCK8), immunofluorescence, immunohistochemistry, Western Blot (WB), flow cytometry, and hematoxylin-eosin (HE) staining. According to the corresponding findings, the survival rate of MDA-MB-231 cells gradually decreased as RSV treatment concentration increased. The RNA-seq analysis results demonstrated that genes affected by RSV treatment were mainly involved in apoptosis and the p53 signaling pathway. Moreover, apoptosis of MDA-MB-231 cells induced by RSV was observed to be mainly mediated by POLD1. When treated with RSV, the expression levels of full length PARP1, PCNA, and BCL-2 were found to be significantly reduced, and the expression level of Cleaved-PARP1 as well as Cleaved-Caspase3 increased significantly. Additionally, the mRNA expression of POLD1 was significantly reduced after treatment with RSV, and the protein expression level was also inhibited by RSV in a concentration-dependent manner. The prediction of domain interaction suggested that RSV may bind to at least five functional domains of the POLD1 protein (6s1m, 6s1n, 6s1o, 6tny and 6tnz). Furthermore, after RSV treatment, the anti-apoptotic index (PCNA, BCL-2) of MDA-MB-231 cells was found to decrease while the apoptosis index (caspase3) increased. Moreover, the overexpression of POLD1 reduced the extent of apoptosis observed in MDA-MB-231 cells following RSV treatment. Moreover, animal experimental results showed that RSV had a significant inhibitory effect on the growth of live tumors, while POLD1 overexpression was shown to antagonize this inhibitory effect. Accordingly, this study's findings reveal that RSV may

promote the apoptosis of TNBC cells by reducing the expression of POLD1 to activate the apoptotic pathway, which may serve as a potential therapy for the treatment of TNBC.

**Keywords: resveratrol, triple negative breast cancer, apoptosis, RNA-seq, POLD1**

## INTRODUCTION

In 2018, there were about 2.1 million newly diagnosed female breast cancer cases globally, accounting for nearly a quarter of all female cancer cases (1). According to the expression levels of estrogen receptor [ER], progesterone receptor [PR], and human epidermal growth factor receptor 2 [HER2] protein, breast cancer can be divided into four subtypes: luminal -A, luminal-B, HER-2 positive, and triple negative breast cancer (TNBC) (2, 3). Among them, TNBC accounts for about 15% - 20% of breast cancer (4), and compared to hormonal receptor positive or HER2 positive diseases, TNBC is characterized by its highly aggressive clinical progression due to its earlier onset age, greater metastatic potential and worse clinical results (5, 6). TNBC progresses very rapidly, and due to the lack of common therapeutic targets, current methods in controlling disease development are very limited (7). TNBC patients usually receive anthracycline and cyclophosphamide chemotherapy, and subsequently take taxane (anthracycline/taxane [ACT]) as standard care. However, only about one-third of patients attain a pathological complete response (PCR), while remaining patients relapse and eventually succumb to the disease (8). Several studies have shown that resveratrol (RSV) possesses anticancer properties (9) in breast cancer (10) and may serve as a potential therapeutic candidate for TNBC.

RSV is a non-flavonoid polyphenolic compound produced by plants when treated. It is a bioactive component in wine and grape juice and can be synthesized in grape leaves and grape skins (11, 12). Research has shown that RSV has functions in anti-oxidation, anti-inflammatory, anti-cancer, and cardiovascular protection (11, 13–15). Moreover, RSV has a significant inhibitory effect on a variety of tumor cells, such as liver cancer, breast cancer, colon cancer, gastric cancer, and leukemia (9, 16). RSV can enhance cancer radiotherapy and effectively inhibit the role of cancer stem cells (17). For TNBC cells such as MDA-MB-231, RSV can inhibit its metastasis by reversing TGF-β1-induced epithelial matrix transformation (18). However, due to the complex anti-tumor mechanism of RSV, researchers have yet to reach a consensus on its mechanism of action, hence, the anti-cancer mechanism of RSV on TNBC remains unclear. In addition, the DNA polymerase delta catalytic subunit gene (POLD1) is one of the subunits of polδ in DNA polymerases (19). High expression or point mutations may lead to DNA replication and cell cycle abnormality of common cells, which may then progress to cancer cells. POLD has been confirmed to be regulated by a variety of upstream factors, such as p53 and SIRT1 (20, 21), which are the direct regulatory targets of RSV. However, no studies have discussed the regulation of POLD1 by RSV. Additionally, the role of POLD1 within RSV-mediated apoptosis of cancer cells is also unclear.

Therefore, this study aims to explore the specific mechanism surrounding RSV-mediated apoptosis of TNBC cells. The corresponding flow chart of this research is shown in **Figure 1**. RNA sequencing was used to observe the changes of POLD1, other apoptosis-related pathways and factors in MDA-MB-231 under RSV treatment. Additionally, genes and pathways related to POLD1's potential role were analyzed, and changes in the transcription and translation levels of POLD1 and its related genes were verified. Subsequently, *via* ectopic expression of POLD1, the role of POLD1 in RSV-mediated breast cancer cell apoptosis *in vivo* and *in vitro* were further explored. The obtained results suggested that RSV may promote apoptosis of TNBC cells by reducing the expression of POLD1 to activate the apoptotic pathway, which may be a potential mechanism pertaining to its anticancer effects on TNBC.

## MATERIALS AND METHODS

### Materials and Ethical Approval

In the Cancer Genome Atlas (TCGA, https://www.cancer.gov/) database, the transcriptome data of breast cancer (BRCA) samples and control samples were downloaded. Moreover, the TNBC cell lines MDA-MB-231 and common breast epithelial cell lines MCF10A were derived from the Shanghai Cell Bank of the Shanghai Academy of Sciences. BALB/c nude female mice (weight 18-22g, 4–6 weeks old) were obtained from the Animal Experiment Center of Guangxi Medical University. All experiments were approved by the Animal Ethics Approval Committee of Guangxi Medical University.

### Effect of RSV on MCF-10A and MDA-MB-231 Cell Survival

Cell Counting Kit-8 (CCK8) (Dojindo, Japan) was used to detect the effect of RSV (Solarbio, China) on the survival of MCF-10A and MDA-MB-231 cells. The cells in the logarithmic growth phase were adjusted to a concentration of $5 \times 10^4$/ml and were inoculated in 96-well plates (100 μl per well). The experiment was divided into eight groups, and each group was set up with five duplicate wells that were incubated in a 37 °C, 5% $CO_2$ incubator overnight. After the cells were adhered, the medium was removed, and 100 μl of DMEM (Gibco, USA) containing RSV at concentrations of 0, 3.125, 6.25, 12.5, 25, 50, 100, and 200 μM were added in groups. The control group had 100 μl of 0.1% DMSO in DMEM added, which was then incubated for 24 h under the same conditions. Next, 10 μl of CCK8 solution was added to each well and incubation continued for 3 h. A microplate reader was used to measure absorbance (A) at 450 nm. The survival rates of the eight groups of MCF-10A and MDA-MB-231 cells were then compared, and the experiment was repeated six times.

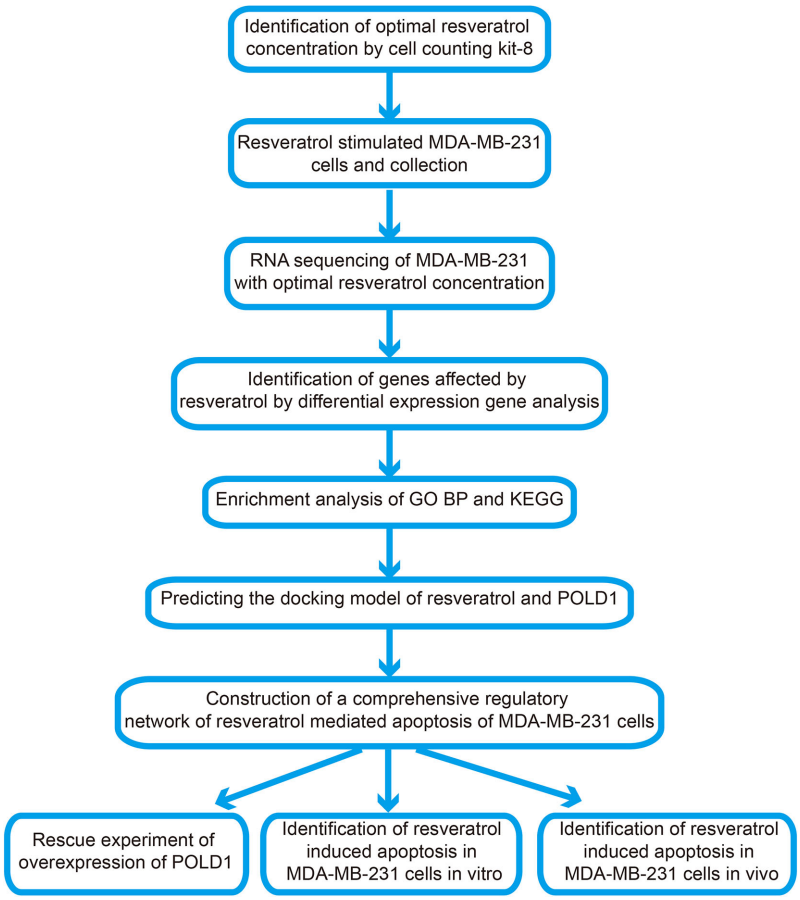


**FIGURE 1** | Flow chart of present study.

The concentration of RSV that produced significant differences in survival rates between the two cell lines was chosen as the optimum concentration for further experiments.

## The Treatment of MDA-MB-231 Cells With Resveratrol

Here, $5 \times 10^4$ cells/well of MDA-MB-231 cells in the logarithmic growth phase were taken and inoculated into 6-well plates, after which 10% FBS serum DMEM medium was added and incubated in a 37°C, 5% $CO_2$ incubator. When MDA-MB-231 cells were observed to reach 80% confluence, PBS was used to wash the cells three times, and the serum-containing DMEM was replaced with serum-free DMEM. The cells were starved overnight and were then divided into the control group and RSV treatment group. On the next day, after removing the DMEM medium, a new serum-free DMEM medium was added to the control group, and an optimum concentration RSV containing DMEM medium was added to the RSV treatment group, which was then cultured in a 37°C, 5% $CO_2$ incubator for 24 h. Subsequently, the culture medium was removed, and 1 ml of PBS was added to each well, followed by gentle washing and removal. After this operation was repeated twice, 1 ml of trypsin was added to each well and digested in a 5% $CO_2$ incubator at 37°C for 1 to 1.5 min, and 2 ml of 10% FBS complete medium was added. Then, digestion was stopped, and all cells and liquid were collected into 15 ml centrifuge tubes.

## RNA Extraction and Sequencing

After treatment of MDA-MB-231 cells with resveratrol, RNA from MDA-MB-231 cells treated by the optimal concentration of resveratrol were extracted using Trizol. In order to ensure that the samples were qualified and appropriate for sequencing, Nanodrop, Qubit 2.0 and Aglient 2100 were used to detect the purity, concentration, and integrity of RNA samples, respectively. The optical density (OD) 260/280 of the sample must be greater than 1.8, and it must be free of protein, or visible impurities. Library construction and RNA sequences were performed according to the manufacturer's instructions. RNA sequencing was performed on MDA-MB-231 cells using NovaSeq. After RNA-seq, the clean data was first filtered to remove low-quality data and joints to obtain high-quality clean data. The results were then stored in a FASTQ file format. Then, fastqc software (22) was used to perform a quality inspection of the FASTQ file format. BWA software (23) was used to compare the sequencing results of each sample with the reference genome and generated Sam files. Samtools (24) was used to convert Sam

files to BAM files and sort them. The featurecounts tool (25) was used to convert BAM files to counts files, which were then used for the construction of expression profiles.

## Differentially Expressed Genes Analysis and Functional Enrichment Analysis

The sequencing data and TCGA data were standardized using rlogTransformation and varianceStabilizingTransformation of the DESeq2 package (26), respectively. DESeq of the DESeq2 package was used for differentially expressed genes' analysis. Genes with P value adjusted by the false discovery rate (FDR) <0.01 were considered significant, and differentially expressed genes (DEGs) with opposite expressions in sequencing data and TCGA data were defined to be the genes affected by RSV in the treatment of breast cancer. In terms of genes affecting RSV in the treatment of breast cancer, an enrichment analysis was performed using enrichGO and enrichKEGG of the clusterProfiler package (27). The pathway with a P Value <0.05 was considered to be significant.

## Gene Set Variation Analysis (GSVA) and Correlation Analysis

In regard to the enrichment results of the KEGG pathway, the expression spectra of the KEGG pathway were made using gsva of the GSVA package (28), which were used to visualize heat maps. In addition, ggcor of the ggcor package was used to visualize the correlation pathway map.

## Predicting the Docking Model of Resveratrol and POLD1 and the Construction of a Comprehensive Regulation Network

The PDB files for the five POLD1 domains (6s1m, 6s1n, 6s1o, 6tny, 6tnz) (29) were downloaded from the Protein data bank database (PDB, http://www.rcsb.org/pdb/results/results.do?tabtoshow=Current&qrid=9D5B948E) (30). The sdf file of RSV was downloaded from the PubChem database (https://pubchem.ncbi.nlm.nih.gov/) and converted to pdb using Open Babel (31). Then, AutoDockTools (32) was used to predict the docking model of resveratrol and POLD1, eventually attaining the pdbqt file. Open Babel was used to convert pdbqt files into pdb files and visualize the molecular docking results using PyMOL (33). In addition, based on the String database (34), a comprehensive regulation network of the POLD1-targets-pathway was constructed, which was visualized using Cytoscape (35).

## Effect of RSV on POLD1 Expression Gradient

The MDA-MB-231 cells in logarithmic growth phase were adjusted to a concentration of $5 \times 10^4$ cells/well into 6-well plates and were inoculated in 6-well plates containing 10% FBS serum DMEM. Subsequently, the MDA-MB-231 cells were placed in a 37 °C, 5% $CO_2$ incubator and incubated until 80% confluence, and the blank DMEM medium was used to starve overnight. RSV was divided according to different treatment concentrations into 0, DMSO, 12.5, 25, 50, 100, and 200μM groups, and the MDA-MB-231 cells were treated for 24 h. The cells of each group were collected in a 1.5 ml EP tube, lysed with RIPA cell lysate, and the protein concentration was measured by BCA. The experimental protein samples were then adjusted to the same concentration with RIPA. The protein samples were loaded for 1.5 h following electrophoresis and transferred to a membrane blocked with a 5% skim milk powder blocking solution for 2 h. The primary antibody was incubated overnight (4 °C), and on the next day, it was dipped in TBST for 1 h, which was then incubated with the corresponding secondary antibody for 2 h. Subsequently, it was immersed in TBST for 45 min, and developed with an ECL chemiluminescence developer (Beyotime Biotechnology, China).

## POLD1 Overexpression Transfects Verification

MDA-MB-231 cells in logarithmic growth phase were inoculated into 6-well plates at 5 × 104 cells/well. After 12 h of culturing, POLD1 over-expressing recombinant lentivirus (pCMV-EGFP-POLD1) was added. In addition, a control group and no-load negative control group without viruses were established, and 2 ug/L virus enhancement solution was added at the same time. After 12 h, the medium was changed to a fresh complete medium, and following 72 h, puromycin (2 mg/L) was added for screening. After 1 week, the concentration of puromycin was observed to be reduced by half, and the screening was continued for 1 week. MDA-MB-231/POLD1- Overexpression (OE) and MDA-MB-231/POLD1- Normal control (NC) cell lines were obtained for the subsequent experiments. Transfection efficiency was determined by fluorescence, WB and qPT-PCR.

## Detection of Apoptotic Protein in POLD1 Overexpressing MDA-MB-231 Cells Under RSV Treatment

This experiment was divided into the control group, RSV group and RSV + POLD1-OE group. The protein was extracted 24 h following RSV treatment of the MDA-MB-231 cells. The protein expression levels of POLD1, PARP1, Cleaved-PARP1, PCNA, BCLl-2, and Cleaved-caspase 3 were detected *via* WB. The POLD1 antibody was acquired from Abcam (USA), and GAPDH, Bcl-2, PCNA, PARP1, and cleared Caspase3 antibody were obtained from CST (United States).

## Detection of Apoptotic in POLD1 Overexpressing MDA-MB-231 Cells Under RSV Treatment

The cells in logarithmic growth phase were taken and adjusted to a cell concentration of $5 \times 10^4$/ml, after which they were inoculated in 96-well plates (200 μl per well). Next, they were divided into 5 groups with 5 replicates in each group and incubated overnight in a 37 °C, 5% $CO_2$ incubator. After the cells adhered, the medium was removed, and the experiment was divided into a control group, a virus no-load control group NC, a no-load control group NC + RSV group, a POLD1 overexpression + RSV group, and a POLD1 overexpression group. Incubation continued under the same conditions for

36 h, after which 10 μl of CCK8 solution was added to each well, and incubation was continued for 3 h. A microplate reader was then used to measure absorbance (A) at 450 nm, and the survival rates of the four groups of cells were compared. The experiment was repeated three times, and the experiment was divided into control group, a virus no-load control group NC, a POLD1-OE group, a POLD1-OE + RSV group, and a no-load control group NC + RSV group. After 36 h of processing, detection was performed using flow cytometry using the AnnexinV APC-7AAD kit (Becton, Dickinson and Company, USA) double standard method.

## Animal Experiments

Nine nude mice were divided into three groups (n = 3) by random grouping into the blank control (Ctrl), RSV, and RSV + POLD1-OE groups. MDA-MB-231 and MDA-MB-231/POLD-OE cells in logarithmic growth-phase were prepared as a suspension of 1 × 107 cells per ml, and 0.1 ml was inoculated subcutaneously into the right lateral axillae of the nude mice. After pinching, the pinholes were clamped with tweezers to prevent cell fluid from leaking. The injection site was observed for ulceration and swelling daily and was ready for use after about 1 week of subcutaneous inoculation. The solvent in the control group was intraperitoneally injected with a 100 μl mixture of PEG400: DMSO: sterile deionized water [1: 1: 3]. The RSV group and the RSV + POLD1-OE group were then injected intraperitoneally with 25 mg/kg RSV containing PEG400: DMSO: sterile deionized water [1: 1: 3] mixed solution (36, 37). After subcutaneous tumorigenesis (generally on the 7th day), the drug was given every other day 8 times.

## Xenograft Assessment, Histopathology, and Immunohistochemistry Assay

During the administration period, the body weight of the nude mice was measured every 4 days, and the longest diameter (a) and shortest diameter (b) of the tumor were measured with a Vernier caliper. Accordingly, 48 h after the last administration, the experimental animals were euthanized, the tumor was weighed, and the tumor inhibition rate was calculated. The tumor tissues were fixed in a 10% formaldehyde solution for 24h and were subsequently fixed in formalin and embedded in paraffin. Sections of the dissected biopsies were stained with hematoxylin and eosin (H&E) using standard procedure and were examined under light microscopy. Paraffin-embedded sections were stained with anti-PCNA (Abcam, USA), anti-Ki-67 (Maixin, China), and anti-Cleaved-Caspase3 monoclonal antibody (CST, USA). HRP-conjugated anti-mouse secondary antibody was added and detected according to the manufacturer's protocol (Maixin, China). Moreover, the imageJ software was used for image analysis.

## Statistical Analysis

The data was displayed as mean ± standard deviation (x ± s). One-way analysis of variance (One-Way ANOVA) was used for comparison between groups, least significant difference (LSD) test was used for pairwise comparison when variance was uniform, and Dunnett's T3 test was used for uneven variance. The two groups of data were analyzed by paired T test, and $P<0.05$ was considered as statistically significant. All data were analyzed using SPSS for Windows 17.0 (Chicago, Illinois, USA).

# RESULTS

## Resveratrol's Therapeutic Potential in Triple Negative Breast Cancer

Assessment of the RSV target demonstrated that the target mutation rate of RSV was low (**Figure 2A**), suggesting fewer mutations at the site of action of RSV are present. Circplot of RSV multiomics suggested that the target proteins of RSV may serve as potential drivers for TNBC (**Figure 2B**). CCK8 showed (**Table S1**) that different concentrations of RSV could reduce the survival rate of MDA-MB-231 and MCF-10A. Moreover, with the increase in RSV concentration, the cell viability decreased gradually with increased concentrations of RSV. By comparing cells treated with different concentrations of RSV at 24 h, 36 h, and 48 h, a significant difference was found between the relative survival rate of TNBC cells (**Figure 2C**). When the RSV concentration was 25μM, 50μM, and 100μM, the survival rate of MDA-MB-231 cells and MCF-10A cells had the largest difference. However, at 25 μM concentration (36h), MDA-MB-231 cells had a higher survival rate and slower killing effect. At 100 μM concentration (36 h), the survival rate of MCF-10A cells was lower. The relative survival rate of MDA-MB-231 cells was 52.24% ± 7.03% after 36 h of treatment with 50 μM, suggesting 50 μM was the optimal treating concentration of RSV.

## Effects of Resveratrol on MDA-MB-231 Cells

To further identify genes affected by RSV in the treatment of breast cancer, the RNA of MDA-MB-231 cells treated with an optimal concentration for RNA sequencing were extracted. The results of the differentially expressed genes analysis (**Figure 3A**) showed that compared to MDA-MB-231 cells without RSV treatment, 8,527 DEGs in MDA-MB-231 cells treated with RSV were present. Additionally, compared to control samples, the BRCA samples had 16,241 DEGs. After comparison, 6,487 DEGs were identified as TNBC genes affected by RSV (**Figure 3B**). **Figure 3C** showed that RSV-treated MDA-MB-231 cells possessed distinct hierarchical clustering from control MDA-MB-231 cells (**Figure 3C**). In addition, the Circplot of RSV targets showed that the expression of some RSV targets changed little after treatment (**Figure 3D**). The heat map of gene expression in the apoptotic pathway illustrates that apoptotic genes were generally elevated in TNBC cells treated with RSV (**Figures 3E, F**). Furthermore, apoptosis-related proteins (PARP1, PCNA, and BCL-2) were detected, and POLD1 and PARP1 expression of MDA-MB-231 cells treated with the optimal concentration of RSV verified the mechanism of TNBC cell apoptosis. Western Blot (**Figure 3G**, **Table S2**) demonstrated that after 24 h of RSV (50uM) treatment, the protein expressions of PARP1 ($P<0.05$), PCNA ($P<0.05$), and BCL-2 ($P<0.05$) were significantly lower than those of the control

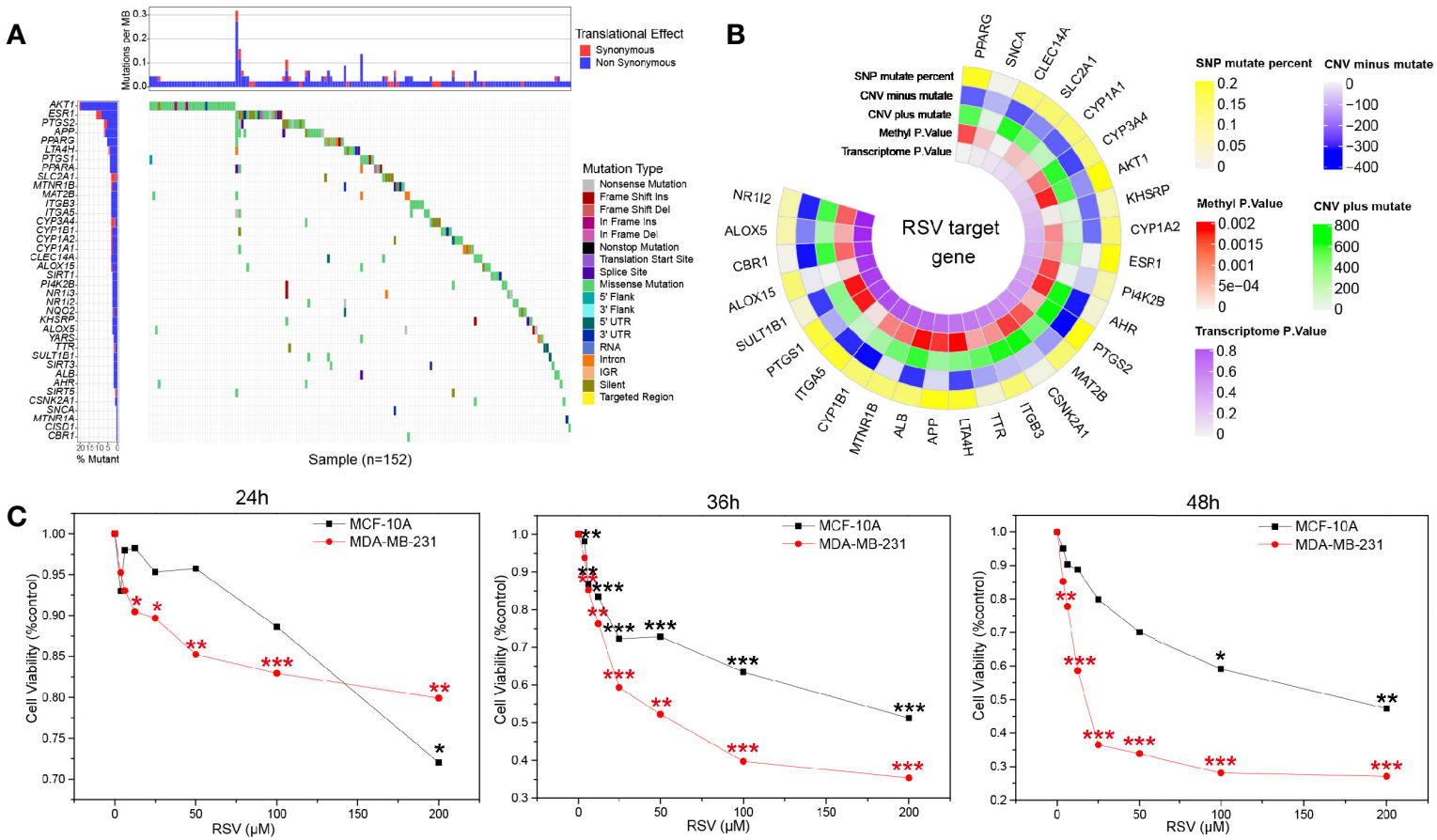


**FIGURE 2** | Resveratrol treatment potential in breast cancer. **(A)** Waterfall map of resveratrol target in drugbank and resveratrol target domain protein in protein data bank (TCGA download breast cancer data). **(B)** Multiomics circplot of resveratrol target in drugbank and resveratrol target domain protein in protein data bank (TCGA download breast cancer data). **(C)** Resveratrol inhibited the survival of MDA-MB-231 and MCF-10A cells at different concentrations (24 h, 36 h, 48 h). *p<0.05, **p<0.01, ***p<0.001.

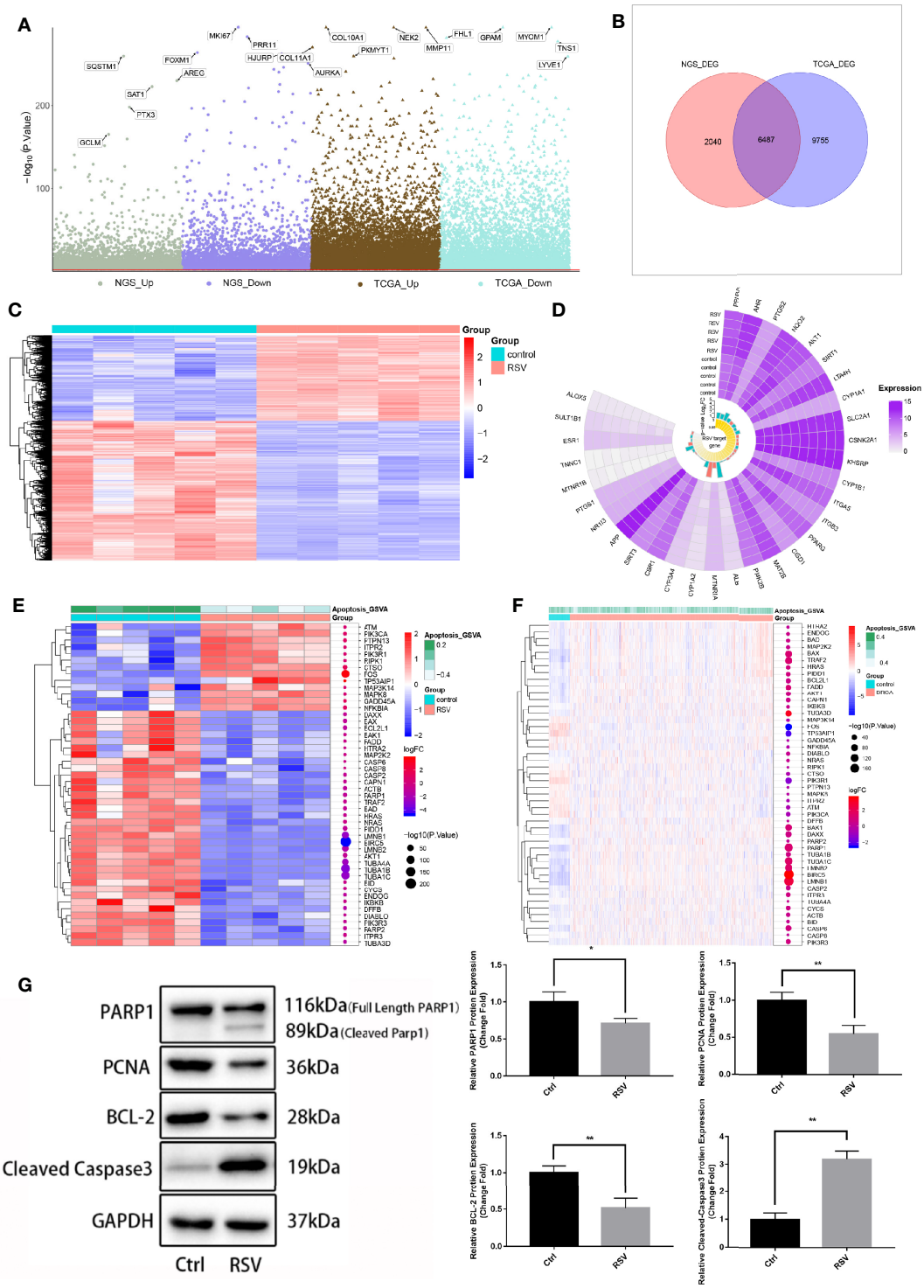


**FIGURE 3** | Genes affecting resveratrol in the treatment of MDA-MB-231 cells. **(A)** Manhattan map. The differential expression analysis of the sequencing data of 50 μM resveratrol-treated MDA-MB-231 cell samples -control samples and the differential expression analysis of breast cancer samples - control samples of the TCGA database are respectively displayed. **(B)** Venn diagram. The intersection in the figure is the gene with the opposite differential expression, which is defined as the gene affected by resveratrol in the treatment of breast cancer. **(C)** Expression heat map of genes affected by resveratrol in breast cancer treatment. **(D)** Circplot of resveratrol target in drugbank and resveratrol target domain protein in protein data bank (RNA sequencing data). **(E)** Apoptotic pathway-differential gene expression heat map (RNA sequencing data). **(F)** Apoptotic pathway-differential gene expression heat map (TCGA download breast cancer data). **(G)** Expression of apoptosis-related proteins in MDA-MB-231 cells after optimal resveratrol treatment (PARP1: **P*=0.03, PCNA: ***P*=0.008, BCL-2: ***P*=0.006, Cleaved Caspased 3: ***P*=0.001).

group, and levels of both Cleaved-PARP1 and Cleaved-Caspase3 ($P<0.05$) were found to be increased.

## Biological Processes and Pathways of Resveratrol in Treating TNBC

In order to further explore the biological process and KEGG pathway affected by RSV in the treatment of TNBC, a functional enrichment analysis was conducted for genes affected by RSV in the treatment of TNBC. The results showed (**Figure 4A**) that genes affected by RSV in TNBC cells were mainly involved in biological processes such as the regulation of mitotic cell cycle phase transition, regulation of cell cycle phase transition, chromosome segregation, DNA replication, and cell cycle DNA replication. Moreover, these genes were mainly involved in the KEGG pathways such as autophagy – animal, MAPK signaling pathway, apoptosis, p53 signaling pathway, and the cell cycle (**Figure 4B**). Most genes affected by resveratrol were found to be enriched in apoptosis related pathways, suggesting that resveratrol can promote the apoptosis of TNBC cells.

## POLD1 Acts as an Intermediary Mediator of MDA-MB-231 Cell Apoptosis

Previous studies have suggested that POLD1 may be associated with the malignant survival of tumor cells and that POLD1 is generally highly expressed in BRCA tissues (38). In this study, this result was verified in BRCA data of TCGA database [**Figure 5A(a)**]. Moreover, we also found that POLD1 was downregulated in MDA-MB-231 cells treated with RSV [**Figure 5A(b)**], suggesting it may serve as an intermediary for RSV in the treatment of TNBC. As shown in **Figure 5B** (**Table S3**), after RSV treatment, protein and mRNA expression of POLD1 gradually decreased with the increase in treatment concentration. The molecular docking results of RSV and POLD1 indicated (**Figure 5C**) that the docking energy with

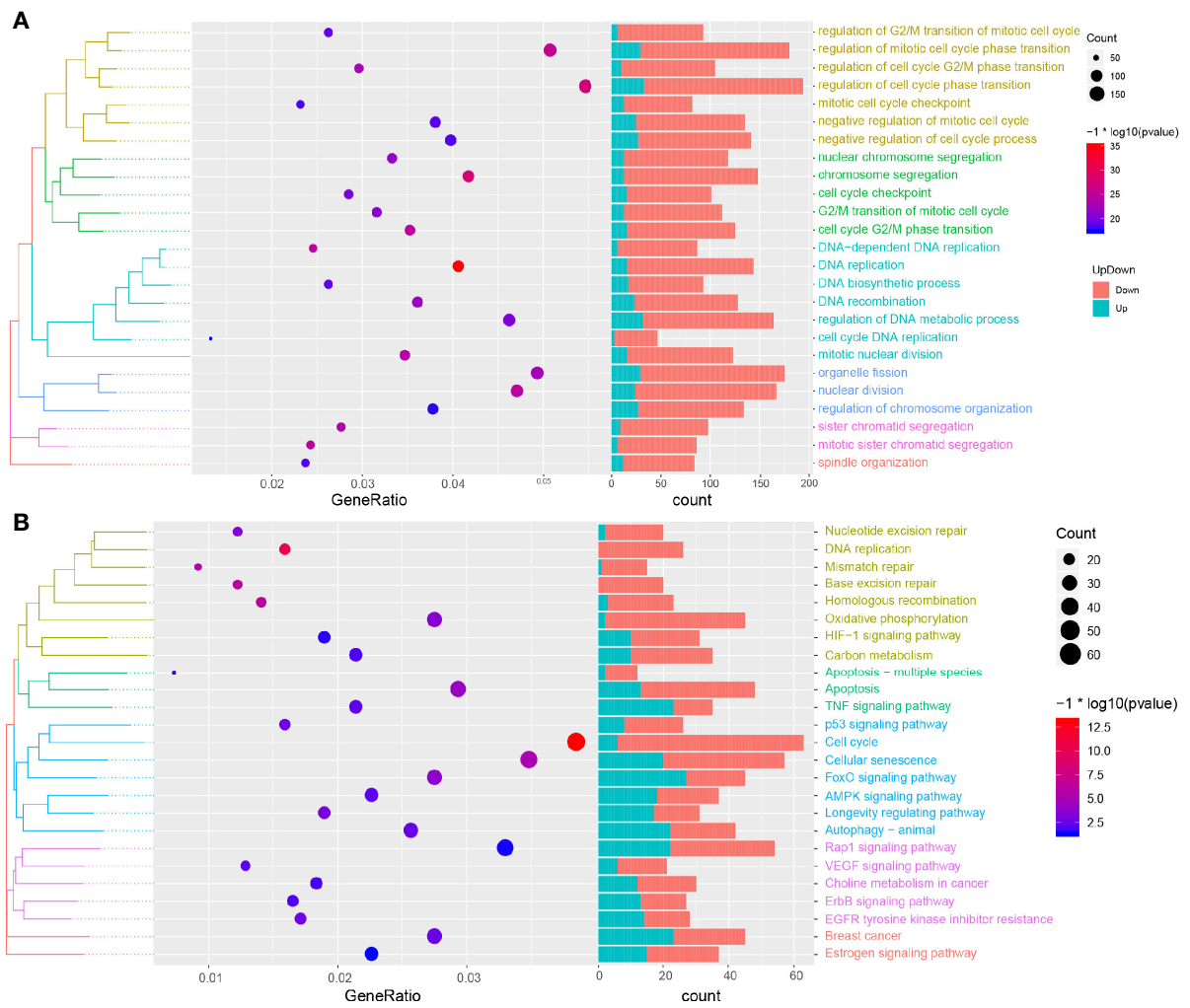


**FIGURE 4** | Functional enrichment analysis and GSEA analysis. **(A)** Biological processes involved in resveratrol affected genes. **(B)** KEGG pathways involved in resveratrol affected genes.

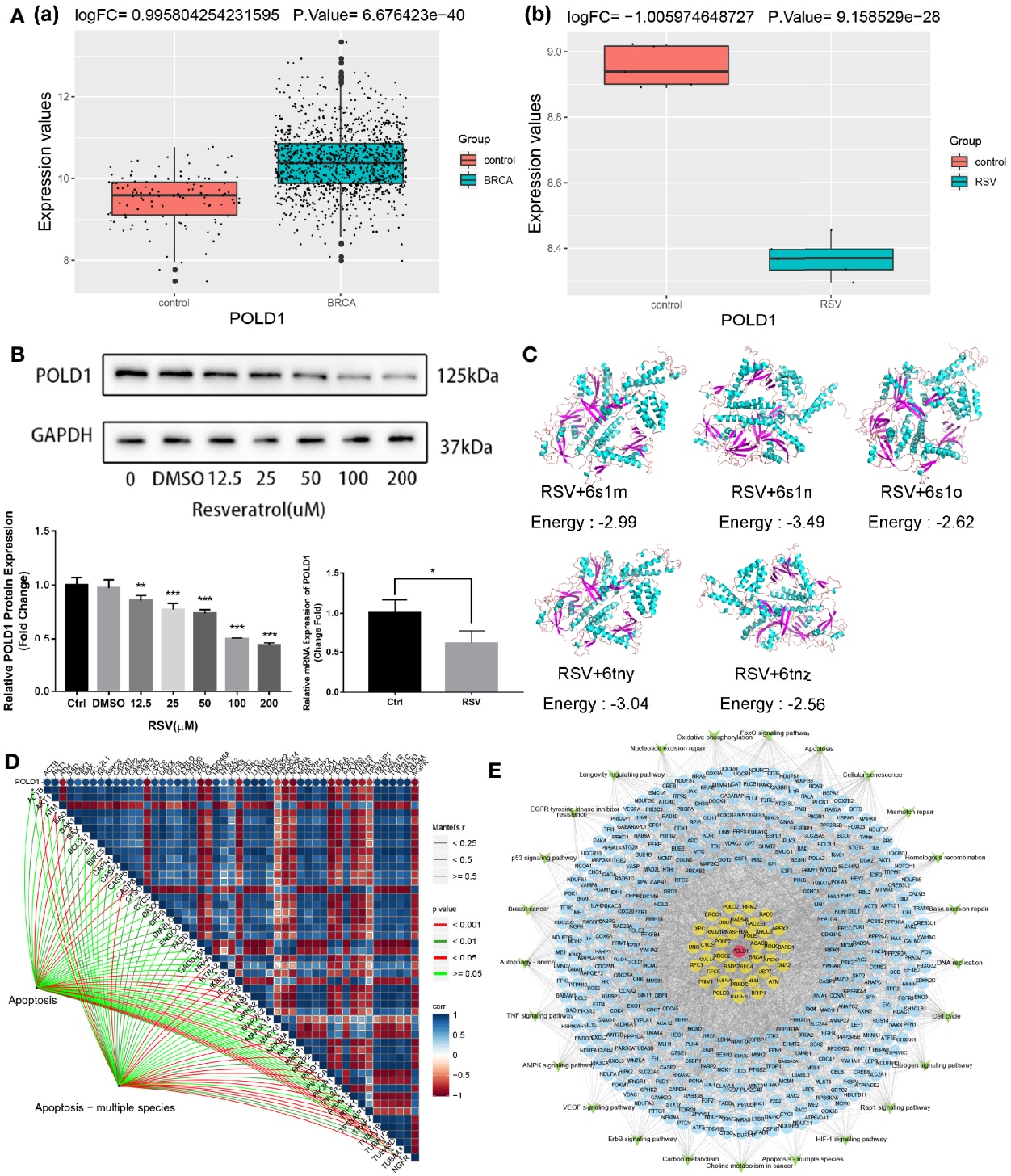


**FIGURE 5** | Comprehensive regulatory network for resveratrol in treating MDA-MB-231 cells. **(A)** (a) POLD1 expression in BRCA samples of TCGA database. (b) POLD1 expression in MDA-MB-231 cells samples after resveratrol treatment. **(B)** Protein expression of POLD1 after treatment with different concentrations of resveratrol (*$P$=0.043, **$P$=0.004, ***$P$<0.001). **(C)** Combined prediction model of resveratrol and POLD1 domain. **(D)** POLD1-differential apoptotic pathway gene-apoptotic pathway correlation pathway map. **(E)** Comprehensive regulatory network diagram. Red represents POLD1, yellow represents genes that interact with POLD1, blue represents genes that are affected by other resveratrol treatments for TNBC, and green represents pathways.

five domains of POLD1 (6s1m, 6s1n, 6s1o, 6tny and 6tnz) was generally less than 0 kcal/mol, suggesting that POLD1 may serve as a potential target of RSV. In addition, the results of the correlation pathway map (**Figure 5D**) showed that POLD1 was related to most genes in the apoptotic pathway, suggesting that RSV may inhibit TNBC by reducing the expression of POLD1 and mediating TNBC's potential mechanisms of apoptosis. Finally, a comprehensive regulatory map of TNBC cell genes treated by RSV was constructed (**Figure 5E**). The network diagram illustrates that TNBC cells treated by RSV mainly affect the protein encoded by other genes through POLD1, which then affect different pathways.

## Overexpression of POLD1 Reduces Apoptosis of MDA-MB-231 Cell Induced by Resveratrol

To further verify whether POLD1 is an intermediary for RSV in the treatment of TNBC, a rescue experiment of POLD1 overexpression (OE) was performed. The results of the POLD1 lentivirus-transfected cells showed that the transfection efficiency was over 90% (×100-fold) (**Figure 6A**). WB and qRT-PCR showed that the expression of POLD1 protein (nearly 2 times) and mRNA (about 25 times) in POLD1-OE group were highly expressed (**Figures 6B, C**, **Table S4**). In addition, the proteins after RSV treated MDA-MB-231 cells for 24 h were extracted, and protein was detected in expression levels of POLD1, PARP1, Cleaved-PARP1, PCNA, BCL-2, Cleaved-Caspase3, and other proteins using WB. Accordingly, the results demonstrated that the protein expression level of POLD1 in the RSV + POLD1-OE group was significantly higher than that in the RSV group ($P<0.01$), and the expression level of BCL-2 ($P<0.05$) was also significantly higher than that in the RSV group (**Figure 6D**, **Table S5**). However, the expression of Cleaved-PARP1 ($P<0.01$) and Cleaved-Caspase3 ($P<0.05$) was significantly lower. Although the expression of full length PARP1 decreased, the ratio of Cleaved-PARP1/full length PARP1 ($P<0.01$) decreased significantly. Overexpression of POLD1 and RSV treatment can synergistically lead to a further reduction in PARP1 expression, however, POLD1 overexpression can reduce the ratio of Cleaved-PARP1/full length PARP1, indicating apoptosis. CCK8 showed (**Figure 6E**, **Table S6**) that RSV could significantly promote MDA-MB-231 cell apoptosis, while POLD1 overexpression could slightly increase the proliferation ability of MDA-MB-231 cells. Moreover, overexpression of POLD1 could significantly reduce RSV's pro-apoptotic effect on MDA-MB-231 cells. At the same time, flow cytometry demonstrated (**Figure 6F**) that RSV could significantly promote MB-231 cell apoptosis, while overexpression of POLD1 could reduce the apoptotic effect of RSV on MB-231 cells.

## Resveratrol Mediates MDA-MB-231 Cell Apoptosis Through a POLD1-Driven Apoptosis Pathway

Animal experiments showed that RSV has a direct inhibitory effect on TNBC in nude mouse models, while overexpression of the POLD1 gene was found to reduce the inhibitory effect of RSV on tumors. Compared to the control group (**Figure 7A**, **Table S7**), the RSV and RSV + POLD1-OE groups had a smaller final tumor volume (493.66 ± 138.30mm3 vs. 222.70 ± 102.55mm3 and 313.48 ± 140.93mm3, $P<0.01$ $P>0.05$) and lower wet weight (0.54 ± 0.10 g vs. 0.26 ± 0.13 g and 0.34 ± 0.14 g, $P<0.01$, $P<0.05$). HE staining showed that the tumor tissue of the RSV group had obvious necrosis, while the RSV + POLD1-OE group had less fibrous tissue than the RSV group (**Figure 7B**). In addition, immunohistochemistry illustrated (**Figure 7C**, **Table S8**) that RSV can reduce the expression of PCNA ($P<0.001$) and Ki-67 ($P<0.01$) and increase the expression of Cleaved-Caspase3 ($P<0.001$). However, the POLD1 overexpression group antagonized these inhibitory or promotive effects (× 200-fold), signifying that POLD1 was an intermediary for RSV in treating MDA-MB-231 cells. Mechanistically, RSV may drive the apoptosis gene by reducing the expression of POLD1, activating the apoptosis pathway in the apoptosis of TNBC cells (**Figure S1**).

# DISCUSSION

RSV has previously been found to inhibit breast cancer cells by hindering the proliferation of breast cancer cells through its cell cycle and inducing apoptosis (39). Moreover, RSV possesses abrogate stemness properties and can reduce the expression of self-renewal signaling molecules in stem-like breast cancer cells (40). However, its anti-cancer mechanism on TNBC has not been clarified. In this study, *via* CCK8 experiments, the survival rates of MDA-MB-231 and MCF-10A were observed to gradually decrease following treatment with different concentrations of RSV, indicating that RSV can inhibit the survival of TNBC cells. By comparing the survival rates of MDA-MB-231 and MCF-10A treated by different concentrations of RSV, 50 μM was identified to be the optimal concentration of RSV, and MDA-MB-231 cells treated with this concentration were extracted for RNA sequencing.

According to the results of the differentially expressed gene analysis, the results of the two DEG groups were compared, and DEGs were defined with opposite expressions in the two groups as genes affected by RSV treatment in TNBC cells. Moreover, WB showed that apoptosis related proteins like Cleaved-Caspase 3 and BCL-2 were detected in MDA-MB-231 treated by RSV. In tumor therapy, apoptosis is a well-known mechanism of cell death, involving the activation of caspases (41). Caspases are key mediators in programmed cell death or apoptosis, where caspase 3 catalyzes the specific cleavage of many key cellular proteins (42). Additionally, BCL2 is originally characterized with respect to their roles in controlling outer mitochondrial membrane integrity and apoptosis (43, 44). The high expression of BCL2 is closely related to tumorigenesis, and the overexpression of BCL2 family proteins promotes the occurrence and development of tumors, while its inhibition is related to anti-tumor characteristics (45, 46). These results indicate that RSV can reduce the survival rate of TNBC cells by promoting apoptosis. To this effect, a functional enrichment analysis showed that genes affected by the corresponding RSV in the treatment of

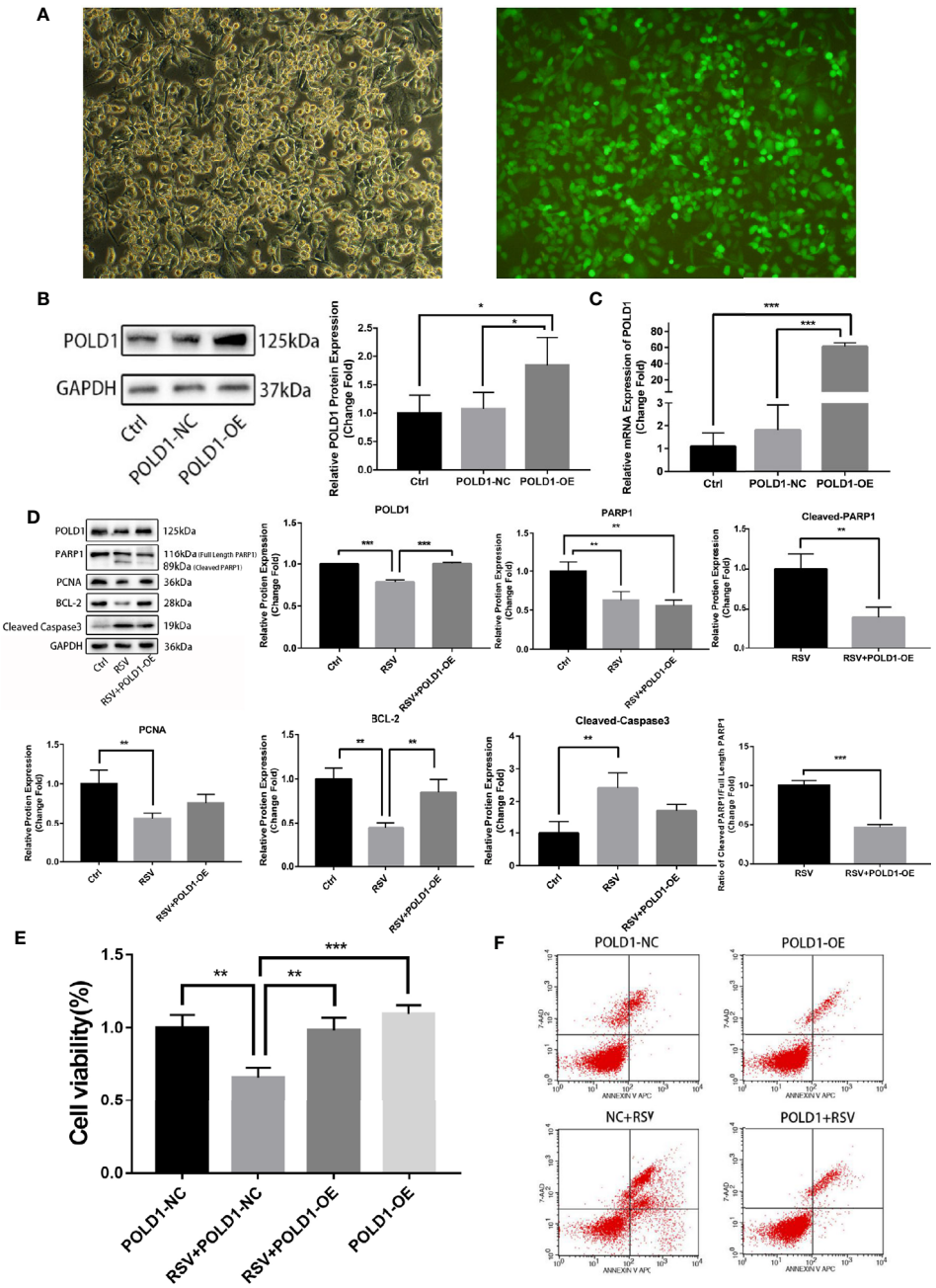


**FIGURE 6** | POLD1 rescue experiment **(A)** Immunofluorescence of POLD1 transfected with lentivirus. **(B)** POLD1 protein expression after transfection (control and POLD1-NC: *$P$=0.035, POLD1-NC and POLD1-OE: *$P$=0.048). **(C)** Gene expression of POLD1 after transfection (control and POLD1-NC: **$P$=0.007, POLD1-NC and POLD1-OE: **$P$=0.007). **(D)** Apoptosis indicators of breast cancer cells after transfection (POLD1:***$P$<0.001, PARP1: control and RSV+POLD1-OE: **$P$=0.004, RSV and RSV+POLD1-OE: **$P$=0.001, Cleaved PARP1/Full Length PARP1: ***$P$<0.001, PCNA: **$P$=0.004, BCL-2:control and RSV: **$P$=0.001, RSV and RSV +POLD1-OE: **$P$=0.006, Cleaved Caspased 3: **$P$=0.003),. **(E)** CCK8 detection of resveratrol treated breast cancer cell survival after transfection (**$P$=0.001, ***$P$<0.001). **(F)** Flow cytometry detection of resveratrol-treated apoptosis of breast cancer cells after transfection (on the two-parameter scatter diagram of flow cytometry, the lower left quadrant represents living cells; the upper left quadrant represents necrotic cells; the lower right quadrant represents apoptotic cells (late apoptotic cells), and the upper right quadrant represents early apoptotic cells).

TNBC were significantly involved in both the apoptotic signal pathway and P53 signal pathway. P53 is a tumor suppressor protein that regulates the expression of various genes including apoptosis, growth inhibition, inhibition of cell cycle progression, differentiation, and accelerated DNA repair (47, 48). In general, p53 can regulate cell growth by promoting apoptosis and DNA repair under stress. However, when p53 mutates, it loses its regulatory function, leading to abnormal cell proliferation and

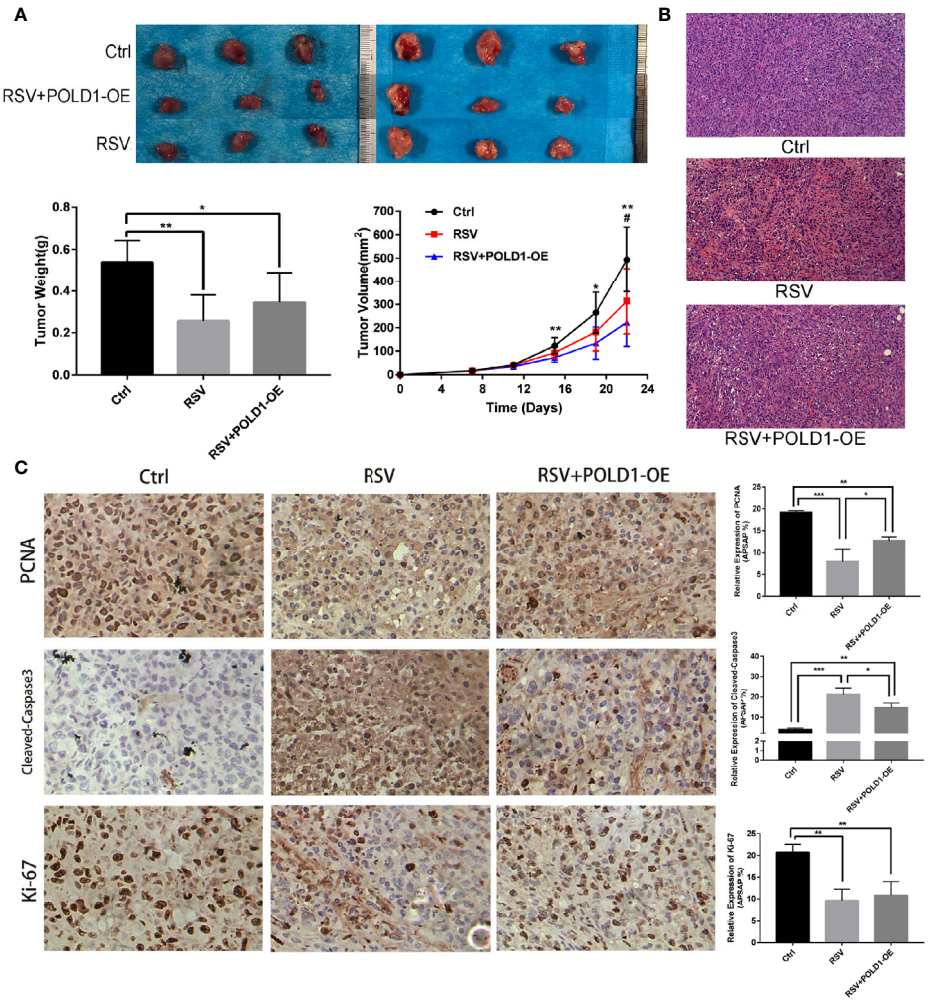


**FIGURE 7** | Identification of RSV induced apoptosis in MDA-MB-231 cells *in vitro* and *in vivo*. **(A)** Breast cancer proliferation after resveratrol and resveratrol + POLD1-OE treatment in mouse model. **(B)** Apoptosis was detected by hematoxylin-eosin (HE) staining after Resveratrol and Resveratrol + POLD1-OE treatment in mice. **(C)** Immunohistochemistry of related apoptotic proteins after resveratrol and resveratrol + POLD1-OE treatment in mice. *p<0.05, **p<0.01, ***p<0.001.

tumor progression (49). Apoptosis refers to programmed cell death, resulting in the orderly and effective removal of damaged cells, such as DNA damage or cell damage caused during development (50, 51). Apoptosis may be triggered *via* intracellular signals (such as genotoxic stress) or external signals (such as the binding of ligands to cell surface death receptors) (52, 53). Deregulation of apoptotic cell death mechanisms is a feature of cancer. Here, the genes of TNBC cells treated by RSV were found to be significantly involved in signal pathways like apoptosis and P53, suggesting that RSV can activate apoptosis of TNBC cells.

Previous studies have shown that POLD1 may be associated with the malignant proliferation of tumor cells and that a high expression of POLD1 is associated with the poor prognosis of breast cancer (38). The present study found that the low expression of POLD1 in TNBC cells treated by RSV may be related to the treatment of RSV. Further experimentation demonstrated that as the RSV treatment concentration rose, the protein expression of POLD1 in TNBC cells gradually decreased. Molecular docking suggested that RSV may bind to POLD1, and POLD1 possesses a strong correlation with DEGs in the apoptotic pathway. Hence, a comprehensive regulatory landscape of RSV-treated TNBC cells was constructed. According to the network, POLD1 was observed to interact with ATM, which is a DNA damage response gene commonly mutated in cancer. ATM activation serves as a key factor in balancing between aging and apoptosis as well as autophagy (54). In this study, ATM was found to be highly expressed in RSV affected MDA-MB-231 cells, which may be related to its apoptosis promoting mechanism. A rescue experiment was then performed with POLD1 overexpression, demonstrating that the expression levels of POLD1, PCNA, and BCL-2 in MDA-MB-231 cells treated with RSV after the overexpression of POLD1 were higher than those in the RSV treated group, while the levels of Cleaved-Caspase3 and Cleaved-PARP1 reduced. Among them, PCNA was considered to be a molecular marker of proliferation due to its role in replication (55). Here, the expression of PCNA treated with RSV

decreased, while the proliferation ability of POLD1 overexpression treatment was relatively high, indicating that POLD1 has an effect on the proliferation of TNBC cells. In addition, PARP1 was discovered to be a molecular target of anti-tumor drugs. In melanoma, breast cancer, lung cancer, and other neoplastic diseases, the expression of PARP1 is often increased (56). Therefore, the corresponding results demonstrate that POLD1 overexpression could reduce the apoptosis effect of RSV on MDA-MB-231 cells. Moreover, CCK8 and flow cytometry revealed that RSV can promote TNBC cell apoptosis, while the overexpression of POLD1 can reduce the apoptosis effect of RSV on MDA-MB-231 cells, further suggesting that RSV can mediate TNBC cell apoptosis by reducing the expression of POLD1.

Further animal experiments showed that compared to the control group, the final tumor volume and wet weight of the RSV and RSV + POLD1-OE groups were smaller. HE staining illustrated that the distribution of cancer cells was sparse, and the proportion of fiber components was observed to be significantly higher. Immunohistochemistry of the animal models showed that RSV could reduce the expression of PCNA and Ki-67 while increasing the expression of Cleaved-Caspase3. However, the POLD1 overexpression group antagonized these inhibitory or promoting effects. Ki-67 is a human nuclear antigen and forms an integral part of cell division in both normal and malignant tissue (57). High expression of Ki-67 serves as a marker for poor prognosis in breast cancer (58, 59), and the obtained results demonstrated that RSV can inhibit the growth of TNBC cells and promote necrosis in cancer cells *in vivo* but was limited in the overexpression of POLD1. This suggested that the overexpression of POLD1 can antagonize the inhibitory effect of RSV on TNBC *in vivo* and serves as an important regulatory target of RSV in the treatment of TNBC.

Although this study explored and identified a potential mechanism for the anticancer effect of RSV on TNBC cells, various limitations exist. First, relatively few samples were used in this experiment, and the results should be verified in larger sample studies. Second, this study used only one triple negative cell line and verified the proliferation and apoptosis of MDA-MB-231 cells treated by RSV at the gene level, protein level and individual animal level. However, the relationship between RSV and POLD1 requires further elucidation. More importantly, although the anti-TNBC effect of RSV has been clarified, due to poor solubility and bioavailability of RSV, as well as adverse reactions, its clinical use has been restricted. Therefore, making RSV into a drug to better treat breast cancer remains to be studied.

## CONCLUSION

In conclusion, this study determined a potential anticancer mechanism of RSV against TNBC by conducting bioinformatics and experimental studies. Accordingly, RSV was found to promote the apoptosis of TNBC cells by reducing POLD1 expression, thereby activating the respective apoptosis pathways. However, since this study is a basic mechanism study, this method has not yet been applied to human patients.

## DATA AVAILABILITY STATEMENT

We have uploaded the raw data to the Sequence Read Archive database. You can access it through the following link: https://www.ncbi.nlm.nih.gov/sra/PRJNA680177.

## ETHICS STATEMENT

The animal study was reviewed and approved by Guangxi Medical University.

## AUTHOR CONTRIBUTIONS

C-YW and H-ML developed the research design, evaluated all of the results, and were responsible for the article. Z-JL and YW developed the experimental design and analyzed the data. D-DZ, M-XW, H-MJ, D-LH, L-FL, M-JC, and W-PY performed research and contributed to the writing of this paper. All authors contributed to the article and approved the submitted version.

## FUNDING

The authors disclosed receipt of the following financial support for the research, authorship, and/or publication of this article: This work was financially supported by the National Natural Science Foundation of China (81760346, 81860341), Natural Science Foundation of Guangxi Province (2018GXNSFAA281148, 2020JJA140036), Innovation Project of Guangxi Graduate Education (YCBZ2018041), the Scientific Research & Technology Development Program of Nanning City (20173021-2, 20183037-1, 20191034), the Nanning Excellent Young Scientist Program and Guangxi Beibu Gulf Economic Zone Major Talent Program (RC20180201, RC20190206), Self-financing research Project of Guangxi Health and Family Planning Commission (Z20180679, Z20190139), and the Youth Science Foundation of Guangxi Medical University (GXMUYSF201808).

## ACKNOWLEDGMENTS

The authors would like to thank the Life-Ontology Biological Technology Co., Ltd for assisting with bioinformatics analysis.

## SUPPLEMENTARY MATERIAL

The Supplementary Material for this article can be found online at: https://www.frontiersin.org/articles/10.3389/fonc.2021.569295/full#supplementary-material

**Supplementary Figure 1** | Potential mechanisms of resveratrol promoting apoptosis of triple negative breast cancer cells.

**Supplementary Table 1 |** The result of CCK8 detection of cell viability after RSV treatment.

**Supplementary Table 2 |** Protein expression of PCNA, BCL-2, Cleaved-PARP1 and Cleaved-Caspase3 after RSV treated.

**Supplementary Table 3 |** WB and qRT-PCR of POLD1 after RSV treated.

**Supplementary Table 4 |** Protein expression and mRNA expression of POLD overexpression.

**Supplementary Table 5 |** Rescue experiment of POLD1 overexpression.

**Supplementary Table 6 |** The result of CCK8 detection of cell viability after rescue experiment.

**Supplementary Table 7 |** Weight and volume of nude mouse models after RSV treated.

**Supplementary Table 8 |** PCNA, Cleaved-Caspase3 and Ki67 of immunohistochemistry after RSV treated.

## REFERENCES


1. Beauvarlet J, Bensadoun P, Darbo E, Labrunie G, Rousseau B, Richard E, et al. Modulation of the ATM/autophagy pathway by a G-quadruplex ligand tips the balance between senescence and apoptosis in cancer cells. *Nucleic Acids Res* (2018) 47(6):2739–56. doi: 10.3322/caac.21492
2. Nielsen TO, Hsu FD, Jensen K, Cheang M, Karaca G, Hu Z, et al. Immunohistochemical and clinical characterization of the basal-likesubtype of invasive breast carcinoma. *Clin Cancer Res*(2004) 10(16):5367–74. doi: 10.1158/1078-0432.CCR-04-0220
3. Garrido-Castro AC, Lin NU, Polyak K. Insights into Molecular Classifications of Triple-Negative Breast Cancer: Improving Patient Selection for Treatment. *Cancer Discovery* (2019) 9(2):176–98. doi: 10.1158/2159-8290.CD-18-1177
4. Lee KL, Kuo YC, Ho YS, Huang YH. Triple-Negative Breast Cancer: Current Understanding and Future Therapeutic Breakthrough Targeting Cancer Stemness. *Cancers (Basel)* (2019) 11(9). doi: 10.3390/cancers11091334
5. Brown M, Tsodikov A, Bauer KR, Parise CA, Caggiano V. The role of human epidermal growth factor receptor 2 in the survivalof women with estrogen and progesterone receptor-negative, invasive breast cancer: the California Cancer Registry, 1999-2004. *Cancer* (2008) 112(4):737–47. doi: 10.1002/cncr.23243
6. Dent R, et al. Triple-negative breast cancer: clinical features and patterns of recurrence. *Clin Cancer Res* (2007) 13(15 Pt 1):4429–34. doi: 10.1158/1078-0432.CCR-06-3045
7. Liedtke C, et al. Response to neoadjuvant therapy and long-term survival in patients with triple-negative breast cancer. *J Clin Oncol* (2008) 26(8):1275–81. doi: 10.1200/JCO.2007.14.4147
8. Tan DS, Marchio C, Tan DS, Jones RL, Savage K, Smith IE, et al. Triple negative breast cancer: molecular profiling and prognostic impact in adjuvant anthracycline-treated patients. *Breast Cancer Res Treat* (2008) 111(1):27–44. doi: 10.1007/s10549-007-9756-8
9. Carter LG, D'Orazio JA, Pearson KJ. Resveratrol and cancer: focus on in vivo evidence. *Endocr Relat Cancer* (2014) 21(3):R209–25. doi: 10.1530/ERC-13-0171
10. Sinha D, Sarkar N, Biswas J, Bishayee A. Resveratrol for breast cancer prevention and therapy: Preclinical evidence and molecular mechanisms. *Semin Cancer Biol* (2016) 40–41:209–32. doi: 10.1016/j.semcancer.2015.11.001
11. Jardim FR, de Rossi FT, Nascimento MX, da Silva Barros RG, Borges PA, Prescilio IC, et al. Resveratrol and Brain Mitochondria: a Review. *Mol Neurobiol* (2018) 55(3):2085–101. doi: 10.1007/s12035-017-0448-z
12. Fremont L. Biological effects of resveratrol. *Life Sci* (2000) 66(8):663–73. doi: 10.1016/S0024-3205(99)00410-5
13. Chaplin A, Carpene C, Mercader J. Resveratrol, Metabolic Syndrome, and Gut Microbiota. *Nutrients* (2018) 10(11). doi: 10.3390/nu10111651
14. Hou CY, Tain YL, Yu HR, Huang LT. The Effects of Resveratrol in the Treatment of Metabolic Syndrome. *Int J Mol Sci* (2019) 20(3). doi: 10.3390/ijms20030535
15. Huang XT, Li X, Xie ML, Huang Z, Huang YX, Wu GX, et al. Resveratrol: Review on its discovery, anti-leukemia effects and pharmacokinetics. *Chem Biol Interact* (2019) 306:29–38. doi: 10.1016/j.cbi.2019.04.001
16. Huminiecki L, Horbanczuk J. The functional genomic studies of resveratrol in respect to its anti-cancer effects. *Biotechnol Adv* (2018) 36(6):1699–708. doi: 10.1016/j.biotechadv.2018.02.011
17. Jiang Z, Chen K, Cheng L, Yan B, Qian W, Cao J, et al. Resveratrol and cancer treatment: updates. *Ann N Y Acad Sci* (2017) 1403(1):59–69. doi: 10.1111/nyas.13466
18. Sun Y, Zhou QM, Lu YY, Zhang H, Chen QL, Zhao M, et al. Resveratrol Inhibits the Migration and Metastasis of MDA-MB-231 Human Breast Cancer by Reversing TGF-beta1-Induced Epithelial-Mesenchymal Transition. *Molecules* (2019) 24(6). doi: 10.3390/molecules24061131
19. Nicolas E, Golemis EA, Arora S. POLD1: Central mediator of DNA replication and repair, and implication in cancer and other pathologies. *Gene* (2016) 590(1):128–41. doi: 10.1016/j.gene.2016.06.031
20. Li B, Lee MY. Transcriptional regulation of the human DNA polymerase delta catalytic subunit gene POLD1 by p53 tumor suppressor and Sp1. *J Biol Chem* (2001) 276(32):29729–39. doi: 10.1074/jbc.M101167200
21. Xu Y, Qin Q, Chen R, Wei C, Mo Q. SIRT1 promotes proliferation, migration, and invasion of breast cancer cell line MCF-7 by upregulating DNA polymerase delta1 (POLD1). *Biochem Biophys Res Commun* (2018) 502 (3):351–7. doi: 10.1016/j.bbrc.2018.05.164
22. Brown J, Pirrung M, McCue LA. FQC Dashboard: integrates FastQC results into a web-based, interactive, and extensible FASTQ quality control tool. *Bioinformatics* (2017) 33(19):3137–9. doi: 10.1093/bioinformatics/btx373
23. Jo H, Koh G. Faster single-end alignment generation utilizing multi-thread for BWA. *BioMed Mater Eng* (2015) 26(Suppl 1):S1791–6. doi: 10.3233/BME-151480
24. Li H, Handsaker B, Wysoker A, Fennell T, Ruan J, Homer N, et al. The Sequence Alignment/Map format and SAMtools. *Bioinformatics* (2009) 25 (16):2078–9. doi: 10.1093/bioinformatics/btp352
25. Liao Y, Smyth GK, Shi W. featureCounts: an efficient general purpose program for assigning sequence reads to genomic features. *Bioinformatics* (2014) 30(7):923–30. doi: 10.1093/bioinformatics/btt656
26. Love MI, Huber W, Anders S. Moderated estimation of fold change and dispersion for RNA-seq data with DESeq2. *Genome Biol* (2014) 15(12):550. doi: 10.1186/s13059-014-0550-8
27. Yu G, Wang LG, Han Y, He QY. clusterProfiler: an R package for comparing biological themes amonggene clusters. *OMICS* (2012)16(5):284–7. doi: 10.1089/omi.2011.0118
28. Hanzelmann S, Castelo R, Guinney J. GSVA: gene set variation analysis for microarray and RNA-seq data. *BMC Bioinf* (2013) 14:7. doi: 10.1186/1471-2105-14-7
29. Lancey C, Tehseen M, Raducanu VS, Rashid F, Merino N, Ragan TJ, et al. Structure of the processive human Pol delta holoenzyme. *Nat Commun* (2020) 11(1):1109. doi: 10.1038/s41467-020-14898-6
30. Burley SK, et al. RCSB Protein Data Bank: Sustaining a living digital data resource that enables breakthroughs in scientific research and biomedical education. *Protein Sci* (2018) 27(1):316–30. doi: 10.1002/pro.3331
31. O'Boyle NM, et al. Open Babel: An open chemical toolbox. *J Cheminform* (2011) 3:33. doi: 10.1186/1758-2946-3-33
32. Morris GM, et al. AutoDock4 and AutoDockTools4: Automated docking with selective receptor flexibility. *J Comput Chem* (2009) 30(16):2785–91. doi: 10.1002/jcc.21256
33. Dilip A, et al. Ligand-based virtual screening interface between PyMOL and LiSiCA. *J Cheminform* (2016) 8(1):46. doi: 10.1186/s13321-016-0157-z
34. von Mering C, et al. STRING: a database of predicted functional associations between proteins. *Nucleic Acids Res* (2003) 31(1):258–61. doi: 10.1093/nar/gkg034
35. Shannon P, Markiel A, Ozier O, Baliga NS, Wang JT, Ramage D, et al. Cytoscape: a software environment for integrated models of biomolecular interaction networks. *Genome Res* (2003) 13(11):2498–504. doi: 10.1101/gr.1239303
36. Pan J, Pan J, Pan J, Du C, Chen D, Xu L. *Resveratrol promotes MICA/B expression and natural killer cell lysis ofbreast cancer cells by suppressing c-Myc/miR-17 pathway. Oncotarget* (2017) 8(39):65743–58. doi: 10.18632/oncotarget.19445.
37. Tan L, Wang W, He G, Kuick RD, Gossner G, Kueck AS, et al. Resveratrol inhibits ovarian tumor growth in an in vivo mouse model. *Cancer* (2016) 122 (5):722–9. doi: 10.1002/cncr.29793

38. Qin Q, Tan Q, Li Q, Yang W, Lian B, Mo Q, et al. Elevated expression of POLD1 is associated with poor prognosis inbreast cancer. *Oncol Lett* (2018) 16 (5):5591–8. doi: 10.3892/ol.2018.9392
39. Wu H, Chen L, Zhu F, Han X, Sun L, Chen K, et al. The Cytotoxicity Effect of Resveratrol: Cell Cycle Arrest and Induced Apoptosis of Breast Cancer 4T1 Cells. *Toxins (Basel)* (2019) 11(12). doi: 10.3390/toxins11120731
40. Suh J, Kim DH, Surh YJ. Resveratrol suppresses migration, invasion and stemness of human breast cancer cells by interfering with tumor-stromal cross-talk. *Arch Biochem Biophys* (2018) 643:62–71. doi: 10.1016/j.abb.2018.02.011
41. Green DR, Llambi F. Cell Death Signaling. *Cold Spring Harb Perspect Biol* (2015) 7(12). doi: 10.1101/cshperspect.a006080
42. Porter AG, Janicke RU. Emerging roles of caspase-3 in apoptosis. *Cell Death Differ* (1999) 6(2):99–104. doi: 10.1038/sj.cdd.4400476
43. Chipuk JE, Moldoveanu T, Llambi F, Parsons MJ, Green DR, et al. The BCL-2 family reunion. *Mol Cell* (2010) 37(3):299–310. doi: 10.1016/j.molcel.2010.01.025
44. Siddiqui WA, Ahad A, Ahsan H. The mystery of BCL2 family: Bcl-2 proteins and apoptosis: an update. *Arch Toxicol* (2015) 89(3):289–317. doi: 10.1007/s00204-014-1448-7
45. Kelly PN, Strasser A. The role of Bcl-2 and its pro-survival relatives in tumourigenesis and cancer therapy. *Cell Death Differ* (2011) 18(9):1414–24. doi: 10.1038/cdd.2011.17
46. Czabotar PE, Lessene G, Strasser A, Adams JM. Control of apoptosis by the BCL-2 protein family: implications for physiology and therapy. *Nat Rev Mol Cell Biol* (2014) 15(1):49–63. doi: 10.1038/nrm3722
47. Meek DW. Regulation of the p53 response and its relationship to cancer. *Biochem J* (2015) 469(3):325–46. doi: 10.1042/BJ20150517
48. Sigal A, Rotter V. Oncogenic mutations of the p53 tumor suppressor: the demons of theguardian of the genome. *Cancer Res* (2000) 60(24):6788–93.
49. Kanapathipillai M. Treating p53 Mutant Aggregation-Associated Cancer. *Cancers (Basel)* (2018) 10(6). doi: 10.3390/cancers10060154
50. Pistritto G, Trisciuoglio D, Ceci C, Garufi A, D'Orazi G. Apoptosis as anticancer mechanism: function and dysfunction of itsmodulators and targeted therapeutic strategies. *Aging (Albany NY)* (2016) 8(4):603–19. doi: 10.18632/aging.100934
51. Elmore S. Apoptosis: a review of programmed cell death. *Toxicol Pathol* (2007) 35(4):495–516. doi: 10.1080/01926230701320337
52. Ghobrial IM, Witzig TE, Adjei AA. Targeting apoptosis pathways in cancer therapy. *CA Cancer J Clin* (2005) 55(3):178–94. doi: 10.3322/canjclin.55.3.178
53. Goldar S, Khaniani MS, Derakhshan SM, Baradaran B. Molecular mechanisms of apoptosis and roles in cancer developmentand treatment. *Asian Pac J Cancer Prev* (2015) 16(6):2129–44. doi: 10.7314/APJCP.2015.16.6.2129
54. Beauvarlet J, et al. Modulation of the ATM/autophagy pathway by a G-quadruplex ligand tips the balance between senescence and apoptosis in cancer cells. *Nucleic Acids Res* (2019) 47(6):2739–56. doi: 10.1093/nar/gkz095
55. Wang SC. PCNA: a silent housekeeper or a potential therapeutictarget? *Trends Pharmacol Sci* (2014) 35(4):178–86. doi: 10.1016/j.tips.2014.02.004
56. Malyuchenko NV, Kotova EY, Kulaeva OI, Kirpichnikov MP, Studitskiy VM, et al. PARP1 Inhibitors: antitumor drug design. *Acta Naturae* (2015) 7(3):27–37. doi: 10.32607/20758251-2015-7-3-27-37
57. Mannell A. The role of Ki-67 in breast cancer. *S Afr J Surg* (2016) 54(2):10–3.
58. Urruticoechea A, Smith IE, Dowsett M. Proliferation marker Ki-67 in early breast cancer. *J Clin Oncol* (2005) 23(28):7212–20. doi: 10.1200/JCO.2005.07.501
59. Petrelli F, Viale G, Cabiddu M, Barni S. Prognostic value of different cut-off levels of Ki-67 in breast cancer: a systematic review and meta-analysis of 64,196 patients. *Breast Cancer Res Treat* (2015) 153(3):477–91. doi: 10.1007/s10549-015-3559-0


**Conflict of Interest:** The authors declare that the research was conducted in the absence of any commercial or financial relationships that could be construed as a potential conflict of interest.

frontiers in Oncology

ORIGINAL RESEARCH
published: 13 April 2021
doi: 10.3389/fonc.2021.630432

# High Expression of microRNA-223 Indicates a Good Prognosis in Triple-Negative Breast Cancer

*Li Chen*[1,2†], *Xiuzhi Zhu*[1,2,3†], *Boyue Han*[1,2,3†], *Lei Ji*[3], *Ling Yao*[1,2*] *and Zhonghua Wang*[1,2*]

[1] Key Laboratory of Breast Cancer in Shanghai, Fudan University Shanghai Cancer Center, Shanghai, China, [2] Department of Breast Surgery, Fudan University Shanghai Cancer Center, Shanghai, China, [3] Department of Oncology, Shanghai Medical College, Fudan University, Shanghai, China

OPEN ACCESS

**Edited by:**
*Zhijie Jason Liu,*
*The University of Texas Health Science Center at San Antonio, United States*

**Reviewed by:**
*Claudia Cava,*
*National Research Council, Italy*
*Zhi-Gang Zhuang,*
*Shanghai First Maternity and Infant Hospital, China*
*Chuan-Gui Song,*
*Affiliated Union Hospital of Fujian Medical University, China*

***Correspondence:**
*Ling Yao*
*yaoling19852@126.com*
*Zhonghua Wang*
*wangzhonghua2691@sina.com*

[†]*These authors have contributed equally to this work*

**Specialty section:**
*This article was submitted to Women's Cancer, a section of the journal Frontiers in Oncology*

**Received:** *17 November 2020*
**Accepted:** *12 March 2021*
**Published:** *13 April 2021*

**Citation:**
*Chen L, Zhu X, Han B, Ji L, Yao L and Wang Z (2021) High Expression of microRNA-223 Indicates a Good Prognosis in Triple-Negative Breast Cancer. Front. Oncol. 11:630432. doi: 10.3389/fonc.2021.630432*

**Purpose:** MicroRNAs can influence many biological processes and have shown promise as cancer biomarkers. Few studies have focused on the expression of microRNA-223 (miR-223) and its precise role in breast cancer (BC). We aimed to examine the expression level of miR-223 and its prognostic value in BC.

**Methods:** Tissue microarray (TMA)-based miRNA detection *in situ* hybridization (ISH) with a locked nucleic acid (LNA) probe was used to detect miR-223 expression in 450 BC tissue samples. Overall survival (OS) and disease-free survival (DFS) were compared between two groups using the Kaplan-Meier method and Cox regression model.

**Results:** OS and DFS were prolonged in the high miR-223 expression group compared to the low miR-223 expression group ($p < 0.0001$ and $p = 0.017$, respectively), especially in patients with the triple-negative breast cancer (TNBC) subtype ($p = 0.046$ and $p < 0.001$, respectively). Univariate and multivariate Cox regression analyses revealed that TNM stage ($p = 0.008$), the molecular subtype ($p = 0.049$), and miR-223 ($p < 0.001$) were independently associated with OS and DFS. External validation was performed with the METABRIC and The Cancer Genome Atlas (TCGA) databases *via* online webtools and was consistent with the data described above.

**Conclusions:** This study provides evidence that high miR-223 expression at diagnosis is associated with improved DFS and OS for BC patients, especially those with the TNBC subtype. miR-223 is a valid and independent prognostic biomarker in BC.

**Keywords: microRNA-223, breast cancer, triple-negative, *in situ* hybridization, prognostic factor**

**Abbreviations:** miR-223, microRNA-223; BC, breast cancer; TMA, tissue microarray; ISH, *in situ* hybridization; LNA, locked nucleic acid; OS, overall survival; DFS, disease-free survival; TNBC, triple-negative breast cancer; TCGA, The Cancer Genome Atlas; ER, estrogen receptor; PR, progesterone receptor; HER2, human epidermal growth factor receptor 2; FFPE, formalin-fixed and paraffin-embedded; FUSCC, Fudan University Shanghai Cancer Center; SSC, saline sodium citrate; SI, staining index; HRs, hazard ratios.

## INTRODUCTION

Breast cancer (BC) has overtook lung cancer as leading cause of cancer worldwide (https://www.iarc.who.int/wp-content/uploads/2021/02/pr294_E.pdf). In 2020, BC made up 11.7% of all new cancer cases globally, followed by lung cancer (11.4%) and colorectal cancer (10.0%). Due to the molecular heterogeneity of BC, individual biomarkers for BC are necessary (1). Since the groundbreaking work of Sørlie T and colleagues (2, 3) at the beginning of the 21st century, BC has been believed to consist of at least four different clinically relevant molecular subtypes, Luminal A, Luminal B, HER2 enriched, and triple-negative, classified according to the expression of estrogen receptor (ER), progesterone receptor (PR), human epidermal growth factor receptor 2 (HER2), and Ki-67. Although the PAM50 test, MammaPrint test, Oncotype DX test, and others have been used for clinical treatment and prognosis prediction (4), there are still no recognized clinically relevant biomarkers or effective therapeutic targets for BC except for ER, PR, and HER2 (5). Meanwhile, numerous new biomarkers are still being researched to help optimize personalized treatment in the management of BC, especially triple-negative breast cancer (TNBC), which has a high risk of recurrence and no effective targeted therapy (6, 7).

MicroRNAs (miRNAs) are a series of single-stranded, non-coding RNAs usually 21–25 nt in length (8). MiRNA expression profiling is gaining popularity because miRNAs, as key regulators in posttranscriptional gene expression networks, can influence many biological processes and have shown promise as biomarkers for cancer (9–11). In addition, miRNAs can generally be well preserved in body fluids, formalin-fixed and paraffin-embedded (FFPE) tissues, and other types of specimens for easy preservation and evaluation (9). Functional studies have confirmed that miRNA dysregulation is causal in many cancers, with miRNAs acting as tumor suppressors or oncogenes (12). The role of miRNAs in BC has been widely studied. Several oncogenic miRNAs are correlated with tumor aggressiveness and a poor prognosis, such as miR-221 (13), miR-301a (14), miR-493 (15), miR-200c, and miR-141 (16). Other tumor suppressor miRNAs, such as miR-34 (17, 18), miR-361-5p (19), miR-548p (20), and miR-205 (21, 22), can reduce migration and invasion capabilities upon their stably high expression.

MicroRNA-223 (miR-223), located at q12 of chromosome X, has been observed primarily in the myeloid lineage, especially neutrophils (23–27). To date, no consensus between the level of miR-223 and the type of disease or disease progression has been reached (28). In cancers, the role of miR-223 is conflicting. For example, the elevated expression of miR-223 is associated with a poor prognosis and drug resistance in non-small cell lung cancer (29) and gastric cancer (30, 31). In contrast, miR-223 plays a tumor suppressor role in human prostate cancer (32), bladder cancer (33), cervical cancer (34), and hepatocellular carcinoma (35, 36).

Until now, few studies have focused on the expression of miR-223 and its precise role in BC. Previous studies suggested that miR-223 improved treatment response in BC, including increasing the sensitivity to CDK4/6 inhibition (37) and suggesting a good response to radiotherapy (38). But none of them specifically focused on TNBC research. Xu Sun et al. demonstrated that miR-223 increased the sensitivity of TNBCs to apoptosis by targeting HAX-1 (39), but their study lacked clinical cohorts and specimens to validation. Therefore, we aimed to examine the expression level of miR-223 in our center's well-developed tissue microarray (TMA) and its specific function and potential prognostic value in BC, especially TNBC.

## MATERIALS AND METHODS

### Study Cohort

A total of 150 female patients diagnosed with stage I-III TNBC from August 2003 to November 2007 at Fudan University Shanghai Cancer Center (FUSCC; Shanghai, China) were consecutively recruited. According to the ratio approximately equal to 1.5 (ratio = TNBCs/other subtypes), 300 patients with other BC subtypes (Luminal A, Luminal B, and HER2-enriched) in the same period were randomly selected to avoid selection bias. All participants were diagnosed with invasive ductal carcinoma BC as the only primary tumor and underwent surgery, and their miR-223 expression levels were available. Overall survival (OS) was calculated as the time from the initial pathological diagnosis to death from any cause. Disease-free survival (DFS) was defined as the period from the initial pathological diagnosis to recurrence or metastasis or BC-specific death. The last follow-up time was March 2018, and the median follow-up time was 96.02 months.

Written permission was obtained for the collection of data from the FUSCC database. This study was ethically approved by the Ethical Committee and Institutional Review Board of FUSCC, and all the methods were performed in accordance with the approved guidelines.

### Tissue Microarrays (TMAs)

FFPE samples were obtained from the above BC patients before cancer treatment. The TMAs were constructed from FFPE samples by the Department of Pathology at FUSCC. Details on the development of the TMAs have been described in our previous studies (15, 19, 40–43). Briefly, an instrument was built for creating holes in the recipient array blocks and for acquiring tissue cores from the donor blocks (43). Stereotactic microscope was used to best select the areas of interest, with an additional bright light source under each block. After the block construction was completed, 8-μm sections of the resulting tumor tissue microarray block were cut with a microtome. An adhesive-coated tape system was a useful method for sectioning the tumor array blocks. The microtome knife cuts underneath a piece of tape that is placed over the block surface. The thin tissue section adheres to the tape, which is then rolled on an adhesive-coated microscope slide to transfer the section to the slide. Nearly all of the malignant tumors retain their histological pattern through the entire 3-mm-deep block. To reduce errors and improve accuracy, the TMAs were designed in duplicate cores in different areas of the same tumor.

### *In Situ* Hybridization (ISH)

ISH was performed on the TMAs using digoxigenin (DIG)-labeled miRCURY LNA robes from Exiqon (Vedbeak, Denmark) and

anEnhanced Sensitive ISH Detection Kit I from Boster (Wuhan, China). The miR-223 probe sequence was 5′-TGGGGTATTTGACAAACTGAC-3′. Detailed ISH procedures have been described previously (15, 41). Briefly, TMAs were rewarmed at 65°C for 4 h, deparaffinized in xylene, and sequentially hydrated in gradient ethanol solutions (three times in 100%, once in 95%, once in 85%, and once in 75%). Then, TMAs were washed with PBS three times and incubated with 3% hydrogen peroxide for 10 min at room temperature. Next, TMAs were washed with 0.1% DEPC-H2O for 5 min, and then incubated with pepsin diluted 10-fold by citrate at 37°C for 20 min. After the digestion procedure exposing the nucleic acid fraction of RNA, TMAs were washed with PBS three times for 5 min each and with 0.1% DEPC-H2O once for 5 min. After incubation with prehybridization solution for 3 h at 37°C, the TMAs were incubated with 200 μl miRNA probe (20 nmol/L) that had been preheated for 10 min at 80°C and quickly transferred to an ice/water mixture for 5 min, in a hybridization box at 60°C overnight. The next day, TMAs were subjected to a stringent washing procedure with 2× saline sodium citrate (SSC), 0.5× SSC, and 0.2× SSC. After a 30-min wash in blocking solution, TMAs were sequentially incubated with biotinylated digoxin (60 min), streptavidin–biotin complex (20 min), and peroxidase (20 min) with a 5-min wash in 0.5 mol/L PBS between each. The results were visualized after staining with 3, 3-diaminobenzidine and counterstained with Gill hematoxylin.

## Staining Evaluation

ISH staining was evaluated by two experienced pathologists independently in a blinded fashion. The staining index (SI) was used to incorporate the intensity and percentage of positive cells (15, 41). The intensity of staining was graded as follows: 0, no staining; 1, weak; 2, moderate; and 3, strong. The percentage of cells stained was graded as follows: 0, no staining; 1, <10%; 2, 10–50%; and 3, >50% tumor cells. The SI was calculated by multiplying the two scores. Samples with SIs >4 were defined as miR-223 high expression, whereas samples with SIs ≤4 were defined as miR-223 low expression. A third pathologist was consulted if there was a disagreement between the two observers. Examples of high and low expression stains are shown in **Figure 1**.

## miR-223 Expression in the METABRIC and TCGA Databases

The public data of miR-223 expression in the METABRIC and TCGA databases can be accessed online at Kaplan-Meier plotter https://kmplot.com/, which is a validation of survival biomarkers and capable of assessing the effect of 54k genes (mRNA, miRNA, and protein) on survival in 21 cancer types. A total of 1,262 BC patients from the METABRIC database and 1,078 BC patients from the TCGA database had complete follow-up data, pathological information, and miR-223 expression levels. All the details concerning how to use the online webtools have been described in the paper published by Lanczky et al. (44).

## Statistical Analysis

The relationships between miR-223 expression and clinicopathological parameters were based on Pearson's $\chi 2$ tests or Fisher's exact tests when necessary. OS and DFS were compared between the two groups using the Kaplan-Meier method and a Cox regression model. All p values were two-tailed, and a p value <0.05 was considered statistically significant. SPSS version 22.0 software (SPSS, Chicago, IL, USA) and R software version 3.5.3. (The R Project for Statistical Computing, https://www.r-project.org/) were used for the calculations and analyses. The R packages "survminer",

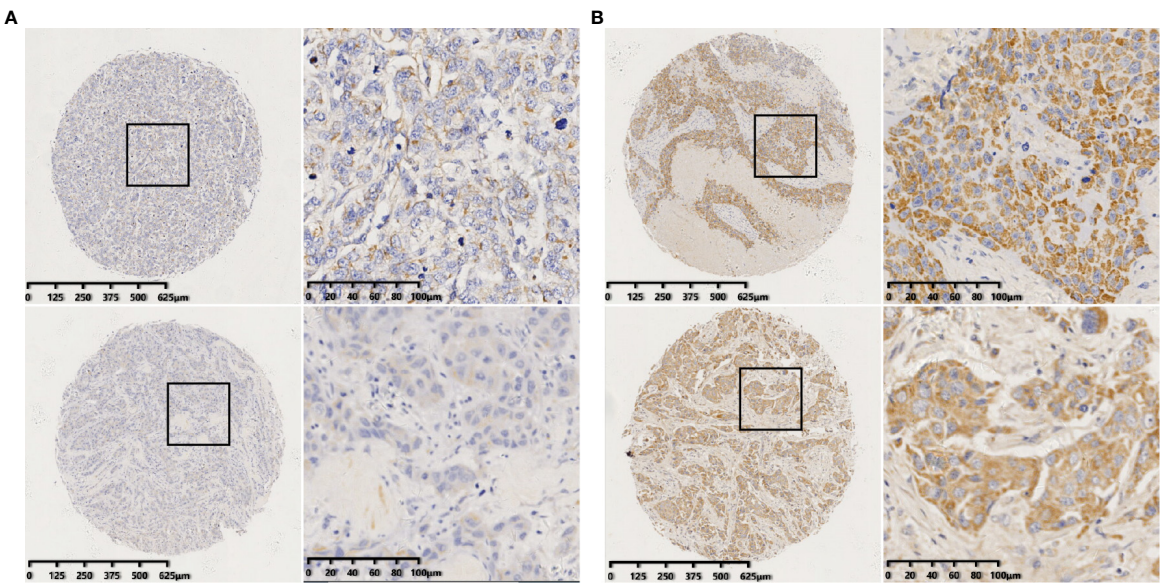


**FIGURE 1** | Identification of miR-223 in breast tumors by *in situ* hybridization (ISH). **(A)** Representative staining of negative miR-223 staining (staining index ≤4); **(B)** Representative staining of positive miR-223 staining (staining index >4) (scale bar of low-magnification = 125 μm and scale bar of high-magnification = 20 μm).

"readr", and "survival" with the appropriate libraries were used. "Kaplan-Meier plotter" was utilized to test miR-223 as a biomarker of BC patient survival.

# RESULTS

## Patient Characteristics and miR-223 Expression Patterns

For the 450 patients with invasive BC enrolled in this study, the median age was 51.31 years, and 49.1% of patients were menopausal. Among all patients, 55.11% were grade II and 26% were grade III. In addition, 56% (252/450) of patients had no lymph node metastasis, and 46.67% (210/450) had a tumor size ≤2 cm. Based on TNM stage, the proportions of patients in stage I, II, and III were 30.89, 54.67, and 11.11%, respectively. In the overall cohort, the four molecular subtypes (Luminal A, Luminal B, HER2-enriched, and triple-negative, definitions described in **Table 1**) accounted for 22, 24, 20.67, and 33.33%, respectively. In the staining evaluation, high staining for miR-223 was observed in 36.66% (165/450) of tumors. No significant associations were observed between miR-223 expression and clinicopathologic characteristics. Other related and detailed characteristics of the patients are shown in **Table 1**.

**TABLE 1** | Characteristics of the study cohort.

| Variable | Number | miR-223 expression, number (%) | | $P^a$ value |
|---|---|---|---|---|
| | | Low | High | |
| **Total** | 450 | 285 | 165 | |
| **Age (years)** | | | | 0.399 |
| ≤40 | 52 (11.56%) | 36 (8.00%) | 16 (3.56%) | |
| 40–60 | 330 (73.33%) | 210 (46.67%) | 120 (26.67%) | |
| >60 | 68 (15.11%) | 39 (8.67%) | 29 (6.44%) | |
| **Menopausal status** | | | | 0.438 |
| pre | 229 (50.89%) | 149 (33.11%) | 80 (17.78%) | |
| post | 221 (49.11%) | 136 (30.22%) | 85 (18.89%) | |
| **Differentiation** | | | | 0.811 |
| II | 248 (55.11%) | 155 (34.44%) | 93 (20.67%) | |
| III | 117 (26.00%) | 77 (17.11%) | 40 (8.89%) | |
| Missing | 85 (18.89%) | 53 (11.78%) | 32 (7.11%) | |
| **Tumor size (cm)** | | | | 0.369 |
| ≤2 | 210 (46.67%) | 131 (29.11%) | 79 (17.56%) | |
| 2–5 | 211 (46.89%) | 133 (29.56%) | 78 (17.33%) | |
| >5 | 20 (4.44%) | 13 (2.89%) | 7 (1.56%) | |
| Missing | 9 (2.00%) | 8 (1.78%) | 1 (0.22%) | |
| **Lymph node status** | | | | 0.539 |
| Negative | 252 (56.00%) | 153 (34.00%) | 99 (22.00%) | |
| Positive | 198 (44.00%) | 132 (29.33%) | 66 (14.67%) | |
| **ER** | | | | 0.622 |
| Negative | 255 (56.67%) | 164 (36.44%) | 91 (20.22%) | |
| Positive | 195 (43.33%) | 121 (26.89%) | 74 (16.44%) | |
| **PR** | | | | 0.195 |
| Negative | 298 (66.22%) | 195 (43.33%) | 103 (22.89%) | |
| Positive | 152 (33.78%) | 90 (20.00%) | 62 (13.78%) | |
| **HER2** | | | | 0.233 |
| Negative | 248 (55.11%) | 151 (33.56%) | 97 (21.56%) | |
| Positive | 202 (44.89%) | 134 (29.78%) | 68 (15.11%) | |
| **TNM stage** | | | | 0.784 |
| I | 139 (30.89%) | 84 (18.67%) | 55 (12.22%) | |
| II | 246 (54.67%) | 157 (34.89%) | 89 (19.78%) | |
| III | 50 (11.11%) | 34 (7.56%) | 16 (3.56%) | |
| Missing | 15 (3.33%) | 10 (2.22%) | 5 (1.11%) | |
| **Molecular subtype**[b] | | | | 0.635 |
| Luminal A | 99 (22.00%) | 58 (12.89%) | 41 (9.11%) | |
| Luminal B | 108 (24.00%) | 72 (16.00%) | 36 (8.00%) | |
| HER2-enriched | 93 (20.67%) | 61 (13.56%) | 32 (7.11%) | |
| Triple-negative | 150 (33.33%) | 94 (20.89%) | 56 (12.44%) | |

*ER, estrogen receptor; PR, progesterone receptor; HER2, human epidermal growth factor receptor 2.*

[a] *Based on Pearson's $\chi 2$ test; Fisher's exact test was used when needed.*

[b] *Definitions of subtypes: Luminal A (ER- and/or PR-positive, HER2-negative, PR high expression, and Ki-67 low expression), Luminal B (ER- and/or PR-positive, HER2-positive; ER-and/or PR-positive, HER2-negative, and Ki-67 high expression or PR low expression), HER2-enriched (ER- and PR-negative, HER2-positive), and triple-negative (ER-negative, PR-negative, and HER2-negative).*

## Elevated miR-223 Expression Is Associated With Good Clinical Outcomes in BC Patients

By the end of the study, a total of 20.22% (91/450) of patients experienced disease recurrence or metastasis, and 9.78% (44/450) died of BC. Among the 91 patients, 85.71% (78/91) had low miR-223 expression; among the 44 patients who died of BC, 79.55% (35/44) had low miR-223 expression. Kaplan-Meier analysis showed that the OS and DFS of the high miR-223 expression group were significantly better than those of the low miR-223 expression group ($p < 0.001$ and $p = 0.017$, respectively, **Figures 2A, B**). The 5-year DFS and OS rates of the low miR-223 expression group (76.24 and 90.43%, respectively) were significantly lower than those of the high miR-223 expression group (94.35 and 95.79%, respectively). Notably, both OS and DFS were significantly better in the high miR-223 TNBC group ($p = 0.046$ and $p < 0.001$, respectively, **Figures 2C, D**) and HER2-enriched group ($p = 0.099$ and $p = 0.014$, respectively, **Figures S1E, F**) than in the low miR-223 TNBC group, although the same trend was not observed in the other subtypes (**Figure S1**). In conclusion, high miR-223 expression indicates a better clinical outcome in BC patients, especially TNBC patients.

## Univariate and Multivariate Analyses of Prognostic Factors in BC Patients

Univariate and multivariate Cox regression analyses revealed that TNM stage ($p = 0.008$), the molecular subtype ($p = 0.049$), and miR-223 ($p < 0.001$) were independently associated with DFS (**Table 2**). The same factors were also determined to affect OS independently (**Table S1**). Since TNM stage overlapped with tumor size and lymph node status and the molecular subtype overlapped with ER, PR, and HER2 status, we did not incorporate TNM stage and the molecular subtype into the multivariate analyses to avoid study bias. The hazard ratios (HRs) of the low miR-223 expression group were 2.373 (95% CI: 1.140–4.937) for OS and 3.960 (95% CI: 2.201–7.126) for DFS, with the high miR-223 expression group used as a reference. All the results from the univariate analysis and multivariate Cox regression model are presented in **Tables 2** and **S1**.

In addition to the Cox prognosis, we explored the competing-risk nomogram. All of the validated factors in **Table 2** were incorporated to develop the competing-risks nomogram for predicting the 3-, 5-, and 10-year probability of DFS and OS by calculating the sum of the point values corresponding to each patient's characteristics. **Figure S2** showed that expression of miR-223 was the strongest contributor to DFS, while TNM stage

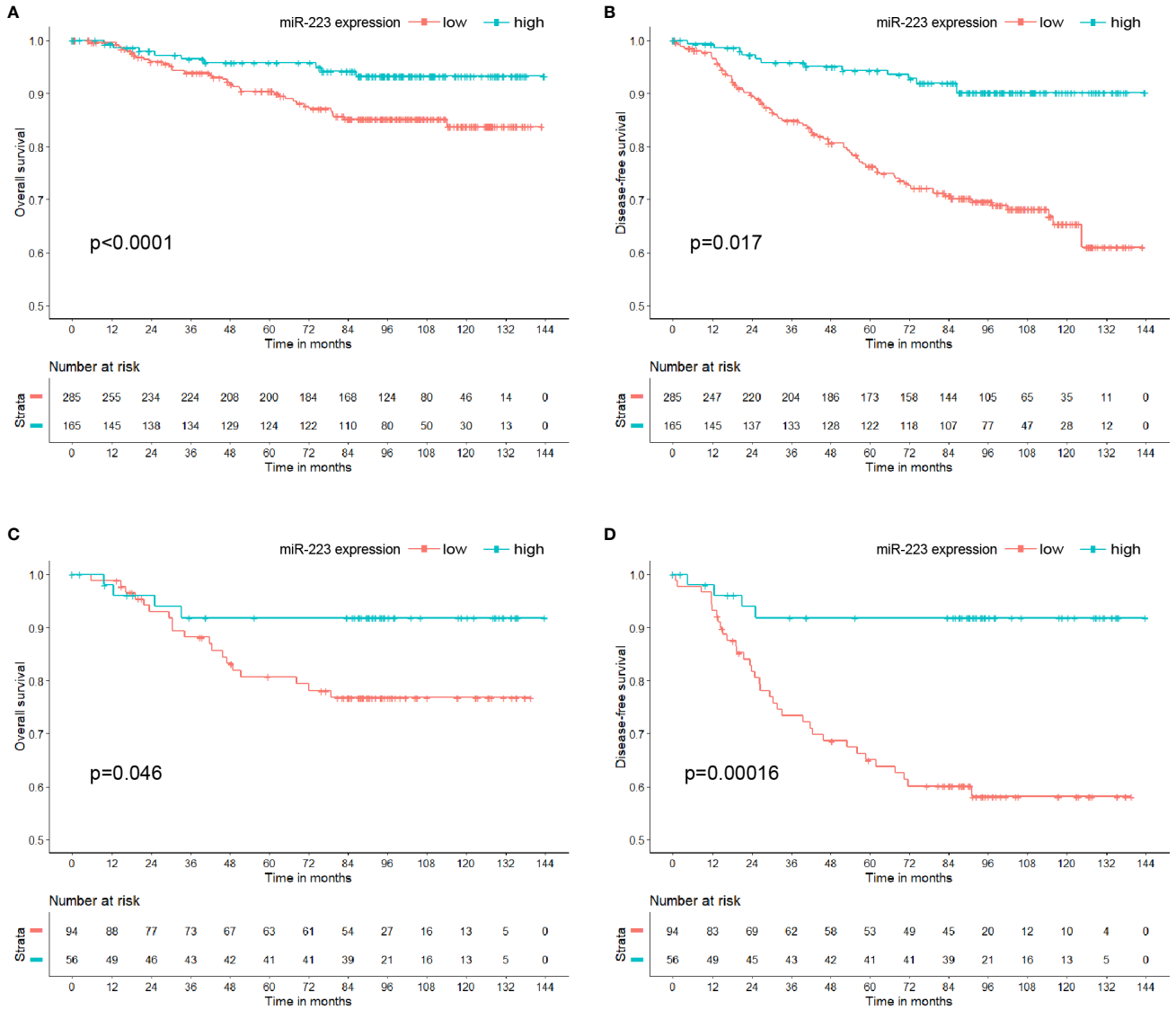


**FIGURE 2** | Kaplan-Meier curve of miR-223 expression in breast cancer patients. **(A)** Overall survival in breast cancer patients; **(B)** disease-free survival in breast cancer patients; **(C)** overall survival in triple-negative breast cancer patients; **(D)** disease-free survival in triple-negative breast cancer patients.

was the strongest contributor to OS. But unfortunately, we did not have external calibrations to verify it.

## Subgroup Analysis: miR-223 Is an Effective Predictive Factor of Clinical Outcomes in TNBC

In the subgroup analysis, miR-223 expression exhibited predictive potential for DFS and OS only in the TNBC subgroup (HR = 5.997, 95% CI 2.128–16.903, p = 0.001 for DFS; HR = 3.142, 95% CI 1.063–9.283, p = 0.038 for OS; **Table 3**) but not in the Luminal A (p = 0.217 for DFS, p = 0.277 for OS), Luminal B (p = 0.127 for DFS, p = 0.528 for OS), or HER2-enriched (p = 0.081 for DFS, p = 0.958 for OS) subgroup. Interestingly, among the 93 patients with HER2-enriched BC, five patients, all in the low miR-223 expression group, died, and no patient in the high expression group died. In addition, of the 15 patients who experienced relapse, 14 were in the low expression group, and only one was in the high expression group. This finding may explain why the statistics were slightly skewed. In summary, miR-223 is an effective predictor of clinical outcomes in TNBC, but it is worthy of further study in HER2-enriched BC.

## External Validation in the METABRIC and TCGA Databases *via* Online Webtools

To test the correlation between miR-223 expression and clinical prognosis, we performed survival analysis on data from publicly available datasets. As a survival biomarker discovery and validation tool based on a meta-analysis, Kaplan-Meier plotter is capable of assessing the effect of a miRNA on survival in BC patients.

**TABLE 2 |** Univariate and multivariate analyses for disease-free survival.

| | Univariate | | | Multivariate | | |
|---|---|---|---|---|---|---|
| **Variable** | HR | 95% CI | *P* value | HR | 95% CI | *P* value |
| **Age** | | | 0.594 | | | |
| ≤40 *vs* >60 | 1.351 | 0.626–2.914 | 0.444 | | | |
| 40–60 *vs* >60 | 0.994 | 0.548–1.803 | 0.984 | | | |
| **Menopausal status** | | | | | | |
| pre *vs* post | 0.737 | 0.487–1.113 | 0.147 | | | |
| **Differentiation** | | | | | | |
| II *vs* III | 0.730 | 0.457–1.164 | 0.186 | | | |
| **TNM stage** | | | 0.008 | | | **0.008** |
| II *vs* I | 1.421 | 0.860–2.346 | 0.170 | 1.485 | 0.887–2.485 | 0.132 |
| III *vs* I | 2.758 | 1.446–5.259 | 0.002 | 2.858 | 1.469–5.563 | 0.002 |
| **Molecular subtype** | | | 0.194 | | | **0.049** |
| Luminal B *vs* Luminal A | 1.106 | 0.580–2.107 | 0.760 | 0.813 | 0.415–1.593 | 0.546 |
| HER2-enriched *vs* Luminal A | 0.986 | 0.497–1.956 | 0.967 | 0.701 | 0.337–1.458 | 0.342 |
| Triple-negative *vs* Luminal A | 1.626 | 0.930–2.843 | 0.088 | 1.493 | 0.849–2.626 | 0.164 |
| **miR-223** | | | | | | |
| low *vs* high | 3.960 | 2.201–7.126 | <0.001 | 3.789 | 2.098–6.843 | **<0.001** |

*CI, confidence interval; HR, hazard ratio.*
*The covariates in the Cox model were all categorical variables, and the adjusted p value and HR were derived from the model.*
*The p value of the univariate analysis is marked bold.*

**TABLE 3 |** Multivariate Cox regression analysis for miR-223 as a prognostic marker for DFS and OS.

| | DFS | | | OS | | |
|---|---|---|---|---|---|---|
| Variable | HR | 95% CI | *P* value | HR | 95% CI | *P* value |
| **Molecular subtype** | | | | | | |
| Luminal A | 1.924 | 0.681–5.433 | 0.217 | 2.452 | 0.487–12.341 | 0.277 |
| Luminal B | 2.681 | 0.756–9.512 | 0.127 | 0.597 | 0.120–2.960 | 0.528 |
| HER2-enriched | 6.421 | 0.793–51.969 | 0.081 | 100402 | 0.000–6.4E+191 | 0.958 |
| Triple-negative | 5.997 | 2.128–16.903 | **0.001** | 3.142 | 1.063–9.283 | **0.038** |

*CI, confidence interval; HR, hazard ratio; DFS, disease-free survival; OS, overall survival. The covariates in the Cox model included miR-223 and TNM stage. The adjusted p value and HR were derived from the Cox model; miR-223 = 1 was used as a reference.*
*The p value of multivariate cox regression analysis for miR-223 in TNBC subtype is marked bold.*

Data from Kaplan-Meier plotter showed that patients with high expression levels of miR-223 experienced a significantly longer OS time than those with low expression levels of miR-223 in both the METABRIC and TCGA databases ($p < 0.001$ and $p = 0.0045$, **Figures 3A, B**, respectively). In the detailed subtype analysis, we found that high miR-223 expression levels were associated with prolonged OS in patients with TNBC but not in those with the other subtypes based on data from the METABRIC database ($p = 0.0054$; **Figure 3C**), consistent with the results described above. The same trend was observed in the TCGA database, but there was no statistical significance ($p = 0.067$), which may be related to the deficiency of TNBC data (n = 98, **Figure 3D**).

The same results were also confirmed in patients with rectal adenocarcinoma (n = 160, $p = 0.025$), stomach adenocarcinoma (n = 436, $p = 0.031$), thymoma (n = 124, $p = 0.03$), and kidney renal papillary cell carcinoma (n = 291, $p = 0.049$); high expression levels of miR-223 were associated with prolonged OS (data not shown, available online at https://kmplot.com/).

## DISCUSSION

Insights into the roles of miRNAs in disease development, particularly cancer, have made miRNAs attractive tools for novel biomarkers as well as therapeutic approaches (12). There is considerable evidence to indicate that miRNAs and their biogenesis machinery are involved in cancer development. The dysregulation of miRNA in tumors can be roughly divided into three parts. First, the dysregulation of miRNA biogenesis enzymes, such as downregulation of the miRNA biogenesis proteins Drosha and Dicer, is associated with poor patient outcomes (45–48). The other two points are the dysregulation of miRNAs with oncogenic function and the dysregulation of tumor suppressor miRNAs (described above). A mimic of the tumor suppressor miR-34 reached a phase I clinical trial (NCT01829971) for treating cancer. Currently, there is no universally recognized miRNA as a clinical prognostic biomarker or even as a clinical therapeutic target in BC. The search for effective biomarkers to guide treatment and predict prognosis is particularly important in TNBC, which is associated with high recurrence and lacks targeted therapy (49).

Our study is the first to evaluate the relationship between the expression of miR-223 and clinical outcomes in BC specimens. We found that the OS and DFS of the high miR-223 expression group were significantly better than those of the low miR-223 expression group, which was consistent with the results of some previous basic researches (37–39). The same results were also confirmed in the METABRIC and TCGA databases *via* online webtools. However, there was a study that differed from our results (50),

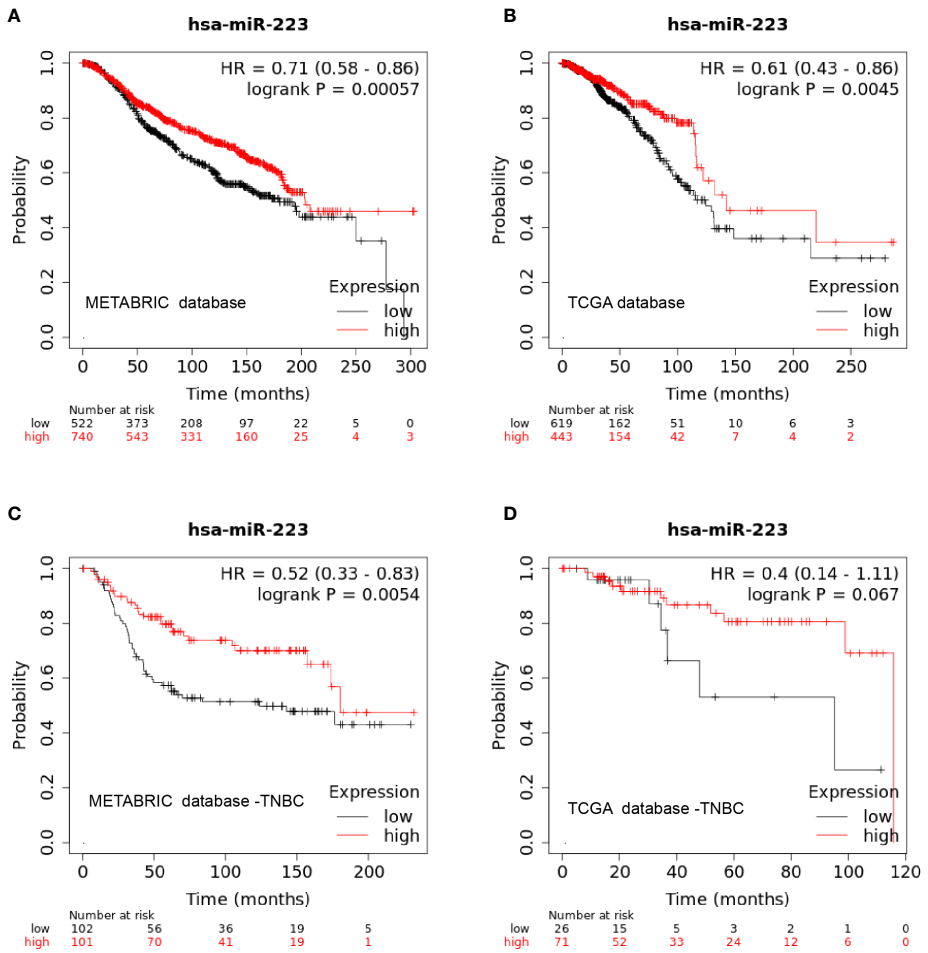


**FIGURE 3** | Kaplan-Meier curve of miR-223 expression in the METABRIC and TCGA databases. **(A)** overall survival in the METABRIC database; **(B)** overall survival in the TCGA database; **(C)** overall survival of triple-negative breast cancer patients in the METABRIC database; **(D)** overall survival of triple-negative breast cancer patients in the TCGA database.

which may be caused by different race, follow-up time, cohort size, as well as miR-223 detection methods. So far, no consensus has been reached between the expression level of miR-223 and the progression of the disease. This is also worthy of further study in the future. Surprisingly, no significant associations were observed between miR-223 expression and clinicopathologic characteristics. To a certain extent, miR-223 might be an important biomarker which was independent of these clinicopathological features, and needed to be paid attention to by clinical practice. The subsequent univariate and multivariate analyses confirmed that miR-223 is an independent prognostic factor for OS and DFS. Therefore, we speculate that miR-223 may be a protective factor in the prognosis of BC and can be detected to guide clinical practice in the future. Whether miR-223 is a tumor suppressor miRNA in BC requires further mechanistic research. In previous studies, miR-223 has been found to affect the cell cycle in acute myeloid leukemia by targeting the transcription factor E2F1 (51). Xu and coworkers found that miR-223 targets the tumor suppressor Fbxw7/Cdc4 (52). The latest research proved that miR-223 plays a key role in controlling steatosis-to-NASH progression by inhibiting two downstream targets, Cxcl10 and Taz (36).

In the subgroup analysis, the expression of miR-223 showed predictive potential for DFS and OS only in patients with TNBC but not in those with Luminal A, Luminal B, or HER2-enriched BC. According to the results from the METABRIC and TCGA database, miR-223 was also an effective predictive factor of clinical outcomes in TNBC. Regarding patients with HER2-enriched BC, DFS was better in the high miR-223 expression group, while statistical significance was not obtained for OS based on the small sample size. Unfortunately, miR-223 expression data on patients with HER2-enriched BC in the METABRIC and TCGA databases are less than our data. Interestingly, we analyzed miR-223 expression in the pan-cancer species *via* Kaplan-Meier plotter and found that high miR-223 expression was associated with a good prognosis in patients with rectal adenocarcinoma, stomach adenocarcinoma, thymoma, and kidney renal papillary cell carcinoma. Of course, this speculation needs further research and additional evidence.

In addition, several limitations to this study should be noted. First, our cohort is not representative of the composition of BC, and there were more patients with TNBC than with any of the other subtypes. Second, this was a retrospective analysis in a relatively small patient cohort. The use of the METABRIC and TCGA databases in the validation of the results might help attenuate these limitations. Third, we cannot explain the association between miR-223 and prognosis or why a high level of miR-223 indicates a good prognosis in adenocarcinoma but a poor prognosis in squamous cell carcinoma.

In conclusion, by using one of the largest BC TMAs available combined with a large public RNA sequencing database, this study provides evidence that high miR-223 expression at diagnosis is associated with prolonged DFS and OS in BC patients, especially those with the TNBC subtype. MiR-223 is a valid and independent prognostic biomarker in BC.

## DATA AVAILABILITY STATEMENT

The original contributions presented in the study are included in the article/**Supplementary Material**. Further inquiries can be directed to the corresponding authors.

## ETHICS STATEMENT

All procedures performed in studies involving human participants were in accordance with the ethical standards of the institutional and/or national research committee and with the 1964 Helsinki declaration and its later amendments or comparable ethical standards. Informed consent was obtained from all individual participants included in the study.

## AUTHOR CONTRIBUTIONS

ZW and LY designed the concept of the study. LC, LY, and XZ were responsible for data gathering. XZ and BH were responsible for statistical analysis and interpretation. LC and XZ wrote the final manuscript. LJ modified the manuscript. All authors contributed to the article and approved the submitted version.

## FUNDING

This research was supported by the Natural Science Foundation of Shanghai (19ZR1411200) and Shanghai Anti-cancer Association (SACA-AX201904).

## SUPPLEMENTARY MATERIAL

The Supplementary Material for this article can be found online at: https://www.frontiersin.org/articles/10.3389/fonc.2021.630432/full#supplementary-material

## REFERENCES

1. Sachs N, de Ligt J, Kopper O, Gogola E, Bounova G, Weeber F, et al. A Living Biobank of Breast Cancer Organoids Captures Disease Heterogeneity. *Cell* (2018) 172(1-2):373–86. doi: 10.1016/j.cell.2017.11.010
2. Perou CM, Sørlie T, Eisen MB, van de Rijn M, Jeffrey SS, Rees CA, et al. Molecular portraits of human breast tumours. *Nature* (2000) 406(6797):747–52. doi: 10.1038/35021093
3. Sørlie T, Perou CM, Tibshirani R, Aas T, Geisler S, Johnsen H, et al. Gene expression patterns of breast carcinomas distinguish tumor subclasses with clinical implications. *Proc Natl Acad Sci USA* (2001) 98(19):10869–74. doi: 10.1073/pnas.191367098
4. Kwa M, Makris A, Esteva FJ. Clinical utility of gene-expression signatures in early stage breast cancer. *Nat Rev Clin Oncol* (2017) 14(10):595–610. doi: 10.1038/nrclinonc.2017.74
5. Harbeck N, Gnant M. Breast cancer. *Lancet* (2017) 389(10074):1134–50. doi: 10.1016/S0140-6736(16)31891-8
6. Waks AG, Winer EP. Breast Cancer Treatment: A Review. *JAMA* (2019) 321 (3):288–300. doi: 10.1001/jama.2018.19323
7. Zhu X, Chen L, Huang B, Wang Y, Ji L, Wu J, et al. The prognostic and predictive potential of Ki-67 in triple-negative breast cancer. *Sci Rep* (2020) 10 (1):225. doi: 10.1038/s41598-019-57094-3
8. Lu TX, Rothenberg ME. MicroRNA. *J Allergy Clin Immunol* (2018) 141 (4):1202–7. doi: 10.1016/j.jaci.2017.08.034
9. Armand-Labit V, Pradines A. Circulating cell-free microRNAs as clinical cancer biomarkers. *Biomol Concepts* (2017) 8(2):61–81. doi: 10.1515/bmc-2017-0002
10. Pritchard CC, Cheng HH, Tewari M. MicroRNA profiling: approaches and considerations. *Nat Rev Genet* (2012) 13(5):358–69. doi: 10.1038/nrg3198
11. Gyparaki MT, Basdra EK, Papavassiliou AG. MicroRNAs as regulatory elements in triple negative breast cancer. *Cancer Lett* (2014) 354(1):1–4. doi: 10.1016/j.canlet.2014.07.036
12. Rupaimoole R, Slack FJ. MicroRNA therapeutics: towards a new era for the management of cancer and other diseases. *Nat Rev Drug Discov* (2017) 16 (3):203–22. doi: 10.1038/nrd.2016.246
13. Santolla MF, Lappano R, Cirillo F, Rigiracciolo DC, Sebastiani A, Abonante S, et al. miR-221 stimulates breast cancer cells and cancer-associated fibroblasts (CAFs) through selective interference with the A20/c-Rel/CTGF signaling. *J Exp Clin Cancer Res* (2018) 37(1):94. doi: 10.1186/s13046-018-0767-6
14. Zheng JZ, Huang YN, Yao L, Liu YR, Liu S, Hu X, et al. Elevated miR-301a expression indicates a poor prognosis for breast cancer patients. *Sci Rep* (2018) 8(1):2225. doi: 10.1038/s41598-018-20680-y
15. Yao L, Liu Y, Cao Z, Li J, Huang Y, Hu X, et al. MicroRNA-493 is a prognostic factor in triple-negative breast cancer. *Cancer Sci* (2018) 109(7):2294–301. doi: 10.1111/cas.13644
16. Zhang G, Zhang W, Li B, Stringer-Reasor E, Chu C, Sun L, et al. MicroRNA-200c and microRNA- 141 are regulated by a FOXP3-KAT2B axis and associated with tumor metastasis in breast cancer. *Breast Cancer Res* (2017) 19(1):73. doi: 10.1186/s13058-017-0858-x
17. Imani S, Wu RC, Fu J. MicroRNA-34 family in breast cancer: from research to therapeutic potential. *J Cancer* (2018) 9(20):3765–75. doi: 10.7150/jca.25576
18. Zhang L, Liao Y, Tang L. MicroRNA-34 family: a potential tumor suppressor and therapeutic candidate in cancer. *J Exp Clin Cancer Res* (2019) 38(1):53. doi: 10.1186/s13046-019-1059-5
19. Cao ZG, Huang YN, Yao L, Liu YR, Hu X, Hou YF, et al. Positive expression of miR-361-5p indicates better prognosis for breast cancer patients. *J Thorac Dis* (2016) 8(7):1772–9. doi: 10.21037/jtd.2016.06.29

20. Liang Y, Song X, Li Y, Su P, Han D, Ma T, et al. circKDM4C suppresses tumor progression and attenuates doxorubicin resistance by regulating miR-548p/PBLD axis in breast cancer. *Oncogene* (2019) 38(42):6850–66. doi: 10.1038/s41388-019-0926-z
21. Xiao Y, Li Y, Tao H, Humphries B, Li A, Jiang Y, et al. Integrin α5 down-regulation by miR-205 suppresses triple negative breast cancer stemness and metastasis by inhibiting the Src/Vav2/Rac1 pathway. *Cancer Lett* (2018) 433:199–209. doi: 10.1016/j.canlet.2018.06.037
22. Seo S, Moon Y, Choi J, Yoon S, Jung KH, Cheon J, et al. The GTP binding activity of transglutaminase 2 promotes bone metastasis of breast cancer cells by downregulating microRNA-205. *Am J Cancer Res* (2019) 9 (3):597–607.
23. Johnnidis JB, Harris MH, Wheeler RT, Stehling-Sun S, Lam MH, Kirak O, et al. Regulation of progenitor cell proliferation and granulocyte function by microRNA-223. *Nature* (2008) 451(7182):1125–9. doi: 10.1038/nature06607
24. Chen CZ, Li L, Lodish HF, Bartel DP. MicroRNAs modulate hematopoietic lineage differentiation. *Science* (2004) 303(5654):83–6. doi: 10.1126/science.1091903
25. Calvente CJ, Tameda M, Johnson CD, Del PH, Lin YC, Adronikou N, et al. Neutrophils contribute to spontaneous resolution of liver inflammation and fibrosis via microRNA-223. *J Clin Invest* (2019) 129(10):4091–109. doi: 10.1172/JCI122258
26. Zhou W, Pal AS, Hsu AY, Gurol T, Zhu X, Wirbisky-Hershberger SE, et al. MicroRNA-223 Suppresses the Canonical NF-κB Pathway in Basal Keratinocytes to Dampen Neutrophilic Inflammation. *Cell Rep* (2018) 22 (7):1810–23. doi: 10.1016/j.celrep.2018.01.058
27. Neudecker V, Brodsky KS, Clambey ET, Schmidt EP, Packard TA, Davenport B, et al. Neutrophil transfer of miR-223 to lung epithelial cells dampens acute lung injury in mice. *Sci Transl Med* (2017) 9(408):eaah5360. doi: 10.1126/scitranslmed.aah5360
28. Haneklaus M, Gerlic M, O'Neill LA, Masters SL. miR-223: infection, inflammation and cancer. *J Intern Med* (2013) 274(3):215–26. doi: 10.1111/joim.12099
29. Xu YH, Tu JR, Zhao TT, Xie SG, Tang SB. Overexpression of lncRNA EGFR −AS1 is associated with a poor prognosis and promotes chemotherapy resistance in non−small cell lung cancer. *Int J Oncol* (2019) 54(1):295–305. doi: 10.3892/ijo.2018.4629
30. Li BS, Zhao YL, Guo G, Li W, Zhu ED, Luo X, et al. Plasma microRNAs, miR-223, miR-21 and miR-218, as novel potential biomarkers for gastric cancer detection. *PLoS One* (2012) 7(7):e41629. doi: 10.1371/journal.pone.0041629
31. Li J, Guo Y, Liang X, Sun M, Wang G, De W, et al. MicroRNA-223 functions as an oncogene in human gastric cancer by targeting FBXW7/hCdc4. *J Cancer Res Clin Oncol* (2012) 138(5):763–74. doi: 10.1007/s00432-012-1154-x
32. Kurozumi A, Goto Y, Matsushita R, Fukumoto I, Kato M, Nishikawa R, et al. Tumor-suppressive microRNA-223 inhibits cancer cell migration and invasion by targeting ITGA3/ITGB1 signaling in prostate cancer. *Cancer Sci* (2016) 107(1):84–94. doi: 10.1111/cas.12842
33. Sugita S, Yoshino H, Yonemori M, Miyamoto K, Matsushita R, Sakaguchi T, et al. Tumor−suppressive microRNA−223 targets WDR62 directly in bladder cancer. *Int J Oncol* (2019) 54(6):2222–36. doi: 10.3892/ijo.2019.4762
34. Tang Y, Wang Y, Chen Q, Qiu N, Zhao Y, You X. MiR-223 inhibited cell metastasis of human cervical cancer by modulating epithelial-mesenchymal transition. *Int J Clin Exp Pathol* (2015) 8(9):11224–9.
35. Wong QW, Lung RW, Law PT, Lai PB, Chan KY, To KF, et al. MicroRNA-223 is commonly repressed in hepatocellular carcinoma and potentiates expression of Stathmin1. *Gastroenterology* (2008) 135(1):257–69. doi: 10.1053/j.gastro.2008.04.003
36. He Y, Hwang S, Cai Y, Kim SJ, Xu M, Yang D, et al. MicroRNA-223 Ameliorates Nonalcoholic Steatohepatitis and Cancer by Targeting Multiple Inflammatory and Oncogenic Genes in Hepatocytes. *Hepatology* (2019) 70 (4):1150–67. doi: 10.1002/hep.30645
37. Citron F, Segatto I, Vinciguerra G, Musco L, Russo F, Mungo G, et al. Downregulation of miR-223 Expression Is an Early Event during Mammary Transformation and Confers Resistance to CDK4/6 Inhibitors in Luminal Breast Cancer. *Cancer Res* (2020) 80(5):1064–77. doi: 10.1158/0008-5472.CAN-19-1793
38. Fabris L, Berton S, Citron F, D'Andrea S, Segatto I, Nicoloso MS, et al. Radiotherapy-induced miR-223 prevents relapse of breast cancer by targeting the EGF pathway. *Oncogene* (2016) 35(37):4914–26. doi: 10.1038/onc.2016.23
39. Sun X, Li Y, Zheng M, Zuo W, Zheng W. MicroRNA-223 Increases the Sensitivity of Triple-Negative Breast Cancer Stem Cells to TRAIL-Induced Apoptosis by Targeting HAX-1. *PLoS One* (2016) 11(9):e162754. doi: 10.1371/journal.pone.0162754
40. Chen L, Yang L, Qiao F, Hu X, Li S, Yao L, et al. High Levels of Nucleolar Spindle-Associated Protein and Reduced Levels of BRCA1 Expression Predict Poor Prognosis in Triple-Negative Breast Cancer. *PLoS One* (2015) 10(10): e140572. doi: 10.1371/journal.pone.0140572
41. Cao ZG, Li JJ, Yao L, Huang YN, Liu YR, Hu X, et al. High expression of microRNA-454 is associated with poor prognosis in triple-negative breast cancer. *Oncotarget* (2016) 7(40):64900–9. doi: 10.18632/oncotarget.11764
42. Ye FG, Song CG, Cao ZG, Xia C, Chen DN, Chen L, et al. Cytidine Deaminase Axis Modulated by miR-484 Differentially Regulates Cell Proliferation and Chemoresistance in Breast Cancer. *Cancer Res* (2015) 75(7):1504–15. doi: 10.1158/0008-5472.CAN-14-2341
43. Kononen J, Bubendorf L, Kallioniemi A, Bärlund M, Schraml P, Leighton S, et al. Tissue microarrays for high-throughput molecular profiling of tumor specimens. *Nat Med* (1998) 4(7):844–7. doi: 10.1038/nm0798-844
44. Lánczky A, Nagy Á, Bottai G, Munkácsy G, Szabó A, Santarpia L, et al. miRpower: a web-tool to validate survival-associated miRNAs utilizing expression data from 2178 breast cancer patients. *Breast Cancer Res Treat* (2016) 160(3):439–46. doi: 10.1007/s10549-016-4013-7
45. Guo X, Liao Q, Chen P, Li X, Xiong W, Ma J, et al. The microRNA-processing enzymes: Drosha and Dicer can predict prognosis of nasopharyngeal carcinoma. *J Cancer Res Clin Oncol* (2012) 138(1):49–56. doi: 10.1007/s00432-011-1058-1
46. Dedes KJ, Natrajan R, Lambros MB, Geyer FC, Lopez-Garcia MA, Savage K, et al. Down-regulation of the miRNA master regulators Drosha and Dicer is associated with specific subgroups of breast cancer. *Eur J Cancer* (2011) 47 (1):138–50. doi: 10.1016/j.ejca.2010.08.007
47. Allegra D, Bilan V, Garding A, Döhner H, Stilgenbauer S, Kuchenbauer F, et al. Defective DROSHA processing contributes to downregulation of MiR-15/-16 in chronic lymphocytic leukemia. *Leukemia* (2014) 28(1):98–107. doi: 10.1038/leu.2013.246
48. Torres A, Torres K, Paszkowski T, Jodłowska-Jędrych B, Radomański T, Książek A, et al. Major regulators of microRNAs biogenesis Dicer and Drosha are down-regulated in endometrial cancer. *Tumour Biol* (2011) 32(4):769–76. doi: 10.1007/s13277-011-0179-0
49. Bianchini G, Balko JM, Mayer IA, Sanders ME, Gianni L. Triple-negative breast cancer: challenges and opportunities of a heterogeneous disease. *Nat Rev Clin Oncol* (2016) 13(11):674–90. doi: 10.1038/nrclinonc.2016.66
50. Purwanto I, Heriyanto DS, Widodo I, Hakimi M, Hardianti MS, Aryandono T, et al. MicroRNA-223 is Associated with Resistance Towards Platinum-based Chemotherapy and Worse Prognosis in Indonesian Triple-negative Breast Cancer Patients. *Breast Cancer (Dove Med Press)* (2021) 13:1–7. doi: 10.2147/BCTT.S291014
51. Pulikkan JA, Dengler V, Peramangalam PS, Peer ZA, Müller-Tidow C, Bohlander SK, et al. Cell-cycle regulator E2F1 and microRNA-223 comprise an autoregulatory negative feedback loop in acute myeloid leukemia. *Blood* (2010) 115(9):1768–78. doi: 10.1182/blood-2009-08-240101
52. Xu Y, Sengupta T, Kukreja L, Minella AC. MicroRNA-223 regulates cyclin E activity by modulating expression of F-box and WD-40 domain protein 7. *J Biol Chem* (2010) 285(45):34439–46. doi: 10.1074/jbc.M110.152306


**Conflict of Interest:** The authors declare that the research was conducted in the absence of any commercial or financial relationships that could be construed as a potential conflict of interest.

frontiers in Oncology

ORIGINAL RESEARCH
published: 03 May 2021
doi: 10.3389/fonc.2021.630300

# LncRNA PCIR Is an Oncogenic Driver *via* Strengthen the Binding of TAB3 and PABPC4 in Triple Negative Breast Cancer

*Wenhui Guo*[1,2,3†], *Jingyi Li*[4†], *Haobo Huang*[5†], *Fangmeng Fu*[1,2,3†], *Yuxiang Lin*[1,2,3] *and Chuan Wang*[1,2,3*]

[1] Department of Breast Surgery, Fujian Medical University Union Hospital, Fuzhou, China, [2] Department of General Surgery, Fujian Medical University Union Hospital, Fuzhou, China, [3] Breast Cancer Institute, Fujian Medical University, Fuzhou, China, [4] College of Integrated Traditional Chinese and Western Medicine, Fujian University of Traditional Chinese Medicine, Fuzhou, China, [5] Department of Blood Transfusion, Fujian Medical University Union Hospital, Fuzhou, China

OPEN ACCESS

**Edited by:**
Shengtao Zhou,
Sichuan University, China

**Reviewed by:**
Xiuxing Wang,
Nanjing Medical University, China
Yuhong Zhou,
Fudan University, China
Zhe Li,
Fudan University, China
Houbao Liu,
Fudan University, China

***Correspondence:**
Chuan Wang
chuanwangfmu@163.com

[†]These authors have contributed equally to this work

**Specialty section:**
This article was submitted to Women's Cancer, a section of the journal Frontiers in Oncology

**Received:** 17 November 2020
**Accepted:** 06 April 2021
**Published:** 03 May 2021

**Citation:**
Guo W, Li J, Huang H, Fu F, Lin Y and Wang C (2021) LncRNA PCIR Is an Oncogenic Driver via Strengthen the Binding of TAB3 and PABPC4 in Triple Negative Breast Cancer. Front. Oncol. 11:630300. doi: 10.3389/fonc.2021.630300

Long non-coding RNAs (LncRNA) as the key regulators in all stages of tumorigenesis and metastasis. However, the underlying mechanisms are largely unknown. Here, we report a lncRNA RP11-214F16.8, which renamed Lnc-PCIR, is upregulated and higher RNA level of Lnc-PCIR was positively correlated to the poor survival of patients with triple negative breast cancer (TNBC) tissues. Lnc-PCIR overexpression significantly promoted cell proliferation, migration, and invasion *in vitro* and *in vivo*. RNA pulldown, RNA immunoprecipitation (RIP) and RNA transcriptome sequencing technology (RNA-seq) was performed to identify the associated proteins and related signaling pathways. Mechanistically, higher Lnc-PCIR level of blocks PABPC4 proteasome-dependent ubiquitination degradation; stable and highly expressed PABPC4 can further increase the stability of TAB3 mRNA, meanwhile, overexpression of Lnc-PCIR can disrupt the binding status of TAB3 and TAB2 which lead to activate the TNF-α/NF-κB pathway in TNBC cells. Our findings suggest that Lnc-PCIR promotes tumor growth and metastasis *via* up-regulating the mRNA/protein level of TAB3 and PABPC4, activating TNF-α/NF-κB signaling pathway in TNBC.

**Keywords: long non-coding RNA, RP11-214F16.8/Lnc-PCIR, TNF-α/NF-κB signaling pathway, TGF-beta activated kinase 1 (MAP3K7) binding protein 3, poly(A) binding protein cytoplasmic 4**

## BACKGROUND

Breast cancer is the most frequently diagnosed malignancy in women worldwide and is the second leading cause of cancer-related death in the United States (1, 2). Expression of the estrogen receptor (ER), progesterone receptor (PR), and amplification of the HER2 gene define the main breast cancer subtypes in terms of prognostic and therapeutic intervention (3). Triple negative breast cancer (TNBC) is the breast cancer subtype characterized by the absence of expression of the ER, PR and

HER2 (4).Therapies commonly used in other breast cancer subtypes are therefore not suitable for TNBC, and treatment options are largely limited to conventional genotoxic chemotherapy (5, 6). Most of TNBC patients present high rates of metastatic recurrence and very poor long-term prognosis after chemotherapy. Consequently, to explore the underlying mechanisms and identification of molecular targets and the development of new therapeutic avenues remain critically important.

Long non-coding RNAs (lncRNAs) are a class of transcripts longer than 200 nucleotides lacking the open reading frame with no protein-coding ability (7). With advancements in cancer transcriptome profiling, large number of lncRNAs has been demonstrated closely associated with cancer (8, 9). Besides, lncRNAs have also been implicated to regulate a range of biological functions, such as genomic imprinting and transcriptional regulation, plays a critical role in tumorigenesis and metastasis (10–12). During the past decade, numerous studies have showed the important role of NF-κB pathway as a link between inflammation and tumorigenesis (13). NF-κB was first identified as part of the immune system, and become widely accepted as a crucial transcription factor that regulates inflammation, innate and adaptive immunity, cell proliferation, cell differentiation and apoptosis (14, 15). The hyper-activate of NF-κB pathway has been linked to cancer which is regarded as a potential therapeutic target in human cancers (16, 17). TGF-beta activated kinase 1 (MAP3K7) binding protein 3 (TAB3), as a newly identified Transforming growth factor-β-activated kinase 1 (TAK1) binding partner, has been implicated in the immune response, signal transduction, inflammation and autophagy (18–21). Several reports showed TAB3 is markedly overexpressed in various tumor tissues, such as the testis, skin, non-small cell lung cancer (NSCLC), hepatocellular carcinoma (HCC) and small intestinal cancers (19, 22–24). However, the mechanism of overexpressed TAB3 in the process of TNBC remains unclear.

In this study, we sought to identify clinically relevant lncRNAs deregulated specifically in TNBC patients and aim to reveal the functional role and regulatory mechanism of lncRNA in the progress of TNBC. We identified and characterized the lncRNA RP11-214F16.8, renamed Lnc-PCIR (LncRNA Positively Correlated with Inflammatory Responses). Our results showed Lnc-PCIR was upregulated in TNBC tissues, and overexpressed of Lnc-PCIR could accelerated cell growth and metastasis *in vitro* and *in vivo*. For mechanistic investigations, Lnc-PCIR could directly binding with TAB3 and PABPC4. The stability of PABPC4 protein was increased by inhibiting ubiquitin proteasome degradation and overexpressed PABPC4 can enhance the stability of TAB3 mRNA, which known as a key molecular involved in TNF-α/NF-κB signaling pathway. Taken together, these results suggest that Lnc-PCIR may be as the promising therapeutic target for TNBC patients.

**Abbreviations:** LncRNA, Long non-coding RNA; TNBC, Triple Negative Breast Cancer; Lnc-PCIR, LncRNA Positively Correlated with Inflammatory Responses; CCK-8, Cell Counting Kit-8; RIP, RNA Immunoprecipitation; TCGA, The Cancer Genome Atlas; TAB3, TGF-beta activated kinase 1 (MAP3K7) binding protein 3; PABPC4, poly(A) binding protein cytoplasmic 4; TAB2, TGF-beta activated kinase 1 (MAP3K7) binding protein 2; UCSC, University of California, Santa Cruz; qPCR, quantitative real-time PCR; RACE, rapid amplification of cDNA ends; MS, mass spectrometry; ER, estrogen receptor; PR, progesterone receptor; TAK1, Transforming growth factor-β-activated kinase 1; NSCLC, non-small cell lung cancer; HCC, hepatocellular carcinoma; GSEA, Gene Set Enrichment Analysis; GO analysis, Gene Ontology Analysis; EMT, Epithelial-Mesenchymal Transition; CHX, cycloheximide.

# METHODS

## Cell Culture

Human TNBC cell lines used in this study were purchased from Cell Bank of the Chinese Academy of Science (Shanghai, China), the Health Science Research Resources Bank (Osaka, Japan) and American Type Culture Collection (ATCC, Manassas, Virginia, USA). The cell lines were cultured in Dulbecco's modified Eagle's medium (DMEM, Gibco BRL) contained with 10% fetal calf serum (FBS, HyClone) as well as 100 U/ml penicillin and 100 μg/ml streptomycin (Invitrogen). Cells were maintained in a humidified incubator at 37°C in the presence of 5% CO2. Cell lines confirmed to be mycoplasma-free by short tandem repeats (STR) profiling. All the cell lines were used within 15 passages and subjected to routine cell line quality examinations (e.g., morphology, mycoplasma), and thawed fresh every 2 months.

## Patients and Samples

Cohort 1: One hundred and ten paired TNBC and neighboring noncancerous tissues from TCGA database (https://cancergenome.nih.gov/); Cohort 2: Five hundred and fifty paired patients TNBC and neighboring noncancerous tissues were also from TCGA database; Cohort 3: One hundred and ten paired TNBC and neighboring noncancerous tissues obtained from the surgical specimen archives of the Shanghai cancer center of Fudan university, Shanghai, China (collected postoperatively from August 2010 to September 2018); Each sample was snap-frozen in liquid nitrogen and stored at −80°C prior to RNA isolation and qRT-PCR analysis. All patients recruited to this study did not receive any pre-operative treatments. The data do not contain any information that could identify the patients. All patients provided written informed consent. The use of human clinical specimens in the present study was approved by the Institutional Review Board of the Shanghai Medical College of Fudan University. A summary of the clinical information for the 110 patients is available online in **Supplementary Table 1**.

## RNA Isolation and Quantitative PCR (Real-Time RT-PCR)

Total RNA was extracted from tissues or cultured cells using TRIzol reagent (Invitrogen). Total RNA (500 ng) was reverse transcribed to cDNA in a final volume of 10 μl using random primers under standard conditions with the PrimeScript RT Reagent Kit (Takara, Dalian, China). We performed real-time PCR analyses using SYBR Premix Ex Taq (Takara) according to

the manufacturer's instructions. Results were normalized to the expression of glyceraldehyde 3-phosphate dehydrogenase (GAPDH) or β-actin, and data were collected based on the comparative cycle threshold (CT) ($2^{-\Delta\Delta CT}$) method. Specific primer sequences are listed in **Supplementary Table 2**.

## Plasmid Generation and Transfection/Infection

We obtained the full-length Lnc-PCIR, PABPC4 and TAB3 sequence and ligated into the pcDNA3.0 (+) vector (Invitrogen). Additionally, we also cloned the sequence of PABPC4 and TAB3 into the pCMV-Flag or pCMV-HA. Plasmid were transfected into TNBC cells cultured in six-well plates using the Lipofectamine 3000 DNA transfection reagent (life, USA). For lentivirus packaging, $2 \times 10^6$ 293 T cells were co-transfected with packaging plasmid pA2 and pMD2G. After 8 h, the transfection medium was replaced with fresh DMEM supplemented with 10% FBS. Subsequently, cell supernatants containing lentiviruses were collected. For infection, cells were treated with polybrene (8 μg/mL, Sigma) for 0.5 h before incubated with lentiviral, after incubation for 8 to 12 h at 37°C, stable cell lines were selected by puromycin (2 μg/mL, Sigma). Cells were harvested for qRT-PCR or western blot analysis 48 h after transfection. The sequences for the gene-specific primers used are listed in **Supplementary Table 2**.

## Northern Blot Assay

Total RNA (10–15 μg) from samples were separated on 15% denaturing polyacrylamide gels, transferred onto GeneScreen Plus membranes (PerkinElmer), and hybridized using UltraHyb-Oligo buffer (Ambion). Following hybridization at 42°C overnight, the membranes washed twice in 0.1×SSPE and 0.1% SDS at 42°C for 15 min each. Membranes were then exposed to a storage phosphor screen (GE Healthcare Bio-Sciences) for 8 h and imaged using a Typhoon 9410 Variable Mode Imager (GE Healthcare Bio-Sciences). The sequences for probe primers used are listed in **Supplementary Table 2**.

## Western Blotting

Cells were lysed in lysis buffer in the presence of protease inhibitor cocktail (Roche) and phosphatase inhibitor cocktails I and II (Sigma). Equal amounts of protein, as determined by the Bradford assay, were resolved by electrophoresis in a SDS 10% polyacrylamide gel and then transferred to a PVDF membrane (Millipore). The membrane was incubated with the primary antibodies and secondary antibodies, then was detected using an enhanced chemiluminescence kit (ECL, Invitrogen). The details of antibodies used are listed in **Supplementary Table 3**.

## Cell Growth Assay

For cell growth assays, 2000 cells per well were seeded into 96-well plates, with three wells used for each group. Cell numbers were evaluated for 5 days using a cell counting kit-8 (CCK-8) (Dojindo, Japan). 10 μl of CCK-8 reagent was added to each well and the plate was incubated at 37°C for 2 h. Next, the absorbance at 450 nm was measured in each well by using a spectrophotometer (Molecular Devices, CA, USA). For the colony formation assay, 1500 cells well were seed into 6-well plates and routinely cultured for 14 days. The cells were subsequently fixed with 30% formaldehyde for 10 min and stained with 0.1% crystal violet for 10 min. The number of colonies was determined under an optical microscope.

## Cell Migration and Invasion Assays

The migration and invasive ability of the cells was performed using a transwell assay. For Invasion assays, we using the 8-μm pore inserts Millicell chambers which were coated with 30 μg of Matrigel (BD Biosciences, USA). And the Millicell chambers without coating the Matrigel was conducted in the migration assay. Cells (5×10 (4) for migration and 1×10 (5) for invasion) were seeded onto a transwell plate with 8-mm pores, and DMEM supplemented with 20% FBS was used as a chemoattractant. Following a 24-h incubation, non-invading cells were manually removed using a cotton swab. Subsequently, the cells were fixed in 4% paraformaldehyde for 20 min, stained with hematoxylin and then counted under a microscope.

## RNA Pull-Down and Mass Spectrometry Assay

A full-length of sense and antisense Lnc-PCIR sequence were transcribed and biotin-labeled using T7 RNA polymerase (Roche, Basel, Switzerland) and purified using the RNA Clean Kit (ZYMO research, USA) *in vitro*. 1 mg protein lysis of 231 cell extracts was then mixed with 2 μg of biotinylated RNA at 4°C for 1 h, and then incubated with 50 μl of M-280 streptavidin dynabeads (Thermo Scientific, USA) over night at 4°C. After washing with the beads for six times with DEPC-PBS buffer. The RNA–protein complex was boiled in 1×SDS buffer for 5 min. The retrieved protein was detected using standard western blotting techniques and silver staining.

For mass spectrometry process, in brief, which include protein digestion, MS, database retrieval and protein identification. Firstly, protein digestion, each sample was allowed to proceed at 56°C for 1 h in 10 Mm dithiotreitol and add 55 mM iodoacetamide incubated in the dark for 45 min at room temperature. The gel pieces were washed with 100 μl of 25 mm NH4HCO3 for 10 min and dehydrated with 100 μl of 25 mm NH4HCO3 in 50% acetonitrile for 5 min for two times. Following drying in a SpeedVac, the gel pieces were mixed with 12.5 ng/μl of trypsin and incubated on ice for 40 min and 25 mm NH4HCO3 was added as needed to cover the gel pieces. Digestion was then carried out at 37°C overnight. Using 60% acetonitrile, 0.2% TFA to extract the tryptic peptides from the gel pieces. Following 20 min of vortex and 5 min of sonication, the supernatant was taken and saved. Following the evaporation of acetonitrile in a SpeedVac, the sample was desalted with a C18 ZipTip (Millipore), and half of the eluate was analyzed with nanoLC-MS/MS. Secondly, the samples were resuspended with 30 μl solvent C respectively (C: water with 0.1% formic acid), separated by nanoLC and analyzed by on-line electrospray tandem mass spectrometry. 10 μl peptide sample was loaded onto the trap column (Thermo Scientific Acclaim PepMap C18, 100 μm × 2 cm), with a flow of 10 μl/min for 3 min and subsequently separated on the analytical column (Acclaim PepMap C18, 75 μm × 15 cm)

with a 90-min linear gradient, from 5% D (D: ACN with 0.1% formic acid) to 55% D. The column was re-equilibrated at initial conditions for 10 min. The column flow rate was maintained at 300 nl/min. The electrospray voltage of 2 kV versus the inlet of the mass spectrometer was used. Thirdly, tandem mass spectra were processed by PEAKS Studio version 8.5 (Bioinformatics Solutions Inc., Waterloo, Canada). PEAKS DB was set up to search the UniProt-homo sapiens database (version 201712, 72029 entries) assuming trypsin as the digestion enzyme. Peptides were filter by 1% FDR and 1 unique peptide.

## RNA Immunoprecipitation (RIP) Assay

RIP was performed using the EZ-Magna RIP kit (Millipore, Billerica, MA) following the manufacturer's protocol. 231 cells at 80–90% confluency was scraped off the tissue culture plate, then lysed in complete RIP lysis buffer. A total of 200 µl of whole cell extract was incubated with RIP buffer containing magnetic beads conjugated with antibodies against PABPC4 and TAB3 or control IgG (Millipore) overnight at 4°C. The beads were washed with wash buffer, then the complexes were incubated with 0.1% SDS and 0.5 mg/ml Proteinase K (30 min at 55°C) to remove proteins. The RNA concentration was measured using a NanoDrop spectrophotometer (Thermo Scientific, USA) and its quality was assessed using a bioanalyzer (Agilent, Santa Clara, CA). Finally, immunoprecipitated RNA was purified and analyzed by qRT-PCR.

## Subcellular Fractionation

The separation of nuclear and cytosolic fractions was performed using the NE-PER Nuclear and Cytoplasmic Extraction Reagents Kit (Thermo, USA) following the manufacturer's instructions. In brief, for adherent cells, harvest with trypsin-EDTA and then centrifuge at 500 × g for 5 min; Wash cells by suspending the cell pellet with PBS and centrifuge at 500 × g for 2 min for two times; Add ice-cold 200 µl CER I to the cell pellet, and vortex the tube vigorously on the highest setting for 15 s to fully suspend the cell pellet. Incubate the tube on ice for 10 min, add ice-cold 11 µl CER II, vortex the tube for 5 s on the highest setting. Incubate tube on ice for 1 min; Centrifuge the tube for 5 min at 16,000*g*, transfer the supernatant (cytoplasmic extract) to a tube; suspend the pellet with 200 µl ice-cold NER, vortex on the highest setting for 15 s every 10 min, for a total of 40 min; Centrifuge the tube at 16,000 × g for 10 min; Immediately transfer the supernatant (nuclear extract) fraction to a clean pre-chilled tube, store extracts at −80°C until use. RNA isolation using TRIzol reagent (Invitrogen) and using PrimeScript RT Reagent Kit (Takara, Dalian, China) for cDNA production. β-Actin was used as the cytoplasmic endogenous control. U6 small nuclear RNA was used as the nuclear endogenous control for qPCR.

## RACE Assay

We used a SMARTer RACE cDNA Amplification kit (Clontech, California, USA) to determine the transcriptional initiation and termination sites of Lnc-PCIR, according to manufacturer's instructions. The sequences for the gene-specific PCR primers used for 5' and 3' RACE analysis was given in **Supplementary Table 2**.

## RNA Scope Assay

RNA *in situ* hybridization was performed using RNAScope® Multiplex Reagent Kit for Tissues (ACD, Life technologies, USA) to analysis the RNA level of Lnc-PCIR in human TNBC tissues and adjacent normal tissues. In brief, deparaffinized tissue sections were hybridized with the Lnc-PCIR probe and negative control probe at 40°C for 2 h. After hybridizations, sections were subjected to signal amplification, Gill's hematoxylin counterstaining, and scanning (Aperio ScanScope CS, Leica Biosystems, Nussloch, Germany) at 40× magnification. Fast Red semiquantitative image analysis was performed using the Aperio RNA ISH algorithm, which automatically quantifies the staining across whole slides and counts individual molecular signals and clusters in the cells. The obtained results are divided into three ranges: 1, which includes cells containing two to five dots per cell; 2, which includes cells containing 6-20 dots per cell; and 3, which includes cells containing more than 20 dots per cell.

## Tumor Xenograft Experiments

Female NOD/SCID nude mice (4 weeks old) were obtained from the Shanghai Model Organisms Center (Shanghai, China). And housed and maintained in laminar airflow cabinets under specific pathogen-free conditions. Subsequently, the stable lenti-P-Lnc-PCIR or control 231 cells ($1 \times 10^7$ cells/mice in 200 µl sterile PBS) were injected subcutaneously into NOD/SCID nude mice. Tumor growth was measured after 1 week, and tumor volumes were calculated by the formula: volume ($cm^3$) = (length × $width^2$)/2. After 4 weeks, the mice were sacrificed and the tumors were collected and weighed. For *in vivo* metastasis assay, $1 \times 10^6$ lenti-P-Lnc-PCIR or control 231 cells (in 50 µl of sterile PBS) were orthotopically injected directly into the inguinal mammary fat pads of mice in (n = 10 in each group). All procedures were conducted in accordance with the Guidelines for the Care and Use of Laboratory Animals with the approval of the Ethics Committee of the Fujian Medical University.

## Statistical Analysis

All experiments were performed in triplicate. Statistical analyses were performed using SPSS (version 23.0, SPSS Inc.) or GraphPad Prism software (version 7.0, USA). Clinicopathological characteristics were analyzed by chi-square tests. Survival curves were generated using the Kaplan-Meier method and log-rank tests. Univariate and multivariate Cox regression analyses were conducted to identify the independent factors. Student's t-test or the Mann–Whitney U test was used for comparison between two groups depending on distribution. P (two-sided) less than 0.05 was considered to indicate statistical significance. All data were presented as the mean ± standard error of the mean (SEM).

# RESULTS

## Identification of Clinically Relevant lncRNAs Overexpressed in TNBC

In order to identify lncRNAs that play a role in TNBC, we used RNA-sequencing (RNA-seq) data from 1084 patients available in

the TCGA database (The Cancer Genome Atlas). We classified the tumors with available PAM50 (Prediction Analysis of Microarray 50) molecular subtype annotation (25), obtaining a final cohort of 110 TNBC patients (cohort 1) (26). Using differentially expressed gene analysis, we identified a subset of lncRNAs overexpressed with clinically relevant in the TNBC subtype (fold change>4) compared to normal tissue (**Figures 1A, B** and **Supplementary Excel 1**). Subsequently, the top four upregulated lncRNAs are selected: RP11-214F16.8 (Lnc-PCIR), LOC645249, SNHG3, and LINC00160. The RNA level of Lnc-PCIR was confirmed in 550 paired TNBC tissues and paired tumor-adjacent non-tumor tissues (Cohort2) (**Figure 1C**). The univariate Cox proportional hazards regression method revealed that Lnc-PCIR showed the significantly prognostic value in TNBC tissue (**Figure 1C**). So, we choose the Lnc-PCIR for further study. Moreover, the RNA levels of Lnc-PCIR were confirmed by quantitative real-time polymerase chain reaction (q-PCR) analysis in 110 paired TNBC tissues and paired tumor-adjacent non-tumor tissues (Cohort3). Compared with matched normal tissues, Lnc-PCIR was significantly up-regulated in TNBC tissues (**Figure 1D**). We also employed the RNA Scope assay to analyze Lnc-PCIR RNA

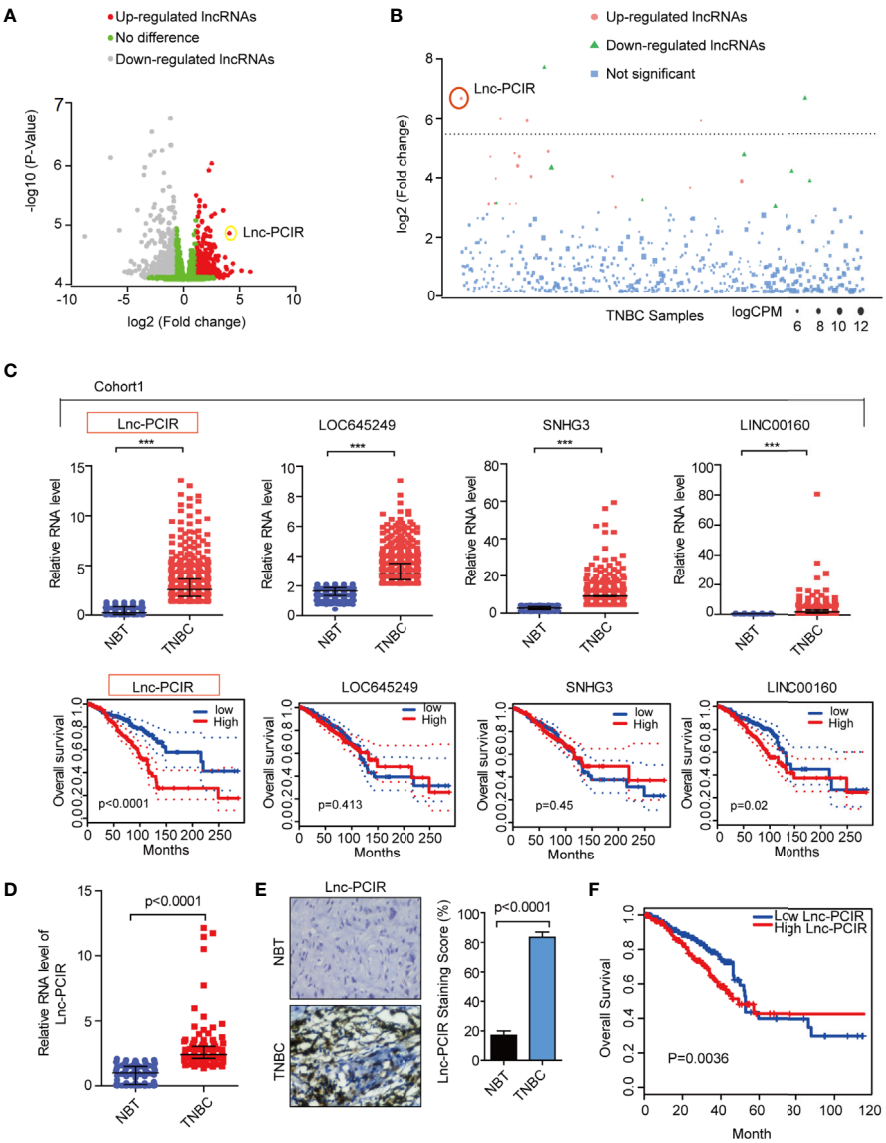


**FIGURE 1** | Lnc-PCIR upregulated and predicted the worse survival in triple negative breast cancer. **(A, B)** Volcano plot and Manhattan plot analysis of RNA-sequencing data of TNBC and normal tissues from TCGA. Red represents up-regulated long non-coding RNAs with $\log_2^{(\text{fold change})}$ >4; **(C)** Relative expression level and overall survival of screened lncRNAs in TCGA data of TNBC samples; **(D)** qRT-PCR results showed that Lnc-PCIR expression was significantly upregulated in 110 pairs of TNBC tissues and non-tumor tissues (NTs); **(E)** RNA Scope assay to detect the Lnc-PCIR RNA level in TNBC and adjacent normal tissues. Left panel: representative images; right panel: statistical analysis of the staining; **(F)** Kaplan-Meier survival analysis of Lnc-PCIR expression in TNBC patients (n = 110). All *p*-values calculated by independent sample t-test (***significant values of <0.001).

level, results confirmed Lnc-PCIR has significantly higher level in TNBC tissues (**Figure 1E**). Patients with higher levels of the Lnc-PCIR exhibited poor survival outcomes ($P$=0.0036) (**Figure 1F**). These data together indicated that Lnc-PCIR was significantly upregulated and related to the overall survival in TNBC tissues, and might be involved in the progression of TNBC.

## Overexpressed Lnc-PCIR Promoted Cell Migration, Invasion, and Proliferation *In Vitro* and *In Vivo*

We first analyzed the basic characteristic of Lnc-PCIR in breast cancer cells. Lnc-PCIR (ENSG00000280710.2) located on 13q32.3 and has only one transcript with three exons (**Supplementary Figure 1A**). Lnc-PCIR is widely expressed in different breast cancer cell lines, and the RNA level was significantly up-regulated in TNBC cell lines (**Supplementary Figure 1B**). Next, we examined the subcellular localization of Lnc-PCIR, finding that Lnc-PCIR predominately resides in the nucleus in 231 and BT549 cells by qRT-PCR (**Supplementary Figure 1C**). By Coding Potential Calculator (27) (http://cpc.cbi.pku.edu.cn/) and the PhyloCSF codon substitution frequency analysis (28), Lnc-PCIR has low protein-coding ability (**Supplementary Figures 1D, E**). Moreover, we performed the RACE assay (rapid amplification of cDNA ends) and Northern blot assay to confirm the Lnc-PCIR is a 987-bp-long intergenic non-protein-coding RNA in breast cancer cells (**Supplementary Figures 1F, G**).

To assess the effect of Lnc-PCIR on TNBC cell migration and invasion, we performed transwell assay and wound-healing assay. Two independent small interfering RNAs (siRNAs) for Lnc-PCIR significantly decreased the migration and invasion of the 231 and BT549 cells (**Figures 2A–D** and **Supplementary Figure 2A**), and vice-versa, Lnc-PCIR overexpression by a lentivirus vector (pCDH- Lnc-PCIR, shorted in P-Lnc-PCIR) promoted 231 and BT549 cells the migration and invasion of the 231 and BT549 cells (**Figures 2E–G** and **Supplementary Figure 2B**). On the other hand, Lnc-PCIR knockdown significantly decreased 231 and BT549 cells growth and colony formation (**Figures 3A–C**), whereas, Lnc-PCIR induction increased cell growth and colony formation (**Figures 3D–F**).

To further explore the growth-promoting effects of Lnc-PCIR on TNBC cells *in vivo*, we evaluated the promoting effects of Lnc-PCIR on cell metastasis. The stable P-Lnc-PCIR 231 cells were transplanted into the fat pad of nude mice. The metastatic nodules in the lung were significantly increased in the P-Lnc-PCIR group (**Figure 4A**). Hematoxylin-eosin staining showed that the metastatic foci derived from the P-Lnc-PCIR cells dramatically increased in the lung (**Figure 4B**). We also subcutaneously injected stable P-Lnc-PCIR 231 cells into nude mice. Both the volumes and weights of the tumors in the P-Lnc-PCIR group were markedly higher than those in the control group (**Figures 4C–E**) with no significant change in body weight of nude mice (**Figure 4F**), demonstrating that P-Lnc-PCIR promotes the tumorigenicity of the TNBC cells *in vivo*. Taken together, these findings suggest that Lnc-PCIR acts as an oncogenic driver in the development and progression of TNBC.

## Identified the Lnc-PCIR Binding Proteins

To explore the molecular mechanism underlying the oncogenic activity of Lnc-PCIR in TNBC progression, we performed RNA pull-down assays to identify the proteins associated with Lnc-PCIR in the 231 cells. The results from three independent Lnc-PCIR pull-down experiments repeatedly showed specific bands at approximately 70 KD and 90 KD *via* mass spectrometry (**Figure 5A** and **Supplementary Table 4**). Nine potential interacting proteins were obtained based on unique peptide number>5 and peptide number>10 in the three independent experiments and were absent in the corresponding antisense groups (**Figure 5A**). After confirming in two independent experiments, we observed that sense but not antisense Lnc-PCIR, was specifically associated with TGF-beta activated kinase 1 (MAP3K7) binding protein 3 (TAB3) and Poly(A) binding protein cytoplasmic 4 (PABPC4) (**Figure 5B**). Moreover, RIP assays showed that the antibodies of TAB3 or PABPC4 could significantly enrich Lnc-PCIR (**Figure 5C**), whereas the GAPDH antibody and IgG as the negative control. In addition, unbiased transcriptome profiling was performed using RNA-sequencing in 231 cells transfected with two independent si-Lnc-PCIR to investigate the related signaling pathways and biological process. GSEA (Gene Set Enrichment Analysis) and GO analysis (Gene Ontology Analysis) showed that top four signaling pathways Lnc-PCIR involved in which include: TNFA signaling *via* NFKB pathway, Hypoxia, Epithelial-mesenchymal Transition (EMT) and Estrogen response early in 231 cells (**Figure 5D** and **Supplementary Excel 2**). Moreover, we verified the top-scoring genes altered in TNFA signaling *via* NFKB pathway and confirmed that Lnc-PCIR dramatically affected the genes expression level that are highly associated with tumorigenesis (**Figure 5E**). Taken together, these findings demonstrated that Lnc-PCIR is an oncogenic driver through activating TNF-α/NF-κB signaling pathway by binding with TAB3 and PABPC4 in TNBC and the molecular mechanisms between them need further explored.

## Lnc-PCIR Enhances the Protein Levels of TAB3 and PABPC4

In order to explore the regulatory mechanism among Lnc-PCIR, TAB3 and PABPC4, we first analysis the binding fragment/domain between them, a series of deletion was constructed based on the secondary structure of Lnc-PCIR (http://www.lncipedia.org/, **Figure 6A**). The 201–507 nt (#2) fragment of Lnc-PCIR mediates the interaction with TAB3, while the 625–987 nt (#3) fragment of Lnc-PCIR is required and sufficient for the association with PABPC4. Additionally, we also construct the FLAG-tagged full-length and truncated TAB3 or PABPC4. RIP assays showed CUE domain (1–244 aa) of TAB3 was the vital domain mediate the interaction with Lnc-PCIR (**Figure 6B**), and PABP-1234 super family domain (11–624 aa) of PABPC4 is required for its association with Lnc-PCIR (**Figure 6C**). Next, we sought to determine the functional relevance of the association between Lnc-PCIR and TAB3/PABPC4. Knockdown of Lnc-PCIR significantly decreased the mRNA level of TAB3, and vice versa (**Figure 6D**). But knockdown and overexpressed Lnc-PCIR

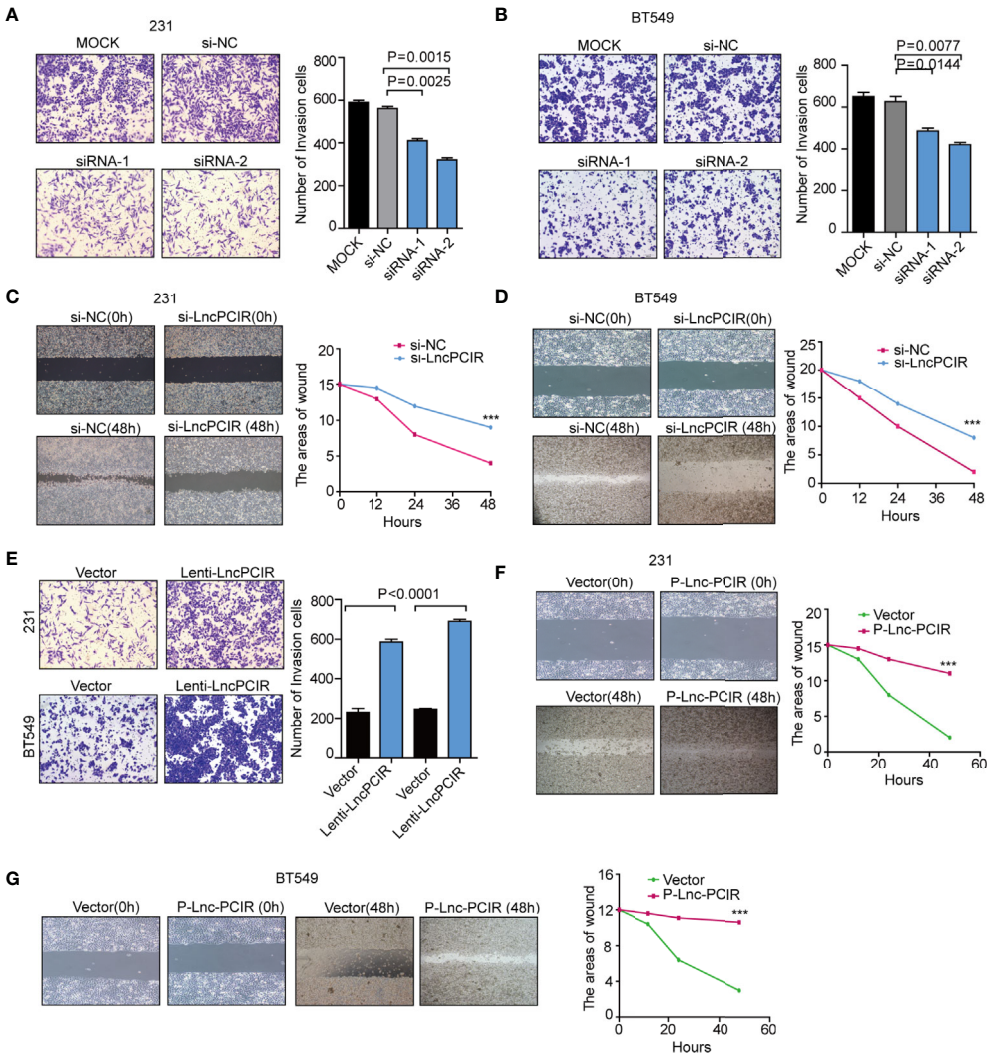


**FIGURE 2** | Lnc-PCIR increases TNBC cell invasion and migration *in vitro*.**(A, B)** Transwell invasion assays in the 231 **(A)** and BT549 **(A)** cells with Lnc-PCIR knockdown; **(C, D)** Wound-healing assays in the 231 **(A)** and BT549 **(A)** cells with Lnc-PCIR knockdown; **(E)** Transwell invasion assays in the 231 **(A)** and BT549 **(A)** cells with Lnc-PCIR overexpressed; **(F, G)** Wound-healing assays in the 231 **(A)** and BT549 **(A)** cells with Lnc-PCIR overexpressed. All *p*-values calculated by independent sample t-test (***significant values of <0.001).

has non-effect of mRNA level of PABPC4 (**Figure 6D**). Western blot assay revealed overexpressed Lnc-PCIR increased the expression level of TAB3 and PABPC4, knockdown of Lnc-PCIR could significantly reduce the protein level of TAB3/PABPC4 in 231 cells (**Figure 6E**). Moreover, actinomycin D, which effectively inhibits the *de novo* synthesis of RNA, was used to explore the stability of TAB3 regulated by Lnc-PCIR. Overexpression of Lnc-PCIR could increase the half-life and steady-state level of TAB3, whereas the depletion of Lnc-PCIR resulted in a decreased half-life and RNA level of TAB3 (**Figure 6F**), revealing that Lnc-PCIR specifically regulate the stability of TAB3 in the TNBC cells. Meanwhile, we found PABPC4 could specifically bind with TAB3 in 231 cells (**Figures 6G, H**). PABPC4, a Poly (A)-binding protein, is expressed at a higher level in colon cancer and lung adenocarcinoma compared to normal tissues (29, 30). However, the expression profile and role of PABPC4 in TNBC remains unknown. Given this, we speculate whether PABPC4 can directly bind to the TAB3 mRNA. RNA pulldown assay was conducted with biotinylated TAB3 mRNA, results showed overexpressed Lnc-PCIR strengthened the binding of PABPC4 and mRNA of TAB3 (**Figure 6I**). Both PABPC4 and TAB3 are overexpressed in TNBC tissues, and a strong correlation between them (**Supplementary Figures 3A–C**). Furthermore, knockdown of PABPC4 or TAB3 reduced the cell growth and invasion abilities of the 231 cells (**Supplementary Figures 3D, E** and **Supplementary Figures 4A–D**). These findings suggest higher RNA level of Lnc-PCIR could strengthening the stability of TBA3 mRNA, by enhancing the binding state of PABPC4 to TAB3 in TNBC cells.

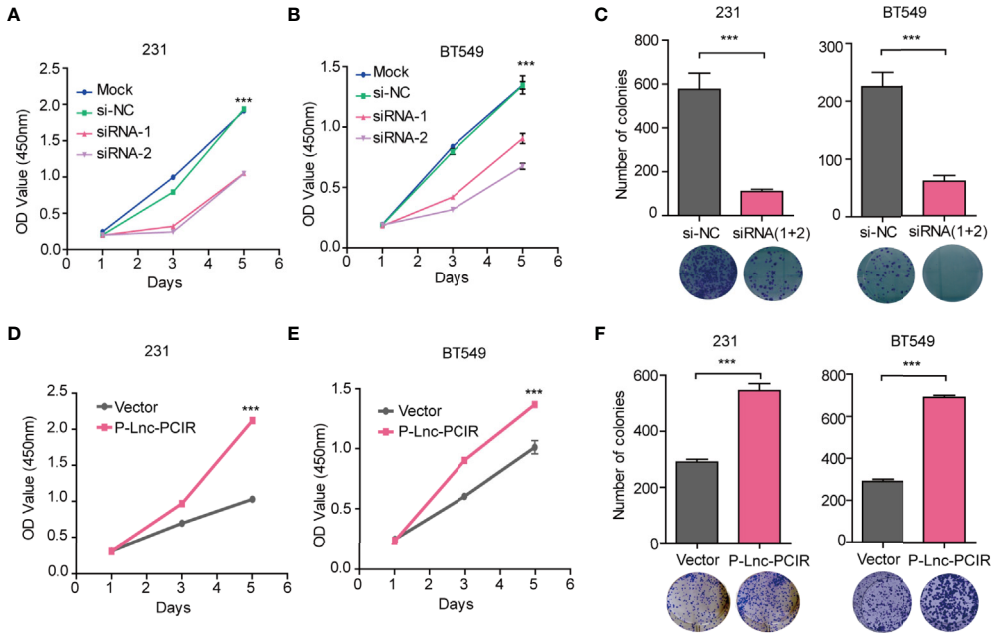


**FIGURE 3** | Lnc-PCIR increases TNBC cell proliferation and colony formation *in vitro*. **(A–C)**. CCK-8 assays **(A, B)** and Colony formation assays **(C)** in the 231 and BT549 cells with knockdown of Lnc-PCIR; **(D–F)**. CCK-8 assays **(D, E)** and Colony formation assays **(F)** in the 231 and BT549 cells with overexpression of Lnc-PCIR. All *p*-values calculated by independent sample t-test (***significant values of <0.001).

## Lnc-PCIR Blocks PABPC4 Proteasome-Dependent Ubiquitination Degradation

Although Lnc-PCIR had no significant effect on the mRNA level of PABPC4 (**Figure 6D**), the protein levels of PABPC4 were dramatically increased when overexpressing Lnc-PCIR and were reduced when silencing Lnc-PCIR in TNBC cells (**Figure 6E**). To explore the mechanisms underlying this phenomenon, we wonder whether it affects the stability of the PABPC4 protein level. Thus, following treatment with a protein-synthesis inhibitor cycloheximide (CHX), Lnc-PCIR knockdown accelerate the PABPC4 degradation, whereas Lnc-PCIR activation increased the half-life of the PABPC4 protein in the TNBC cells (**Figure 7A**). Besides, we also treated cells with a proteasome inhibitor MG132, the accumulation of endogenous PABPC4 in cells overexpressing Lnc-PCIR was remarkable greater (**Figure 7B**), indicating that higher level Lnc-PCIR might inhibit the proteasome-dependent degradation of PABPC4 in TNBC cells. Furthermore, the ubiquitination levels of PABPC4 significantly increased in the sh-Lnc-PCIR cells, whereas the ubiquitination levels of PABPC4 sharply decreased in the overexpressed Lnc-PCIR cells (**Figure 7C**). Collectively, these results indicated that Lnc-PCIR can increase the stability of PABPC4 through blocking its ubiquitin/proteasome-dependent degradation.

## TAB3 as the Functional Downstream Mediator of Lnc-PCIR to Activating TNF-α/NF-κB Pathway

Previous studies have shown that TAB2 which tightly associated with TAB3 is involved in NF-κB activation (31). Considering the effect of Lnc-PCIR on TAB3 protein level, we hypothesize that Lnc-PCIR may exert its biological effects through regulating the association of TAB3 and TAB2. The Co-IP study showed that endogenous TAB2, were detected in the immunoprecipitant with TAB3 antibody, and the association of TAB2 and TAB3 was remarkable decreased due to Lnc-PCIR overexpression (**Figure 7D**). Furthermore, functional recovery assay showed deleting TAB3 in the P-Lnc-PCIR cells significantly inhibited the invasion abilities, indicating that TAB3 is an important downstream effector of P-Lnc-PCIR in TNBC cells (**Figure 7E**). On the other hand, the activation of NF-κB signaling by treatment with TNFα (10 ng/ml) rescued the decreased cell invasion induced by the knockdown of TAB3. We also treated cells with the NF-κB inhibitor caffeic acid phenethyl ester (CAPE, 10 ng/ml), the transwell assay showed that blockade of NF-κB signaling dramatically decreased Lnc-PCIR induced cell migration and invasion (**Figure 7E**). To further clarify the mechanism by which Lnc-PCIR regulates *via* the NF-κB signaling in TNBC cells, we measured the changes in phosphorylated IκBα (p-IκBα), phosphorylated-p65 (p-p65) and total p65 expression in Lnc-PCIR knockdown or overexpression 231 cells. The results showed that the knockdown of Lnc-PCIR can significantly decrease p-IκB and p-p65 in 231 cells and vice-versa (**Figure 7F**). TNBC patients in the high TAB3 expression group had a much shorter median survival time than those in the low TAB3 expression group (**Figure 7G**). And TAB3 showed a positive correlation with Lnc-PCIR in TNBC tissues (**Figure 7H**). Taken together, Lnc-PCIR as the oncogenic driver in TNBC, they make a meaningful

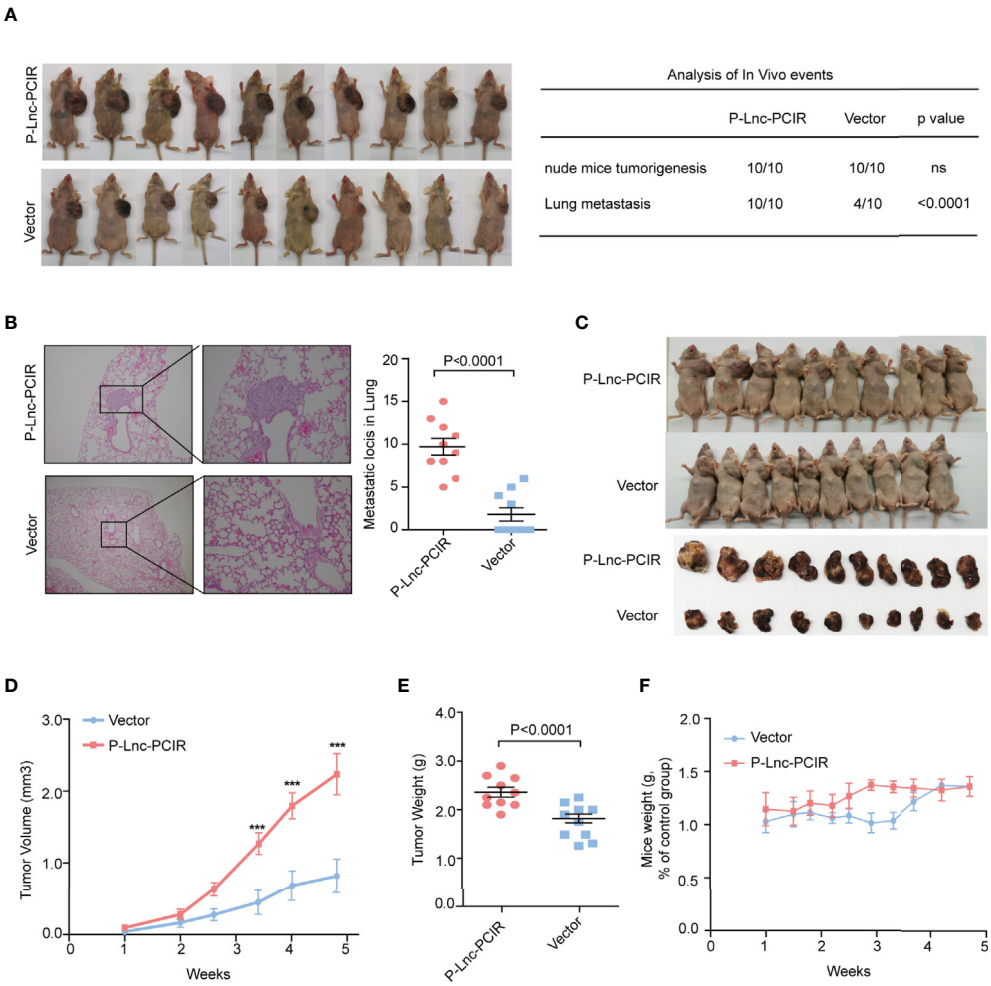


**FIGURE 4** | Lnc-PCIR increases TNBC cell metastasis and cell growth *in vivo*.**(A, B)** Statistics analysis of the metastatic foci in the lung obtained from nude mice injection with the stable P-Lnc-PCIR 231 cells detected by hematoxylin-eosin staining; **(C–E)**. Representative image of nude mouse models bearing subcutaneous tumor xenografts **(C)**; Tumor volumes **(D)** and tumor weights **(E)** were measured in the P-Lnc-PCIR 231 cells and negative-control groups in the xenograft mouse models; **(F)** The weight of nude mice in the P-Lnc-PCIR 231 cells group and negative-control group. All *p*-values calculated by independent sample t-test (***significant values of <0.001).

contribution to tumor progression through activating the NF-κB signaling by associated with TAB3.

## DISCUSSION

Long non-coding RNAs were found to be deregulated in a variety of diseases, especially cancer (32). Understanding the precise molecular mechanism by which lncRNAs function is vital for exploring new potential strategies for early diagnosis and therapy. In this study, from RNA-sequencing data, we identified Lnc-PCIR, is a clinically relevant lncRNA displays a remarkable trend of increased expression in TNBC tissue. Importantly, higher Lnc-PCIR levels predicted lower overall survival rates in TNBC patients, supporting that Lnc-PCIR may be a promising prognostic biomarker for TNBC. Lnc-PCIR showed the strong oncogenic activity by promoting TNBC cell tumor invasion and metastasis, proliferation, tumorigenicity *in vitro* and *in vivo*. And these results may suggest Lnc-PCIR involved in cancer-related biological processes and pathways which lead to TNBC tumorigenesis and progression.

Through the study on the mechanisms driven by Lnc-PCIR, we performed RNA Pulldown and RNA-sequencing assay, and found Lnc-PCIR could directly binds to TAB3 and PABPC4. TAB3 bind to the 5′ terminus of Lnc-PCIR (210–624 nt), whereas the 3’ terminus of Lnc-PCIR (625–987 nt) accounts for its association with PABPC4; therefore, it was not surprising that these two proteins could bind to each other.

TABs family which include TAB1, TAB2 and TAB3 have been identified as the specific binding partner proteins of TAK1

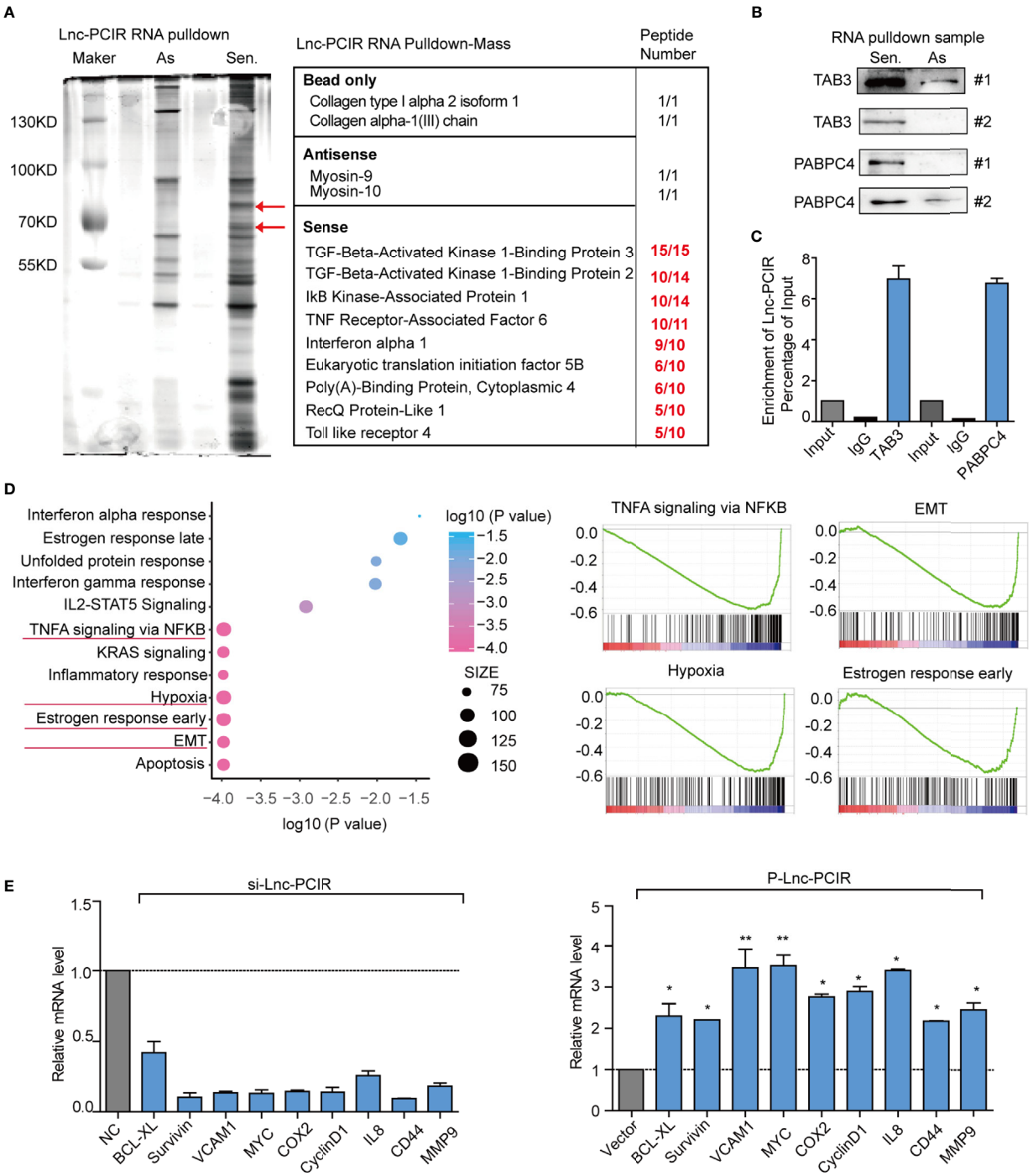


**FIGURE 5** | Lnc-PCIR specific directly binding with TAB3 and PABPC4 in 231 cells. **(A)** Silver staining of SDS-PAGE gel of biotinylated Lnc-PCIR RNA pull-down assays. Red arrows indicated the Lnc-PCIR-Sense-specific bands; **(B)** Western blot to analysis the interaction partners of Lnc-PCIR using RNA pull-down samples in 231 cell lines; **(C)** RIP analyses were performed using antibodies against endogenous TAB3 and PABPC4, with IgG as a negative control. The RNA level of the Lnc-PCIR was detected using RT-PCR and normalized to the input; **(D)** GSEA analysis of RNA-sequencing primary data when knockdown of Lnc-PCIR by two independent siRNAs and representative image of top four signaling pathways showed by GSEA analysis; **(E)** Top key genes regulated by TNF-α/NF-κB pathway were verified by qRT-PCR when knockdown or overexpressed Lnc-PCIR in TNBC cells. All *p*-values calculated by independent sample t-test (*significant values of <0.05; **significant values of <0.01).

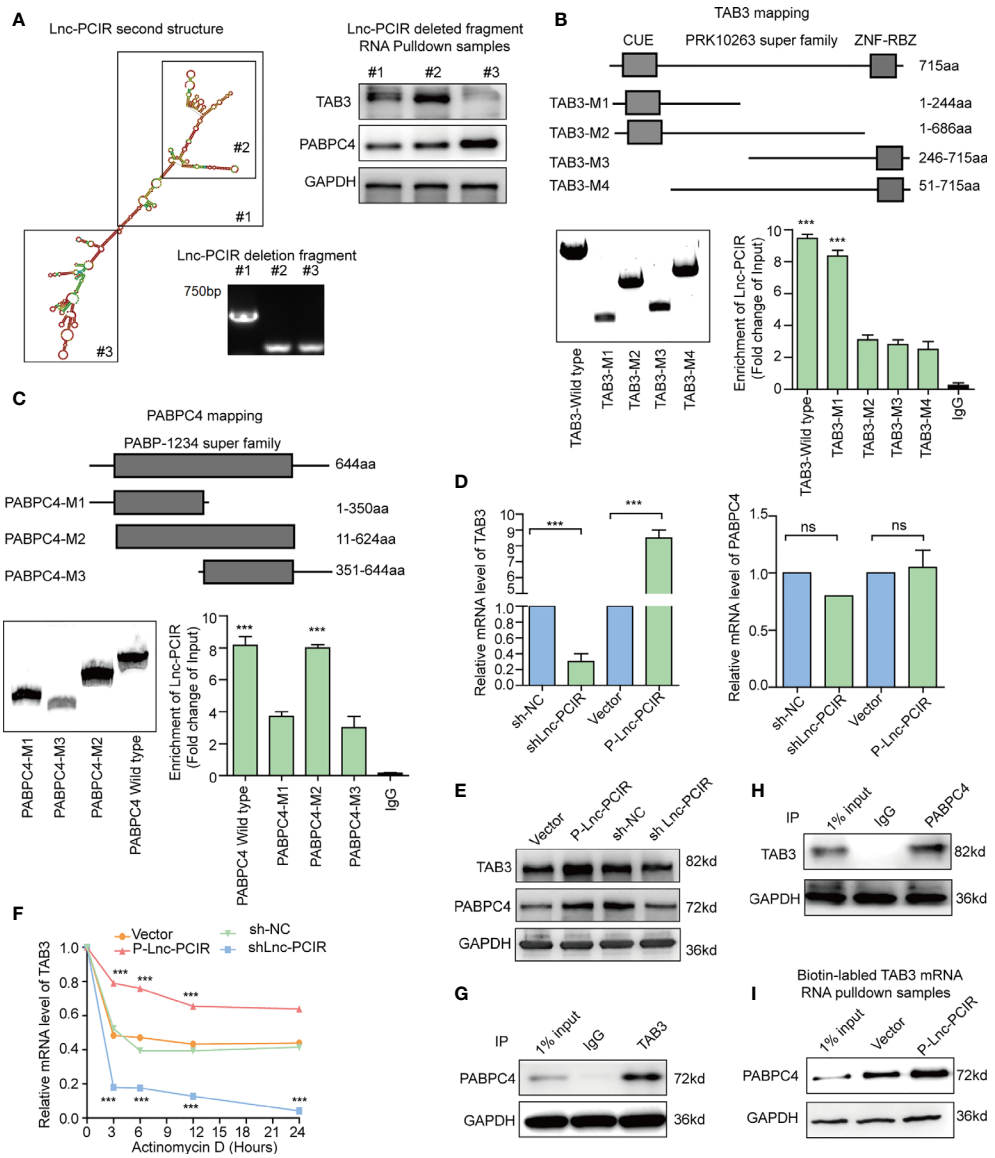


**FIGURE 6** | Lnc-PCIR enhances the protein levels of TAB3 and PABPC4. **(A)** Deletion mapping of the Lnc-PCIR according to the second structure (https://lncipedia.org/); Western blot of TAB3 or PABPC4 in pull-down samples by full-length biotinylated-Lnc-PCIR or truncated biotinylated- Lnc-PCIR RNA motifs, with GAPDH as the negative control; **(B, C)** RIP analysis of deletion mapping for the domains of TAB3 **(B)** or PABPC4 **(C)** that bind to Lnc-PCIR; **(D)** The mRNA levels of TAB3 or PABPC4 were quantified by qRT-PCR with Lnc-PCIR knockdown or overexpression; **(E)** The protein levels of TAB3 or PABPC4 after Lnc-PCIR overexpression or knockdown. GAPDH served as the internal control; **(F)** The half-life of TAB3 after treatment with actinomycin D for indicated times, with Lnc-PCIR knockdown or overexpression; **(G, H)** Co-IP assay to detect the association between TAB3 and PABPC4; **(I)** Western blot to analysis the interaction of PABPC4 with biotinylated-TAB3 mRNA using RNA pull-down samples in 231 cell lines. All *p*-values calculated by independent sample t-test (***significant values of <0.001). ns, no significance.

(TGF-β activated kinase 1) which implicated in regulating diverse range of cellular processes that include embryonic development, differentiation, autophagy, apoptosis and cell survival (18, 22). TAB3, a scaffold protein of TAB2, is involved in IL-1 and TNF-α signaling pathways (21). Several reports demonstrated TAB3 is widely expressed and constitutively overexpressed in certain tumor tissues, which as the oncogene to driving the occurrence and development of tumors (24, 33). Here, our findings showed that Lnc-PCIR have a strong impact on TAB3 mRNA stability, and interacting with and upregulating the TAB3 protein level which contribute to the promoting effects on activating TNF-α/NF-κB pathway in TNBC cells. Next, we further explored the mechanisms that stabilize TAB3 mRNA by Lnc-PCIR.

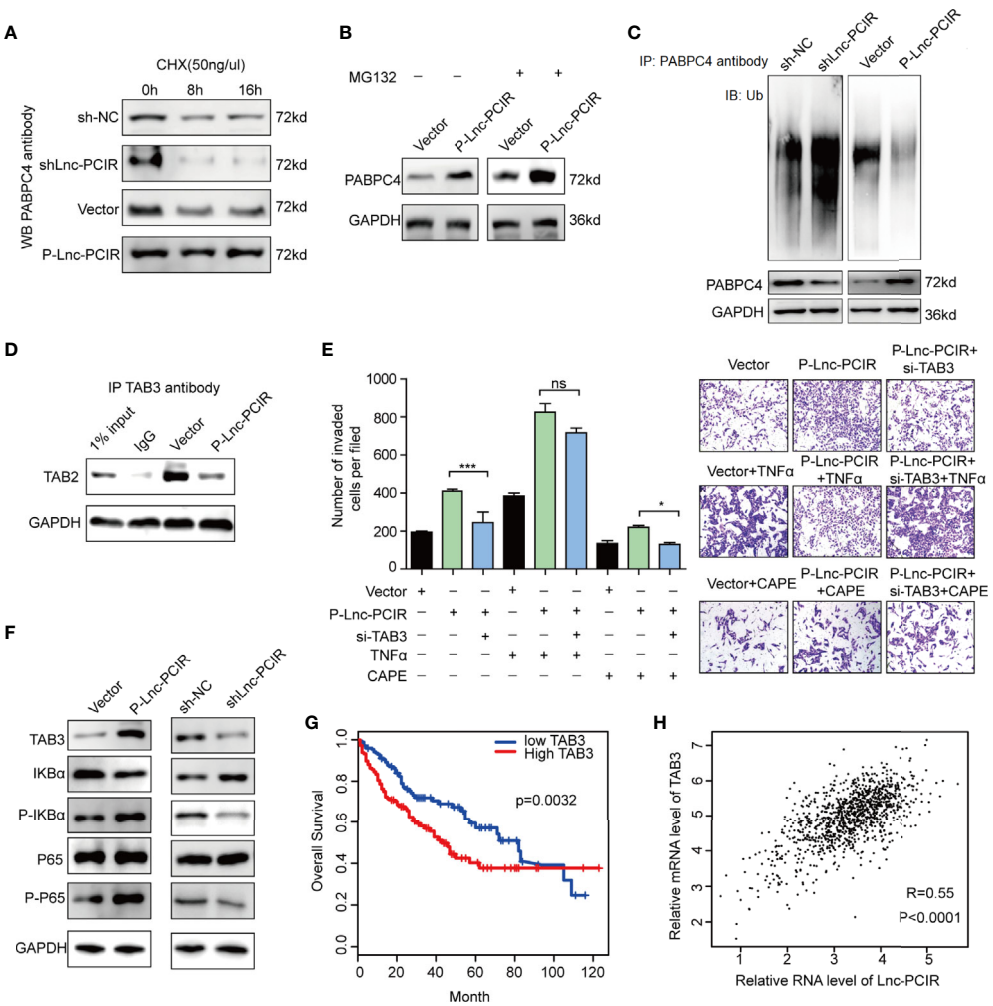


**FIGURE 7** | Lnc-PCIR blocks proteasome-dependent ubiquitination degradation of PABPC4. **(A)** Western blot to detect the protein level of PABPC4 in sh-Lnc-PCIR, P-Lnc-PCIR or the control cells which treated with CHX for the indicated times; **(B)** Western blot to detect the protein level of PABPC4 in P-Lnc-PCIR or control cells were treated with MG132 for 12 h; **(C)** IP assay with either control IgG or endogenous PABPC4 antibody and immunoblotted with the ubiquitin-specific antibody, endogenous PABPC4 and GAPDH served as the loading control; **(D)** Co-IP assay to detect the association between TAB3 and TAB2 after Lnc-PCIR overexpression, GAPDH served as the loading control; **(E)** Rescue assays of transwell invasion assay were performed after silencing TAB3 in P-Lnc-PCIR cells with or without TNFα/CAPE treatment; **(F)** Protein expression levels of TAB3, IKBa, p-IKBa, P65 and p-P65 transfected with P-Lnc-PCIR and vector in 231 cells; **(G)** Kaplan-Meier survival analysis of TAB3 expression in TNBC patients (n = 110); **(H)** Correlation analysis between TAB3 and Lnc-PCIR in TNBC patients (n = 110). All *p*-values calculated by independent sample t-test (**significant values of <0.01). ns, no significance.

PABPC4, another associated protein of Lnc-PCIR, which has been demonstrated related to the inflammatory biomarker (C-reactive protein) and anti-hepatitis C response, is expressed at a higher level in tumor tissues (34, 35). However, the mechanisms underlying the upregulated protein level of PABPC4 remain unclear. In the present study, we provided a new regulatory mechanism for PABPC4 *via* Lnc-PCIR. Higher level of Lnc-PCIR blocks PABPC4 proteasome-dependent ubiquitination degradation to promote the oncogenic effects of PABPC4 on carcinogenesis of TNBC. Stable and highly expressed PABPC4 can further increase the stability of TAB3 mRNA, and the association of PABPC4 and TAB3 can disrupt the binding of TAB3 and TAB2 to activate the TNF-α/NF-κB pathway.

## CONCLUSION

This study identifies clinically relevant lncRNA Lnc-PCIR using a large cohort of samples from TCGA and identified it have prognostic value and may be directly implicated in the oncogenic phenotype. Our results show that Lnc-PCIR acts as an oncogene

and significantly promotes TNBC cells tumorigenicity and metastasis *in vitro* and *in vivo*. Mechanistically, higher levels of Lnc-PCIR inhibits PABPC4 ubiquitination and degradation. Moreover, higher PABPC4 protein level strengthen the interaction of PABPC4 and TAB3 mRNA, weakens the interaction between TAB3 and TAB2, positively regulated TNF-α/NF-κB signaling pathway. Therefore, our study implies the Lnc-PCIR may provide a potential target for TNBC treatment.

## DATA AVAILABILITY STATEMENT

The original contributions presented in the study are included in the article/**Supplementary Material**. Further inquiries can be directed to the corresponding author.

## ETHICS STATEMENT

The studies involving human participants were reviewed and approved by Shanghai Cancer Center of Fudan University. The patients/participants provided their written informed consent to participate in this study. The animal study was reviewed and approved by Fujian Medical University.

## AUTHOR CONTRIBUTIONS

CW, WG, and HH designed the study. WG, JL, HH, and FF performed the experiments. WG and HH analyzed the results. YL carried out bioinformatics analyses. WG, HH, and CW wrote the paper with comments from all authors. All authors contributed to the article and approved the submitted version.

## FUNDING

This work was supported by grants from Joint funds for the innovation of science and Technology of Fujian province (2018Y9019, 2018Y9055), Joint funds for the youth research project of Fujian provincial health department (2011-1-14) and minimally invasive medicine center of Fujian Province.

## SUPPLEMENTARY MATERIAL

The Supplementary Material for this article can be found online at: https://www.frontiersin.org/articles/10.3389/fonc.2021.630300/full#supplementary-material

## REFERENCES

1. DeSantis CE, Ma J, Gaudet MM, Newman LA, Miller KD, Goding Sauer A, et al. Breast Cancer Statistics, 2019. *CA: Cancer J Clin* (2019) 69:438–51. doi: 10.3322/caac.21583
2. Bray F, Ferlay J, Soerjomataram I, Siegel RL, Torre LA, Jemal A. Global Cancer Statistics 2018: GLOBOCAN Estimates of Incidence and Mortality Worldwide for 36 Cancers in 185 Countries. *CA: Cancer J Clin* (2018) 68:394–424. doi: 10.3322/caac.21492
3. Cancer Genome Atlas N. Comprehensive Molecular Portraits of Human Breast Tumours. *Nature* (2012) 490:61–70. doi: 10.1038/nature11412
4. Garrido-Castro AC, Lin NU, Polyak K. Insights Into Molecular Classifications of Triple-Negative Breast Cancer: Improving Patient Selection for Treatment. *Cancer Discov* (2019) 9:176–98. doi: 10.1158/2159-8290.CD-18-1177
5. Lehmann BD, Bauer JA, Chen X, Sanders ME, Chakravarthy AB, Shyr Y, et al. Identification of Human Triple-Negative Breast Cancer Subtypes and Preclinical Models for Selection of Targeted Therapies. *J Clin Invest* (2011) 121:2750–67. doi: 10.1172/JCI45014
6. Carey LA, Dees EC, Sawyer L, Gatti L, Moore DT, Collichio F, et al. The Triple Negative Paradox: Primary Tumor Chemosensitivity of Breast Cancer Subtypes. *Clin Cancer Res* (2007) 13:2329–34. doi: 10.1158/1078-0432.CCR-06-1109
7. Prensner JR, Chinnaiyan AM. The Emergence of lncRNAs in Cancer Biology. *Cancer Discov* (2011) 1:391–407. doi: 10.1158/2159-8290.CD-11-0209
8. Quinn JJ, Chang HY. Unique Features of Long non-Coding RNA Biogenesis and Function. *Nat Rev Genet* (2016) 17:47–62. doi: 10.1038/nrg.2015.10
9. Li Z, Lu X, Liu Y, Zhao J, Ma S, Yin H, et al. Gain of LINC00624 Enhances Liver Cancer Progression by Disrupting the HDAC6-TRIM28-ZNF354C Corepressor Complex. *Hepatology* (2020). doi: 10.1002/hep.31530
10. Gupta RA, Shah N, Wang KC, Kim J, Horlings HM, Wong DJ, et al. Long non-Coding RNA HOTAIR Reprograms Chromatin State to Promote Cancer Metastasis. *Nature* (2010) 464:1071–6. doi: 10.1038/nature08975
11. Tsai MC, Manor O, Wan Y, Mosammaparast N, Wang JK, Lan F, et al. Long Noncoding RNA as Modular Scaffold of Histone Modification Complexes. *Science* (2010) 329:689–93. doi: 10.1126/science.1192002
12. Niknafs YS, Han S, Ma T, Speers C, Zhang C, Wilder-Romans K, et al. The lncRNA Landscape of Breast Cancer Reveals a Role for DSCAM-AS1 in Breast Cancer Progression. *Nat Commun* (2016) 7:12791. doi: 10.1038/ncomms12791
13. Pikarsky E, Porat RM, Stein I, Abramovitch R, Amit S, Kasem S, et al. NF-Kappab Functions as a Tumour Promoter in Inflammation-Associated Cancer. *Nature* (2004) 431:461–6. doi: 10.1038/nature02924
14. Caamano J, Hunter CA. NF-Kappab Family of Transcription Factors: Central Regulators of Innate and Adaptive Immune Functions. *Clin Microbiol Rev* (2002) 15:414–29. doi: 10.1128/CMR.15.3.414-429.2002
15. Tornatore L, Thotakura AK, Bennett J, Moretti M, Franzoso G. The Nuclear Factor Kappa B Signaling Pathway: Integrating Metabolism With Inflammation. *Trends Cell Biol* (2012) 22:557–66. doi: 10.1016/j.tcb.2012.08.001
16. Ding J, Zhao J, Huan L, Liu Y, Qiao Y, Wang Z, et al. Inflammation-Induced Long Intergenic Noncoding Rna (Linc00665) Increases Malignancy Through Activating the Double-Stranded Rna-Activated Protein Kinase/Nuclear Factor Kappa B Pathway in Hepatocellular Carcinoma. *Hepatology* (2020) 72 (5):1666–81. doi: 10.1002/hep.31195
17. Jin X, Ding D, Yan Y, Li H, Wang B, Ma L, et al. Phosphorylated RB Promotes Cancer Immunity by Inhibiting NF-Kappab Activation and PD-L1 Expression. *Mol Cell* (2019) 73:22–35.e26. doi: 10.1016/j.molcel.2018.10.034
18. Sakurai H, Miyoshi H, Mizukami J, Sugita T. Phosphorylation-Dependent Activation of TAK1 Mitogen-Activated Protein Kinase Kinase Kinase by TAB1. *FEBS Lett* (2000) 474:141–5. doi: 10.1016/S0014-5793(00)01588-X
19. Cheung PC, Nebreda AR, Cohen P. TAB3, a New Binding Partner of the Protein Kinase TAK1. *Biochem J* (2004) 378:27–34. doi: 10.1042/bj20031794
20. Ishitani T, Takaesu G, Ninomiya-Tsuji J, Shibuya H, Gaynor RB, Matsumoto K. Role of the TAB2-related Protein TAB3 in IL-1 and TNF Signaling. *EMBO J* (2003) 22:6277–88. doi: 10.1093/emboj/cdg605
21. Kim SI, Kwak JH, Na HJ, Kim JK, Ding Y, Choi ME. Transforming Growth Factor-Beta (TGF-beta1) Activates TAK1 Via TAB1-mediated Autophosphorylation, Independent of TGF-beta Receptor Kinase Activity in Mesangial Cells. *J Biol Chem* (2009) 284:22285–96. doi: 10.1074/jbc.M109.007146

22. Jin G, Klika A, Callahan M, Faga B, Danzig J, Jiang Z, et al. Identification of a Human NF-kappaB-activating Protein, TAB3. *Proc Natl Acad Sci USA* (2004) 101:2028–33. doi: 10.1073/pnas.0307314101
23. Ding J, Huang S, Wang Y, Tian Q, Zha R, Shi H, et al. Genome-Wide Screening Reveals That miR-195 Targets the TNF-alpha/NF-kappaB Pathway by Down-Regulating IkappaB Kinase Alpha and TAB3 in Hepatocellular Carcinoma. *Hepatology* (2013) 58:654–66. doi: 10.1002/hep.26378
24. Chen J, Gu J, Feng J, Liu Y, Xue Q, Ni T, et al. TAB3 Overexpression Promotes Cell Proliferation in non-Small Cell Lung Cancer and Mediates Chemoresistance to CDDP in A549 Cells Via the NF-kappaB Pathway. *Tumour Biol* (2016) 37:3851–61. doi: 10.1007/s13277-015-3896-y
25. Parker JS, Mullins M, Cheang MC, Leung S, Voduc D, Vickery T, et al. Supervised Risk Predictor of Breast Cancer Based on Intrinsic Subtypes. *J Clin Oncol* (2009) 27:1160–7. doi: 10.1200/JCO.2008.18.1370
26. Sørlie T, Perou CM, Tibshirani R, Aas T, Geisler S, Johnsen H, et al. Gene Expression Patterns of Breast Carcinomas Distinguish Tumor Subclasses With Clinical Implications. *Proc Natl Acad Sci USA* (2001) 98:10869–74. doi: 10.1073/pnas.191367098
27. Kong L, Zhang Y, Ye ZQ, Liu XQ, Zhao SQ, Wei L, et al. CPC: Assess the Protein-Coding Potential of Transcripts Using Sequence Features and Support Vector Machine. *Nucleic Acids Res* (2007) 35:W345–9. doi: 10.1093/nar/gkm391
28. Lin MF, Jungreis I, Kellis M. PhyloCSF: A Comparative Genomics Method to Distinguish Protein Coding and non-Coding Regions. *Bioinformatics* (2011) 27:i275–282. doi: 10.1093/bioinformatics/btr209
29. Hsu CH, Hsu CW, Hsueh C, Wang CL, Wu YC, Wu CC, et al. Identification and Characterization of Potential Biomarkers by Quantitative Tissue Proteomics of Primary Lung Adenocarcinoma. *Mol Cell Proteom* (2016) 15:2396–410. doi: 10.1074/mcp.M115.057026
30. Liu D, Yin B, Wang Q, Ju W, Chen Y, Qiu H, et al. Cytoplasmic Poly(a) Binding Protein 4 is Highly Expressed in Human Colorectal Cancer and Correlates With Better Prognosis. *J Genet Genomics* (2012) 39:369–74. doi: 10.1016/j.jgg.2012.05.007
31. Kanayama A, Seth RB, Sun L, Ea CK, Hong M, Shaito A, et al. TAB2 and TAB3 Activate the NF-kappaB Pathway Through Binding to Polyubiquitin Chains. *Mol Cell* (2004) 15:535–48. doi: 10.1016/j.molcel.2004.08.008
32. Du Z, Fei T, Verhaak RG, Su Z, Zhang Y, Brown M, et al. Integrative Genomic Analyses Reveal Clinically Relevant Long Noncoding RNAs in Human Cancer. *Nat Struct Mol Biol* (2013) 20:908–13. doi: 10.1038/nsmb.2591
33. Grimsey NJ, Lin Y, Narala R, Rada CC, Mejia-Pena H. Trejo J. G Protein-Coupled Receptors Activate P38 MAPK Via a non-Canonical TAB1-TAB2- and TAB1-TAB3-dependent Pathway in Endothelial Cells. *J Biol Chem* (2019) 294:5867–78. doi: 10.1074/jbc.RA119.007495
34. Kini HK, Kong J, Liebhaber SA. Cytoplasmic Poly(a) Binding Protein C4 Serves a Critical Role in Erythroid Differentiation. *Mol Cell Biol* (2014) 34:1300–9. doi: 10.1128/MCB.01683-13
35. Yang H, Duckett CS, Lindsten T. iPABP, an Inducible Poly(a)-Binding Protein Detected in Activated Human T Cells. *Mol Cell Biol* (1995) 15:6770–6. doi: 10.1128/MCB.15.12.6770

**Conflict of Interest:** The authors declare that the research was conducted in the absence of any commercial or financial relationships that could be construed as a potential conflict of interest.

frontiers in Oncology

ORIGINAL RESEARCH
published: 27 May 2021
doi: 10.3389/fonc.2021.604801

# MET and FASN as Prognostic Biomarkers of Triple Negative Breast Cancer: A Systematic Evidence Landscape of Clinical Study

*Weihua Jiang*[1†], *Xiao-Liang Xing*[2†], *Chenguang Zhang*[1], *Lina Yi*[1], *Wenting Xu*[1], *Jianghua Ou*[1] *and Ning Zhu*[2*]

[1] The Affiliated Tumor Hospital of Xinjiang Medical University, Wulumuqi, China, [2] Hunan University of Medicine, Huaihua, China

**Background:** To know the expression of Mesenchymal–Epithelial Transition factor (MET) and Fatty Acid Synthase (FASN) in Triple Negative Breast Cancer (TNBC) patients, as well as its relationship with clinical pathological characteristic and prognosis.

**Methods:** we used immunohistochemistry staining to detect the expression of MET and FASN for those 218 TNBC patients, and analyze their relationship with the clinical pathological characteristic and prognosis.

**Results:** 130 and 65 out of 218 TNBC patients were positive for MET in the cancer and adjacent tissues respectively. 142 and 30 out of 218 TNBC patients were positive for FASN in the cancer and adjacent tissues respectively. Positive expression of MET and FASN were significantly correlated with lymph node metastasis, pathological TNM, and pathological Stage. In addition, the positive expression of MET and FASN were correlated with recurrence and metastasis. The combined use of MET and FASN can better predict the survival condition.

**Conclusions:** Our results indicated that MET and FASN showed good predictive ability for TNBC. Combined use of MET and FASN were recommended in order to make a more accurate prognosis for TNBC.

**Keywords: TNBC, MET, FASN, recurrence, metastasis, prognosis biomarker**

OPEN ACCESS

***Edited by:***
*Zhijie Jason Liu,*
*The University of Texas Health Science Center at San Antonio, United States*

***Reviewed by:***
*Dylan Lei,*
*Harvard Medical School, United States*
*Huichang Gao,*
*South China University of Technology, China*

****Correspondence:***
*Ning Zhu*
*82478637@qq.com*

*[†]These authors have contributed equally to this work*

***Specialty section:***
*This article was submitted to Women's Cancer, a section of the journal Frontiers in Oncology*

***Received:*** *10 September 2020*
***Accepted:*** *30 April 2021*
***Published:*** *27 May 2021*

***Citation:***
*Jiang W, Xing X-L, Zhang C, Yi L, Xu W, Ou J and Zhu N (2021) MET and FASN as Prognostic Biomarkers of Triple Negative Breast Cancer: A Systematic Evidence Landscape of Clinical Study. Front. Oncol. 11:604801. doi: 10.3389/fonc.2021.604801*

## INTRODUCTION

Breast Cancer (BC) is the most commonly diagnosed cancer and the leading cause of cancer death (1). In 2018, there are almost 2.1 million new cases of BC have been diagnosed which account for about 1/4 cancer cases among women (1). Depend on molecular and histological evidences, BC could be classified into BC expressing hormone receptor (estrogen receptor ($ER^+$) or progesterone receptor ($PR^+$)), BC expressing human epidermal receptor 2 ($HER2^+$) and triple-negative breast cancer (TNBC) ($ER^-$, $PR^-$, $HER2^-$) (2, 3). About 25% of early breast cancer patients still experience local recurrence and develop distant metastases after active treatment (4). TNBC is one of the most aggressive subtypes of BC, which accounts for about 10–15% of all breast cancers (5). Currently, there are few effective treatments for TNBC. And the prognosis of TNBC is worse than that of non-TNBC (6, 7).

Previous studies indicated that the treatment approaches for BC should be based on their molecular characteristics. Therefore, it is important to search for suitable prognostic biomarkers for the prognosis diagnosis and clinical treatment of TNBC.

MET (Mesenchymal–epithelial transition factor) is a receptor tyrosine kinase which could be activated by its ligand hepatocyte growth factor (HGF). The activation of MET and its downstream signaling pathway involved in a number of important biological activities, including tumor cells growth, proliferation and metastasis (8, 9). Recently, increasing evidences indicated that MET is closely correlated with the development of BC (10, 11). MET positive TNBC patients have a shorter overall survival, their death risk is 1.8 times that of negative patients (12). MET is highly expressed in TNBC cell lines. And inhibition of MET could reduce cell proliferation and migration (12). Fatty acid synthase (FASN) is a key enzyme in fat biosynthesis, which plays an important role in regulating the expression of genes involved in apoptosis and DNA repair (13). It is highly expressed in various sex hormone-related malignant tumors and closely related to the proliferation, invasion, metastasis, drug resistance, and apoptosis of tumor cells (13). Current studies have shown that FASN is closely related to the development of BC (14–16). The expression degree of FASN is positively correlated with malignant degree, recurrence, metastasis and death of tumor (17).

In this study, we detect the expression of MET and FASN in TNBC, and analysis the correlation of MET and FASN with clinic pathological characteristics. 130 and 65 out of 218 TNBC patients were positive for MET in the cancer and adjacent tissues respectively. 142 and 30 out of 218 TNBC patients were positive for FASN in the cancer and adjacent tissues respectively. Positive expression of MET and FASN were correlated with lymph node metastasis, pathological TNM, and pathological Stage. In addition, the positive expression of MET and FASN were correlated with recurrence and metastasis. The combined use of MET and FASN can better predict the survival condition. Combined analysis indicated that the TNBC patients with MET and FASN positive expression displayed a worse overall survival. And the AUC was higher than 0.6, which indicated that the combined used of MET and FASN could predict the survival situation more accurately.

# MATERIALS AND METHODS

## Patients

This study was carried out in accordance with the World Medical Association's Declaration of Helsinki and approved by the Research Ethics Committee in The Affiliated Tumor Hospital of Xinjiang Medical University. A total of 218 TNBC patients which confirmed by pathological examination in the affiliated tumor hospital of Xinjiang medical university from 2013 to 2015 were collected (**Table 1**).

**TABLE 1** | Clinical characteristic.

| Category | | Case (218) |
|---|---|---|
| Age | <40 | 65 |
| | ≥40 | 153 |
| Operation method | Improved radical mastectomy | 127 |
| | Breast-conserved radical mastectomy | 72 |
| | Breast reconstruction surgery | 19 |
| Treatment | Neoadjuvant chemotherapy | 72 |
| | Adjuvant chemotherapy | 146 |

## Immunohistochemistry

MET antibody (ZA-0636) was purchased from Beijing Zhong Shan Jin Qiao Biotechnology Company. FASN antibody (FNab-03019) was purchased from Wuhan Enfei Biotechnology Company. The operation of immunohistochemistry was strictly in accordance with the content of quality control. (1) The surgically resected tissue of TNBC patients was treated with 10% formalin fixation and paraffin embedding, and then histological sections were performed (4μm). (2) After routine dewaxing and rehydration, we washed the histopathological sections with PBS (pH =7.4) for three times at 5 min interval. After heat-induced epitope recovery, we washed the histopathological sections with $ddH_2O$. (3) We used hydrogen peroxide solution to block endogenous catalase activity (at room temperature, 10 min). (4) The primary antibody (Dilution: MET, 1:200; FASN, 1:100) was incubated at 4°C overnight. Then washed it with PBS for 5 min and repeated three times. (5) Biotin conjugated secondary antibody was added and incubated at room temperature for 30 min, following with three times wash by PBS for 5 min/time. (6) Add chromogenic reagent for incubation 3 min, hematoxylin dyeing for nuclear staining and dehydration for seal the slide.

## Criteria for Result Analysis

The expression of MET and FASN protein was observed by two-person use double-blind method. All slides contain multiple tissue sections and set antibody or PBS as positive control and negative control. The results were determined by two-person double-blind observation. The ratio of positive cells and the intensity of cell staining were considered to be the judgment criteria. The score criteria for the ratio of MET positive cells were displayed as follows: negative represented 0, <25% represented 1, 26–50% represented 2, 51–75% represented 3, and >75% represented 4. The score criteria for the dyeing intensity were displayed as follows: negative represented 0, light yellow represented 1, dark yellow represented 2, and brown represented 3. A patient is considered to positive for MET if the sum of those two indexes was greater than 4, and negative if they are not (**Figures 1A, B**) (18). The score criteria for the ratio of FASN positive cells were displayed as follows: ≤1% represented 0, 2–10% represented 1, 11–50% represented 2, 51–80% represented 3, and ≥81% represented 4. The score criteria for the dyeing intensity were displayed as follows: negative represented 0, light brown represented 1, brown represented 2, and dark brown represented 3. A patient is considered to positive for MET if the sum of those two indexes was greater than 4, and negative if they are not (**Figures 1C, D**) (19).

## Follow-Up Records

The follow-up time of this study was calculated from the postoperative period. The primary survival assessment was disease-free survival (DFS) for five years. DFS time referred to

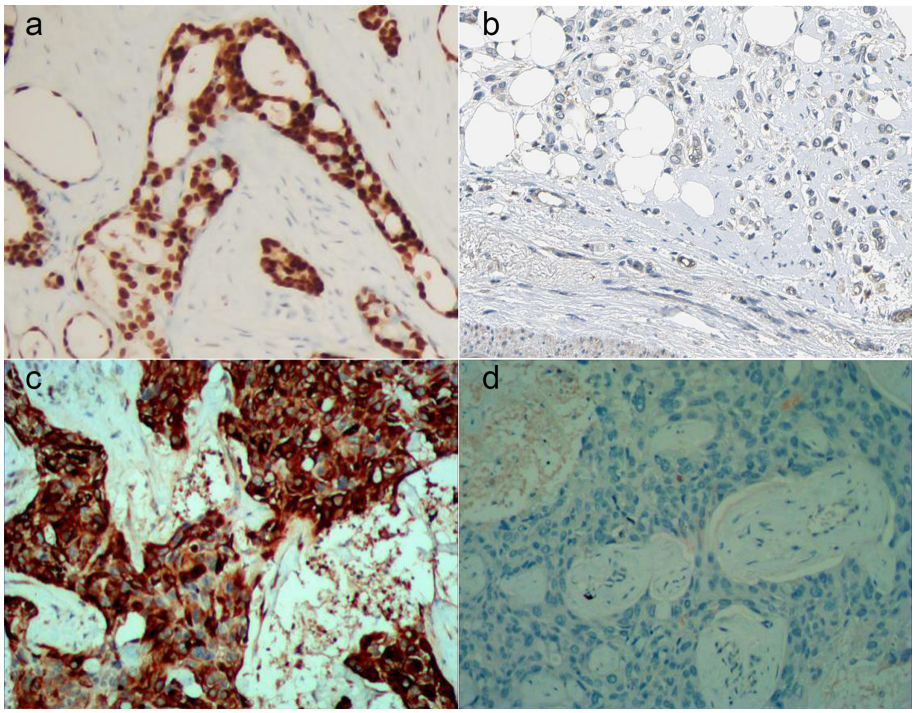


**FIGURE 1** | Expression detection of MET and FASN by Immunohistochemistry. **(A, B)**, positive **(A)** and negative **(B)** expression of MET by immunohistochemistry. **(C, D)**, positive **(C)** and negative **(D)** expression of FASN by immunohistochemistry.

the time from the first day after surgery to local recurrence, regional recurrence, or distant metastasis.

## Construction of the TNBC Prognostic Model

We first marked patients with both MET and FASN positive as 2 points, marked patients with MET or FASN positive as 1 point, marked patients with MET and FASN negative as 0 point. After the assignment, we classify the sample as following:①Group 1: 1 and 2 points, Group 2: 0 point. ②Group 1: 2 points, Group 2: 0 and 1 point. After group divided, we carried our univariate Cox hazards regression analysis and time-dependent receiver operating characteristic (ROC) curves analysis.

## Statistical Analysis

IBM SPSS 22 software was used to carry out univariate and multivariate Cox regression analysis, and chi-square test analysis, Kaplan–Meier analysis. P <0.05 was considered statistically significant.

# RESULTS

## Expression of MET and FASN in Cancer and Adjacent Tissues of TNBC

In this present study, we used IHC staining to detect the expression of MET and FASN. We found that 130 and 65 out of 218 TNBC patients were positive for MET in the cancer and adjacent tissues respectively. The positive rates were 59.6 and 29.8% (**Table 2**). 142 and 30 out of 218 TNBC patients were positive for FASN in the cancer and adjacent tissues respectively. The positive rates were 65.1 and 13.8%. The positive rate for MET and FASN in cancer tissues of TNBC were higher significantly than those in the adjacent tissue (**Table 2**). There were 83 TNBC patients with both positive expression of MET and FASN.

## The Relationship of MET and FASN With the Clinical Pathological Features

To know the relationship of MET and FASN with the clinical pathological features, we carried out the correlation analysis and found that the positive expression of MET and FASN were significantly correlated with lymph node metastasis, pathological TNM, and pathological Stage. In addition, we also found that the positive expression of FASN was significantly correlated with diabetes and body mass index (**Table 3**). Those

**TABLE 2** | Expression of MET and FASN in cancer and adjacent tissues.

| Group | MET | | FASN | |
|---|---|---|---|---|
| | Positive | Negative | Positive | Negative |
| Cancer Tissue | 130 (59.6) | 88 (40.4) | 142 (65.1) | 76 (34.9) |
| Adjacent Tissue | 65 (29.8) | 153 (70.2) | 30 (13.8) | 188 (86.2) |
| Chi-square value | 39.19 | | 120.4 | |
| p value | <0.001 | | <0.001 | |

**TABLE 3 |** The relationship of MET and FASN with the clinical pathological features in TNBC.

| Clinical pathological features | | n | MET | | chi-square value | p value | FASN | | chi-square value | p value |
|---|---|---|---|---|---|---|---|---|---|---|
| | | | positive | negative | | | positive | negative | | |
| Tumor size (cm) | ≤2 | 55 | 29 (52.7) | 26 (47.3) | 1.648 | 0.439 | 30 (54.5) | 25 (45.5) | 4.114 | 0.128 |
| | 2–5 | 124 | 78 (62.9) | 46 (37.1) | | | 87 (70.2) | 37 (29.8) | | |
| | ≥5 | 39 | 23 (59.0) | 16 (41.0) | | | 25 (64.1) | 14 (35.9) | | |
| Lymph node | metastasis | 66 | 46 (69.7) | 20 (30.3) | 3.983 | **0.046** | 50 (75.8) | 16 (24.2) | 4.701 | **0.030** |
| | no-metastasis | 152 | 84 (55.3) | 68 (44.7) | | | 92 (60.5) | 60 (39.5) | | |
| Pathological TNM | I | 50 | 22 (44.0) | 28 (56.0) | 6.643 | **0.036** | 21 (42.0) | 29 (58.0) | 16.30 | **0.001** |
| | II | 110 | 70 (63.6) | 40 (36.4) | | | 79 (71.8) | 31 (28.2) | | |
| | III | 58 | 38 (65.5) | 20 (34.5) | | | 42 (72.4) | 16 (27.6) | | |
| Pathologic Stage | I | 15 | 5 (33.3) | 10 (66.7) | 6.365 | **0.041** | 4 (26.7) | 11 (73.3) | 11.18 | **0.004** |
| | II | 129 | 75 (58.1) | 54 (41.9) | | | 85 (65.9) | 44 (34.1) | | |
| | III | 74 | 50 (67.6) | 24 (32.4) | | | 53 (71.6) | 21 (28.4) | | |
| Diabetes | Positive | 29 | 16 (55.2) | 13 (44.8) | 0.276 | 0.599 | 24 (82.8) | 5 (17.2) | 4.574 | **0.032** |
| | Negative | 189 | 114 (60.3) | 75 (39.7) | | | 118 (62.4) | 71 (37.6) | | |
| Body mass index | <18.5 | 4 | 1 (25.0) | 3 (75.0) | 2.053 | 0.561 | 0 (0.0) | 4 (100) | 13.33 | **0.004** |
| | 18.5–23.9 | 102 | 62 (60.8) | 40 (41.2) | | | 60 (58.8) | 42 (41.2) | | |
| | 24–27.9 | 70 | 42 (60.0) | 28 (40.0) | | | 49 (70.0) | 21 (30.0) | | |
| | ≥28 | 42 | 25 (59.5) | 17 (40.5) | | | 33 (78.6) | 9 (21.4) | | |

*Since the P value is less than 0.05, we highlighted it in bold.*

results indicated that MET and FASN may be the factor affecting the progression of TNBC.

## Associated Analysis of Recurrence and Metastasis With MET and FASN

To know the relationship of positive expression of MET and FASN with their recurrence and metastasis, we followed up those 218 patients for five years. Of 218, 54 TNBC patients had cancer recurrence and metastasis. For MET, we found the ratio of DFS in positive expression group and negative expression group were 70.0 and 83.0% respectively. The positive expression of MET was significantly correlated with cancer recurrence and metastasis ($X^2 = 4.726$, $p = 0.030$). For FASN, we also found the ratio of DFS in positive expression group and negative expression group were 70.4 and 84.2% respectively. The positive expression of FASN was significantly correlated with cancer recurrence and metastasis ($X^2 = 5.505$, $p = 0.025$) (**Table 4**).

At meanwhile, we carried out univariate Cox regression analysis for MET and FASN. The TNBC patients with negative expression of MET (P = 0.036) and FASN (P = 0.029) displayed a better overall survival. The result of multivariate Cox regression analysis indicated that the expression of MET (B = 0.685, P = 0.025) and FASN (B = 0.757, P = 0.021) were still correlated with the overall survival.

**TABLE 4 |** Correlation analysis of MET and FASN with the recurrence and metastasis.

| Group | MET | | FASN | |
|---|---|---|---|---|
| | Positive | Negative | Positive | Negative |
| Recurred and Metastasis (%) | 39 (72.2) | 15 (27.8) | 42 (77.8) | 12 (22.2) |
| No- recurred and metastasis (%) | 91 (55.5) | 73 (44.5) | 100 (61.0) | 64 (39.0) |
| chi-square value | 4.726 | | 5.505 | |
| p value | 0.030 | | 0.025 | |

To know whether MET and FASN could be combined for TNBC diagnostic analysis, we divided the TNBC patients into two groups as following: Group 1: 1 and 2 points, Group 2: 0 point. We carried out univariate Cox regression analysis and found that there was no significantly difference in overall survival between groups 1 and 2. And then, we divided the TNBC patients into two groups as following: Group 1: 2 points, Group 2: 0 and 1 point. We carried out univariate Cox regression analysis and found that group 1 displayed a worse overall survival (**Figure 2A**). The time-dependent receiver operating characteristic (ROC) curves have area under curve (AUC) values higher than 0.5 significantly, which were 0.6210 (p = 0.0028) (**Figure 2B**).

# DISCUSSIONS

BC is the most commonly diagnosed cancer and the leading cause of cancer death (1). There are almost 2.1 million new cases of BC have been diagnosed which account for about 1/4 cancer cases among women in 2018 (1). TNBC is one of the most aggressive subtypes of BC. It is important to find suitable biomarkers in TNBC patients for prognosis diagnosis.

MET is a protein encoded by the proto-oncogene *MET* which is located in 7q21-q31 of chromosome 7. MET is involved in the activation of multiple signal transduction pathways, including RAS, PI3K and -catenin pathways, which play an important role in the occurrence and development of cancer (20–22). Previous studies have demonstrated that abnormal activation of MET signaling pathway could promote neovascularization, lymphangiogenesis, proliferation and differentiation of tumor cells, malignant tumor invasion and metastasis (23). For example, Bleau et al. (24) found that miR-146a targets c-met and abolishes colorectal cancer liver metastasis. Guo et al. (25) found miRNA-454-3p inhibits cervical cancer cell invasion and migration by targeting Met. Han et al. (26) found miR-1 could inhibit gastric cancer cell proliferation and

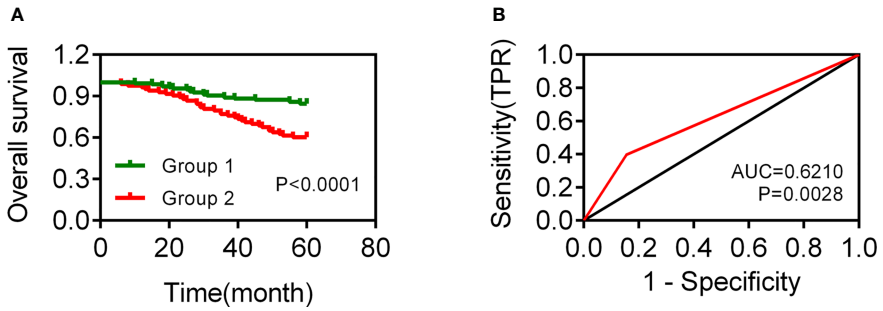


**FIGURE 2** | Analysis of the TNBC prognostic model based on MET and FASN expression. **(A)** The overall survival curve of TNBC patients with group 1 (2 points, both positive expression of MET and FASN) and group 2 (0 and 1 point, positive expression of MET or FASN, and negative expression of MET and FASN). **(B)** The AUC value of ROC curve in 5-year for TNBC patients.

migration by targeting MET. Lee et al. (27) found that inhibition of Met and VEGFR2 in osteoblasts reduced RANKL and M-CSF expression, and associated with reduction of tumor-induced osteolysis. In addition, previous studies indicated abnormal activation of MET was also involved in the development of BC. For example, Meng et al. (11) found that EGFL9 could promote breast cancer metastasis by inducing MET activation and metabolic reprogramming. Zeng et al. (10) found that FEN1 mediates miR-200a methylation and promotes BC cell growth *via* MET and EGFR signaling pathway. Those reports indicated MET played important role in the development of cancer, including BC. In this present study, we found 130 out of 218 TNBC patients (59.6%) was positive for MET in the cancer tissue which were significantly higher than that in adjacent tissues. We also found the positive expression of MET was associated with lymph node metastasis, pathological TNM, and pathological stage in TNBC patients significantly. Our results reinforced the relationship of MET with the development of cancers. In addition, we found that the TNBC patients with positive expression of MET exhibited poorer overall survival. Our results not only enhanced the relationship between MET expression and BC survival rate, but also suggested that MET expression was also closely related to the overall survival of BC subtype TNBC (12). Our results indicated that MET could be a prognostic biomarker for TNBC which was similar to previous studies (28, 29).

FASN is an enzyme that encoded by the *FASN* gene, could catalyzes fatty acid synthesis. Previous study indicated that *FASN* could be a possible oncogene (30). Orlistat was a gastrointestinal lipase inhibitor which could be a potential medicine for cancers (31). Inhibition of FASN could suppress the proliferation, invasion, and metastasis of cancer cells (15, 32, 33). In the present study, we found that 142 out of 218 TNBC patients (65.1%) were positive for FASN in cancer tissue which was significantly higher than that in adjacent tissues. Positive expression of FASN was associated with lymph node metastasis, TNM stage, histological grading, diabetes, and body mass index. In addition, we also found FASN was correlated with the overall survival of TNBC patients. TNBC patients with positive expression of FASN exhibited poorer overall survival. These results indicated that FASN could be a prognostic biomarker for TNBC patients. Our result was consistent with previous reports showed that FASN was an indicator of poor prognosis (34).

## CONCLUSIONS

Combined analysis indicated that the TNBC patients with MET and FASN positive expression displayed a worse overall survival. And the AUC was higher than 0.6, which indicated that the combined used of MET and FASN could predict the survival situation more accurately.

## DATA AVAILABILITY STATEMENT

The raw data supporting the conclusions of this article will be made available by the authors, without undue reservation.

## ETHICS STATEMENT

The studies involving human participants were reviewed and approved by Research Ethics Committee in The Affiliated Tumor Hospital of Xinjiang Medical University. The patients/participants provided their written informed consent to participate in this study.

## AUTHOR CONTRIBUTIONS

WJ and NZ conceived and designed the experiments. CZ, LY, and WX performed the experiments. JO, and X-LX helped to analyze the data. X-LX wrote the paper. All authors contributed to the article and approved the submitted version.

## FUNDING

This project is financially supported by the Natural Science Foundation of Xinjiang (2017D01C407).

## REFERENCES


1. Bray F, Ferlay J, Soerjomataram I, Siegel RL, Torre LA, Jemal A. Global Cancer Statistics 2018: GLOBOCAN Estimates of Incidence and Mortality Worldwide for 36 Cancers in 185 Countries. *CA Cancer J Clin* (2018) 68 (6):394–424. doi: 10.3322/caac.21492
2. Liedtke C, Mazouni C, Hess KR, Andre F, Tordai A, Mejia JA, et al. Response to Neoadjuvant Therapy and Long-Term Survival in Patients With Triple-Negative Breast Cancer. *J Clin Oncol* (2008) 26(8):1275–81. doi: 10.1200/JCO.2007.14.4147
3. Lehmann BD, Bauer JA, Chen X, Sanders ME, Chakravarthy AB, Shyr Y, et al. Identification of Human Triple-Negative Breast Cancer Subtypes and Preclinical Models for Selection of Targeted Therapies. *J Clin Invest* (2011) 121(7):2750–67. doi: 10.1172/JCI45014
4. Kennecke H, Yerushalmi R, Woods R, Cheang MC, Voduc D, Speers CH, et al. Metastatic Behavior of Breast Cancer Subtypes. *J Clin Oncol* (2010) 28 (20):3271–7. doi: 10.1200/JCO.2009.25.9820
5. Perez-Garcia J, Soberino J, Racca F, Gion M, Stradella A, Cortes J. Atezolizumab in the Treatment of Metastatic Triple-Negative Breast Cancer. *Expert Opin Biol Ther* (2020) 20(9):981–9. doi: 10.1080/14712598.2020.1769063
6. Yi YW, You K, Bae EJ, Kwak SJ, Seong YS, Bae I. Dual Inhibition of EGFR and MET Induces Synthetic Lethality in Triple-Negative Breast Cancer Cells Through Downregulation of Ribosomal Protein S6. *Int J Oncol* (2015) 47 (1):122–32. doi: 10.3892/ijo.2015.2982
7. Gaule P, Mukherjee N, Corkery B, Eustace AJ, Gately K, Roche S, et al. Dasatinib Treatment Increases Sensitivity to C-Met Inhibition in Triple-Negative Breast Cancer Cells. *Cancers (Basel)* (2019) 11(4):548. doi: 10.3390/cancers11040548
8. Ren X, Yuan L, Shen S, Wu H, Lu J, Liang Z. c-Met and ERbeta Expression Differences in Basal-Like and Non-Basal-Like Triple-Negative Breast Cancer. *Tumour Biol* (2016) 37(8):11385–95. doi: 10.1007/s13277-016-5010-5
9. Ayoub NM, Al-Shami KM, Alqudah MA, Mhaidat NM. Crizotinib, a MET Inhibitor, Inhibits Growth, Migration, and Invasion of Breast Cancer Cells *In Vitro* and Synergizes With Chemotherapeutic Agents. *Onco Targets Ther* (2017) 10:4869–83. doi: 10.2147/OTT.S148604
10. Zeng X, Qu X, Zhao C, Xu L, Hou K, Liu Y, et al. FEN1 Mediates miR-200a Methylation and Promotes Breast Cancer Cell Growth *Via* MET and EGFR Signaling. *FASEB J* (2019) 33(10):10717–30. doi: 10.1096/fj.201900273R
11. Meng F, Wu L, Dong L, Mitchell AV, James Block C, Liu J, et al. EGFL9 Promotes Breast Cancer Metastasis by Inducing cMET Activation and Metabolic Reprogramming. *Nat Commun* (2019) 10(1):5033. doi: 10.1038/s41467-019-13034-3
12. Simiczyjew A, Dratkiewicz E, Van Troys M, Ampe C, Styczen I, Nowak D. Combination of EGFR Inhibitor Lapatinib and MET Inhibitor Foretinib Inhibits Migration of Triple Negative Breast Cancer Cell Lines. *Cancers (Basel)* (2018) 10(9):335. doi: 10.3390/cancers10090335
13. Bueno MJ, Quintela-Fandino M. Emerging Role of Fatty Acid Synthase in Tumor Initiation: Implications for Cancer Prevention. *Mol Cell Oncol* (2020) 7 (2):1709389. doi: 10.1080/23723556.2019.1709389
14. Menendez JA, Lupu R. Fatty Acid Synthase (FASN) as a Therapeutic Target in Breast Cancer. *Expert Opin Ther Targets* (2017) 21(11):1001–16. doi: 10.1080/14728222.2017.1381087
15. Singh R, Yadav V, Kumar S, Saini N. MicroRNA-195 Inhibits Proliferation, Invasion and Metastasis in Breast Cancer Cells by Targeting FASN, Hmgcr, ACACA and CYP27B1. *Sci Rep* (2015) 5:17454. doi: 10.1038/srep17454
16. Giro-Perafita A, Palomeras S, Lum DH, Blancafort A, Vinas G, Oliveras G, et al. Preclinical Evaluation of Fatty Acid Synthase and EGFR Inhibition in Triple-Negative Breast Cancer. *Clin Cancer Res* (2016) 22(18):4687–97. doi: 10.1158/1078-0432.CCR-15-3133
17. Menendez JA, Lupu R. Fatty Acid Synthase Regulates Estrogen Receptor-Alpha Signaling in Breast Cancer Cells. *Oncogenesis* (2017) 6(2):e299. doi: 10.1038/oncsis.2017.4
18. Harvey JM, Clark GM, Osborne CK, Allred DC. Estrogen Receptor Status by Immunohistochemistry is Superior to the Ligand-Binding Assay for Predicting Response to Adjuvant Endocrine Therapy in Breast Cancer. *J Clin Oncol* (1999) 17(5):1474–81. doi: 10.1200/JCO.1999.17.5.1474
19. Zhou L, Zhao YH, Wang XD, Jiang SF, Li H. [Expression of Fatty Acid Synthase and Adipocyte Fatty Acid-Binding Protein and the Relationship With the Clinicopathological Characteristics in Human Infiltrating Ductal Breast Cancer]. *Sichuan Da Xue Xue Bao Yi Xue Ban* (2015) 46(2):228–33.
20. O'Brien LE, Tang K, Kats ES, Schutz-Geschwender A, Lipschutz JH, Mostov KE. ERK and MMPs Sequentially Regulate Distinct Stages of Epithelial Tubule Development. *Dev Cell* (2004) 7(1):21–32. doi: 10.1016/j.devcel.2004.06.001
21. Gentile A, Trusolino L, Comoglio PM. The Met Tyrosine Kinase Receptor in Development and Cancer. *Cancer Metastasis Rev* (2008) 27(1):85–94. doi: 10.1007/s10555-007-9107-6
22. Monga SP, Mars WM, Pediaditakis P, Bell A, Mule K, Bowen WC, et al. Hepatocyte Growth Factor Induces Wnt-independent Nuclear Translocation of Beta-Catenin After Met-beta-catenin Dissociation in Hepatocytes. *Cancer Res* (2002) 62(7):2064–71.
23. Leonetti E, Gesualdi L, Scheri KC, Dinicola S, Fattore L, Masiello MG, et al. C-Src Recruitment is Involved in C-MET-Mediated Malignant Behaviour of NT2D1 Non-Seminoma Cells. *Int J Mol Sci* (2019) 20(2):320. doi: 10.3390/ijms20020320
24. Bleau AM, Redrado M, Nistal-Villan E, Villalba M, Exposito F, Redin E, et al. miR-146a Targets C-Met and Abolishes Colorectal Cancer Liver Metastasis. *Cancer Lett* (2018) 414:257–67. doi: 10.1016/j.canlet.2017.11.008
25. Guo Y, Tao M, Jiang M. MicroRNA-454-3p Inhibits Cervical Cancer Cell Invasion and Migration by Targeting C-Met. *Exp Ther Med* (2018) 15 (3):2301–6. doi: 10.3892/etm.2018.5714
26. Han C, Zhou Y, An Q, Li F, Li D, Zhang X, et al. MicroRNA-1 (miR-1) Inhibits Gastric Cancer Cell Proliferation and Migration by Targeting MET. *Tumour Biol* (2015) 36(9):6715–23. doi: 10.1007/s13277-015-3358-6
27. Lee C, Whang YM, Campbell P, Mulcrone PL, Elefteriou F, Cho SW, et al. Dual Targeting C-Met and VEGFR2 in Osteoblasts Suppresses Growth and Osteolysis of Prostate Cancer Bone Metastasis. *Cancer Lett* (2018) 414:205–13. doi: 10.1016/j.canlet.2017.11.016
28. Van Der Steen N, Zwaenepoel K, Mazzaschi G, AL R, PG D, Op de Beeck K, et al. The Role of c-Met as a Biomarker and Player in Innate and Acquired Resistance in Non-Small-Cell Lung Cancer: Two New Mutations Warrant Further Studies. *Molecules* (2019) 24(24):4443. doi: 10.3390/molecules24244443
29. Tsakonas G, Botling J, Micke P, Rivard C, LaFleur L, Mattsson J, et al. c-MET as a Biomarker in Patients With Surgically Resected Non-Small Cell Lung Cancer. *Lung Cancer* (2019) 133:69–74. doi: 10.1016/j.lungcan.2019.04.028
30. Baron A, Migita T, Tang D, Loda M. Fatty Acid Synthase: A Metabolic Oncogene in Prostate Cancer? *J Cell Biochem* (2004) 91(1):47–53. doi: 10.1002/jcb.10708
31. Flavin R, Peluso S, Nguyen PL, Loda M. Fatty Acid Synthase as a Potential Therapeutic Target in Cancer. *Future Oncol* (2010) 6(4):551–62. doi: 10.2217/fon.10.11
32. Long XH, Mao JH, Peng AF, Zhou Y, Huang SH, Liu ZL. Tumor Suppressive microRNA-424 Inhibits Osteosarcoma Cell Migration and Invasion *Via* Targeting Fatty Acid Synthase. *Exp Ther Med* (2013) 5(4):1048–52. doi: 10.3892/etm.2013.959
33. Chang L, Fang S, Chen Y, Yang Z, Yuan Y, Zhang J, et al. Inhibition of FASN Suppresses the Malignant Biological Behavior of Non-Small Cell Lung Cancer Cells *Via* Deregulating Glucose Metabolism and AKT/ERK Pathway. *Lipids Health Dis* (2019) 18(1):118. doi: 10.1186/s12944-019-1058-8
34. Wu K, Yin X, Jin Y, Liu F, Gao J. Identification of Aberrantly Methylated Differentially Expressed Genes in Prostate Carcinoma Using Integrated Bioinformatics. *Cancer Cell Int* (2019) 19:51. doi: 10.1186/s12935-019-0763-8


**Conflict of Interest:** The authors declare that the research was conducted in the absence of any commercial or financial relationships that could be construed as a potential conflict of interest.

frontiers in Oncology

ORIGINAL RESEARCH
published: 02 June 2021
doi: 10.3389/fonc.2021.602222

# Epithelial-Mesenchymal-Transition-Like Circulating Tumor Cell-Associated White Blood Cell Clusters as a Prognostic Biomarker in HR-Positive/HER2-Negative Metastatic Breast Cancer

*Xiuwen Guan[1], Chunxiao Li[2], Yiqun Li[1], Jiani Wang[1], Zongbi Yi[1], Binliang Liu[1], Hongyan Chen[2], Jiasen Xu[3], Haili Qian[2]*, Binghe Xu[1,2]* and Fei Ma[1,2]**

*[1] Department of Medical Oncology, National Cancer Center/National Clinical Research Center for Cancer/Cancer Hospital, Chinese Academy of Medical Sciences and Peking Union Medical College, Beijing, China, [2] State Key Laboratory of Molecular Oncology, National Cancer Center/Cancer Hospital, Chinese Academy of Medical Sciences and Peking Union Medical College, Beijing, China, [3] SurExam Bio-Tech, Guangzhou, China*

OPEN ACCESS

**Edited by:**
*Zhijie Jason Liu, The University of Texas Health Science Center at San Antonio, United States*

**Reviewed by:**
*Chun Wang, Thomas Jefferson University, United States*
*Michel Rigaud, Istituto Scientifico Romagnolo per lo Studio e la Cura dei Tumori (IRST-IRCCS), Italy*

***Correspondence:**
*Fei Ma*
*drmafei@126.com*
*Binghe Xu*
*xubinghe@medmail.com.cn*
*Haili Qian*
*qianhaili001@163.com*

**Specialty section:**
*This article was submitted to Women's Cancer, a section of the journal Frontiers in Oncology*

**Received:** *02 September 2020*
**Accepted:** *05 May 2021*
**Published:** *02 June 2021*

**Citation:**
*Guan X, Li C, Li Y, Wang J, Yi Z, Liu B, Chen H, Xu J, Qian H, Xu B and Ma F (2021) Epithelial-Mesenchymal-Transition-Like Circulating Tumor Cell-Associated White Blood Cell Clusters as a Prognostic Biomarker in HR-Positive/HER2-Negative Metastatic Breast Cancer. Front. Oncol. 11:602222. doi: 10.3389/fonc.2021.602222*

**Background:** Although positive Circulating tumor cells (CTCs) status has been validated as a prognostic marker in breast cancer, the interaction between immune cells and CTCs during the progress of Epithelial-mesenchymal-transition (EMT), and the clinical implications of CTC-associated white blood cell clusters (CTC-WBC clusters) for metastatic breast cancer are largely uncharacterized.

**Methods:** We optimized a filter-based method combined with an RNA *in situ* hybridization technique according to the epithelial- and mesenchymal-markers to analyze EMT in CTC-WBC clusters. Serial peripheral blood samples from 135 patients with Hormone receptor (HR)-positive/HER2-negative metastatic breast cancer receiving first-line chemotherapy with docetaxel plus capecitabine were prospectively collected until disease progression from Nov 2013 to March 2019. Follow-up data collection was conducted until July 2020.

**Results:** A total of 452 blood samples at all time-points were collected and analyzed. Median age of the cohort was 51.0 years (range, 27 to 73 years), and most of them (76.3%) had visceral metastases. Median progression-free survival (PFS) was 10.6 months (95% CI, 8.8 to 12.3 months). The presence of EMT-like CTC-WBC clusters was more frequently evident among patients with simultaneous bone and lymph node metastases (87.5% *vs* 36.2%, $P$=0.006), whereas no associations were observed between CTC-WBC clusters and other clinicopathologic characteristics before chemotherapy. The patients with EMT-like CTC-WBC clusters tended to show a significantly increased number of total CTC count (median,19.0 *vs* 5.0, $P$<0.001). The patients with at least one detectable EMT-like CTC-WBC cluster at baseline were

characterized by significantly worse PFS, when compared to the patients with no EMT-like CTC-WBC clusters detected (7.0 *vs* 10.7 months, *P*=0.023), and those with five or more epithelial-based CTCs detected per 5mL of peripheral blood (7.0 *vs* 12.7 months, *P*=0.014). However, the total CTC-WBC clusters were not correlated with patients' survival in the cohort (8.4 *vs* 10.6 months, *P*=0.561).

**Conclusions:** Our data provide evidence that the emergence of CTC-WBC clusters underwent EMT before treatment is associated with significantly poorer PFS in HR-positive/HER2-negative metastatic breast cancer patients receiving docetaxel plus capecitabine, which may be used as a parameter to predict the clinical outcomes and a potential target for individualized therapy.

**Keywords: metastatic breast cancer, circulating tumor cells, white blood cell, epithelial-mesenchymal-transition, prognosis**

## INTRODUCTION

Circulating tumor cells (CTCs), potentially involved in the metastatic cascade (1), has been identified as a poor prognostic clinical factor in breast, lung, colorectal, and prostate cancer, which plays a key role in tumor cell dissemination for metastatic formation (2–6). Owing to the independent prognostic value of CTC count proved in multiple studies, the 8th edition of the American Joint Committee on Cancer (AJCC) cancer staging manual suggested CTCs as an adverse prognosis factor for patients with primary and metastatic breast cancer (7). However, carcinoma cells may undergo an epithelial-mesenchymal-transition (EMT) process and result in decreased expression of epithelial markers, which leads to false-negative findings by traditional epithelial marker-based CTC capturing methods (8).

The process of EMT is a key event in promoting stationary tumor cells to invade and migrate during metastatic cascade (6), which may also result in down-regulated expression of epithelial markers and an increase in mesenchymal proteins in CTCs. CTCs with the expression of mesenchymal markers, like TWIST1, SNAIL1, or vimentin were more likely to be identified in patients with advanced cancer compared to those with early-stage cancer, suggesting the potential role in metastatic dissemination and disease progression (8). Previous evidence in breast, lung, and colorectal cancer showed the presence of CTCs undergoing EMT was correlated with a higher risk of treatment failure and poor prognosis (9–13). Whereas, traditional epithelial marker-based CTC capturing methods, such as Cellsearch, may partially leak the detection of CTCs underwent EMT, thus it is necessary to optimize the enrichment and characterization system based on the expression of both epithelial- markers and mesenchymal-markers.

Moreover, CTCs may have direct interactions with immune cells during cancer dissemination, and correlate with the inflammatory state in the target organ of metastatic extravasation (14). Analyses of the interaction between CTCs and immune cells may provide reference for real-time therapy stratification and prognosis prediction. Although positive CTC status has been validated as a prognostic marker for recurrence-free survival, progression-free survival and overall survival in breast cancer (2, 3, 15), the interaction between immune cells and CTCs during the process of EMT, and the clinical implications of CTC-associated white blood cell clusters (CTC-WBC clusters) for metastatic breast cancer are largely uncharacterized. To address the technical challenges in a practical method and further investigate its clinical value, we optimized a filter-based method combined with an RNA *in situ* hybridization technique according to the epithelial- and mesenchymal-markers to analyze EMT in CTC-WBC clusters, and investigated the predictive value of different phenotypes of CTC-WBC clusters as a prognostic biomarker in a prospective study for Hormone receptor (HR)-positive/HER2-negative metastatic breast cancer.

## METHODS

### Isolation and Classification of CTCs and CTC-WBC Clusters

We optimized the CanPatrol® CTC enrichment technique for the detection of CTC and CTC-WBC clusters (16, 17). CTCs were isolated using a filter-based method combined with an RNA *in situ* hybridization method based on the branched DNA signal amplification technology according to the epithelial-markers EpCAM and CK8/18/19, the mesenchymal-markers vimentin and twist, and the leukocyte-marker CD45.

A total of 5 ml of patient peripheral blood sample was collected in a K2-EDTA tube and transferred to a sample preservative tube which contained lysing buffer *via* a tailored connection device. Erythrocytes were lysed by the red blood cell lysis buffer in 30 min at room temperature. The cell pellets were collected by centrifugation at 600g for 5 min and then PBS containing 4% formaldehyde was used to resuspend the remaining cells for 8 min. At last, CTCs were isolated in a filtration system by a calibrated membrane with 8μm pores filters which can separate small leukocytes from the large epithelial cells.

A multiplex mRNA *in situ* hybridization (ISH) assay was used to identify and classify CTCs. The assay was performed in a 24-well plate at 40°C for 3 hours and a set of probes (EMT markers) was utilized *in situ* hybridization. The epithelial-markers

expressed on CTCs were detected by a multi-marker probe (such as EpCAM, CK8, CK18 and CK19), and the mesenchymal-markers expressed on CTC were detected by a multi-marker probe (such as Twist1 and Vimentin). The CD45 probe was used as the leukocyte-marker. Finally, the cells were stained with DAPI for 10 min and analyzed with an automated imaging fluorescence microscope. The red and green fluorescent signals represent epithelial and mesenchymal markers expression, respectively. A bright white fluorescent signal represents CD45 expression. As **Figure 2A** depicted, CTC-WBC cluster was defined as CTC karyotype connected to typical WBC karyotype cells, on which CD45 fluorescence signal points expressed.

## Patient Cohort Selection

A total of 135 patients with HR-positive/HER2-negative metastatic breast cancer receiving first-line chemotherapy with docetaxel plus capecitabine were prospectively enrolled in the observation cohort to investigate the clinical implications of different phenotypes of CTC-WBC clusters. The patients were recruited after an agreement from the local Ethical committee between Nov 2013 to March 2019 from 32 clinical centers in China. Key eligibility included (1) confirmed histologic/cytologic diagnosis of HR-positive/HER2-negative metastatic breast cancer, (2) previously untreated with first-line chemotherapy, (3) age≥18, (4) Eastern Cooperative Oncology Group performance status < 2, (5) with measurable lesions defined by revised Response Evaluation Criteria in Solid Tumors guidelines version 1.1 (RECIST 1.1), and (6) adequate hematologic, hepatic and renal function.

The clinicopathological characteristics, including age, estrogen receptor (ER) status, progesterone receptor (PR) status, disease free survival (DFS), position of metastatic sites, and previous endocrinotherapy after confirmed tumor relapse were collected before enrollment. Enrolled patients received first-line chemotherapy of docetaxel plus capecitabine for a maximum of 6 cycles or until disease progression, intolerable adverse events, or patient withdrawal occurred, and those with stable disease or a partial or complete response after initial chemotherapy received the maintenance chemotherapy of capecitabine. Blood samples were collected from the baseline and dynamically tracked every 6 weeks during the treatment until disease progression. Follow-up data collection was conducted until July 2020.

## Statistical Analyses

The associations between the distribution of different subtypes of CTCs and the heterogeneity of CTC-WBC clusters were analyzed by Mann-Whitney U test. $\chi^2$ test or Fisher's exact test were used to compare the distribution of clinicopathological characteristics between different groups and described in percentages of categorical variables. Kaplan-Meier analysis was performed to investigate the prognostic value of CTC-WBC clusters and CTC-WBC clusters under EMT. Multivariate hazard ratios for PFS were estimated with Cox proportional hazards regression analysis. The statistical analyses were performed using SPSS software, version 23.0 (SPSS Inc., Chicago, IL, USA). All *P* values were 2-sided and considered to be statistically significant when less than 0.05.

# RESULTS

## Clinicopathologic Characteristics of the Enrolled Cohort

A total of 135 female patients with HR-positive/HER2-negative metastatic breast cancer were recruited in the study for CTC assessment. The median age of the cohort was 51.0 years (range, 27 to 73 years). Among them, 103 (76.3%) of the patients had visceral metastasis. 20 (14.8%) of the patients were *de novo* Stage IV breast cancer and 36 (26.7%) of them were found relapsed or metastasis within 24 months. 32 (23.7%) of the Luminal-like patients received endocrinotherapy after confirmed tumor relapse.

In the study, disease progression was observed in totally 108 patients and the median follow-up was 36.0 months (95% CI, 27.8 to 44.3 months). Median progression-free survival of the cohort was 10.6 months (95% CI, 8.8 to 12.3 months).

## Association Between Different Subtypes of CTCs and the Heterogeneity of CTC-WBC Clusters

Serial peripheral blood samples from the enrolled 135 patients were prospectively collected during the first-line chemotherapy of docetaxel plus capecitabine, with the median of 3 serial samples collected from each patient. A total of 452 blood samples at all time-points were collected and analyzed (**Figure 1**). In the whole cohort,381 (84.3%) of the blood samples at all time-points were detected with more than one CTCs and 42 (9.3%) were detected with CTC-WBC clusters. In the study, totally 53 CTC-WBC clusters were captured, including 10 epithelial CTC-WBC clusters (with epithelial biomarkers detected on CTCs), 39 biphenotypic epithelial/mesenchymal CTC-WBC clusters (with both epithelial and mesenchymal biomarkers detected on CTCs) and 4 mesenchymal CTC-WBC clusters (with mesenchymal biomarkers detected on CTCs).

As **Table 1** showed, the patients with CTC-WBC clusters detected were simultaneously observed in significantly increased enumeration of each subtypes of CTC count, especially in E/M-CTCs and M-CTCs. Among the patients with more than 5 CTCs, the percentage of the emergency of CTC-WBC clusters in the cohorts was eight times increased than those with CTC<5 (14.4% *vs* 1.6%, $\chi^2$ = 21.1, *P*<0.001). Moreover, in the patients with more than 20 CTCs, the presence of CTC-WBC clusters was more than three times frequency than those CTC<20 (25.6% *vs* 5.9%, $\chi^2$ = 29.9, *P*<0.001).

As for the patients detected with CTC-WBC clusters underwent mesenchymal transformation (EMT-like CTC-WBC clusters, including biphenotypic epithelial/mesenchymal CTC-WBC clusters and mesenchymal CTC-WBC clusters), a significantly increased number of total CTCs, E/M-CTCs and M-CTCs were simultaneously observed when compared to those without EMT-like CTC-WBC clusters detected (*P*<0.05, **Figure 2B** and **Table 1**). Besides that, significantly increased

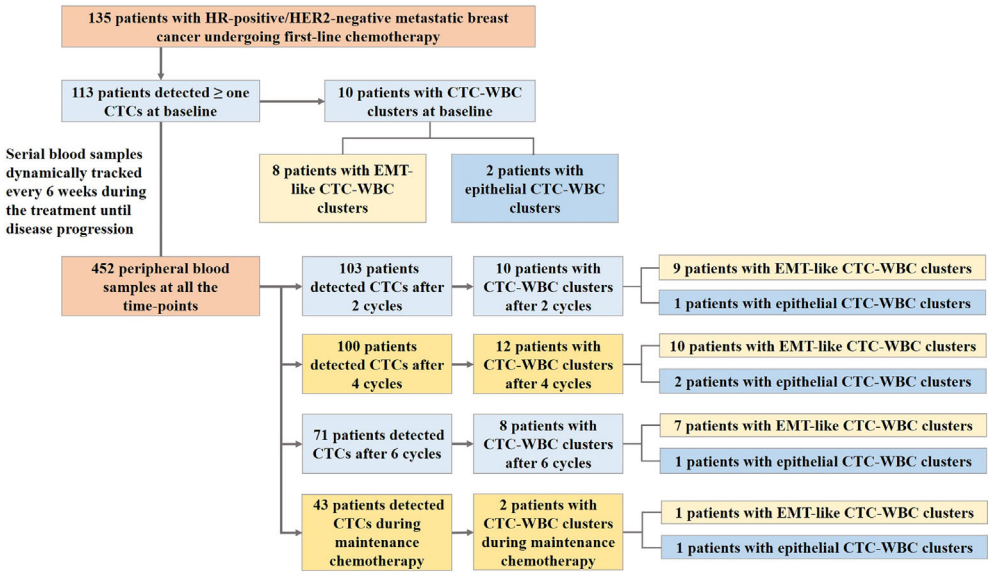


**FIGURE 1** | Flow diagram of the study.

**TABLE 1** | The correlation between different subtypes of CTCs and the presence of CTC-WBC clusters as well as EMT-like CTC-WBC clusters.

| | CTC-WBC clusters | | | | EMT-like CTC-WBC clusters | | | |
|---|---|---|---|---|---|---|---|---|
| | with | without | Z score | *P* value | with | without | Z score | *P* value |
| Total CTCs† | 19.0 (8.0,28.0) | 5.0 (2.0,13.0) | -5.975 | <0.001 | 19.0 (8.0,28.0) | 5.0 (2.0,13.0) | -5.432 | <0.001 |
| E-CTCs† | 2.0 (0,6.25) | 0 (0,2.0) | -3.099 | 0.002 | 1.0 (0,5.0) | 1.0 (0,2.5) | -1.649 | 0.099 |
| E/M-CTCs† | 8.0 (3.0,24.0) | 2 (0,7.0) | -5.658 | <0.001 | 9.0 (4.0,24.0) | 2.0 (0,6.5) | -5.702 | <0.001 |
| M-CTCs† | 2.0 (0,9.25) | 1 (0,2.0) | -3.299 | 0.001 | 3.0 (0,10.0) | 1.0 (0,2.0) | -3.387 | 0.001 |
| EMT-CTCs† | 13.5 (6.0,27.0) | 4 (1.0,10.0) | -5.553 | <0.001 | 16.0 (6.0,28.0) | 4.0 (1.0,10.0) | -5.628 | <0.001 |
| Proportion of EMT-CTCs | 90.8% | 82.0% | -1.904 | 0.057 | 94.7% | 80.0% | -2.773 | 0.006 |

†*median (interquartile range, per 5mL).*

*E-CTCs, epithelial CTCs; E/M-CTCs, biphenotypic epithelial/mesenchymal CTCs; M-CTCs, mesenchymal CTCs; EMT-CTCs, CTCs underwent EMT, including E/M-CTCs and M-CTCs.*

proportion of EMT-CTCs (CTCs underwent EMT, including E/M-CTCs and M-CTCs) in total CTC count was observed in the patients with EMT-like CTC-WBC clusters captured (median, 94.7% *vs* 80.0%, *P*=0.006). Similarly, in patients with more than 5 CTCs and those with more than 20 CTCs, the frequency of presence of EMT-like CTC-WBC clusters was significantly higher than those with low CTC counts (For CTCs≥5 *vs* CTCs<5: 11.9% *vs* 1.6%, $\chi 2 = 15.8$, *P*<0.001; For CTCs≥20 *vs* CTCs <20: 21.8% *vs* 4.8%, $\chi 2 = 26.1$, *P*<0.001).

## Association Between the Emergence of CTC-WBC Clusters and Clinicopathological Features

Before the start of first-line chemotherapy with docetaxel plus capecitabine at baseline, 113 (83.7%) of the 135 patients had more than one detectable CTCs with a median number of 6 CTCs per 5 ml of peripheral blood sample (range, 1 to 151 CTCs/5mL). Meanwhile, CTC-WBC clusters were detectable in 10 patients at baseline, of whom 8 patients had EMT-like CTC-WBC clusters.

When comparing the clinicopathological characteristics between the cohort with EMT-like CTC-WBC cluster detected at baseline and those without, the presence of CTC-WBC clusters had no association with age, menstrual status, ER status, PR status, DFS, and previous endocrinotherapy after confirmed relapse or metastasis (**Table 2**). Concerning the association with different metastatic sites of the enrolled patients, the presence of EMT-like CTC-WBC clusters at baseline was more frequently evident among patients with simultaneous bone metastases and lymph node metastases (87.5% *vs* 36.2%, *P*=0.006, **Figure 2C**), whereas no significant correlation was observed between the detection of EMT-like CTC-WBC clusters and other metastatic sites (**Table 2**).

## Association Between the Heterogeneity of CTC-WBC Clusters and Progression-Free Survival

In this relatively homogeneous HR-positive/HER2-negative metastatic breast cancer cohort, no significant difference was observed in the progression-free survival (PFS) between the

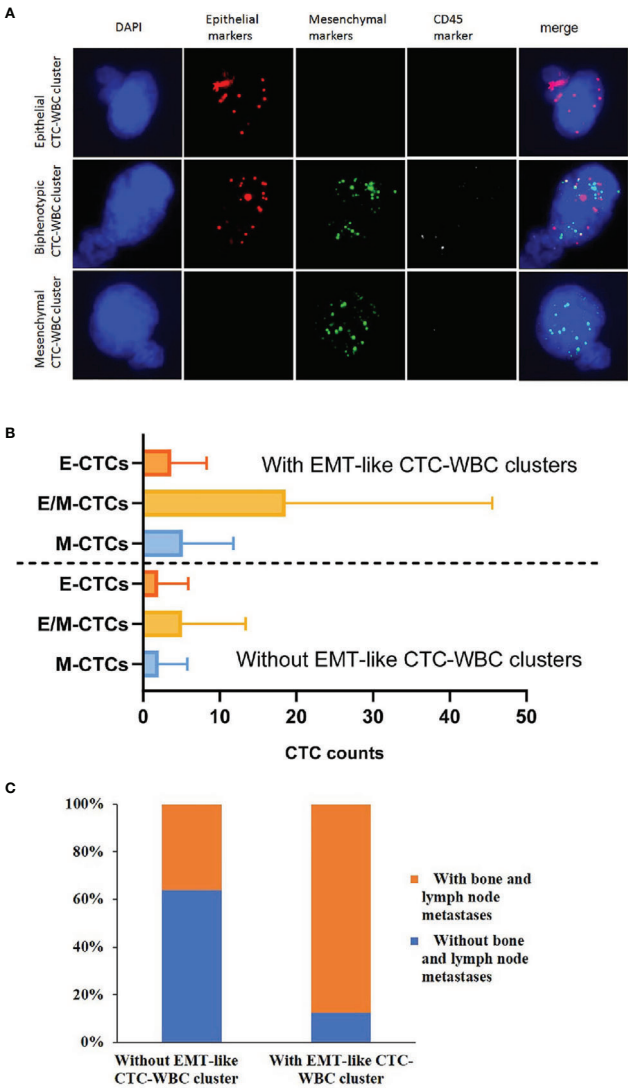


**FIGURE 2** | Association of the detection of EMT-like CTC-WBC clusters with different subtypes of CTCs and the clinicopathological characteristics. **(A)** Representative images of CTC-WBC clusters classified by categorical markers. **(B)** The distribution of different CTC subtypes in the patients with EMT-like CTC-WBC clusters and those patients without. **(C)** Association between the detection of EMT-like CTC-WBC clusters and metastatic sites.

**TABLE 2** | The association between the presence of EMT-like CTC-WBC clusters and the clinicopathological characteristics of 135 enrolled patients with HR-positive/HER2-negative metastatic breast cancer undergoing docetaxel plus capecitabine as first-line chemotherapy.

| | Without EMT-like CTC-WBC clusters at baseline | With EMT-like CTC-WBC clusters at baseline | *P* value |
|---|---|---|---|
| Age | | | 0.353 |
| <60 | 101 (79.5%) | 8 (100.0%) | |
| ≥60 | 26 (20.5%) | 0 | |
| Menstrual status | | | 0.138 |
| Premenopausal | 54 (42.5%) | 6 (75.0%) | |
| Menopause | 73 (57.5%) | 2 (25.0%) | |
| ER status | | | 0.267 |
| Positive | 123 (96.9%) | 7 (87.5%) | |
| Negative | 4 (3.1%) | 1 (12.5%) | |
| PR status | | | 1.000 |
| Positive | 116 (91.3%) | 8(100.0%) | |
| Negative | 11 (8.7%) | 0 | |
| Disease-free survival | | | 0.439 |
| <24 months | 33 (26.0%) | 3 (37.5%) | |
| ≥24 months | 94 (74.0%) | 5 (62.5%) | |
| Position of metastatic site | | | 0.090 |
| Non-visceral | 28 (22.0%) | 4 (50.0%) | |
| Visceral | 99 (78.0%) | 4 (50.0%) | |
| Liver metastases | | | 0.726 |
| Without | 68 (53.5%) | 5 (62.5%) | |
| With | 59 (46.5%) | 3 (37.5%) | |
| Lung metastases | | | 0.154 |
| Without | 59 (46.5%) | 6 (75.0%) | |
| With | 68 (53.5%) | 2 (25.0%) | |
| Bone metastases | | | 0.144 |
| Without | 53 (41.7%) | 1 (12.5%) | |
| With | 74 (58.3%) | 7 (87.5%) | |
| Lymph node metastases | | | 0.268 |
| Without | 44 (34.6%) | 1 (12.5%) | |
| With | 83 (65.4%) | 7 (87.5%) | |
| Simultaneous bone and lymph node metastases | | | 0.006 |
| Without | 81 (63.8%) | 1 (12.5%) | |
| With | 46 (36.2%) | 7 (87.5%) | |
| Previous endocrinotherapy (after confirmed relapse) | | | 0.849 |
| None | 97 (76.4%) | 6 (75.0%) | |
| 1st-line | 26 (20.5%) | 2 (25.0%) | |
| 2nd-line or more | 4 (3.1%) | 0 | |

patients with five or more CTCs and those with fewer than five CTCs per 5 mL of peripheral blood at baseline before initiation of first-line chemotherapy (9.5 months *vs* 11.2 months, *P*=0.387). Nevertheless, the patients with at least one detectable EMT-like CTC-WBC clusters at baseline were characterized by significantly worse PFS, when compared to the patients with no EMT-like CTC-WBC clusters detected (7.0 months *vs* 10.7 months, *P*=0.023; **Figure 3A**), as well as the patients with at least one CTC detected per 5 ml of peripheral blood (7.0 months *vs* 11.2 months, *P*=0.019), and those with five or more epithelial-based CTCs (including E-CTCs and E/M-CTCs, parallel to isolation of CTCs by epithelial markers; 7.0 months *vs* 12.7 months, *P*=0.014; **Figure 3B**). Moreover, multivariate analysis showed the presence of EMT-like CTC-WBC clusters remained the only significantly independently predictive factors associated with PFS, with the adjusted HR of 2.415 (95% CI:1.046, 5.574, *P*=0.039, detail data of other clinical indexes in the multivariate analysis showed in **Supplementary Table 1**). However, the total CTC-WBC clusters and epithelial-based CTC-WBC clusters (including epithelial CTC-WBC clusters and biphenotypic epithelial/mesenchymal CTC-WBC clusters) were not correlated with patients' survival in the cohort, respectively (8.4 months *vs* 10.6 months, *P*=0.561, **Figure 3C**; 8.4 months *vs* 10.7 months, *P*=0.511, **Table 3**).

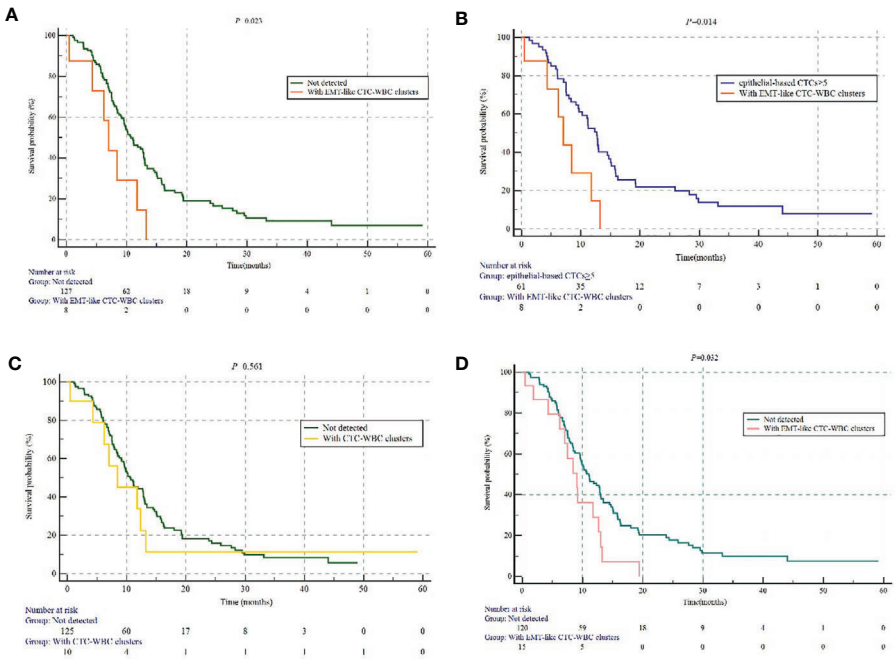


**FIGURE 3** | The prognostic value of different subtypes of CTC-WBC clusters. **(A)** Kaplan-Meier analysis-based estimation of PFS probabilities of comparing the patients with at least one EMT-like CTC-WBC clusters to those without. **(B)** Kaplan-Meier analysis-based estimation of PFS probabilities of comparing the patients with at least one EMT-like CTC-WBC clusters to those to five or more epithelial-based CTCs. **(C)** Kaplan-Meier analysis-based estimation of PFS probabilities of comparing the patients with at least one CTC-WBC clusters to those without. **(D)** Kaplan-Meier analysis-based estimation of PFS probabilities of comparing the patients with at least one EMT-like CTC-WBC clusters within 6 weeks after the start of chemotherapy to those without.

As for patients detected with EMT-like CTC-WBC clusters within 6 weeks after the initiation of chemotherapy (within the first follow-up visit), statistically significantly shorter PFS was observed when compared with the patients without (9.1 months *vs* 11.0 months, $P$=0.032, **Figure 3D**). However, no parallel results can be summarized from the patients with EMT-like CTC-WBC clusters detected after 6 weeks during the first-line treatment.

## DISCUSSIONS

Despite the prognostic value of CTCs has been discussed in many attempts, the clinical significance of the interaction between immune cells and CTCs during the process of Epithelial-mesenchymal-transition are largely uncharacterized. We optimized a filter-based method combined with an RNA *in situ* hybridization technique according to both the epithelial- and mesenchymal-markers, and investigated the predictive value of different phenotypes of CTC-WBC clusters as a prognostic biomarker. Our study revealed the prognostic value of CTC-WBC cluster underwent mesenchymal transformation in a prospective cohort composed of relatively homogeneous participants who were all HR-positive/HER2-negative metastatic breast cancer underwent first-line chemotherapy of docetaxel plus capecitabine, on which epithelial-to-mesenchymal transition was correlated with drug resistance (18, 19).

Several studies illuminated CTC clusters were more likely to be present in patients with high enumeration of CTCs (20, 21). Similar association was found between CTC-WBC clusters and single CTCs in our present study, that is, the frequency of presence of CTC-WBC clusters increased in patients with high enumeration of CTC count, especially in those with high numbers of M-CTCs and E/M-CTCs. Owing to the fact bone marrow was a common homing organ for metastatic tumor cells (22), the detection of EMT-like CTC-WBC clusters at baseline was associated with simultaneous bone metastases and lymph node metastases in the present study, suggesting the correlation between tumor cells and immune cells during tumor dissemination. Increased metastatic propensity of CTC clusters in mouse models and adverse prognosis in breast cancer patients with abundant CTC clusters, suggested the role of CTC clusters as critical mediators of cancer metastasis (23). However, the correlation between CTC clusters and immune cells during cancer dissemination was unclear.

CTCs in the peripheral blood left the immunosuppressive microenvironment of the primary tumor and might be vulnerable to immune surveillance, which required immune–escape mechanisms if they were to form metastases, including alterations in the expression of MHC molecules, NK-cell ligands, FAS, FAS ligand, and immune-checkpoint molecules, such as CD47 and programmed cell death 1 ligand 1 (PD–L1) (14). Analyses of the interaction between CTCs and immune cells may provide reference for real-time therapy stratification and prognosis prediction. In a

**TABLE 3 |** Detail description of Kaplan-Meier analysis-based estimation of Progression-free survival for different subtypes of CTCs and CTC-WBC clusters at baseline.

| | different subtypes of CTCs and CTC-WBC clusters at baseline | No. of patients | No. of patients progressed | Median Progression-free survival (months) | *P* value |
|---|---|---|---|---|---|
| Index 1 | Total CTC counts≥5 | 84 | 71 | 11.2 | 0.387 |
| | Total CTC counts<5 | 51 | 37 | 9.5 | |
| Index 2 | epithelial-based CTCs≥5 | 68 | 57 | 11.8 | 0.362 |
| | epithelial-based CTCs<5 | 67 | 51 | 9.6 | |
| Index 3 | EMT-like CTC-WBC clusters | 8 | 7 | 7.0 | 0.023 |
| | no EMT-like CTC-WBC clusters | 127 | 101 | 10.7 | |
| Index 4 | EMT-like CTC-WBC clusters | 8 | 7 | 7.0 | 0.019 |
| | Total CTC counts≥1 | 105 | 87 | 11.2 | |
| Index 5 | EMT-like CTC-WBC clusters | 8 | 7 | 7.0 | 0.013 |
| | Total CTC counts≥5 | 77 | 65 | 12.3 | |
| Index 6 | EMT-like CTC-WBC clusters | 8 | 7 | 7.0 | 0.014 |
| | epithelial-based CTCs≥5 | 61 | 51 | 12.7 | |
| Index 7 | CTC-WBC clusters | 10 | 8 | 8.4 | 0.561 |
| | no CTC-WBC clusters | 125 | 100 | 10.6 | |
| Index 8 | epithelial-based CTC-WBC clusters | 9 | 7 | 8.4 | 0.511 |
| | no epithelial-based CTC-WBC clusters | 126 | 101 | 10.7 | |

cohort of 106 patients with advanced non-small-cell lung cancer receiving first-line cisplatin-based chemotherapy, Ilié M et al. (24) found a trend for longer PFS and OS was observed in those with PD-L1 expression in CTCs or circulating WBCs. A recent study investigated the association between WBCs and CTCs during blood-borne dissemination by single-cell RNA sequencing and revealed that neutrophils directly interact with CTCs which drives cell cycle progression in circulation and accelerates the metastatic potential of CTCs (25). Szczerba BM et al. (25) observed that the patients of invasive breast cancer in whom at least one CTC-neutrophil cluster were detected per 7.5 ml of peripheral blood were correlated with significantly worse PFS compared to patients with five or more CTCs in 7.5 ml of peripheral blood. However, the study of Szczerba BM et al. (25) focused on the mechanism of interaction between CTCs and WBCs in breast cancer patients and mouse models, while the human samples involved in the study were very heterogeneous because of the recruitment from merely 34 patients with detectable CTCs of different tumor subtypes, TNM stage and diverse treatment. Thus, the statistical power of heterogenous group may be influenced by confounding factors. Moreover, the study did not disclose the clinical implications of CTC-WBC clusters during the progress of epithelial-mesenchymal transition.

However, when carcinoma cells are undergoing EMT process, reduced expression of epithelial markers and upregulated expression of mesenchymal markers on CTCs may result in false-negative findings in the cell surface epithelial marker-based CTC capturing methods (8). Therefore, the identification of additional upregulated mesenchymal markers on CTCs during EMT may lessen the leak detection of CTCs. Previous studies by Yu M et al. (11) and our research group (26) suggested that in patients with metastatic breast cancer, the fluctuation of proportion of CTCs underwent mesenchymal transformation may be more appropriate for predicting prognosis and evaluating therapeutic resistance compared to total CTC enumeration. Whereas, the clinical implications of EMT marker composition in CTC-WBC clusters were uncharacterized before.

In the present study, the patients with at least one EMT-like CTC-WBC clusters before treatment showed significantly shorter PFS compared to those with five or more epithelial-based CTCs. However, epithelial-based CTC-WBC clusters, including epithelial CTC-WBC clusters and biphenotypic epithelial/mesenchymal CTC-WBC clusters, did not reach the statistical power to predict the disease outcome in our study, owing to the lack of mesenchymal composition detected. In this prospective cohort composed of relatively homogeneous participants who were all HR-positive/HER2-negative breast cancer patients receiving first-line chemotherapy of docetaxel plus capecitabine, epithelial-to-mesenchymal transition was positively correlated with drug resistance (18, 19), which may lead to the failure in the prognostic prediction of simple total CTC count and epithelial-based CTC-WBC clusters. Even though the occurrence of EMT-like CTC-WBC clusters seemed to be lower than CTCs, it may be a more accurate marker to differentiate the special population who were more likely resistant to the current treatment, for whom the combination of targeting residual EMT-driven cancer cells in addition to conventional therapy may decrease metastasis formation and drug resistance (27). Meanwhile, blocking the process of epithelial-to-mesenchymal transition and reducing EMT-like CTC-WBC clusters may provide a therapeutic target to control metastatic spread and increase the efficacy of anticancer treatments. To our knowledge, the study is the first attempt to characterize the prognostic value of EMT-like CTC-WBC clusters in a homogeneous cohort, which provide evidence for clinical transformation. However, limited sample size influenced the statistical power to draw firm conclusions, and further large-scale external validation containing data of overall survival is warranted. Besides that, the expression of some EMT-related genes, such as ESRP1 and RBFOX2 (28), which correlated with cancer progression, may also be explored in the EMT-like CTC-WBC clusters in further study to enrich the prognostic model.

In summary, our investigation suggested that the presence of EMT-like CTC-WBC clusters before treatment was associated with significantly poorer PFS in HR-positive/HER2-negative metastatic breast cancer patients receiving first-line chemotherapy of docetaxel plus capecitabine, raising a concern on the optimized choice of first-line treatment for these patients. The results suggested that taking both the cancer cells and immune cells into consideration in the liquid-microenvironment biopsy, EMT-like CTC-WBC clusters may serve as a potential biomarker for prognosis prediction and a rationale target for individualized therapy in HR-positive/HER2-negative metastatic breast cancer patients.

## DATA AVAILABILITY STATEMENT

The raw data supporting the conclusions of this article will be made available by the authors, without undue reservation.

## ETHICS STATEMENT

The studies involving human participants were reviewed and approved by the Independent Ethics Committee of Cancer Hospital, Chinese Academy of Medical Sciences and National GCP Center for Anticancer Drugs. The patients/participants provided their written informed consent to participate in this study. Written informed consent was obtained from the individual(s) for the publication of any potentially identifiable images or data included in this article.

## AUTHOR CONTRIBUTIONS

FM, BX, and HQ conceived the study. XG, CL, YL, JW, ZY, BL, HC, and JX collected and analyzed the data. XG wrote the whole manuscript. All authors contributed to the article and approved the submitted version.

## FUNDING

The study was supported with National Nature Science Foundation of China (81874122), CAMS Initiative for Innovative Medicine (2017-I2M-3-004), PUMC Innovation Fund for Doctors (2018-1002-02-24) and China Postdoctoral Science Foundation(2020M680455).

## ACKNOWLEDGMENTS

We thank all the physicians and patients involved in the study for their contributions.

## SUPPLEMENTARY MATERIAL

The Supplementary Material for this article can be found online at: https://www.frontiersin.org/articles/10.3389/fonc.2021.602222/full#supplementary-material

**Supplementary Table 1 |** Multivariate analysis of clinicopathological characteristics and the detection of CTCs and EMT-like CTC-WBC clusters for predicting the progression-free survival in HR-positive/HER2-negative metastatic breast cancer patients.

## REFERENCES

1. Rack B, Schindlbeck C, Jückstock J, Andergassen U, Hepp P, Zwingers T, et al. Circulating Tumor Cells Predict Survival in Early Average-to-High Risk Breast Cancer Patients. *J Natl Cancer Inst* (2014) 106(5):dju066. doi: 10.1093/jnci/dju066
2. Cristofanilli M, Budd GT, Ellis MJ, Stopeck A, Matera J, Miller MC, et al. Circulating Tumor Cells, Disease Progression, and Survival in Metastatic Breast Cancer. *N Engl J Med* (2004) 351:781–91. doi: 10.1056/NEJMoa040766
3. Bidard FC, Peeters DJ, Fehm T, Nolé F, Gisbert-Criado R, Mavroudis D, et al. Clinical Validity of Circulating Tumour Cells in Patients With Metastatic Breast Cancer: A Pooled Analysis of Individual Patient Data. *Lancet Oncol* (2014) 15:406–14. doi: 10.1016/S1470-2045(14)70069-5
4. Maheswaran S, Sequist LV, Nagrath S, Ulkus L, Brannigan B, Collura CV, et al. Detection of Mutations in EGFR in Circulating Lung-Cancer Cells. *N Engl J Med* (2008) 359:366–77. doi: 10.1056/NEJMoa0800668
5. Cohen SJ, Punt CJ, Iannotti N, Saidman BH, Sabbath KD, Gabrail NY, et al. Relationship of Circulating Tumor Cells to Tumor Response, Progression-Free Survival, and Overall Survival in Patients With Metastatic Colorectal Cancer. *J Clin Oncol* (2008) 26:3213–21. doi: 10.1200/JCO.2007.15.8923
6. de Bono JS, Scher HI, Montgomery RB, Parker C, Miller MC, Tissing H, et al. Circulating Tumor Cells Predict Survival Benefit From Treatment in Metastatic Castration-Resistant Prostate Cancer. *Clin Cancer Res* (2008) 14:6302–9. doi: 10.1158/1078-0432.CCR-08-0872
7. Amin MB, Edge SB, Greene FL, Byrd DR, Brookland RK, Washington MK, et al. *AJCC Cancer Staging Manual. 8th ed.* New York: Springer (2016).
8. Alix-Panabieres C, Pantel K. Challenges in Circulating Tumour Cell Research. *Nat Rev Cancer* (2014) 14:623–31. doi: 10.1038/nrc3820
9. Hamilton G, Rath B. Mesenchymal-Epithelial Transition and Circulating Tumor Cells in Small Cell Lung Cancer. *Adv Exp Med Biol* (2017) 994:229–45. doi: 10.1007/978-3-319-55947-6_12
10. Lindsay CR, Faugeroux V, Michiels S, Pailler E, Facchinetti F, Ou D, et al. A Prospective Examination of Circulating Tumor Cell Profiles in Non-Small-Cell Lung Cancer Molecular Subgroups. *Ann Oncol* (2017) 28:1523–31. doi: 10.1093/annonc/mdx156
11. Yu M, Bardia A, Wittner BS, Stott SL, Smas ME, Ting DT, et al. Circulating Breast Tumor Cells Exhibit Dynamic Changes in Epithelial and Mesenchymal Composition. *Science* (2013) 339:580–4. doi: 10.1126/science.1228522
12. Bulfoni M, Gerratana L, Del Ben F, Marzinotto S, Sorrentino M, Turetta M, et al. In Patients With Metastatic Breast Cancer the Identification of Circulating Tumor Cells in Epithelial-to-Mesenchymal Transition Is Associated With a Poor Prognosis. *Breast Cancer Res* (2016) 18:30. doi: 10.1186/s13058-016-0687-3
13. Satelli A, Mitra A, Brownlee Z, Xia X, Bellister S, Overman MJ, et al. Epithelial-Mesenchymal Transitioned Circulating Tumor Cells Capture for Detecting Tumor Progression. *Clin Cancer Res* (2015) 21:899–906. doi: 10.1158/1078-0432.CCR-14-0894
14. Mohme M, Riethdorf S, Pantel K. Circulating and Disseminated Tumour Cells - Mechanisms of Immune Surveillance and Escape. *Nat Rev Clin Oncol* (2017) 14:155–67. doi: 10.1038/nrclinonc.2016.144
15. Goodman CR, Seagle BL, Friedl TWP, Rack B, Lato K, Fink V, et al. Association of Circulating Tumor Cell Status With Benefit of Radiotherapy and Survival in Early-Stage Breast Cancer. *JAMA Oncol* (2018) 4:e180163. doi: 10.1001/jamaoncol.2018.0163
16. Wu S, Liu S, Liu Z, Huang J, Pu X, Li J, et al. Classification of Circulating Tumor Cells by Epithelial-Mesenchymal Transition Markers. *PloS One* (2015) 10:e0123976. doi: 10.1371/journal.pone.0123976
17. Qi LN, Xiang BD, Wu FX, Ye JZ, Zhong JH, Wang YY, et al. Circulating Tumor Cells Undergoing Emt Provide a Metric for Diagnosis and Prognosis of Patients With Hepatocellular Carcinoma. *Cancer Res* (2018) 78:4731–44. doi: 10.1158/0008-5472.CAN-17-2459
18. Prieto-Vila M, Usuba W, Takahashi RU, Shimomura I, Sasaki H, Ochiya T, et al. Single-Cell Analysis Reveals a Preexisting Drug-Resistant Subpopulation in the Luminal Breast Cancer Subtype. *Cancer Res* (2019) 79:4412–25. doi: 10.1158/0008-5472.CAN-19-0122
19. Toden S, Okugawa Y, Jascur T, Wodarz D, Komarova NL, Buhrmann C, et al. Curcumin Mediates Chemosensitization to 5-Fluorouracil Through miRNA-induced Suppression of Epithelial-to-Mesenchymal Transition in Chemoresistant Colorectal Cancer. *Carcinogenesis* (2015) 36:355–67. doi: 10.1093/carcin/bgv006
20. Paoletti C, Miao J, Dolce EM, Darga EP, Repollet MI, Doyle GV, et al. Circulating Tumor Cell Clusters in Patients With Metastatic Breast Cancer: A

SWOG S0500 Translational Medicine Study. *Clin Cancer Res* (2019) 25 (20):6089–97. doi: 10.1158/1078-0432.CCR-19-0208
21. Larsson AM, Jansson S, Bendahl PO, Levin Tykjaer Jörgensen C, Loman N, Graffman C, et al. Longitudinal Enumeration and Cluster Evaluation of Circulating Tumor Cells Improve Prognostication for Patients With Newly Diagnosed Metastatic Breast Cancer in a Prospective Observational Trial. *Breast Cancer Res* (2018) 20(1):48. doi: 10.1186/s13058-018-0976-0
22. Alix-Panabières C, Riethdorf S, Pantel K. Circulating Tumor Cells and Bone Marrow Micrometastasis. *Clin Cancer Res* (2008) 14:5013–21. doi: 10.1158/1078-0432.CCR-07-5125
23. Aceto N, Bardia A, Miyamoto DT, Donaldson MC, Wittner BS, Spencer JA, et al. Circulating Tumor Cell Clusters Are Oligoclonal Precursors of Breast Cancer Metastasis. *Cell* (2014) 158:1110–22. doi: 10.1016/j.cell.2014.07.013
24. Ilié M, Szafer-Glusman E, Hofman V, Chamorey E, Lalvée S, Selva E, et al. Detection of PD-L1 in Circulating Tumor Cells and White Blood Cells From Patients With Advanced Non-Small-Cell Lung Cancer. *Ann Oncol* (2018) 29:193–9. doi: 10.1093/annonc/mdx636
25. Szczerba BM, Castro-Giner F, Vetter M, Krol I, Gkountela S, Landin J, et al. Neutrophils Escort Circulating Tumour Cells to Enable Cell Cycle Progression. *Nature* (2019) 566:553–7. doi: 10.1038/s41586-019-0915-y
26. Guan X, Ma F, Li C, Wu S, Hu S, Huang J, et al. The Prognostic and Therapeutic Implications of Circulating Tumor Cell Phenotype Detection Based on Epithelial-Mesenchymal Transition Markers in the First-Line Chemotherapy of HER2-Negative Metastatic Breast Cancer. *Cancer Commun* (2019) 39(1):1. doi: 10.1186/s40880-018-0346-4
27. Yeung KT, Yang J. Epithelial-Mesenchymal Transition in Tumor Metastasis. *Mol Oncol* (2017) 11:28–39. doi: 10.1002/1878-0261.12017
28. Fici P, Gallerani G, Morel AP, Mercatali L, Ibrahim T, Scarpi E, et al. Splicing Factor Ratio as an Index of Epithelial-Mesenchymal Transition and Tumor Aggressiveness in Breast Cancer. *Oncotarget* (2017) 8(2):2423–36. doi: 10.18632/oncotarget.13682

**Conflict of Interest:** JX was employed by SurExam Bio-Tech.

The remaining authors declare that the research was conducted in the absence of any commercial or financial relationships that could be construed as a potential conflict of interest.

frontiers in Oncology

ORIGINAL RESEARCH
published: 15 June 2021
doi: 10.3389/fonc.2021.682021

# Transcriptome Analysis Reveals MFGE8-HAPLN3 Fusion as a Novel Biomarker in Triple-Negative Breast Cancer

*Meng-Yuan Wang*[*†], *Man Huang*[†], *Chao-Yi Wang*[†], *Xiao-Ying Tang*, *Jian-Gen Wang*, *Yong-De Yang*, *Xin Xiong* and *Chao-Wei Gao*

*Department of Breast Surgery, Chongqing University Three Gorges Hospital, Chongqing, China*

**Background:** Triple-negative breast cancer (TNBC) is a highly aggressive cancer with poor prognosis. The lack of effective targeted therapies for TNBC remains a profound clinical challenge. Fusion transcripts play critical roles in carcinogenesis and serve as valuable diagnostic and therapeutic targets in cancer. The present study aimed to identify novel fusion transcripts in TNBC.

**Methods:** We analyzed the RNA sequencing data of 360 TNBC samples to identify and filter fusion candidates through SOAPfuse and ChimeraScan analysis. The characteristics, including recurrence, fusion type, chromosomal localization, TNBC subgroup distribution, and clinicopathological correlations, were analyzed in all candidates. Furthermore, we selected the promising fusion transcript and predicted its fusion type and protein coding capacity.

**Results:** Using the RNA sequencing data, we identified 189 fusion transcripts in TNBC, among which 22 were recurrent fusions. Compared to para-tumor tissues, TNBC tumor tissues accumulated more fusion events, especially in high-grade tumors. Interestingly, these events were enriched at specific chromosomal loci, and the distribution pattern varied in different TNBC subtypes. The vast majority of fusion partners were discovered on chromosomes 1p, 11q, 19p, and 19q. Besides, fusion events mainly clustered on chromosome 11 in the immunomodulatory subtype and chromosome 19 in the luminal androgen receptor subtype of TNBC. Considering the tumor specificity and frameshift mutation, we selected *MFGE8-HAPLN3* as a novel biomarker and further validated it in TNBC samples using PCR and Sanger sequencing. Further, we successfully identified three types of *MFGE8-HAPLN3* (E6-E2, E5-E3, and E6-E3) and predicted the ORF of E6-E2, which could encode a protein of 712 amino acids, suggesting its critical role in TNBC.

**Conclusions:** Improved bioinformatic stratification and comprehensive analysis identified the fusion transcript *MFGE8-HAPLN3* as a novel biomarker with promising clinical application in the future.

**Keywords: triple-negative breast cancer, *MFGE8-HAPLN3*, biomarker, target, precision treatment, fusion**

OPEN ACCESS

***Edited by:***
*Yi-Zhou Jiang,*
*Fudan University, China*

***Reviewed by:***
*Gen-Hong Di,*
*Fudan University, China*
*Xiang Cui,*
*First People's Hospital of Shangqiu, China*

***Correspondence:**
*Meng-Yuan Wang*
*wmyuan8899@163.com*

[†]*These authors have contributed equally to this work*

***Specialty section:***
*This article was submitted to Breast Cancer, a section of the journal Frontiers in Oncology*

***Received:*** *17 March 2021*
***Accepted:*** *24 May 2021*
***Published:*** *15 June 2021*

***Citation:***
*Wang M-Y, Huang M, Wang C-Y, Tang X-Y, Wang J-G, Yang Y-D, Xiong X and Gao C-W (2021) Transcriptome Analysis Reveals MFGE8-HAPLN3 Fusion as a Novel Biomarker in Triple-Negative Breast Cancer. Front. Oncol. 11:682021. doi: 10.3389/fonc.2021.682021*

## INTRODUCTION

Triple-negative breast cancer (TNBC) lacks the expression of estrogen receptor (ER), progesterone receptor (PR), and human epidermal growth factor receptor 2 (HER2) and accounts for 10% to 20% of the newly diagnosed breast cancer cases (1, 2). While recognized as the most aggressive breast cancer subtype, women with TNBC have larger tumors, a higher rate of node positivity, and an increased likelihood of distant recurrence (3). Chemotherapy is yet the primary mode of treatment for early and advanced disease owing to the lack of molecular targets for therapy. Although several targeted therapies are showing potent efficacy, patients with TNBC have a worse prognosis compared to those with other breast cancer subtypes (4–6).

Fusion genes, formed by chromosomal rearrangements that juxtapose two different genes, can lead to abnormal activation of one or both genes and drive tumorigenesis (7). Based on the development of sequencing technologies and bioinformatics approaches, a number of fusion genes have been revealed over the past few decades (8, 9). Recently, fusion genes involving *ZNF384* have been identified in B-cell precursor acute lymphoblastic leukemia; eight fusion partners have been reported for the *ZNF384* gene. Moreover, the clinical features of patients depend on the functional defect of the fusion partner gene of *ZNF384* (10). Fusion transcripts, chimeric RNAs encoded by fusion genes or generated through subsequent cis-splicing and trans-splicing of mRNA in the absence of DNA rearrangements, serve as frequent drivers in a wide range of tumor types (11–13). Many fusion transcripts preferentially present in tumors compared to normal tissues, and contribute to tumor progression by enhancing cell proliferation and invasion (14). Significantly, the discovery that cancers harbor specific fusion genes or transcripts has enhanced the development of novel diagnostic and therapeutic strategies. For instance, tyrosine kinase inhibitors, such as imatinib, have been highly effective in the treatment of cancers harboring kinase fusions in leukemia and other cancers (15, 16).

Previous studies demonstrated that fusion candidates are involved in the tumorigenesis and progression of breast cancer. However, recurrent gene fusions have only been identified in rare subtypes of breast cancer. For example, some secretory carcinomas of the breast are driven by an *ETV6-NTRK3* fusion resulted from t(12;15)(p13;q25) chromosomal translocation (17). Similarly, adenoid cystic carcinomas of the breast are largely driven by a t(6;9)(q22-23;p23-24) translocation that forms a *MYB-NFIB* gene fusion (18). In addition to fusion genes, several fusion transcripts specifically present in breast cancer have been identified, including *CRTC1-MAML2*, *SCNN1A-TNFRSF1A*, and *CTSD-IFITM10* (19–21). Interestingly, some of the recurrent fusion transcripts encode membrane proteins, raising the possibility that they are breast cancer-specific cell surface markers and could be targeted by antibody drug conjugates (19). However, only little is known about fusion genes or transcripts in TNBC.

In the present study, we comprehensively revealed the landscape of fusion transcripts in TNBC. We also investigated the characteristics, including recurrence, fusion type, clinical relevance, and subgroup distribution. We discovered a novel fusion transcript *MFGE8-HAPLN3* in TNBC, highlighting the potential implications of fusion transcripts in cancer development and response to therapy.

## MATERIALS AND METHODS

### Patient Cohorts

RNA-seq data used in the current study were downloaded from the Gene Expression Omnibus (GEO) (GSE118527) (https://www.ncbi.nlm.nih.gov/geo/) and The National Omics Data Encyclopedia (NODE) (OEP000155) (http://www.biosino.org/node). The RNA-seq data of 360 tumor tissues and 88 adjacent normal breast tissues were obtained. In addition, the corresponding clinicopathological characteristics, including age, histological type of the tumor, tumor size, lymph node status, histological grade, clinical stage and ER, PR, HER2, and Ki67 status, were collected (5). Our study was approved by the independent Ethics Committee/Institutional Review Board of Chongqing University Three Gorges Hospital.

### Identification of Fusion Transcripts in TNBC

RNA sequencing data were analyzed using ChimeraScan (22) and SOAPfuse (23) algorithms, which identify gene fusion candidates by detecting read pairs discordantly mapped to two different genes. The RNA-seq data of 448 samples (360 tumor samples and 88 adjacent normal breast tissues) were analyzed in random order. Fusion candidate that could be detected in at least one sample by two different algorithms was defined as double-positive fusion transcript (DPFT). We compared the frequency of fusion between tumor tissues and normal breast tissues and also described the characteristics, such as recurrence, fusion type, protein-coding capacity, chromosomal localization, and TNBC subgroup distribution, in all candidates. Subsequently, patients with DPFT were divided into low-fusion transcripts (low FTs) and high-fusion transcripts (high FTs) groups to evaluate the correlation between the expression level of fusion candidates and the clinicopathological features. Patients with fusion transcripts <4 were grouped as low FTs, while those with fusion transcripts ≥ 4 were grouped as high FTs.

### Promising Novel Fusion Screening

We selected promising fusion transcripts according to the following conditions: (1) recurrent fusion transcripts; (2) fusion transcripts with different functions formed by promoter swapping in the non-coding regions or frameshift in the coding regions; (3) fusion transcripts whose partner genes are associated with tumor; (4) fusion transcripts overexpressed in tumor tissue but unexpressed or expressed in low amounts in the adjacent normal breast tissue. We further predicted the open reading frame (ORF) and protein-coding capacity of the fusion transcripts according to the nucleotide sequence.

### Statistical Analyses

The data distribution was characterized by frequency tabulation and summary statistics. The data were examined for normality

using the Shapiro-Wilk test. The continuous variables with normal distribution were assessed using the *t*-test or one-way analyses of variance (ANOVA), while the variables that did not meet the normal distribution were analyzed using the Mann-Whitney Wilcoxon test or Kruskal-Wallis test; Pearson's Chi-square test or Fisher's exact test was used to compare the categorical variables. In addition, the correlations were analyzed using the Pearson or Spearman test according to the normality of the distribution. All tests were two-sided, and P<0.05 indicated statistical significance. All statistical analyses were performed using SPSS 25.0 or R Studio (version 1.1.463, www.R-project.org).

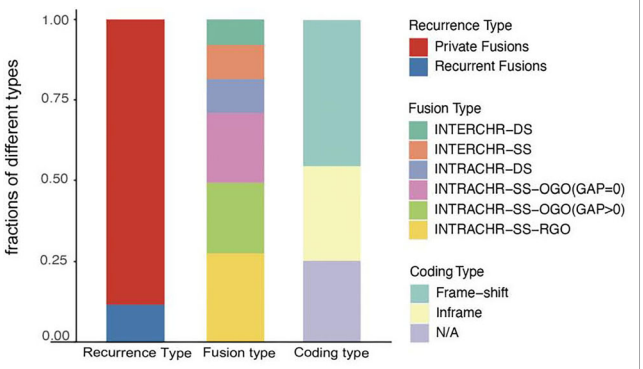


**FIGURE 2** | Characterization of fusion transcripts detected in TNBC. N/A, noncoding.

# RESULTS

## Fusion Transcripts Screening

To detect fusion transcripts, RNA-seq data from a set of 448 frozen samples (360 tumor tissues and 88 adjacent normal tissues) were analyzed (**Figure 1A**). A total of 203 fusion candidates, confirmed to be DPFT, were identified from 123 samples (66 tumor samples and 57 adjacent normal tissues) using both ChimeraScan and SOAPfuse algorithms (**Figure 1B**). Among these, 166 fusion transcripts were tumor-specific, while only 23 fusion transcripts were present in both tumor tissues and adjacent normal tissues (**Figure 1B** and **Supplementary Table 1**). Next, we investigated the frequency of fusion events in each sample. Compared to the adjacent normal tissues, more candidates were detected in TNBC tissues (mean fusions per sample: 4.106 *vs.* 1.807, P<0.05, **Supplementary Table 2**). These findings suggested that TNBC tissues are more likely to harbor fusion events compared to adjacent normal tissues.

## Characteristics of Selected Fusion Transcripts

Next, we analyzed the characteristics, including recurrence, fusion type, and protein-coding capacity of 189 candidates (**Figure 2**) and found that 11.6% (22/189) of all candidates were present in two or more tumor tissues. In order to elucidate the mechanism, the fusion type was further analyzed using SOAPfuse algorithm. According to the relative locations of fusion partner genes, five types of fusion transcripts (INTERCHR-DS, INTERCHR-SS, INTRACHR-DS, INTRACHR-SS-OGO, INTRACHR-SS-RGO) were identified. These transcripts involving sequences from the same chromosomes constituted 81.5% of the total, thereby indicating that the majority of the fusion events occur at the transcriptional level. We also inferred the protein-coding capacity based on the junction sequence. Among these, 141 candidates (including 86 frameshift and 55 in-frame variants) could encode chimeric proteins, suggesting that the majority of the fusion transcripts have the potential to encode functional proteins.

## Clinical Association of Fusion Transcript Frequency in TNBC

To explore the association between the frequency of fusion events and clinicopathological features, we divided 66 patients with TNBC into high and low FTs groups according to the number of fusion transcripts. The difference in the clinicopathological factors, including age, histological type of the tumor, Ki67 status, and clinical stage, was not statistically significant between two groups (**Figure 3**). Notably, an apparent discrepancy in the

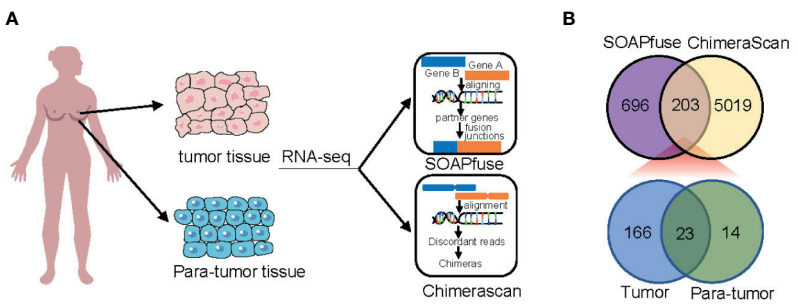


**FIGURE 1** | Identification of fusion transcripts in TNBC. **(A)** Flowchart of fusion transcripts screening. **(B)** Venn diagram summarizing the fusion transcripts detected using ChimeraScan and SOAPfuse algorithms.

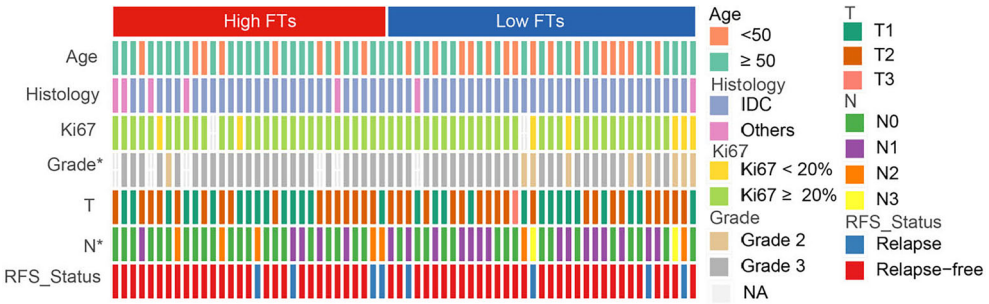


**FIGURE 3** | Association between frequency of fusion events and clinicopathological features. FTs, fusion transcripts; high FTs, patients whose fusion transcripts equal to or greater than 4; low FTs, patients whose fusion transcripts less than 4; IDC, infiltrated ductal carcinoma; NA, not available. *$p < 0.05$.

frequency of fusion events in different pathological grades (P<0.05) indicated that fusion events preferentially expressed in high-grade tumors.

## Subtype-Specific Chromosome Distribution of Fusion Transcripts

Furthermore, we found that fusion transcripts were not randomly distributed on chromosomes (**Figure 4**). A disproportionately large number of fusion partner genes were detected in some specific chromosomes (hot spot region, chromosome arms 1p, 2p, 3q, 9p, 11q, 17q, 19p and 19q). Conversely, only a few fusion partner genes appeared in the cold spot region (chromosomes 10, 13, 21, and 22).

Jiang and colleagues preciously presented a multiomics profiling of 465 Chinese patients with TNBCs, thus providing a large data set of comprehensively profiled TNBCs (5). Herein, they classified the

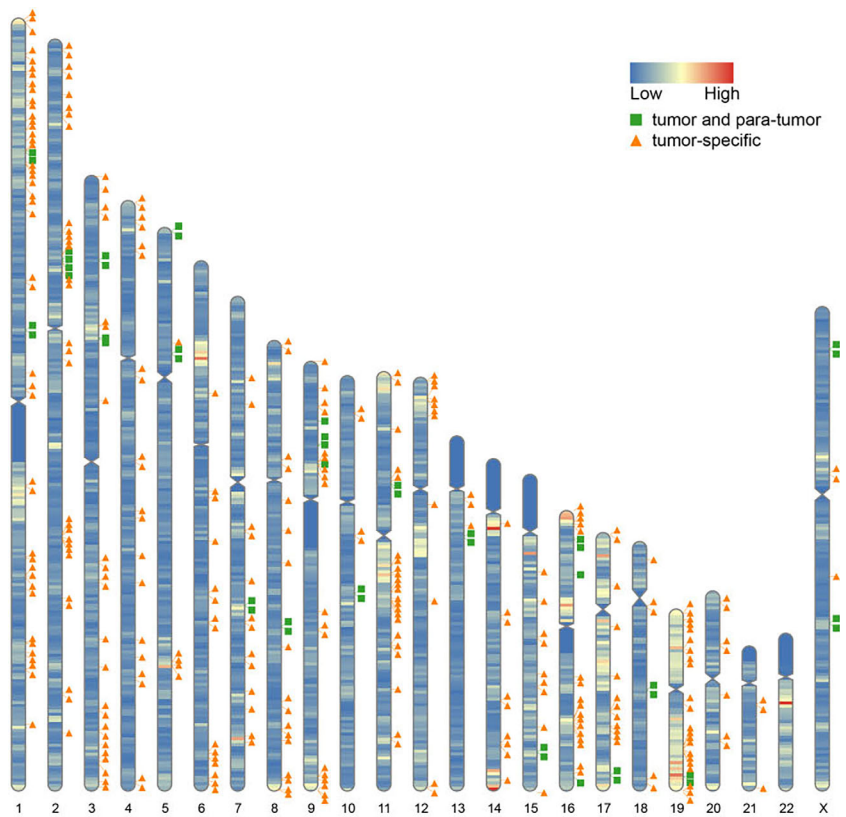


**FIGURE 4** | Chromosomal distribution of fusion partner genes. Green box indicates fusion partner genes in both tumor and para-tumor tissues; Orange triangle indicates fusion partner genes especially in tumor tissues.

TNBCs into four mRNA subtypes with distinct molecular features: 1) luminal androgen receptor (LAR), 2) immunomodulatory (IM), 3) basal-like immune-suppressed (BLIS), and 4) mesenchymal-like (MES). Then, the chromosome distribution of fusion transcripts across different molecular subtypes was characterized (**Figure 5**). The fusion accumulation at chromosome 11 in IM subtype and chromosomes 17 and 19 in LAR subtype suggested a subtype specificity of fusion candidates. Interestingly, our analysis indicated that fusion events were enriched in chromosomes 7, 9, and 15 in MES subtype and were rare in chromosomes 2 and 3. In addition, the frequency of fusion transcripts was significantly different between subtypes (**Supplementary Table 3**). BLIS subtype contained a vast majority of candidates detected in TNBC samples. Conversely, fusion transcripts were rare in MES subtype. Overall, our analysis demonstrated that fusion transcripts in specific chromosomes might exert isoform-specific roles in different molecular subtypes of TNBC.

## *MFGE8-HAPLN3* Fusion in TNBC

To further explore biomarkers of clinical relevance, we selected fusion transcripts from 189 observed fusion candidates, according to the criteria described above. Finally, *MFGE8-HAPLN3* (16.7% in TNBC tumor tissues *vs.* 3.5% in adjacent normal breast tissues) was screened out. Milk fat globule-EGF factor 8 protein (*MFGE8*) and Hyaluronan And Proteoglycan Link Protein 3 (*HAPLN3*) were both located on the long arm of chromosome 15 (15q26.1, **Figure 6A**), suggesting that this fusion could be attributed to transcriptional read-through.

According to PCR and Sanger sequencing, three types of *MFGE8-HAPLN3* fusions, including E6-E2 (most frequently, **Figure 6B**), E5-E3, and E6-E3, were identified. Further, we successfully predicted an ORF of *MFGE8-HAPLN3* (E6-E2) that could encode a protein of 712 amino acids. Collectively, these findings suggested that *MFGE8-HAPLN3* fusion exists in TNBC samples and plays a critical role in TNBC. The predicted ORF of *MFGE8-HAPLN3* and its function *in vivo* have yet to be unambiguously characterized and need to be verified in further exploration.

# DISCUSSION

Gene fusions/transcripts are important driver events in neoplasia and serve as valuable diagnostic biomarkers and therapeutic

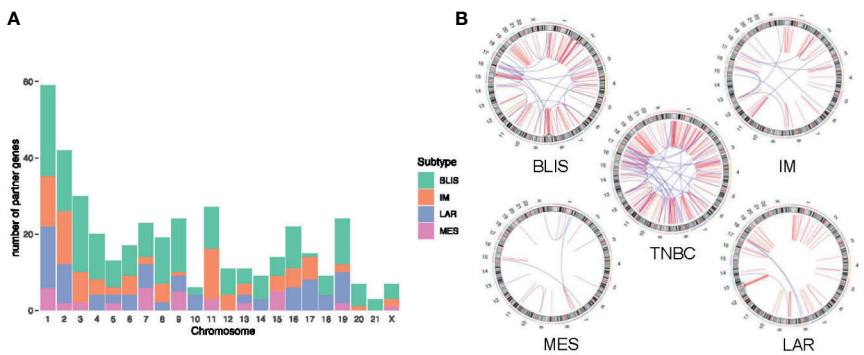


**FIGURE 5** | Distribution of fusion partner genes in different molecular subtypes of TNBC. **(A)** Frequency of fusion partner genes in each chromosome. **(B)** Relative locations of fusion partner genes. Intrachromosomal fusions are shown in red, and interchromosomal fusions are shown in blue. TNBC, triple-negative breast cancer; BLIS, basal-like immune-suppressed; IM, immunomodulatory; LAR, luminal androgen receptor; MES, mesenchymal-like.

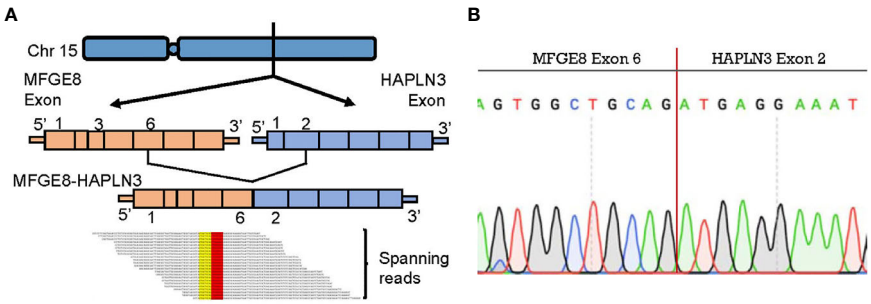


**FIGURE 6** | *MFGE8-HAPLN3* fusion in TNBC. **(A)** Schematic representation of the *MFGE8-HAPLN3* fusion transcript identified in TNBC. **(B)** PCR and Sanger sequencing verified the *MFGE8-HAPLN3* fusion.

targets in cancer. Aberrant fusions have been widely described in multiple tumor types, such as non-small-cell lung cancer (24) and lymphoid neoplasms (25). The current study comprehensively explored the fusion transcripts in TNBC. We discovered 189 novel fusion transcripts and identified *MFGE8-HAPLN3* as a potential biomarker in TNBC.

As reported previously, tumor samples displayed more fusions than normal tissues. In accordance with these studies, our analysis revealed that TNBC tumor tissues accumulated a significantly higher number of fusion events than adjacent normal breast tissues. Typically, tumor characterized by a high frequency of fusion has been implicated in chromosomal instability (26, 27). Structural chromosome rearrangements effectuate the exchange of DNA sequences, inducing cancer cell progression (28). For example, Mitani et al. contended that *MYB-NFIB* gene fusion promoted the aggressive behavior in adenoid cystic carcinoma (29). In addition to chromosomal instability, aberrant regulation of the transcriptional process may also result in fusion transcripts. Herein, we observed a lot of fusion events involving genes on the same chromosome, suggesting that abundant fusions occur at the transcriptional level. An increasing number of studies supported that the disturbance of transcriptional regulation in transcription initiation, alternative splicing, or post-transcriptional modifications also can generate transcriptional read-through and contribute to tumor development (30–32). It is noteworthy that RNA processing of transcripts encoded by fusion genes makes splicing process significantly more complex. Regulatory sites nearby and surrounding the fusion junction sites are essential to the compatibility between sequences and spliceosome, which is necessary to canonical and alternative splicing (33). However, we could not differentiate between the transcriptome-level and genome-level changes. Fusion proteins that encoded by either fusion genes or fusion transcripts play nearly identical biological roles. It will be interesting to further explore the mechanism generating these chimeras.

To better understand the mechanism of novel fusion transcripts, we explored the fusion partner genes' distribution and found they were non-randomly distributed on the chromosome. A majority of partners were enriched on chromosomes 1p, 2p, 9p, 11q, 19p, and 19q. Chromosome 19 has been reported as a fusion "hotspot" for TNBC. All fusion partners in TNBC mapped to clusters were located in the vicinity of 19p13 or 19q13 (34). In addition, we observed a discrepancy in chromosomal distribution between different TNBC subtypes. Fusion events clustered on chromosome 11 in the IM subtype. Differently, fusions are mainly located on chromosomes 17 and 19 in the LAR subtype. These findings demonstrated a strong functional association between the formation of fusion events and the TNBC subtypes.

Furthermore, we demonstrated the presence of a recurrent fusion transcript *MFGE8-HAPLN3*. *MFGE8*, and *HAPLN3* were neighboring genes on the same strand, suggesting that the fusion may be largely attributed to transcriptional read-through. Next, we successfully predicted its ORF and corresponding chimeric proteins. MFGE8 is a kind of soluble glycoprotein found in vertebrates and was initially discovered as a critical component of the milk fat globule. MFGE8 has been studied as a key regulator of various biological functions, including phagocytic removal of apoptotic cells in many tissues, the maintenance of intestinal epithelial homeostasis, and the promotion of mucosal healing (35). Recent studies have clarified the effect of MFGE8 on cell survival, adhesion, and migration in a wide spectrum of tumor types, such as ovarian cancer (36) and hepatocellular carcinoma (37). Consistent with these results, MFGE8 have been found to play a critical role in breast cancer pathobiology and clinical prognosis (38, 39). Furthermore, MFGE8 knockdown significantly inhibited both migration and proliferation of tumor cells, attenuating their tumorigenic properties (40). As for HAPLN3, it has been identified as a novel diagnostic and prognostic biomarker for prostate cancer (41). Besides, the expression of HAPLN3 was shown to be significantly higher in breast cancer tissues compared to the normal breast tissues. It was associated with the metabolism dysregulation, mobility, and migration of cancer cells in TNBC (42, 43). These imply the value of *MFGE8-HAPLN3* in guiding diagnosis and treatment choices in cancer.

Inevitably, there are some limitations in our study. First, we could not distinguish fusions occurring at the transcriptome level from those at the genome level by algorithms we used. Future studies are required for a comprehensive understanding of the selected fusions. Second, due to the small sample size, it is difficult to make any rigorous conclusions regarding the subtype-specific distribution of fusion transcripts. Studies are needed to point out the frequency of *MFGE8-HAPLN3* in different subtypes to distinguish patients with clinical benefit from targeted therapy in the future. Furthermore, the predicted ORF of *MFGE8-HAPLN3* and its pathologic and therapeutic role in TNBC requires further experimental validation.

In conclusion, our large-scale analysis revealed a number of fusion transcripts in TNBC for the first time. Remarkably, *MFGE8-HAPLN3* could be a candidate biomarker and potential therapeutic target in TNBC. Further investigations are required to elucidate the underlying mechanisms and their biological functions.

## DATA AVAILABILITY STATEMENT

The data sets presented in this study can be found in online repositories. The names of the repository/repositories and accession number(s) can be found in the article/**Supplementary Material**.

## ETHICS STATEMENT

Our study was approved by the independent ethics committee/ institutional review board of Chongqing University Three Gorges Hospital. Written informed consent for participation was not required for this study in accordance with the national legislation and the institutional requirements.

## AUTHOR CONTRIBUTIONS

M-YW: conception of the work, data collection, data analysis and interpretation, drafting the article, critical revision of the article, and final approval of the version to be published. MH and C-YW: conception of the work, data collection, critical revision of the article, and final approval of the version to be published. X-YT, J-GW, Y-DY, XX, and C-WG: data collection, critical revision of the article, and final approval of the version to be published. All authors contributed to the article and approved the submitted version.

## FUNDING

This work was supported by the Natural Science Foundation Project of Chongqing, China (cstc2016jcyjA0338).

## SUPPLEMENTARY MATERIAL

The Supplementary Material for this article can be found online at: https://www.frontiersin.org/articles/10.3389/fonc.2021.682021/full#supplementary-material

## REFERENCES


1. Foulkes WD, Smith IE, Reis-Filho JS. Triple-Negative Breast Cancer. *New Engl J Med* (2010) 363(20):1938–48. doi: 10.1056/NEJMra1001389
2. Sharma P. Biology and Management of Patients With Triple-Negative Breast Cancer. *Oncol* (2016) 21(9):1050–62. doi: 10.1634/theoncologist.2016-0067
3. Dent R, Trudeau M, Pritchard KI, Hanna WM, Kahn HK, Sawka CA, et al. Triple-Negative Breast Cancer: Clinical Features and Patterns of Recurrence. *Clin Cancer Res* (2007) 13(15 Pt 1):4429–34. doi: 10.1158/1078-0432.Ccr-06-3045
4. Bianchini G, Balko JM, Mayer IA, Sanders ME, Gianni L. Triple-Negative Breast Cancer: Challenges and Opportunities of a Heterogeneous Disease. *Nat Rev Clin Oncol* (2016) 13(11):674–90. doi: 10.1038/nrclinonc.2016.66
5. Jiang YZ, Ma D, Suo C, Shi J, Xue M, Hu X, et al. Genomic and Transcriptomic Landscape of Triple-Negative Breast Cancers: Subtypes and Treatment Strategies. *Cancer Cell* (2019) 35(3):428–40.e5. doi: 10.1016/j.ccell.2019.02.001
6. Jiang YZ, Liu Y, Xiao Y, Hu X, Jiang L, Zuo WJ, et al. Molecular Subtyping and Genomic Profiling Expand Precision Medicine in Refractory Metastatic Triple-Negative Breast Cancer: The FUTURE Trial. *Cell Res* (2020) 31 (2):178–86. doi: 10.1038/s41422-020-0375-9
7. Mitelman F, Johansson B, Mertens F. Fusion Genes and Rearranged Genes as a Linear Function of Chromosome Aberrations in Cancer. *Nat Genet* (2004) 36(4):331–4. doi: 10.1038/ng1335
8. Heyer EE, Deveson IW, Wooi D, Selinger CI, Lyons RJ, Hayes VM, et al. Diagnosis of Fusion Genes Using Targeted RNA Sequencing. *Nat Commun* (2019) 10(1):1388. doi: 10.1038/s41467-019-09374-9
9. Annala MJ, Parker BC, Zhang W, Nykter M. Fusion Genes and Their Discovery Using High Throughput Sequencing. *Cancer Lett* (2013) 340 (2):192–200. doi: 10.1016/j.canlet.2013.01.011
10. Hirabayashi S, Ohki K, Nakabayashi K, Ichikawa H, Momozawa Y, Okamura K, et al. ZNF384-Related Fusion Genes Define a Subgroup of Childhood B-Cell Precursor Acute Lymphoblastic Leukemia With a Characteristic Immunotype. *Haematologica* (2017) 102(1):118–29. doi: 10.3324/haematol.2016.151035
11. Zhu HH, Yang MC, Wang F, Lou YJ, Jin J, Li K, et al. Identification of a Novel NUP98-RARA Fusion Transcript as the 14th Variant of Acute Promyelocytic Leukemia. *Am J Hematol* (2020) 95(7):E184–e6. doi: 10.1002/ajh.25807
12. Yang RY, Yang CX, Lang XP, Duan LJ, Wang RJ, Zhou W, et al. Identification of a Novel RUNX1-TACC1 Fusion Transcript in Acute Myeloid Leukaemia. *Br J Haematol* (2020) 189(2):e52–6. doi: 10.1111/bjh.16444
13. Haas BJ, Dobin A, Li B, Stransky N, Pochet N, Regev A. Accuracy Assessment of Fusion Transcript Detection Via Read-Mapping and De Novo Fusion Transcript Assembly-Based Methods. *Genome Biol* (2019) 20(1):213. doi: 10.1186/s13059-019-1842-9
14. Jang JE, Kim HP, Han SW, Jang H, Lee SH, Song SH, et al. Nfatc3-Pla2g15 Fusion Transcript Identified by RNA Sequencing Promotes Tumor Invasion and Proliferation in Colorectal Cancer Cell Lines. *Cancer Res Treat* (2019) 51 (1):391–401. doi: 10.4143/crt.2018.103
15. Dai X, Theobard R, Cheng H, Xing M, Zhang J. Fusion Genes: A Promising Tool Combating Against Cancer. *Biochim Biophys Acta Rev Cancer* (2018) 1869(2):149–60. doi: 10.1016/j.bbcan.2017.12.003
16. Dupain C, Harttrampf AC, Boursin Y, Lebeurrier M, Rondof W, Robert-Siegwald G, et al. Discovery of New Fusion Transcripts in a Cohort of Pediatric Solid Cancers at Relapse and Relevance for Personalized Medicine. *Mol Ther J Am Soc Gene Ther* (2019) 27(1):200–18. doi: 10.1016/j.ymthe.2018.10.022
17. Tognon C, Knezevich SR, Huntsman D, Roskelley CD, Melnyk N, Mathers JA, et al. Expression of the ETV6-NTRK3 Gene Fusion as a Primary Event in Human Secretory Breast Carcinoma. *Cancer Cell* (2002) 2(5):367–76. doi: 10.1016/s1535-6108(02)00180-0
18. Persson M, Andrén Y, Mark J, Horlings HM, Persson F, Stenman G. Recurrent Fusion of MYB and NFIB Transcription Factor Genes in Carcinomas of the Breast and Head and Neck. *Proc Natl Acad Sci United States America* (2009) 106(44):18740–4. doi: 10.1073/pnas.0909114106
19. Varley KE, Gertz J, Roberts BS, Davis NS, Bowling KM, Kirby MK, et al. Recurrent Read-Through Fusion Transcripts in Breast Cancer. *Breast Cancer Res Treat* (2014) 146(2):287–97. doi: 10.1007/s10549-014-3019-2
20. Bean GR, Krings G, Otis CN, Solomon DA, García JJ, van Zante A, et al. Crtc1-MAML2 Fusion in Mucoepidermoid Carcinoma of the Breast. *Histopathology* (2019) 74(3):463–73. doi: 10.1111/his.13779
21. Kim J, Kim S, Ko S, In YH, Moon HG, Ahn SK, et al. Recurrent Fusion Transcripts Detected by Whole-Transcriptome Sequencing of 120 Primary Breast Cancer Samples. *Genes Chromosomes Cancer* (2015) 54(11):681–91. doi: 10.1002/gcc.22279
22. Iyer MK, Chinnaiyan AM, Maher CA. ChimeraScan: A Tool for Identifying Chimeric Transcription in Sequencing Data. *Bioinf (Oxford England)* (2011) 27(20):2903–4. doi: 10.1093/bioinformatics/btr467
23. Jia W, Qiu K, He M, Song P, Zhou Q, Zhou F, et al. Soapfuse: An Algorithm for Identifying Fusion Transcripts From Paired-End RNA-Seq Data. *Genome Biol* (2013) 14(2):R12. doi: 10.1186/gb-2013-14-2-r12
24. Soda M, Choi YL, Enomoto M, Takada S, Yamashita Y, Ishikawa S, et al. Identification of the Transforming EML4-ALK Fusion Gene in Non-Small-Cell Lung Cancer. *Nature* (2007) 448(7153):561–6. doi: 10.1038/nature05945
25. Gerds AT, Gotlib J, Bose P, Deininger MW, Dunbar A, Elshoury A, et al. Myeloid/Lymphoid Neoplasms With Eosinophilia and TK Fusion Genes, Version 3.2021, NCCN Clinical Practice Guidelines in Oncology. *J Natl Compr Cancer Netw JNCCN* (2020) 18(9):1248–69. doi: 10.6004/jnccn.2020.0042
26. Mertens F, Johansson B, Fioretos T, Mitelman F. The Emerging Complexity of Gene Fusions in Cancer. *Nat Rev Cancer* (2015) 15(6):371–81. doi: 10.1038/nrc3947
27. Bailey SM, Murnane JP. Telomeres, Chromosome Instability and Cancer. *Nucleic Acids Res* (2006) 34(8):2408–17. doi: 10.1093/nar/gkl303
28. Murnane JP, Sabatier L. Chromosome Rearrangements Resulting From Telomere Dysfunction and Their Role in Cancer. *BioEssays News Rev Mol Cell Dev Biol* (2004) 26(11):1164–74. doi: 10.1002/bies.20125
29. Mitani Y, Rao PH, Futreal PA, Roberts DB, Stephens PJ, Zhao YJ, et al. Novel Chromosomal Rearrangements and Break Points at the T (6,9) in Salivary Adenoid Cystic Carcinoma: Association With MYB-NFIB Chimeric Fusion, MYB Expression, and Clinical Outcome. *Clin Cancer Res* (2011) 17(22):7003–14. doi: 10.1158/1078-0432.Ccr-11-1870
30. Grosso AR, Leite AP, Carvalho S, Matos MR, Martins FB, Vítor AC, et al. Pervasive Transcription Read-Through Promotes Aberrant Expression of Oncogenes and RNA Chimeras in Renal Carcinoma. *eLife* (2015) 4:e09214. doi: 10.7554/eLife.09214

31. Kim HP, Cho GA, Han SW, Shin JY, Jeong EG, Song SH, et al. Novel Fusion Transcripts in Human Gastric Cancer Revealed by Transcriptome Analysis. *Oncogene* (2014) 33(47):5434–41. doi: 10.1038/onc.2013.490
32. Zhang Y, Gong M, Yuan H, Park HG, Frierson HF, Li H. Chimeric Transcript Generated by Cis-Splicing of Adjacent Genes Regulates Prostate Cancer Cell Proliferation. *Cancer Discovery* (2012) 2(7):598–607. doi: 10.1158/2159-8290.Cd-12-0042
33. Neckles C, Sundara Rajan S, Caplen NJ. Fusion Transcripts: Unexploited Vulnerabilities in Cancer? *Wiley Interdiscip Rev RNA* (2020) 11(1):e1562. doi: 10.1002/wrna.1562
34. Asmann YW, Necela BM, Kalari KR, Hossain A, Baker TR, Carr JM, et al. Detection of Redundant Fusion Transcripts as Biomarkers or Disease-Specific Therapeutic Targets in Breast Cancer. *Cancer Res* (2012) 72(8):1921–8. doi: 10.1158/0008-5472.Can-11-3142
35. Yi YS. Functional Role of Milk Fat Globule-Epidermal Growth Factor VIII in Macrophage-Mediated Inflammatory Responses and Inflammatory/Autoimmune Diseases. *Mediators Inflammation* (2016) 2016:5628486. doi: 10.1155/2016/5628486
36. Tibaldi L, Leyman S, Nicolas A, Notebaert S, Dewulf M, Ngo TH, et al. New Blocking Antibodies Impede Adhesion, Migration and Survival of Ovarian Cancer Cells, Highlighting MFGE8 as a Potential Therapeutic Target of Human Ovarian Carcinoma. *PloS One* (2013) 8(8):e72708. doi: 10.1371/journal.pone.0072708
37. Shimagaki T, Yoshio S, Kawai H, Sakamoto Y, Doi H, Matsuda M, et al. Serum Milk Fat Globule-EGF Factor 8 (MFG-E8) as a Diagnostic and Prognostic Biomarker in Patients With Hepatocellular Carcinoma. *Sci Rep* (2019) 9(1):15788. doi: 10.1038/s41598-019-52356-6
38. Kothari C, Osseni MA, Agbo L, Ouellette G, Déraspe M, Laviolette F, et al. Machine Learning Analysis Identifies Genes Differentiating Triple Negative Breast Cancers. *Sci Rep* (2020) 10(1):10464. doi: 10.1038/s41598-020-67525-1
39. Carrascosa C, Obula RG, Missiaglia E, Lehr HA, Delorenzi M, Frattini M, et al. Mfg-E8/lactadherin Regulates Cyclins D1/D3 Expression and Enhances the Tumorigenic Potential of Mammary Epithelial Cells. *Oncogene* (2012) 31(12):1521–32. doi: 10.1038/onc.2011.356
40. Ko DS, Kim SH, Park JY, Lee G, Kim HJ, Kim G, et al. Milk Fat Globule-Egf Factor 8 Contributes to Progression of Hepatocellular Carcinoma. *Cancers (Basel)* (2020) 12(2):403. doi: 10.3390/cancers12020403
41. Haldrup C, Pedersen AL, Øgaard N, Strand SH, Høyer S, Borre M, et al. Biomarker Potential of ST6GALNAC3 and ZNF660 Promoter Hypermethylation in Prostate Cancer Tissue and Liquid Biopsies. *Mol Oncol* (2018) 12(4):545–60. doi: 10.1002/1878-0261.12183
42. Santuario-Facio SK, Cardona-Huerta S, Perez-Paramo YX, Trevino V, Hernandez-Cabrera F, Rojas-Martinez A, et al. A New Gene Expression Signature for Triple Negative Breast Cancer Using Frozen Fresh Tissue Before Neoadjuvant Chemotherapy. *Mol Med (Cambridge Mass)* (2017) 23:101–11. doi: 10.2119/molmed.2016.00257
43. Kuo SJ, Chien SY, Lin C, Chan SE, Tsai HT, Chen DR. Significant Elevation of CLDN16 and HAPLN3 Gene Expression in Human Breast Cancer. *Oncol Rep* (2010) 24(3):759–66. doi: 10.3892/or_00000918


**Conflict of Interest:** The authors declare that the research was conducted in the absence of any commercial or financial relationships that could be construed as a potential conflict of interest.

# Advantages of publishing in Frontiers

**OPEN ACCESS**
Articles are free to read for greatest visibility and readership

**FAST PUBLICATION**
Around 90 days from submission to decision

**HIGH QUALITY PEER-REVIEW**
Rigorous, collaborative, and constructive peer-review

**TRANSPARENT PEER-REVIEW**
Editors and reviewers acknowledged by name on published articles

**Frontiers**
Avenue du Tribunal-Fédéral 34
1005 Lausanne | Switzerland

**Visit us:** www.frontiersin.org
**Contact us:** frontiersin.org/about/contact

**REPRODUCIBILITY OF RESEARCH**
Support open data and methods to enhance research reproducibility

**DIGITAL PUBLISHING**
Articles designed for optimal readership across devices

**FOLLOW US**
@frontiersin

**IMPACT METRICS**
Advanced article metrics track visibility across digital media

**EXTENSIVE PROMOTION**
Marketing and promotion of impactful research

**LOOP RESEARCH NETWORK**
Our network increases your article's readership